Aerodynamic Design of Wind Turbine Blades Utilising Nonconventional Control Systems

I KADE WIRATAMA

A Thesis Submitted in Partial Fulfilment of the Requirements of the University of Northumbria at Newcastle for the Degree of Doctor of Philosophy

A research undertaken in the
School of Computing, Engineering and
Information Sciences

November 2012

Declaration

I declare that the work contained in this thesis has not been submitted for any other award and that it is all my own work. I also confirm that this work fully acknowledges opinions, ideas and contributions from the work of others.

Name I Kade Wiratama

Signature

Date 20 November 2012

Abstract

As a result of the significant growth of wind turbines in size, blade load control has become the main challenge for large wind turbines. Many advanced techniques have been investigated aiming at developing control devices to ease blade loading. Individual pitch control system, adaptive blades, trailing edge microtabs, morphing aerofoils, ailerons, trailing edge flaps, and telescopic blades are among these techniques. Most of the above advanced technologies are currently implemented in, or are under investigation to be utilised, for blade load alleviation. The present study aims at investigating the potential benefits of these advanced techniques in enhancing the energy capture capabilities rather than blade load alleviation. To achieve this goal the research is carried out in three directions: (i) development of a simulation software tool suitable for wind turbines utilising nonconventional control systems, (ii) development of a blade design optimisation tool capable of optimising the topology of blades equipped with nonconventional control systems, and (iii) carrying out design optimisation case studies with the objective of power extraction enhancement towards investigating the feasibility of advanced technologies, initially developed for load alleviation of large blades, for power extraction enhancement. Three nonconventional control systems, namely, microtab, trailing edge flap and telescopic blades are investigated. A software tool, AWTSim, is especially developed for aerodynamic simulation of wind turbines utilising blades equipped with microtabs and trailing edge flap as well as telescopic blades. As part of the aerodynamic simulation of these wind turbines, the control system must be also simulated. The simulation of the control system is carried out via solving an optimisation problem which gives the best value for the controlling parameter at each wind turbine run condition. Developing a genetic algorithm optimisation tool which is especially designed for wind turbine blades and integrating it with AWTSim, a design optimisation tool for blades equipped with nonconventional control system is constructed. The design optimisation tool, AWTSimD, is employed to carry out design case studies. The results of design case studies reveal that for constant speed rotors, optimised telescopic blades are more effective than flaps and microtabs in power enhancement. However, in comparison with flap and microtabs, telescopic blades have two disadvantages: (i) complexity in telescopic mechanism and the added weight and (ii) increased blade loading. It is also shown that flaps are more efficient than microtabs, and that the location and the size of flaps are key parameters in design. It is

also shown that optimisation of the blade pretwist has a significant influence on the energy extraction enhancement. That is, to gain the maximum benefit of installing flaps and microtabs on blades, the baseline blades must be redesigned.

Acknowledgements

First of all I would like to thank the Indonesian Government for the financial support and the opportunity given to me to pursue my PhD study at Northumbria University, United Kingdom.

I would like to express my deepest gratitude to my principal supervisor Dr Alireza Maheri for his great support and guidance to make this project a success. Without his support, this work would have never been completed. I also wish to thank Dr John Tan and Dr Askin Isikveren for their kind assistance, supportive advice and encouragements.

Finally, a million thanks are dedicated to my wife Bhineka for her patience, love and care, as well as to my beloved kids, Wika and Meivi. Their support has been source of my energy and strength giving me spirit to keep forward through many years of the exhausted research. This work is dedicated to them. I also very thankful to all of my relatives for their moral support and motivation, especially to my mother and father who passed away in the first year of my PhD. May my achievement bring pride and joy to them.

Table of Contents

List of Figures

List of Tables

List of Algorithms

Nomenclature

A_0, A_1, A_2	Coefficient in Wilson-Walker state model
A_e	Blade element (segment) area
a	Axial induction factor
a_e	Boundary of heavy and light loading states
a'	Rotational induction factor
B	Number of blades
B_0, B_1, B_2	Coefficient in Classical brake state model
C_1	Child 1
C, c	Blade chord
C_D	Drag coefficient
C_L	Lift coefficient
C_M	Pitching moment coefficient, Torque coefficient
C_{M_0}	Torque coefficient at zero drag
C_p	Power coefficient
C_T	Thrust coefficient
C_{T_0}	Thrust coefficient at zero drag
D	Drag per unit span length, Rotor Diameter
d_F	Width of flap
d_{MT}	Microtabs distance from leading edge
F	Loss factor
f	Function
f_n	Normal force on the blade cross section
fit	Fitness
h_{hub}	Height above ground hub
h_{MT}	Microtabs actuation height
L	Lift per unit span length
M	Rotor torque, Blade bending moment
MT	Microtab
n_{gen}	No. of generation
N_{MT}	Number of microtab
n_{pop}	Population size
n_{co}	Number of crossover
n_{dp}	Number of design points
n_{Mute}	Number of mutation
n_{sec}	Number sector

n_{seg}	Number segment
P_1	Parent 1
P_2	Parent 2
P	Rotor mechanical power
p_c	Probably crossover
p_m	Probably mutation
$pitch$	Pitch angle
q	Controlling parameters
R	Rotor radius, Rayleigh PDF
R_{hub}	Hub radius
R_T	Blade telescopic radius
r	Radial distance from the rotor centre
s_{MT}	Microtab length
T	Rotor thrust
$t_{\max}$	Aerofoil maximum thickness
V	Flow velocity
V_{av}	Site average wind speed
V_{AF}	Stream-wise velocity in the far wake
V_d	Disk velocity
V_{hub}	Wind speed at hub
V_{rel}	Relative velocity
V_w	Wind velocity
V_∞	Free stream velocity
$\vec{V}$	Wind velocity field
$\vec{V}_I$	Induced velocity field
$\vec{V}_{rel}$	Relative velocity field
$\vec{V}_W$	Upstream mean velocity field
$\hat{V}$	Wind turbulence
w	Normalised distribution force
x_0	x-coordinate of the blade pretwist axis
x_{co}	Fraction of total crossover
x_{ip}	Fraction of initial population
z	Height above ground
z_0	Roughness length
α	Angle of attack
α_{opt}	Angle of attack optimum
β	Blade twist angle

β_0	Blade pretwist
β_e	Elastic torsional deformation in the blade
δ	Blade cone angle
δ_F	Flap deployment angle
$\Delta\alpha_c$	Correction applicable to angle of attack
ΔC_L	Change in lift coefficient
ΔC_D	Change in drag coefficient
ε	Tolerance
γ	Rotor yaw angle
λ	Speed ratio
λ_r	Local speed ratio
Ω	Rotor speed
φ	Inflow angle
φ_0	Inflow angle at zero rotational induction
ψ	Blade element azimuth angle
ρ	Air density
σ_r	Local solidity ratio

Subscripts

av	Average
c	Constraint, Crossover
co	Crossover
dp	design point
F	Force, Flap
FB	Flap-wise bending
FW	Far wake
F,e	End of length flaps location
F,s	Start of length flaps location
gen	Generation
hub	Hub
ip	Initial population
l	Lower limit
M	Bending moment
MT	Microtab
MT,e	End of length microtab location
MT,s	Start of length microtab location
m	Mutation
o	Initial point
opt	Optimum
pop	Population
rated	Rated
ref	Reference
rel	Relative

s	Span-wise Secondary
T	Telescopic
T,e	Telescopic part fully deployed
T,s	Fix part of telescopic
T,tip	Tip
u	Upper limit

Superscripts

$*$	Normalised, dimensionless

Systems of coordinates

$n-t-s$	Blade, Figure 2.1
$x-y-z$	Blade and global coordinate, Figure 2.1
$x-r-\psi$	Disk (Rotor), Figure 2.1

Abbreviations

AOA	Angle of Attack
AR	Aspect Ratio
AWT	Aerodynamic Wind Turbine
AWTSim	Aerodynamic Wind Turbine Simulation
AWTSimD	Aerodynamic Wind Turbine Simulation Design
BEMT	Blade Element Momentum Theory
CFD	Computational Fluid Dynamics
CV	Control Volume
GA	Genetic Algorithm
HAWT	Horizontal Axis Wind Turbine
NREL	National Renewable Energy Laboratories
PDF	Probability Distribution (Density) Function
SNL	Sandia National Laboratory

1 Introduction

1.1 Structure of the Thesis

Chapter 1 of this thesis is dedicated to the background of the conventional and nonconventional aero-mechanical control systems, state of the art of blade design optimisation and the aim and the objectives of this project. Chapter 2 elaborates on blade element momentum theory (BEMT), the theory behind the software tool AWTSim developed for aerodynamic analysis of wind turbines. The pseudo codes of the core modules of the software tool are also given in this chapter. Using a stall-regulated constant speed test wind turbine, at the end of this chapter the performance of this software is validated against an accredited analysis tool. Further necessary enhancements to AWTSim, making it capable of simulating wind turbines with nonconventional control systems, is discussed and explained in Chapter 3. For each type of wind turbines, its controlling system is simulated by solving an optimisation problem. Enhanced AWTSim is capable of simulating both constant and variable speed wind turbines with various nonconventional controlling systems. Chapter 4 details the genetic algorithm optimisation method developed for design optimisation of wind turbine blades equipped with nonconventional control systems. In Chapter 5 design optimisation case studies are carried out for wind turbine blades equipped with microtabs and trailing edge flaps as well as telescopic blades. The results of these design case studies have been assessed towards a thorough investigation of their capabilities in enhancing power capture capabilities. Chapter 6 summarises the research carried out, the results obtained, conclusions, critical appraisal of the work and suggested future work.

1.2 Background

1.2.1 Conventional Aero-Mechanical Load and Power Control Systems

Wind turbines are designed to produce maximum power at the most probable wind speed. At high wind speeds, the generated power by a wind turbine far exceeds the generator capacity. To protect wind turbine operation at high wind speeds it is needed to limit the generated power otherwise wind turbine will be overloading its rotors, mechanical power train, as well as its electrical generator leading to failure during operation.

Pitch control and stall regulation are the most popular power control systems both based on controlling the flow angle of attack. Figure (1.1) shows power curve for these two control systems. According to this figure the ideal situation is for the turbine to be able to produce as much power as possible from the wind up to the rated power of the generator, then limits the power production at the rated value.

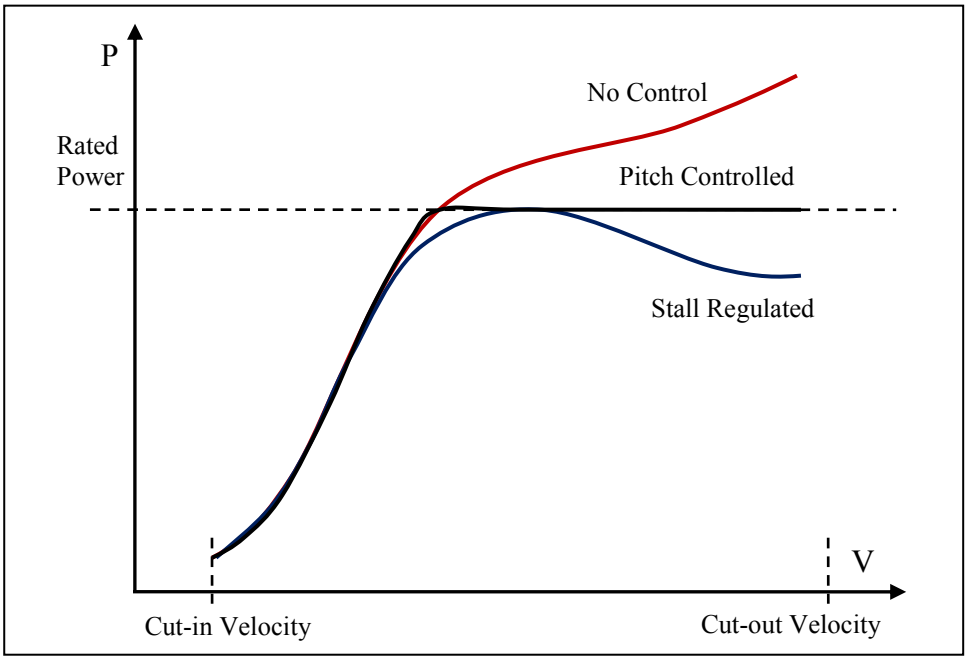

Figure 1.1- Power curve for different power control methods

Stall regulation is mechanically the most simple controlling strategy. In stall regulated wind turbines the blades have been designed to stall in high winds without any pitching control. The rotor is built with the blades fixed on the hub therefore it is rather simple in construction and the pitch of the blades are adjusted only once when the wind turbine is erected. In order to achieve stall-regulation at appropriate wind speeds, the wind turbine blades operate closer to stall and result in lower aerodynamic efficiency below rated power. This does not give a perfectly flat power curve above the rated wind speed.

A stall regulated wind turbine is normally operated at an almost constant rotor speed Ω and thus the angle of attack α increases as the wind speed increases. Figure (1.2) shows the flow diagram of stall regulation at a typical radial location r. According to this figure, as the wind speed V_W increases the inflow angle φ and consequently the angle of attack α increases. Increasing the angle of attack beyond a certain limit, called stall

angle of attack α_s, causes significant drop in lift coefficient and consequently rotor power (see Figure (1.3)).

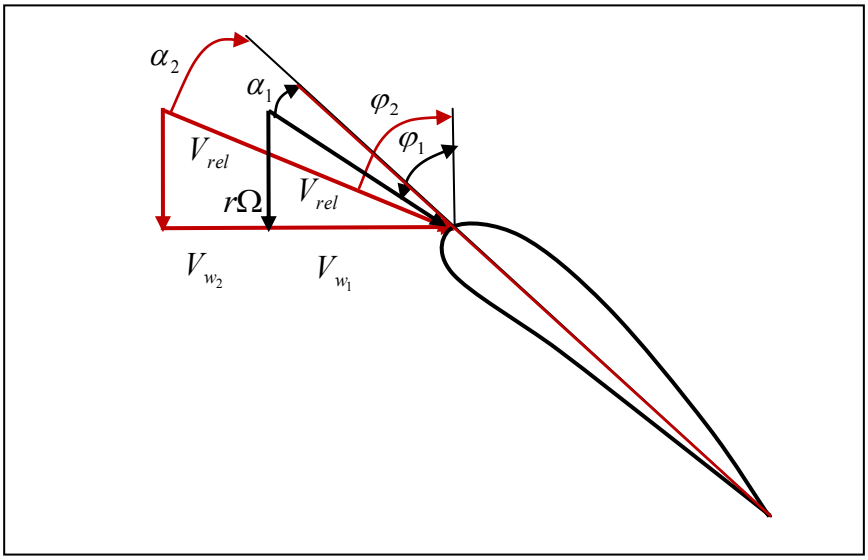

Figure 1.2-Flow kinematics diagram of stall control

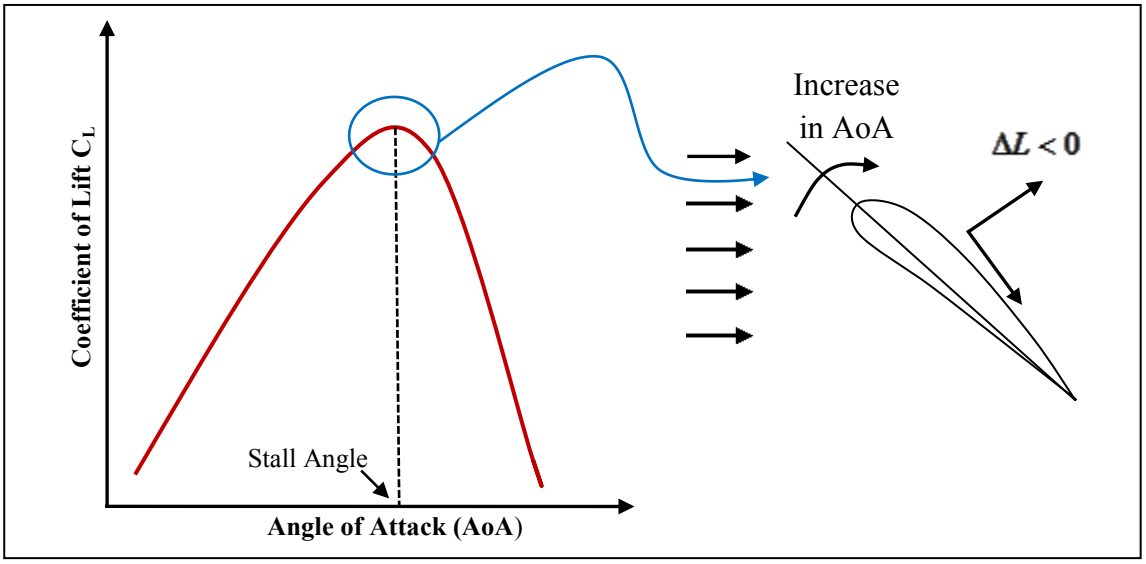

Figure 1.3-Stall regulation

In order for the turbine to stall rather than accelerate in high winds, the rotor speed must be restrained. In a constant speed turbine the rotor speed is restrained by the generator, which is governed by the network frequency, as long as the torque remains below the pull-out torque. In a variable speed turbine, the speed is maintained by ensuring that the generator torque is varied to match the aerodynamic torque. A variable-speed turbine offers the possibility to slow the rotor down in high winds in order to bring it into stall. This means that the turbine can operate further from the stall point in low winds, resulting in higher aerodynamic efficiency. However, this strategy means that when a

gust hits the turbine, the load torque not only has to rise to match the wind torque but also has to increase further in order to slow the rotor down into stall.

Using this type of stall regulating requires carefully designed rotor blade geometry and carefully selected rotor speed to ensure that at higher wind speed, the flow does indeed separate so that an increase in generated power can effectively be prevented.

Pitch control is the most common means of controlling the aerodynamic power generated by the turbine rotor and also has a major effect on the aerodynamic loads generated by wind turbine. The most effective way of influencing the aerodynamic angle of attack and thus power generated is by mechanical adjustment of the blade pitch angle. Pitch control can be used to regulate power generated by decreasing the power to rated power or increasing the power through changes in the blade aerodynamic as shown in Figure (1.4). In this figure the blue curve represents the power curve without pitch control and the red curve represents the power curve when a pitch control system is employed. By pitching the blade around its axis, the blade pitch angle changes the angle of attack and aerodynamic forces. Pitching influences the power generated and load occurred in the rotor blade and is therefore suitable for both power and load control.

Flow kinematics of a pitch control system is shown in Figure (1.5). In this figure β, the blade twist is a combination of the pretwist β_0 and blade pitch angle $pitch$.

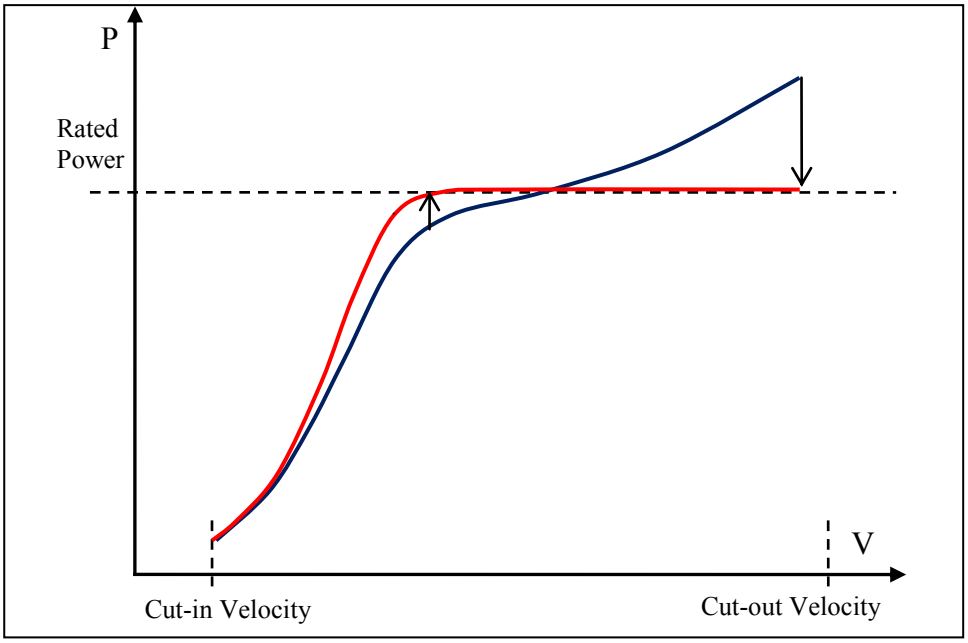

Figure 1.4-Pitch control to enhance/regulate rotor mechanical power

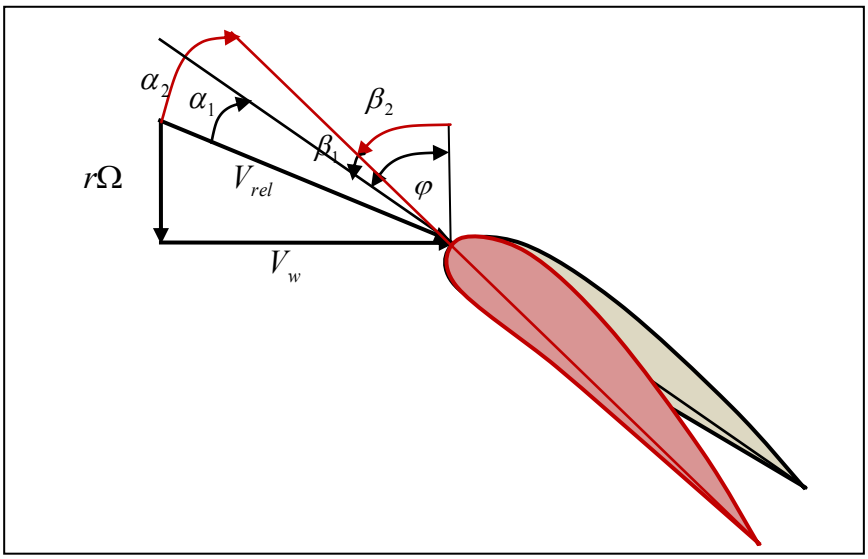

Figure 1.5- Flow kinematics diagram of pitch control

In practice, power control through blade pitch control can be achieved by two methods, conventional pitch and active stall. In conventional approach, shown in Figure (1.6), pitch to stall increases the angle of attack and the lift coefficient (and consequently the rotor mechanical power). Pitching the blade in the direction of the feather position not only reduces the driving force but all forces at the rotor blade and also the resulting stress. By pitching to feather the quasi loads from mean aerodynamic force are reduced at higher wind conditions and during storm therefore when a dangerous operating state occurs (e.g. over-speeding or emergency stop), the blade pitch has to bring the rotor blade to the feather position immediately consequently it will reduce power generated and load generated on the rotor blade.

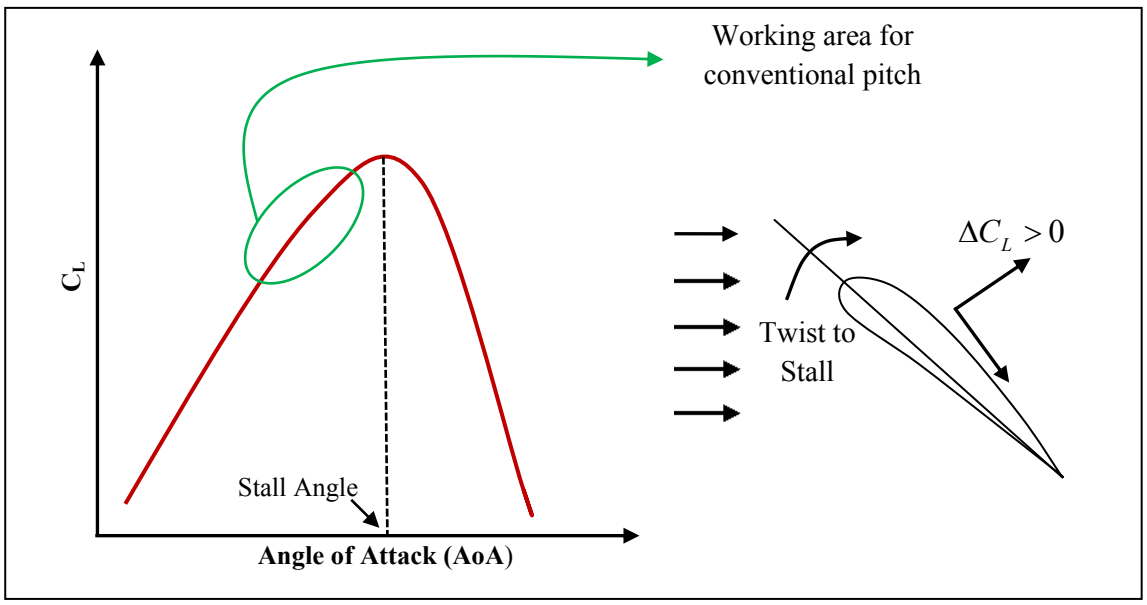

Figure 1.6- Conventional pitch control

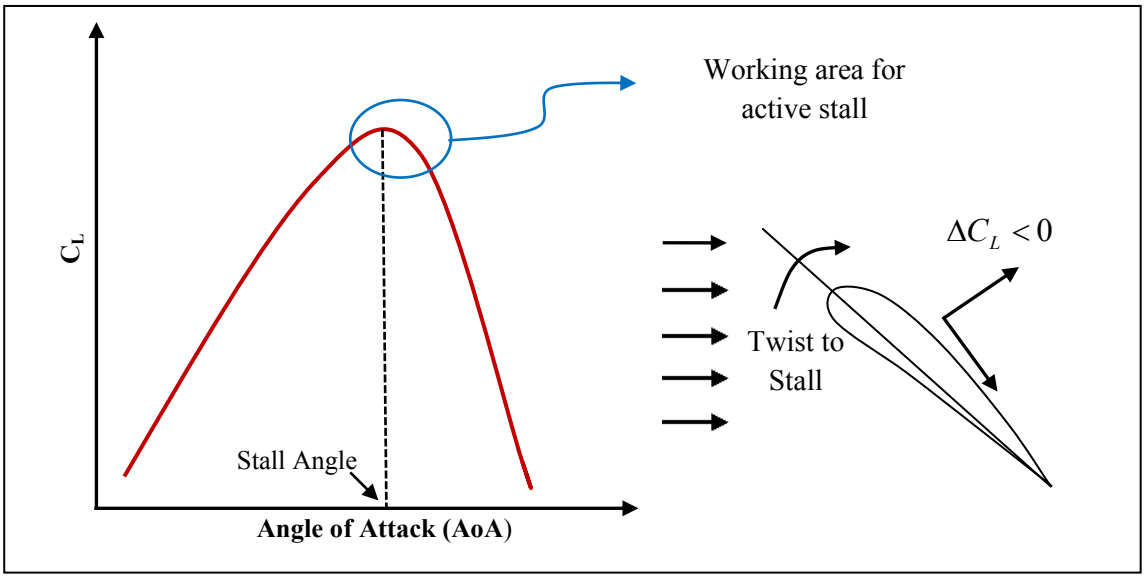

Figure 1.7- Active stall pitch control

In active stall scenario, as shown in Figure (1.7), pitch to stall increases the angle of attack but reduces the lift coefficient (and consequently the rotor mechanical power).

Using mechanical energy for the blade pitch is more suitable at smaller wind turbine for rated power less than 100kW. Hydraulic blade pitch systems are normally used for wind turbines with rated power in the range of 300 kW to the multi-MW. Electrical blade pitch system is also common to most of the wind turbines types. Many manufactures trust in this solution for the pitch systems especially for larger wind turbines for rated power above 500 kW (Robert, 2011).

Mechanisms that adjust blade pitch angle in response to the thrust loading were also quite popular in the early days of the modern wind energy push. Approaches and objectives were quite varied. Cheney (1978) regulated power with a centrifugally loaded mass on an elastic arm. Bottrell (1981) had a system for cyclically adjusting pitch for load balancing. Currin (1981) had a system for passively adjusting pitch for both power and load control. Hohenemser (1981) studied alleviating yaw loads with cyclic pitch adjustments. Corbet (1992) evaluated the use of all available blade loads to effect pitch changes that would regulate the power output of a turbine, aiming at a flat power curve in high winds. They reported that perfect regulation was very difficult to achieve, and that even less than perfect regulation was a challenge. These approaches also depend on quite substantial blade rotations to achieve perfect regulation.

1.2.2 Advanced Aero-Mechanical Methods for Controlling Blade Load

The size of rotor wind turbine has been steady increased over the past decade. Recently, rotors of more than 120 m diameter are in prototype and now, commercial wind turbines are available with capacities up to 3500kW (Herbert, 2007). The rapid increase in size and capacity of commercially manufactured wind turbines between the years 1982 and 2009 is illustrated in Figure (1.8). According to this figure, within a very short time the increase in wind turbine size have been remarkable. In 2010, for example, the largest commercial wind turbine had a capacity of 7.5 MW and a diameter of 126 meters (Robert, 2011).

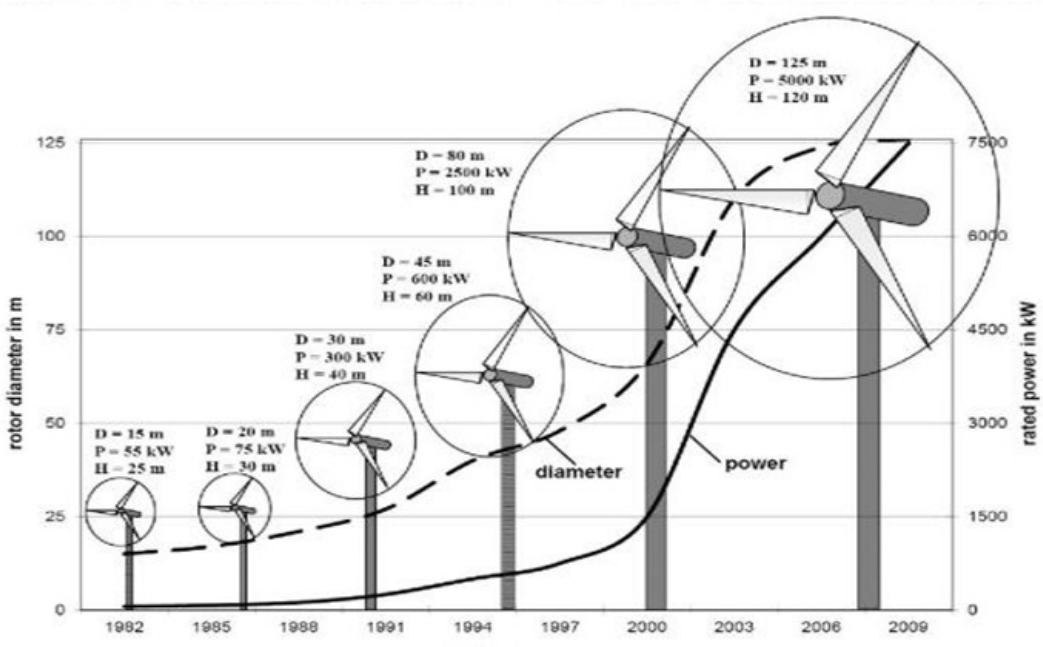

Figure 1.8-Size and power increase of commercial wind turbines over time (Robert, 2011).

As a result of the significant growth of wind turbines in size, blade load control has become the main challenge for large wind turbines (Nijssen 2006 and Johnson 2008). According to Barlas (2010), many advanced techniques have been investigated aiming at developing control devices to ease blade loading. Individual pitch control system, adaptive blades, trailing edge microtabs, morphing aerofoils, ailerons, trailing edge flaps, and telescopic blades are among these techniques.

Though, collective pitch control systems were primarily developed to limit the rotor mechanical power at a rated value and to optimise the energy capture below that value (Bossanyi 2000, Wright 2002, Van der Hooft 2003), recently, individual pitch control systems have been successfully developed and utilised to alleviate low frequency fluctuating loads by pitching the blades individually (Caselitz 1997, Bossanyi 2003, van

Engelen 2003, Larsen 2005, Lovera 2003). The concept of individual pitch control was first introduced for helicopter rotor blades (Johnson 1982). Still some disadvantages are evident, especially for the large scale application for wind turbine blades (Lovera 2003). The response time for individual pitch control systems is not fast enough for high frequency load fluctuation. Moreover, actuation of massive large blades requires significant actuation force and energy.

Also, adopting from the helicopter blade technology, blade twist control based on passive control system is a relatively new field in the wind turbine industry. This approach, known as adaptive or smart blades, employs the blade itself as the controller to sense the wind velocity or rotor speed variations and adjust its aerodynamic characteristics to affect the wind turbine performance. Earlier work was carried out on the project at Reading University by Karaolis (1989) and Kooijiman (1996) and then progressed by other investigators. These blades are made of anisotropic composite materials and change their shapes in response to the variations in wind turbine operating conditions. It has been shown that these blades potentially can be used for both blade load alleviation and enhancing energy capture capabilities (Lobitz, 2001, Maheri 2006, Maheri et al 2006, Maheri et al 2007a, Maheri et al 2007b, Maheri et al 2007c, Maheri and Isikveren 2009a and Maheri and Isikveren 2010) .

A different kind of aerodynamic device proposed for load alleviation is microtabs (Baker and Mayda 2005, Chow 2007 and van Dam et al 2001, 2002, 2005a, 2005b and 2007). Microtabs are small aerodynamic control surfaces with deployment height of order of magnitude of 0.01 of local chord, installed close to the trailing edge of the blade.

Morphing blades, a concept adopted from aircraft morphing wings, has also the potential to improve the system performance over the wind turbine operational envelope (Stuart 1997, Farhan 2008, Barlas 2010). The morphing concept includes a wide spectrum of shape adaptations such as variation in camber, twist, span and plan form area. Camber control is a type of morphing aerofoils and an effective way of controlling the aerodynamic forces by directly changing the shape of the aerofoil. This action has direct effects on the force distribution on the blade, so it can be used for active load alleviation purposes (Farhan 2008, Maheri 2009b).

Aileron, a concept borrowed from aerospace industry, is another active device, which has been used for aerodynamic breaking in the past. Results of a recent research on ailerons via simulating the behaviour of a wind turbine in turbulent wind indicates that aileron load control can assist in power regulation and reduce root flap bending moments during a step-gust and turbulent wind situation (Migliore 1995, Stuart 1996, Enenkl 2002).

The concept of trailing edge flap follows the same principle as aileron, but by deflecting the trailing edge portion of the aerofoil, to change the aerodynamic characteristics of the blade in high-wind conditions and turbulent wind (Troldborg and Buhl 2005, Andersen 2006).

Compact trailing edge flaps made of smart materials is another concept under investigation for load alleviation. Results of a recent research demonstrate large reduction (50 -90%) in vibratory load (Barlas 2010).

Recently, the concept of variable length blades has been also proposed as a means of controlling the load and increasing the energy yield of the turbine. Telescopic blades retract/extend in response to the variations in wind speed (DOE 2005, GE Wind Energy 2006, Pasupulapati 2005, Shrama 2007).

Most of the above advanced technologies are currently implemented in, or are under investigation to be utilised, for blade load alleviation, as the main challenge for design and manufacturing of larger wind turbines. The present research is focused on investigating the application of some these advanced techniques, namely, microtabs, trailing edge flaps and telescopic blades in enhancing the energy capture capabilities rather than blade load alleviation.

Load/power control systems can be divided in two methods: passive and active control. Figure (1.9) summarises nonconventional load/power control systems.

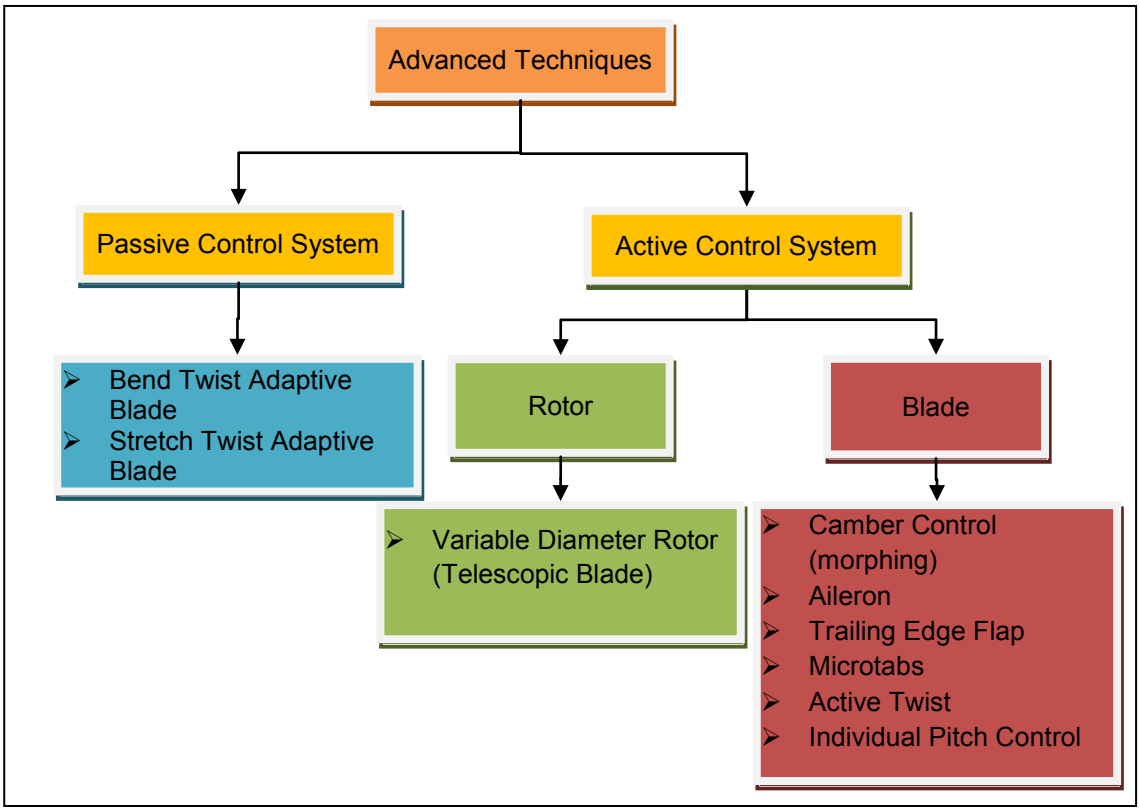

Figure 1.9- Schematic of load control systems

1.2.3 State-of-the-Art in Design and Optimisation of Wind Turbine Blades

Alternative design approaches is another field of research in wind turbines, which recently has become under attention. Integrated design, using computational intelligence techniques in design and optimisation, and modification-based design are examples of this line research. Seki (1996) investigated a method to obtain the optimum blade shape for the rotor of several hundred kW horizontal axis wind turbines. Jureczko (2005) developed a computer program package that would enable optimisation of wind turbine blades with regard to a number of criteria. When designing a wind turbine, the goal is to attain the highest possible power output under specified atmospheric conditions. From the technical point of view, this depends on the shape of the blade. The change of the shape of blade is one of the methods to modify stiffness and stability, but it may influence aerodynamic efficiency of wind turbine. Other method to change dynamic and mechanical properties of wind turbine is modifying the composite material, which the blade is made of. The problem of determining the optimal shape of blade and determining the optimal composite material is a complex one, as the mathematical description of aerodynamic load is complex and a number of constraints and objectives have to be satisfied. These considerations have prompted to take up the problem of the multi-criteria optimum design of wind turbine blades. Mendes (2006) developed a

method to obtain optimal chord and twist distributions in wind turbine blades by using genetic algorithms. The method was based on the use of basic pieces of both aerodynamic techniques for power prediction in wind turbines and also in optimisation tools. The optimisation of chord and pretwist distributions were computed to maximise the mean expected power depending on the Weibull wind distribution at a specific site because in wind power systems optimisation is highly site dependent (Jonkman 2003). To optimise chord and twist distributions BEMT was used (Tangler 2002, Jonkman 2003, Tangler 2004). The BEMT is shown to give good accuracy with respect to computational cost. In most of the optimisation procedures the main computational load is the repetitive goal function evaluation. Therefore, they have implemented a BEM procedure that provided high quality predictions in the linear and in the near stall zones. Also, this procedure was efficient in the use of computational resources.

Ashwill (2007) at Sandia National Laboratories (SNL) developed advanced concepts that enable the utilisation of longer blades that weigh less. These blades are more efficient structurally and aerodynamically. Several of these concepts have been incorporated into subscale prototype blades showing that the concept of flatbacks aerofoils has a structural advantage in the in-board region of the blade, especially towards the root.

More efficient blade designs via integrated design (structure and aerodynamics considered simultaneously) also investigated and reported by Ashwill (2007). Maheri et al (2006) developed a simple algorithm to modify an ordinary blade to a bend-twist adaptive one. Through their algorithm the rotor radius, pretwist and chord distributions of the original blade are modified and the optimum value of the induced twist due to elastic coupling will be predicted. Modifications to the original blade was decided in a manner that limit the output power at its rated value and improve the average power of the wind turbine, while trying to reduce the negative effects on the blade size and loading. Maheri and Isikveren (2008) developed an integrated design approach by proposing an alternative approach for design of adaptive blades. The concept of Variable State Design Parameters (VSDP) was proposed and investigated. It was explained how VSDP can be employed to convert the traditional integrated design process of intrinsically smart aero-structures, to a decoupled and hence computationally efficient design process. Through a design case study they showed the practicality and efficiency of the new approach. Traditional methods of design of aerodynamic surfaces

have been not efficient when applied to design of intrinsically smart aero-structures. Introducing the induced deformation as a Variable State Design Parameter decouples the analysis of these structures therefore the aerodynamic and structural design of these structures can be carried out separately. Their design case study shows that adopting design methodology based on VSDP is enables to design wind turbine smart blades efficiently without any structural analysis involved in the aerodynamic design phase. Using the concept of VSDP they continued by developing a design tool for adaptive blades (Maheri and Isikveren 2009a).

1.3 The Overall Aim and Objectives of the Present Research

The overall aim of this research is to investigate the potentials of nonconventional control systems, which have been initially developed for load control in energy capture capability enhancement. To achieve this goal the following objectives have been defined:

1. To develop the required analysis and simulation tools capable of simulating wind turbines utilising advanced technologies developed for load alleviation of large blades.
2. To develop suitable design optimisation methods and tool for design optimisation of blades equipped with nonconventional control systems.
3. To carry out design optimisation case studies towards investigation of the feasibility of advanced technologies, initially developed for load alleviation of large blades, for power extraction enhancement.

Project has been delivered around three axes: simulation software tool development, design optimisation methodology and tool development and case studies.

2 Aerodynamics of Wind Turbines – Blade Element Momentum Theory

2.1 Introduction

Various methods can be used in order to identify the blade performance and flow characteristics. These methods can be classified mainly as BEMT-based methods and computational fluid dynamics -based methods (Snel 1998, Crespo 1999, Vermeer 2003, Snel 2003, Sanderse 2011).

Computational fluid dynamics (CFD) methods provide more accurate result of analysis compared to BEMT. However, to acquire reliable result from computational method, a vast amount of computational grids are required and advanced turbulence model needs to be applied (Snel 2003, Sanderse 2009). High computational time for turbine wake calculation makes CFD based models less practical in engineering use, particularly as the evaluator module of blade design tools. CFD methods are very useful for understanding the aerodynamic characteristics of rotor blades but it consumes too much time and resources thus it is generally applied at the final performance evaluation stage after all the design process is completed (Madsen,1996). On the other hand, BEMT is a simple, yet efficient method for aerodynamic analysis of rotors. BEMT-based design and analysis codes are somewhat of an industry standard. The evaluator module of almost all wind turbine blade design tools are based on this theory (Moriarty, 2005).

The accuracy of the BEMT model is in general reasonable for a wind turbine in normal operating conditions. A verification study (Madsen,2004) comprising the most common aero-elastic codes in Europe showed a typical difference of 5%-10% between measured and simulated mean blade loads and 5%-20% difference in dynamic blade loads. Madsen investigated both uniformly and non-uniformly loaded actuator disks and the effect of turbulent mixing to show the validity of the BEM theory (Madsen, 1996). It was found that BEMT, with the application of a tip correction, gives a good correlation with the CFD results.

The rest of this Chapter is structured as follows. In Section 2.2 the classical BEMT is explained in details. Some corrections applicable to classical BEMT towards removing some of the shortcomings and enhancing the accuracy of the results are explained in Section 2.3. Section 2.4 and 2.5 detail the software tool developed based on BEMT and its validation against WTPerf (Buhl, 2004), an accredited code by the National Renewable Energy Laboratories, NREL, USA.

2.2 BEMT Method

BEMT combines two methods: Blade Element or Strip Theory and Momentum or Actuator Disk Theory which is used to outline the governing equations for the aerodynamic design and power prediction of a wind turbine rotor (Leishman, 2000). Momentum theory analyses the momentum balance on a rotating annular stream tube passing through a turbine and blade-element theory examines the forces generated by the aerofoil lift and drag coefficients at various sections along the blade. The blade-element theory assumes that the blade can be analysed as a number of independent element in span direction. Combining these theories gives a series of equations that can be solved iteratively.

BEMT postulates the effects of the presence and the rotation of the rotor on the flow field around the rotor by introducing and calculating the field of the induced velocities. This evaluation is based on an iterative algorithm in which the induced velocities are initially assumed and then will be re-calculated by iteration.

The basis of BEMT is well established, but there are some differences among final BEMT models because several strategies are used to solve the non linear equations involved and also because many corrections are proposed to increase the precision of predictions.

2.2.1 Wind, Induced and Relative Velocity Fields

Presence of a wind turbine acting as a partial barrier in the flow field and rotation of its blades cause changes to the wind velocity field as approaches the wind turbine. These changes which are in the form of a reduction in the wind speed and a rotation in the flow field are known as “induced velocity field”. Wind speed retardation depends on the amount of the extracted energy (wind turbine loading), while the induced circumferential velocity depends on the wind turbine angular velocity. Flow in the plane of a wind turbine rotor, referred as rotor disk, can be considered as a combination of the upstream mean velocity field, $\vec{V}_W$ and the induced velocity field, $\vec{V}_I$ (Maheri, 2006).

$$\vec{V} = \vec{V}_W + \vec{V}_I \qquad (2.1)$$

For a moving aerodynamic surface, the aerodynamic performance depends on the "relative velocity field". In case of a wind turbine blade the relative velocity at a general point P located on the blade, as seen by the blade, is defined as:

$$\vec{V}_{rel} = \vec{V} - \vec{V}_P \tag{2.2}$$

in which, $\vec{V}$ is the flow field given by Equation (2.1) and $\vec{V}_P$ is the velocity of point P on the blade.

In order to find the relative velocity, first the following systems of coordinates are defined.

- Cartesian system of coordinates $x - y - z$
- Disk (rotor) system of coordinates $x - r - \psi$, in which x is the rotor axis, $r - \psi$ is the rotor plane, r is the radial coordinate limited between zero and rotor radius $0 \le r \le R$ and ψ is the azimuth angle, measured from horizontal 3 O'clock-clockwise.
- Blade system of coordinates $n - t - s$, in which n is the axis normal to the blade, $t - s$ is the blade plane, $n - t$ is the aerofoil plane and s is the blade span-wise coordinate.

These two systems of coordinates are shown in Figure (2.1). In this figure δ stands for the cone angle, γ is the yaw angle and Ω is the rotor angular velocity. Here, it is assumed that wind velocity has no vertical components.

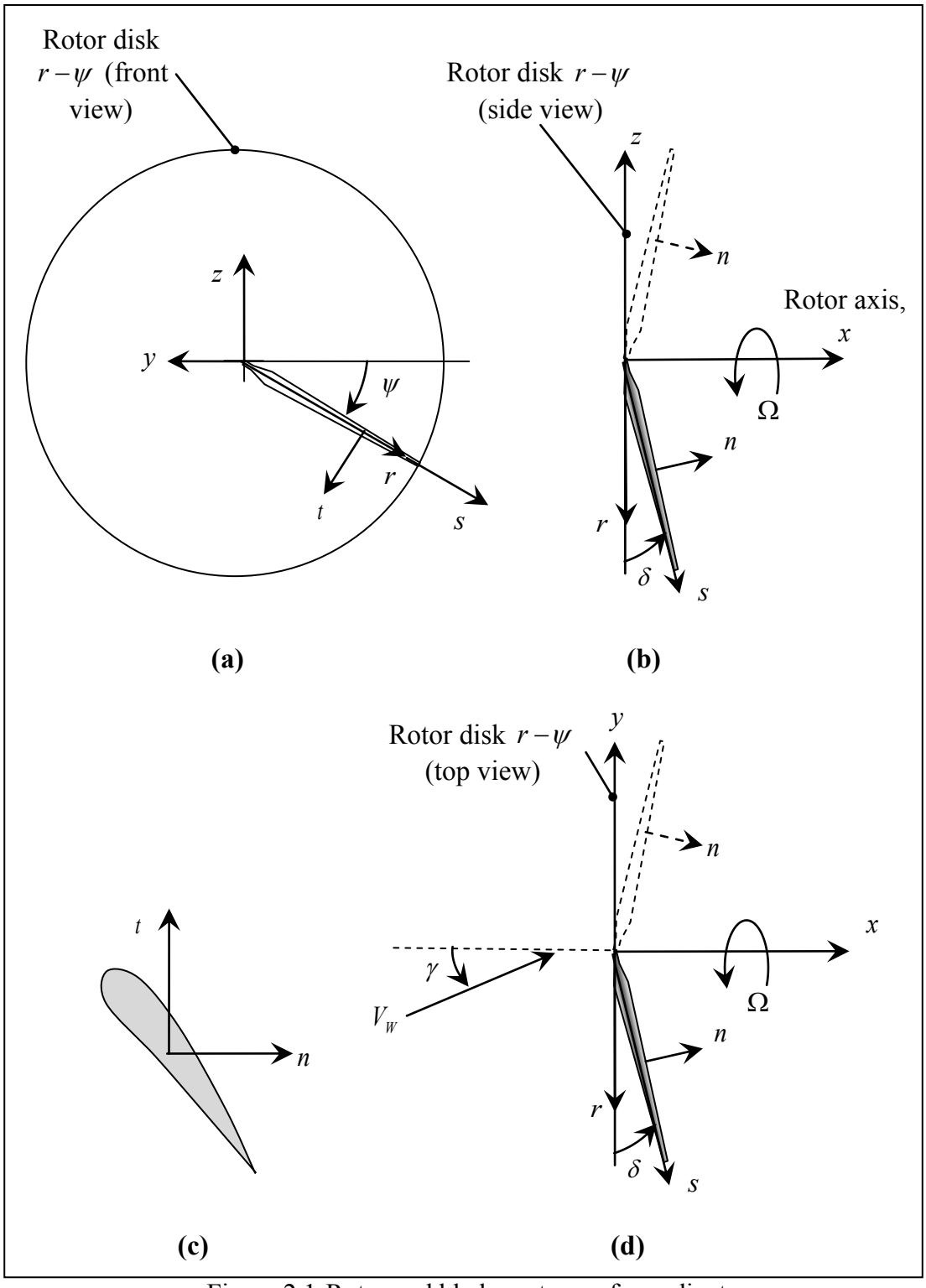

Figure 2.1-Rotor and blade systems of coordinates

Using the $n-t-s$ system of coordinates, wind velocity $\vec{V}_W$ can be expressed as:

$$V_W^t = V_W\left(\cos\gamma\sin\delta+\sin\gamma\cos\delta\right)\sin\psi \tag{2.3.a}$$

$$V_W^s = V_W\left(\cos\gamma\sin\delta-\sin\gamma\cos\delta\cos\psi\right) \tag{2.3.b}$$

$$V_W^n = V_W\left(\cos\gamma\cos\delta + \sin\gamma\sin\delta\cos\psi\right) \tag{2.3.c}$$

Equations (2.3.a) through (2.3.c) for special case of zero yaw angle can be rewritten as:

$$V_W^t = V_W \sin\delta\sin\psi \tag{2.4.a}$$

$$V_W^s = V_W \sin\delta \tag{2.4.b}$$

$$V_W^n = V_W \cos\delta \tag{2.4.c}$$

Cone angle δ is usually very small and therefore $\sin\delta << \cos\delta$, but yaw angle γ can be large enough such that $\sin\gamma$ and $\cos\gamma$ have the same order of magnitude. In case of nonzero yaw angle, neglecting terms including $\sin\delta$ in comparison with the terms including $\cos\delta$, Equations (2.3.a) through (2.3.c) can be rewritten as:

$$V_W^t = V_W \sin\gamma\cos\delta\sin\psi \tag{2.5.a}$$

$$V_W^s = -V_W \sin\gamma\cos\delta\cos\psi \tag{2.5.b}$$

$$V_W^n = V_W \cos\gamma\cos\delta \tag{2.5.c}$$

Induced velocity field, $\vec{V}_I$ has two components of V_I^x and V_I^ψ. V_I^x is directed opposite to the axial component of the wind velocity and V_I^ψ is due to induced angular velocity in the opposite direction of the rotor angular velocity. The components of induced velocity field, V_I^x and V_I^ψ can be related to the axial component of wind speed and the tangential velocity of a general point on the blade located at a radial location r through the following equations:

$$a = \left|V_I^x / V_W^x\right| \tag{2.6}$$

$$a' = \left| V_I^{\psi} / r\Omega \right| \tag{2.7}$$

where a and a' are the axial and rotational induction factors respectively. Using induction factors and knowing that the induced velocity components are in the opposite direction of the axial wind and blade rotation, one can write the induced velocity vector at a general point in $x-r-\psi$ system of coordinates in terms of axial and rotational induction factors and then transform it to $n-t-s$ system of coordinates as:

$$\vec{V}_I = -aV_W^x \hat{i} - r\Omega a' \hat{e}_{\psi} \tag{2.8}$$

$$\vec{V}_I = -aV_W \cos\gamma \cos\delta \hat{e}_n - r\Omega a' \hat{e}_t \tag{2.9}$$

The velocity of point P at radial location r on a blade rotating at an angular speed of Ω is given by:

$$\vec{V}_P = r\Omega \hat{e}_t \tag{2.10}$$

Substituting for $\vec{V}_W$ from Equation (2.5), $\vec{V}_I$ from Equation (2.9) and $\vec{V}_P$ from Equation (2.10) into Equations (2.1) and (2.2), and combining Equations (2.1) and (2.2) leads to:

$$\begin{aligned} \vec{V}_{rel} &= \{V_W \cos\gamma \cos\delta(1-a)\}\hat{e}_n \\ &+ \{V_W \sin\gamma \cos\delta \sin\psi - r\Omega(1+a')\}\hat{e}_t \\ &- \{V_W \sin\gamma \cos\delta \cos\psi\}\hat{e}_s \end{aligned} \tag{2.11}$$

Figure (2.2) shows the relative velocity in the plane of blade aerofoil. Inflow angle and normalised in-plane relative velocity can be derived from this figure as

$$\tan\varphi = \frac{\cos\gamma \cos\delta(1-a)}{\lambda_r(1+a') - \sin\gamma \cos\delta \sin\psi} \tag{2.12}$$

$$\frac{V_{rel}\,|_{n-t}}{V_W} = \frac{\cos\gamma \cos\delta(1-a)}{\sin\varphi} \tag{2.13}$$

where local velocity ratio, λ_r is defined as

$$\lambda_r = \frac{r\Omega}{V_W} \tag{2.14}$$

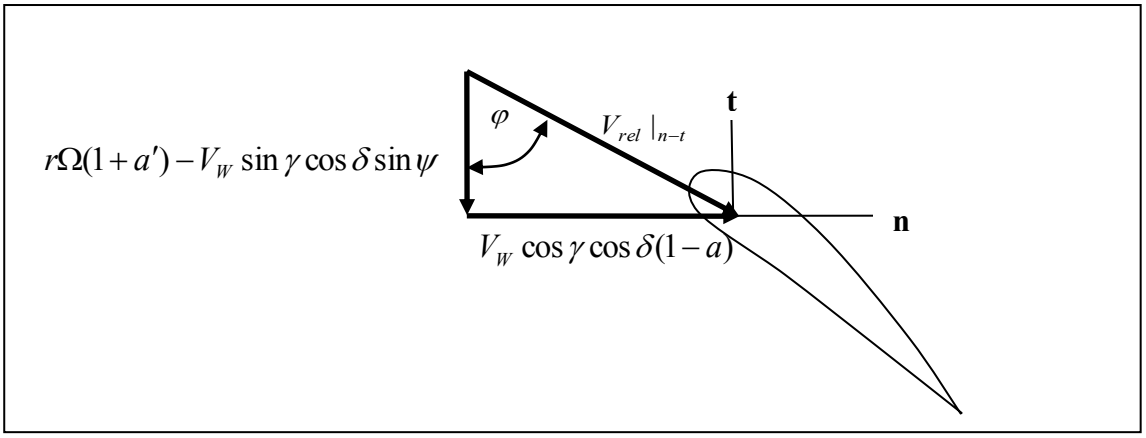

Figure 2.2-Relative velocity in aerofoil plane

In the case of zero yaw angle, $\gamma = 0$, Equations (2.11), (2.12) and (2.13) can be rewritten as:

$$\vec{V}_{rel} = V_W \cos\delta(1-a)\hat{e}_n - r\Omega(1+a')\hat{e}_t \tag{2.15}$$

$$\tan\varphi = \frac{\cos\delta(1-a)}{\lambda_r(1+a')} \tag{2.16}$$

$$\frac{V_{rel}\,|_{n-t}}{V_W} = \frac{\cos\delta(1-a)}{\sin\varphi} \tag{2.17}$$

and the velocity diagram changes to Figure (2.3).

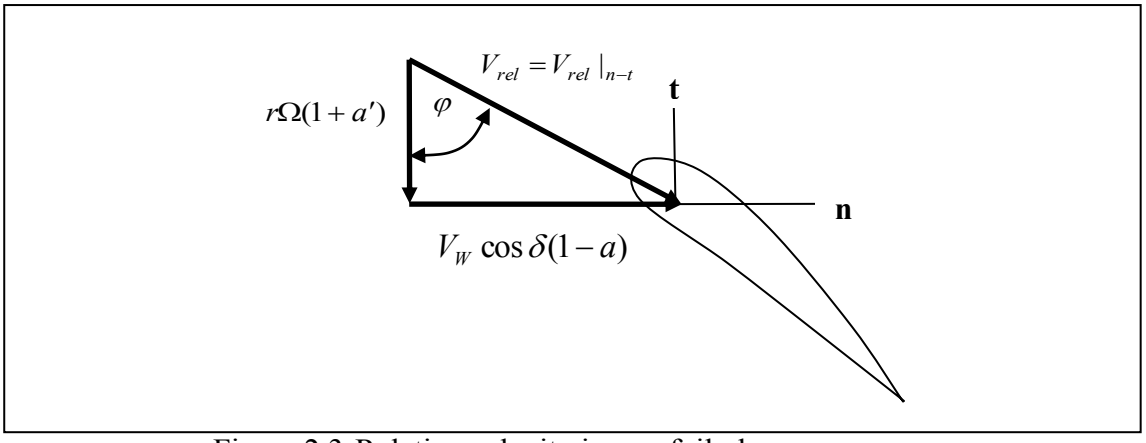

Figure 2.3-Relative velocity in aerofoil plane; zero yaw

It should be noted that the cone angle δ is very small (about 6-7 degrees). In most of published papers and text books, the effect of cone angle on the flow kinematics is completely neglected ($\cos\delta \approx 1$, $\sin\delta \approx 0$ and $\hat{e}_r \approx \hat{e}_s$).

2.2.2 Momentum Theory

Momentum theory applied to the wind turbine aerodynamic is based on three basic assumptions:

1. Axisymmetric flow
2. Steady flow
3. Frictionless flow

Figure (2.4) shows an axisymmetric flow through a wind turbine and typical qualitative variations of pressure, velocity and rotation between upstream of a wind turbine and far wake behind it.

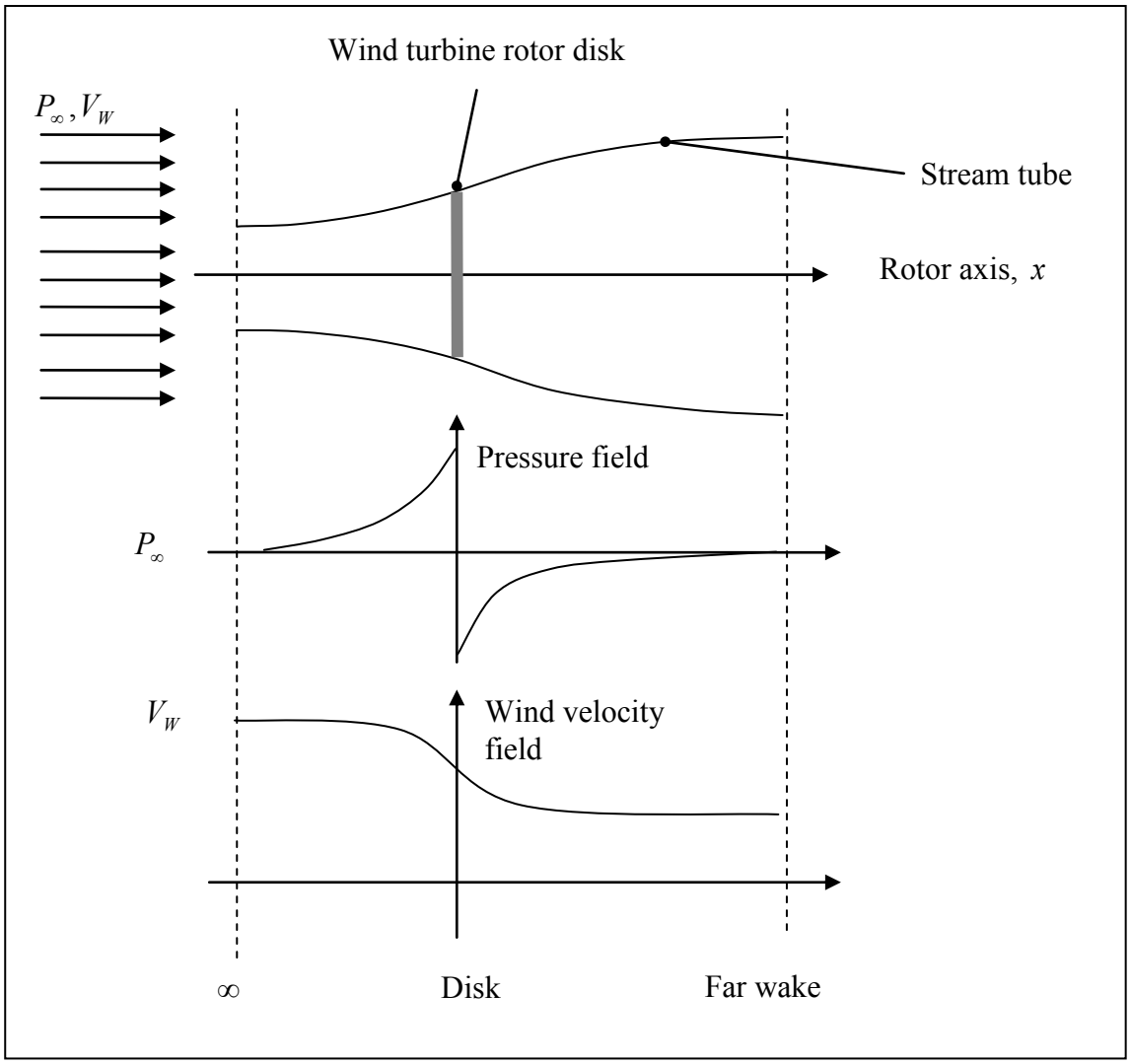

Figure 2.4-Pressure and velocity variations

Now, flow through the rotor disk can be easily found by superposing the x-components of the upstream wind and the induced velocities.

$$V_d = V_W^x - V_I^x = V_W(1-a) \tag{2.18}$$

As wind approaches a wind turbine it slows down. This retardation is a direct result of the presence of the wind turbine acting as a partial barrier in the flow field. Moreover, rotation of blades imposes a rotation in the velocity field. Further reduction in wind speed behind the rotor disk is partly due to extracting energy from wind and partly due to energy losses due to rotation caused by rotating blades. Since in upstream no energy is extracted from the wind yet, a reduction in air velocity causes an increase in pressure. This is equivalent to conversion of energy from kinetic to potential form.

2.2.2.1 Thrust and Torque Coefficients in Terms of Induction Factors

Applying the x-component of linear momentum equation to the annulus control volume shown in Figure (2.5), gives thrust force as $dT_{rotor} = \rho dQ(V_\infty - V_{FW})$,where the volume flow rate $dQ = V_d dA_{disk}$, $V_\infty = V_W$ and $V_d = V_W(1-a)$ and therefore

$$dT_{rotor} = \rho V_W(1-a)(V_W - V_{FW})dA_{disk} \tag{2.19}$$

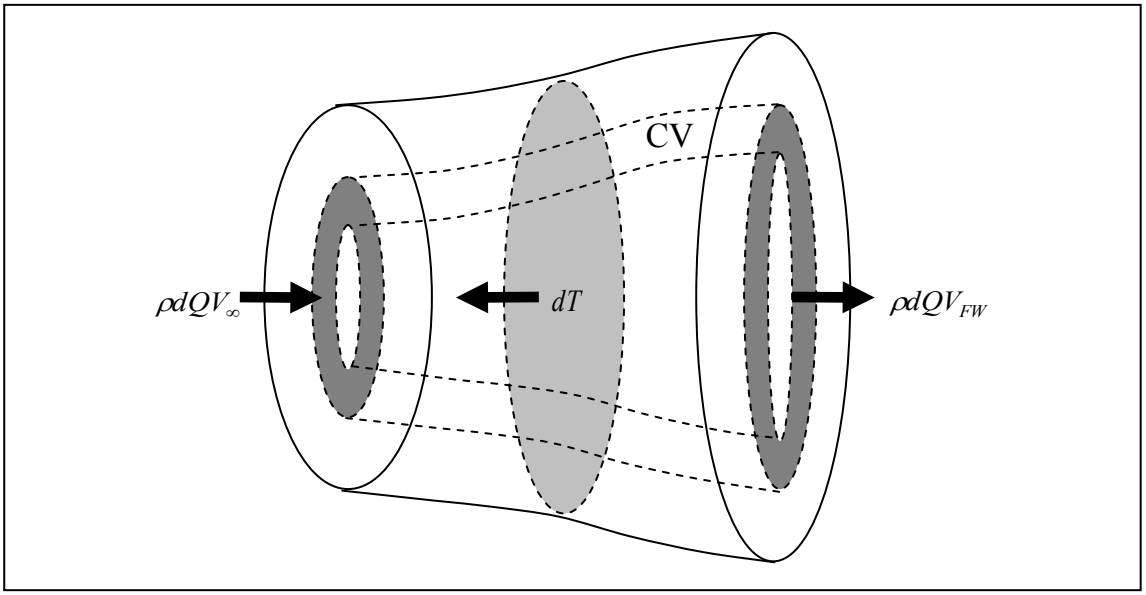

Figure 2.5-Annulus control volume; Linear momentum balance

Applying the energy equation for the same control volume gives the turbine power.

$$dP = 0.5\rho V_d dA_{disk}(V_W^2 - V_{FW}^2) \tag{2.20}$$

Turbine power can also be obtained by multiplying the thrust force and flow velocity at the disk.

$$dP = dTV_d \tag{2.21}$$

Combining Equations (2.19), (2.20) and (2.21) concludes

$$V_{FW} = (1-2a)V_W \tag{2.22}$$

By substituting V_{FW} back into Equation (2.19), dT_{rotor} is determined in terms of the wind velocity at the upstream and the axial induction factor.

$$dT_{rotor} = 2a(1-a)\rho V_W^2 dA_{disk} \tag{2.23}$$

Thrust coefficient by definition is

$$C_T = \frac{dT}{1/2\rho V_W^2 dA_{disk}}\ , \tag{2.24}$$

therefore as a result of Momentum Theory it becomes:

$$C_T = 4a(1-a) \tag{2.25}$$

To determine torque coefficient by the Momentum Theory one can start from applying the angular momentum equation about the x-axis for the control volume shown in Figure (2.6) to find a relation between the rotation in far wake and circumferential velocity at disk as $\left(r^2\omega\right)_{FW} = \left(r^2\omega\right)_{disk} = \left(2rr\omega/2\right)_{disk} = 2rV_{disk}^{\psi}$. Since the circumferential velocity V_{disk}^{ψ} is only due to induction, one can substitute $V^{\psi} = V_I^{\psi}$ from Equation (2.7) in the above equation to find $\left(r^2\omega\right)_{FW}$.

$$\left(r^2\omega\right)_{FW} = 2r^2 a'\Omega \tag{2.26}$$

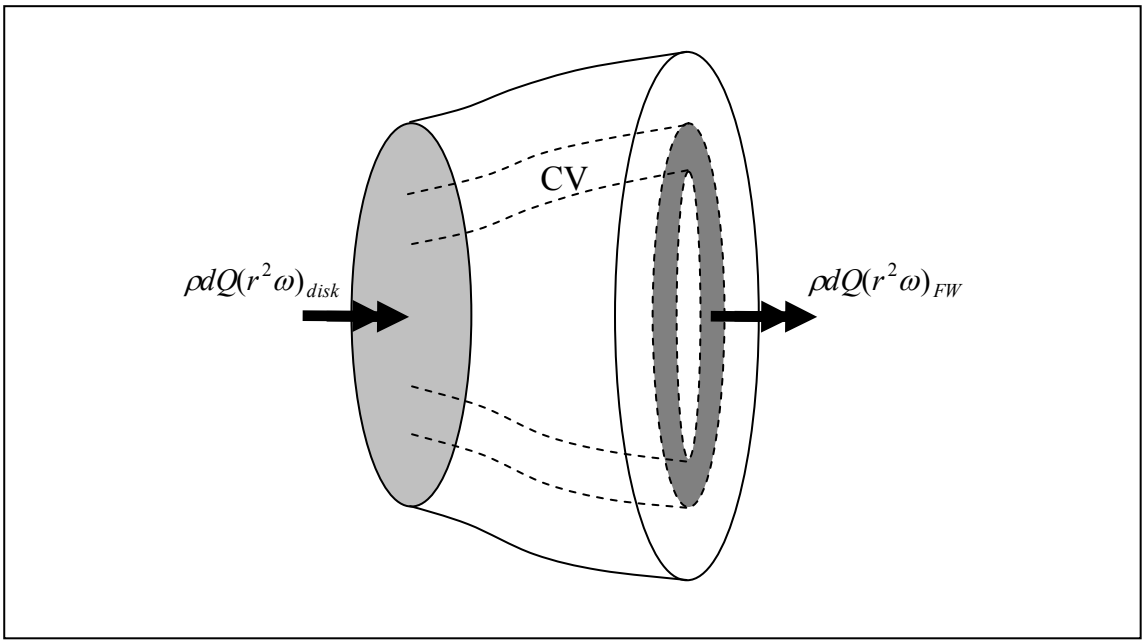

Figure 2.6-Annulus control volume; Angular momentum balance between disk and Far Wake

Applying angular momentum equation about x–axis for the control volume shown in Figure (2.7), the applied torque on the rotor will be determined.

$$dM_x = \rho dQ\left\{\left(r^2\omega\right)_{FW} - \left(r^2\omega\right)_{\infty}\right\} \tag{2.27}$$

Combining Equations (2.26) and (2.27) gives the rotor torque as

$$dM_x = 2\rho\Omega V_w(1-a)a'r^2 dA_{disk} \tag{2.28}$$

Torque coefficient is defined as

$$C_M = \frac{dM_x}{1/2\,\rho V_W^2 r dA_{disk}}, \tag{2.29}$$

and finally, as a result of the Momentum Theory it becomes

$$C_M = 4\lambda_r a'(1-a) \tag{2.30}$$

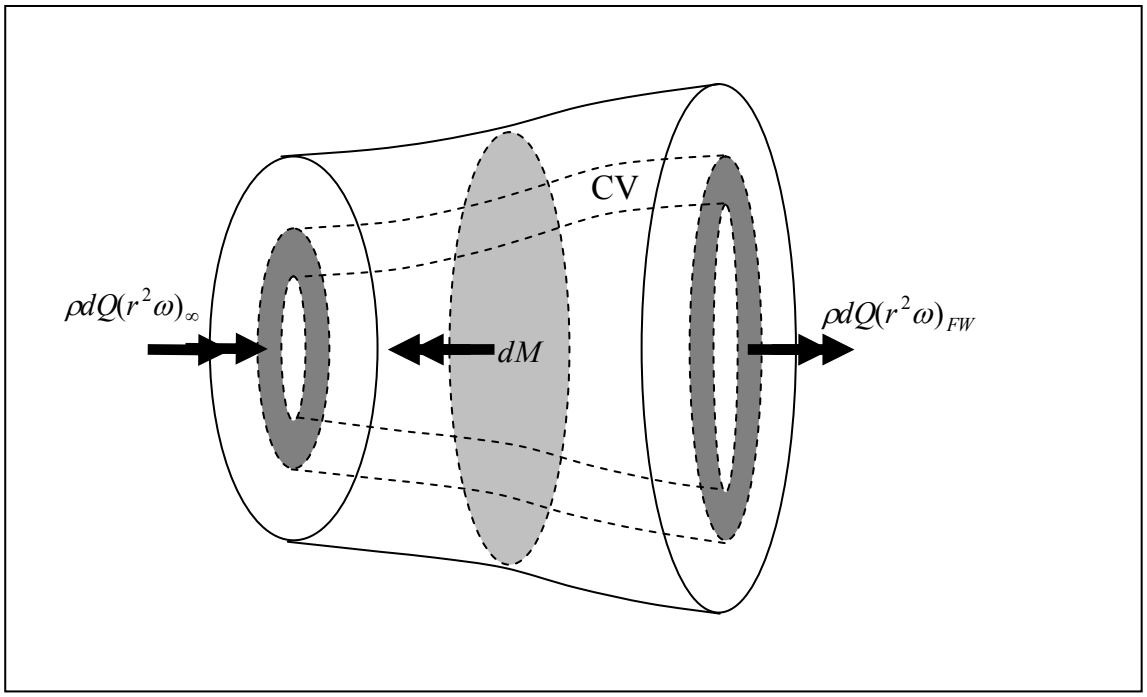

Figure 2.7-Annulus control volume; Angular momentum balance

2.2.2.2 Effect of Tip and Hub Losses on Thrust and Torque Coefficients

In momentum theory, the axisymmetric flow is the basic assumption, which holds if the turbine rotor has an infinite number of blades with zero chord length. In the case of a real turbine with a finite number of blades, the induced velocity on the blades is different from the mean induced velocity in the flow annulus and therefore circumferential symmetry does not hold. The non-uniformity of the induced flow field makes the actual local C_T and C_M to be smaller than the expected values by the optimum actuator disk theory. The departure of the induced velocity, C_T and C_M from their momentum theory values is more significant near the tip and root of the blade. These deviations from the uniform induced velocity flow field are called tip and hub losses. The overall loss factor, F is defined as

$$F = F_{tip} F_{hub} \tag{2.31}$$

in which F_{tip} is unity at inboard parts of the blade and takes smaller values near the tip of the blade and F_{hub} is unity at outboard parts of the blade and takes smaller values near the hub of the blade.

Most of industrial approved and commercial software such as WTPerf (Buhl, 2004) and AeroDyn (Moriarty, 2005) use Wilson-Walker model, in which loss factor F is directly

applied to the disk velocity, $V_d = FV_W(1-a)$ and the difference between the free stream velocity and far wake velocity is defined as $V_W - V_{FW} = 2aV_W$. With the above assumptions thrust and torque coefficients can be calculated as:

$$C_T = 4Fa(1-a) \tag{2.32}$$

$$C_M = 4\lambda_r a' F(1-a) \tag{2.33}$$

For this model the relative velocity diagram becomes as shown in Figure (2.8) and the normalised relative velocity becomes as given by Equation (2.34).

$$\frac{V_{rel}|_{n-t}}{V_W} = \frac{(1-a)F\cos\delta}{\sin\varphi} \tag{2.34}$$

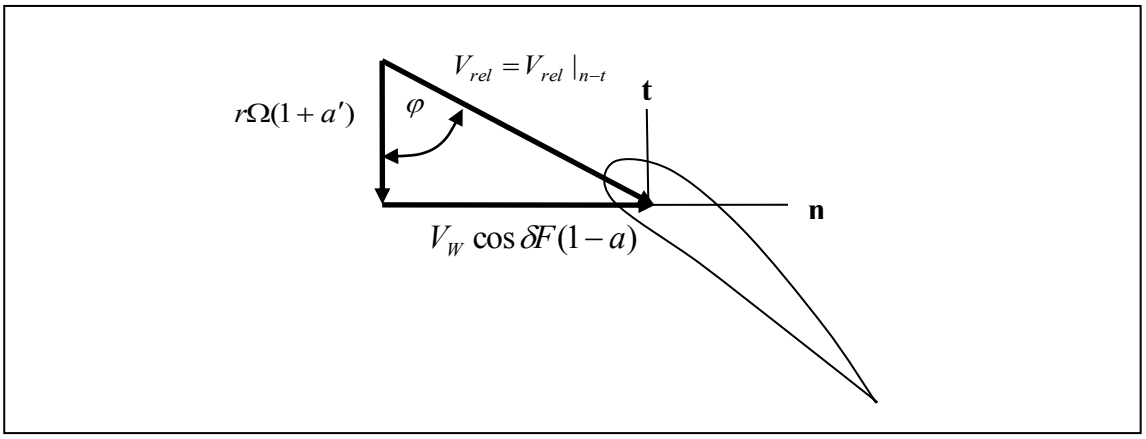

Figure 2.8-Relative velocity in aerofoil plane; zero yaw; Wilson-Walker model

Momentum theory predicts a parabolic variation for thrust coefficient with a maximum value of 1 at $a = 0.5$, while the experimental data show that C_T keeps increasing for $a > 0.5$. For small axial induction factors, $0 < a < a_c \cong 0.4$, known as light loading state, predicted thrust coefficient by the momentum theory is in a good agreement with the experimental data. In the case of heavy loading state, where $a > a_c$, predicted C_T departs dramatically from its actual value. In the extreme loading situation, $a = 1$, wind turbine acts as a drag driven device with a thrust coefficient of $C_T = (C_{T,Drag})_{\max} = 2$ rather than $C_T = 0$ as predicted by Equation (2.25). Extrapolating Equation (2.25), with a maximum value of $C_T = 2$ at $a = 1$, predicts reasonable values for C_T. Separating light and heavy loading state, Equation (2.32) can be re-written as

$$C_T = 4Fa(1-a) \qquad \text{if } a \le a_c \tag{2.35.a}$$

$$C_T = B_0 a^2 + B_1 a + B_2 \qquad \text{if } a > a_c \tag{2.35.b}$$

where

$$B_0 = \frac{2}{(1-a_c)^2} - 4F \tag{2.35.c}$$

$$B_1 = \frac{-4a_c}{(1-a_c)^2} + 4F \tag{2.35.d}$$

$$B_2 = 2 + \frac{4a_c - 2}{(1-a_c)^2} \tag{2.35.e}$$

2.2.2.3 Prandtl Tip and Hub Loss Factors

Among some theories for estimating the tip and hub loss factors, Prandtl theory is simple and efficient and also gives acceptable results (Moriarty, 2005). In Prandtl theory tip and hub loss factors are defined as

$$F_{tip} = \frac{2}{\pi}\cos^{-1}\left\{\exp(-f_{tip})\right\} \qquad \text{if } \left|f_{tip}\right| \le 7 \tag{2.36.a}$$

$$F_{tip} = 1 \qquad \text{if } \left|f_{tip}\right| > 7 \tag{2.36.b}$$

where

$$f_{tip} = \frac{B(R-r)}{2r\sin\varphi} \tag{2.36.c}$$

and

$$F_{hub} = \frac{2}{\pi}\cos^{-1}\left\{\exp(-f_{hub})\right\} \qquad \text{if } \left|f_{hub}\right| \le 7 \tag{2.37.a}$$

$$F_{hub} = 1 \qquad \text{if } |f_{hub}| > 7 \tag{2.37.b}$$

where

$$f_{hub} = \frac{B(r - R_{hub})}{2R_{hub}\sin\varphi} \tag{2.37.c}$$

In the above equations, B is the number of blades, R and R_{hub} are the rotor and hub radius and φ is the inflow angle which can be obtained from Equation (2.12) or Equation (2.16).

2.2.3 Blade Element Analysis

Blade element (strip) theory is based on the main assumption: there is no span-wise pressure gradient and therefore each segment can be analysed independently as a two-dimensional aerofoil. In practice, a three dimensional blade is divided into a number of segments and each segment is analysed as a two dimensional aerofoil. Flow kinematics around each segment (Figure (2.9)) is given by Figure (2.8).

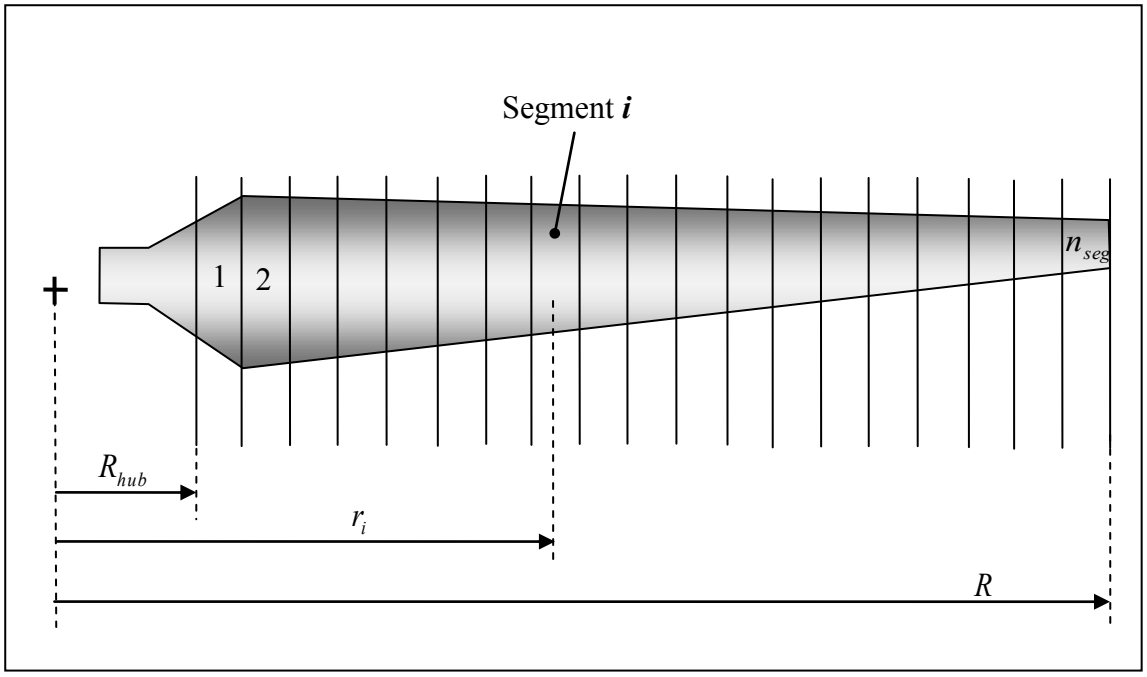

Figure 2.9-Discretisation of blade into n_{seg} segments

2.2.3.1 Thrust and Torque Coefficients via Blade Element Force Analysis

Figure (2.10) shows a blade segment (element) subjected to the aerodynamic forces in the same system of coordinates as introduced in Figure (2.1). Assuming 2-dimentional flow on the aerofoil and neglecting radial forces on the blade ($dF_s = 0$), thrust force on the element can be obtained as $dT = dF_n$ or

$$dT = dL\cos\varphi + dD\sin\varphi \tag{2.38}$$

Lift and drag coefficients are defined as

$$C_L = \frac{dL}{\left(\frac{1}{2}\rho V_{rel}^2\right)_{n-t} dA_e} \tag{2.39}$$

$$C_D = \frac{dD}{\left(\frac{1}{2}\rho V_{rel}^2\right)_{n-t} dA_e} \tag{2.40}$$

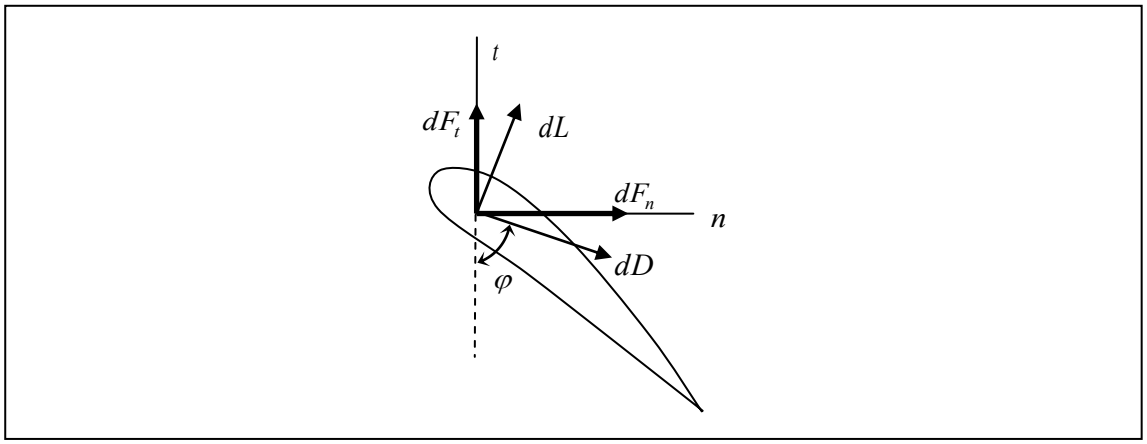

Figure 2.10-Blade element force analysis on a typical segment

where $\left(V_{rel}\right)_{n-t}$ is the relative velocity in the $n-t$ plane (see Figures (2.2) and (2.3)) and $dA_e = cdr$ is the element area. Combining Equations (2.38), (2.39) and (2.40) gives thrust force on a blade element as

$$dT = \frac{1}{2}\rho c\left(V_{rel}^2\right)_{n-t}\left(C_L\cos\varphi + C_D\sin\varphi\right)dr \tag{2.41}$$

and for a turbine with B blades it becomes

$$dT = \tfrac{1}{2}\rho Bc\left(V_{rel}^2\right)_{n-t}\left(C_L\cos\varphi + C_D\sin\varphi\right)dr \tag{2.42}$$

Using Equations (2.24) and (2.17), thrust coefficient can be written as

$$C_T = \frac{\sigma_r\cos^2\delta(1-a)^2\left(C_L\cos\varphi + C_D\sin\varphi\right)}{\sin^2\varphi} \tag{2.43}$$

where σ_r, local solidity ratio, is defined as

$$\sigma_r = \frac{Bc}{2\pi r} \tag{2.44}$$

Aerodynamic forces on the blade element also produce a torque about the rotor axis equal to $dM_x = rdF_t$ (Figure (2.10)). Recalling Equations (2.39) and (2.40), for a turbine with B blades the generated torque about the rotor axis can be expressed as

$$dM_x = \tfrac{1}{2}\rho Bc\left(V_{rel}^2\right)_{n-t}\left(C_L\sin\varphi - C_D\cos\varphi\right)rdr \tag{2.45}$$

Inserting the above result into the definition of the torque coefficient C_M, Equation (2.29), yields to

$$C_M = \frac{\sigma_r\cos^2\delta(1-a)^2\left(C_L\sin\varphi - C_D\cos\varphi\right)}{\sin^2\varphi} \tag{2.46}$$

2.2.4 Blade Element Momentum Theory, BEMT

Equating thrust and torque coefficients obtained from the blade element force analysis (with the assumption of zero drag force) and those obtained from momentum theory is the base of the BEMT. Neglecting drag force in Equations (2.43) and (2.46), thrust and torque coefficients will become

$$C_{T_0} = \frac{\sigma_r\cos^2\delta(1-a)^2 C_L\cos\varphi}{\sin^2\varphi} \tag{2.47}$$

$$C_{M_0} = \frac{\sigma_r \cos^2 \delta (1-a)^2 C_L \sin\varphi}{\sin^2 \varphi} \tag{2.48}$$

Combining Equations (2.47) and (2.48) with Equations (2.35) and (2.33) gives:

$$a = \frac{1-\sqrt{1-\frac{C_{T_0}}{F}}}{2} \qquad \text{if } a \le 0.4 \equiv C_{T_0} \le 0.96F \tag{2.49.a}$$

$$a = \frac{-B_1 + \sqrt{B_1^2 - 4B_0(B_2 - C_{T_0})}}{2B_0} \qquad \text{if } a > 0.4 \equiv C_{T_0} > 0.96F \tag{2.49.b}$$

$$a' = \frac{a\tan\varphi}{\lambda_r \cos\delta} \tag{2.50}$$

Equations (2.16)/(2.12), (2.31), (2.47), (2.49), (2.50) and two set of tabulated data for C_L and C_D can be solved to find a, a', F, φ, C_L, C_D and C_{T_0}. Knowing a, φ, C_L and C_D one can use Equations (2.49) and (2.50) to calculate T and C_T and Equations (2.45) and (2.46) to find M and C_M. Having rotor torque M, turbine mechanical power, P can be easily calculated by

$$P = \int \Omega dM = \Omega M \tag{2.51}$$

and the power coefficient C_P can be determined from the following equation.

$$C_P = \frac{P}{\frac{1}{2}\rho V_W^3 A_{rotor}} = \frac{P}{\frac{1}{2}\rho V_W^3 \pi R^2} \tag{2.52}$$

2.3 BEMT Corrections

BEMT is based on three main assumptions: steady flow, infinite number of blades and axisymmetric flow. These assumptions make BEMT bounded within many limitations. In practice most of these limitations can be removed by (i) applying some corrections,

(ii) averaging, and (iii) employing further assumptions to the original concepts. For example, the ground shear and yaw error contradict the basic assumption of axisymmetric flow. Dividing rotor disk area into a number of sectors and averaging the results is a means to include the effect of ground shear. By employing tip and hub loss correction factors, the effect of finite number of blades can be incorporated in the original BEMT. In case of an unsteady flow, assuming that equilibrium in the wake is maintained at each time step (Snel, 1995), BEMT can be used for determination of the dynamic flow conditions at the rotor disc at each time step.

The accuracy of predicted aerodynamic loads on blades using BEMT strongly depends on the accuracy of the lift and drag coefficients used as well as the validity of its fundamental assumptions. Assuming that the fundamental assumptions are valid, or alternatively violation of the validity of assumptions has been compensated by applying corrections, using the wind tunnel experimental data for lift and drag coefficients makes BEMT somewhat more accurate when compared to CFD methods. Models based on BEMT are sensitive to the aerodynamic characteristics of the aerofoils used in the blade (Tangler, 2002, 2004). Therefore, having a reliable model for predicting the post stall aerodynamic coefficients and considering the effect of stall delay due to blade rotation (Du, 1998) are also necessary for acceptable results. Sanderse (2011) and Snel (1998, 2003) give a comprehensive review of the BEMT and the corrections applicable to remove some of its limitations.

2.3.1 Angle of Attack Corrections

Lift and drag coefficients are functions of the angle of attack and Reynolds number. Angle of attack is in turn a function of the velocity field and the blade geometry and can be expressed as

$$\alpha = \varphi - \beta_0 - pitch + \Delta\alpha_c \tag{2.53}$$

In the above equation φ is the inflow angle, (Equation (2.16)) and β_0 stand for pretwist, $pitch$ is the blade pitch angle and $\Delta\alpha_c$ refers to cascade correction. The cascade correction to the angle of attack has two components

$$\Delta\alpha_c = \Delta\alpha_1 + \Delta\alpha_2 \tag{2.54}$$

where $\Delta\alpha_1$ accounts for the effect of finite aerofoil thickness and $\Delta\alpha_2$ accounts for the effect of finite aerofoil width (Spera 1994).

$$\Delta\alpha_1 = \frac{B\cos\varphi_0 A_a}{2\pi rc} \tag{2.55}$$

$$\Delta\alpha_2 = \frac{1}{4}\left\{\tan^{-1}\frac{(1-a)r}{(1+2a')R} - \tan^{-1}\frac{(1-a)r}{R}\right\} \tag{2.56}$$

φ_0 is the inflow angle prior to rotational induction, ($a'=0$ in Figure (2.3)) and A_a is the aerofoil cross section area, normally taken as $A_a \approx 0.68ct_{\max}$, where $t_{\max}$ is the maximum thickness of the aerofoil.

2.3.2 Effect of Ground Shear

The wind speed profile trends to a lower speed as the altitude move closer to the ground level and this is designated as wind shear. As can be seen from Figure (2.11) the wind speed at certain height (datum of azimuth angle) above ground can be predicated as a function of height above ground z and the roughness length z_0. The wind speed caused by effect wind shear is given by

$$V = V_{hub}\ln\left(\frac{z}{z_0}\right)/\ln\left(\frac{h_{hub}}{z_0}\right) \tag{2.57}$$

in which

$$z = h_{hub} - r\sin\psi \tag{2.58}$$

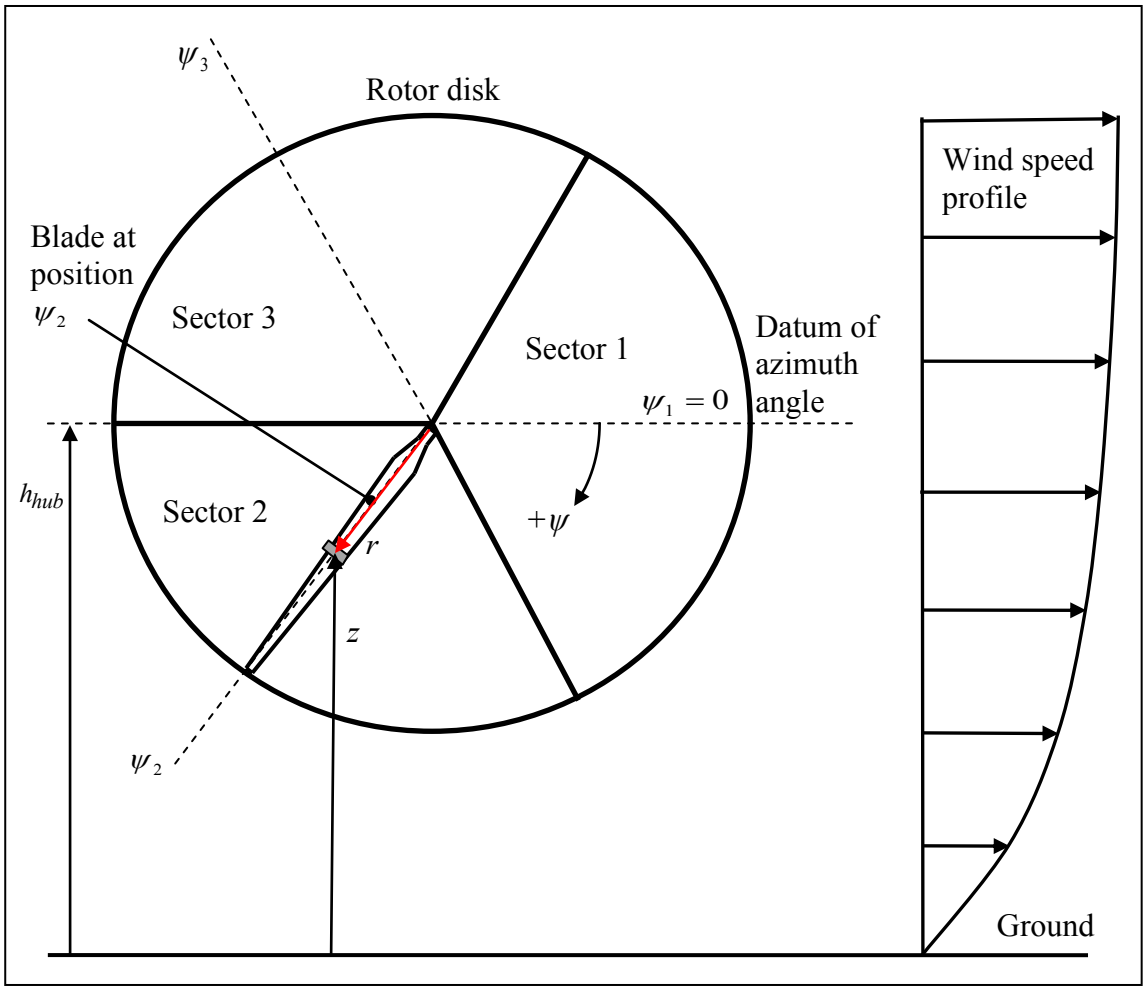

Figure 2.11-Discretising rotor disk into n_{sec} sectors (here, $n_{sec} = 3$) and the azimuth angle associated to each sector

2.4 The software, AWTSim-Advanced Wind Turbine Simulation

Based on the theory explained in Sections 2.2 and 2.3 a software tool has been developed for the analysis of horizontal axis wind turbines. This software includes two primary modules for blade discretisation and BEMT calculations, and some secondary modules for calculating the annual average power and blade external/internal loading. It also includes modules required for analysis of wind turbines utilising unconventional blades which are explained in details in Chapter 3.

In order to analyse the aerodynamic performance of constant speed stall regulated wind turbine, AWTSim requires five sets of inputs:

1. Blade geometry and topology data. These data include span-wise distribution of chord $c(r)$, pretwist $\beta_0(r)$, aerofoil $AF(r)$ and aerofoil maximum thickness $t_{max}(r)$

as well as rotor radius R (or diameter D), hub radius R_{hub} and blade pitch angle $pitch$.

2. Blade aerodynamic data. For each aerofoil used in the blade tabulated $\alpha - C_L$ and $\alpha - C_D$ data are required.
3. Rotor characteristics: rotor speed Ω, cone angle δ, number of blades B and hub height h_{hub}.
4. Wind turbine operating data: Wind speed at hub height V_W and yaw angle γ.
5. Site data: Site average wind speed V_{av} and probability distribution function, and ground surface roughness length z_0.

2.4.1 Blade Discretisation

Algorithm (2.1) describes steps for discretisation of a wind turbine blade as required for BEMT. This algorithm requires blade topology data file as well as the number of segments and sectors. Tables (2.1) and (2.2) show a typical set of the input data defining the topology of a blade. Table (2.3) shows the results of discretisation based on Algorithm (2.1). In this algorithm the normalised chord, radial coordinate and aerofoil maximum thickness are defined as $c^* = c/R$, $r^* = r/R$ and $t^*_{\max} = t_{\max}/c$, respectively.

Algorithm 2.1-Blade discretisation

Given:

- n_{seg} and $n_{\sec}$
- Blade data file $\{ R , R^*_{hub}, c^*(r^*) , \beta_0(r^*) , AF(r^*)$ and $t^*_{\max}(r^*) \}$

Step 1- Calculate length of each blade segment $\Delta r^* = \left(1 - R^*_{hub}\right) \Big/ n_{seg}$

Step 2- Find the centre of each blade segment:

2.1. $r^*_1 = R^*_{hub} + 0.5\Delta r^*$

2.2. For $i = 2 : n_{seg}$, do: $r^*_i = r^*_{i-1} + \Delta r^*$

Step 3- Find blade chord and pretwist at the centre of each segment:

3.1. For $i = 1 : n_{seg}$, do: calculate $c^*(r^*_i)$ and $\beta_0(r^*_i)$ by linear interpolation within the blade data file.

Step 4- Find blade aerofoil index and aerofoil thickness over each segment:

Step 5- Calculate the arc length of each rotor disk sector $\Delta\psi = 360 / n_{\sec}$

Step 6- Find blade position (azimuth angle) for each rotor disk sector:

6.1. $\psi_1 = 0$ (horizontal-3 O'clock)

6.2. For $j = 2 : n_{\sec}$, do: $\psi_j = \psi_{j-1} + \Delta\psi$

Table 2.1-Blade data file-Part 1

r^*	$c^*(r^*)$	$\beta_0(r^*)$
0.086	0.053	6.270
0.109	0.056	6.100
0.155	0.063	5.764
0.223	0.070	5.470
0.269	0.075	5.233
0.315	0.081	4.996
0.360	0.082	4.602
0.406	0.083	4.208
0.452	0.081	3.689
0.497	0.079	3.172
0.543	0.076	2.628
0.589	0.074	2.086
0.634	0.071	1.601
0.680	0.068	1.117
0.726	0.064	0.770
0.772	0.060	0.424
0.806	0.056	0.273
0.840	0.052	0.122
0.863	0.049	0.099
0.886	0.047	0.076
0.918	0.042	0.048
0.936	0.039	0.041
0.954	0.036	0.033
0.963	0.035	0.028
0.973	0.033	0.023
0.986	0.030	0.012
0.995	0.029	0.006
1.000	0.028	0.000

Table 2.2-Blade data file-Part 2

AF index	$t^*_{\max}$	Starts @ r^*	Ends @ r^*
1	0.24	0.086	0.269
2	0.24	0.269	0.360
3	0.24	0.360	0.452
4	0.24	0.452	0.543
5	0.21	0.543	0.634
6	0.21	0.634	0.726
7	0.21	0.726	0.806
8	0.21	0.806	0.863
9	0.21	0.863	0.963
10	0.21	0.963	1.000

Table 2.3-Discretised blade with $n_{seg} = 20$

segment #	r^*	$c^*(r^*)$	$\beta_0(r^*)$	AF index	$t^*_{\max}$
1	0.109	0.056	6.100	1	0.24
2	0.155	0.063	5.764	1	0.24
3	0.200	0.068	5.568	1	0.24
4	0.246	0.073	5.351	1	0.24
5	0.292	0.078	5.114	2	0.24
6	0.337	0.081	4.799	2	0.24
7	0.383	0.083	4.405	3	0.24
8	0.429	0.082	3.949	3	0.24
9	0.475	0.080	3.431	4	0.24
10	0.520	0.078	2.900	4	0.24
11	0.566	0.075	2.357	5	0.21
12	0.612	0.072	1.843	5	0.21
13	0.657	0.069	1.359	6	0.21
14	0.703	0.066	0.944	6	0.21
15	0.749	0.062	0.597	7	0.21
16	0.794	0.057	0.323	7	0.21
17	0.840	0.052	0.122	8	0.21
18	0.886	0.047	0.076	9	0.21
19	0.931	0.040	0.043	9	0.21
20	0.977	0.032	0.019	10	0.21

2.4.2 BEMT Calculator

Algorithm (2.2) shows the steps of calculating the extracted mechanical power by a stall-regulated wind turbine based on the BEMT method explained in Sections 2.2 and 2.3. This algorithm, requires a discretised blade (as shown in Table (2.3)), rotor characteristics and lift and drag tables corresponding to the aerofoils used in the blade.

Algorithm 2.2-BEMT calculator

Given:

- $\{\varepsilon_a, \varepsilon_{a'}\}, \{D, b, \rho, h_{hub}, z_0, \delta, \gamma\}, \{V_{hub}, \Omega, pitch\}$
- $\{n_{seg}, n_{\sec}\}, \{r_i^*, c_i^*, \beta_{0,i}, AF_i, t_{\max,i}^*; i = 1 : n_{seg}\}$ and $\{\psi_j; j = 1 : n_{\sec}\}$ (discretised blade)
- $C_L - \alpha$ and $C_D - \alpha$ tabulated data for all aerofoils used in the blade

Step 1- Initialise $C_{L,i}, C_{D,i}, \varphi_i, \alpha_i, V_{rel,i} \leftarrow 0$; $i = 1 : n_{seg}$.

Step 2- Dimensionalise $\Delta r = R\Delta r^*$ and $r_i = Rr_i^*$, $c_i = Rc_i^*, t_{\max,i} = c_i t_{\max,i}^*$; $i = 1 : n_{seg}$ ($R = 0.5D$).

Step 3- For each azimuth angle ψ_j ; $j = 1 : n_{\sec}$,do:

3.1. Find wind shear field:

3.1.1. $z_i = h_{hub} - r_i \sin\psi_j ; i = 1 : n_{seg}$

3.1.2. $S_{i,j} = \ln(z_i / z_0) / \ln(h_{hub} / z_0); i = 1 : n_{seg}$

3.2. Find wind speed at the centre of each blade segment: $V_{i,j} = V_{hub} S_{i,j}$

Step 4- For $j = 1 : n_{\sec}$, do:

4.1. For $i = 1 : n_{seg}$, do:

4.1.1. Calculate local speed ratio $\lambda_{r_i} = r_i \Omega / V_{i,j}$ and local solidity ratio $\sigma_{r_i} = Bc_i / 2\pi r_i$

4.1.2. Initialise $a \leftarrow 1/3$; $a' \leftarrow 0$; $converged \leftarrow false$

4.1.3. While ($converged = false$) do:

4.1.3.1. Calculate inflow angle

$$\varphi_i = \tan^{-1}\left(\frac{V_{i,j}\cos\delta\cos\gamma(1-a)}{r_i\Omega(1+a') - V_{i,j}\sin\gamma\sin\psi_j\cos\delta}\right)$$

4.1.3.2. Calculate tip and hub losses $F = F_{tip}F_{hub}$.

If $f_{tip} = \left|B(R-r)/2r\sin\varphi\right| \le 7 : F_{tip} = \frac{2}{\pi}\cos^{-1}\{\exp(-f_{tip})\}$; otherwise: $F_{tip} = 1$.

If $f_{hub} = \left|B(r-R_{hub})/2R_{hub}\sin\varphi\right| \le 7 : F_{hub} = \frac{2}{\pi}\cos^{-1}\{\exp(-f_{hub})\}$;otherwise: $F_{hub} = 1$.

4.1.3.3. Calculate inflow angle at zero drag: $\varphi_0 = \tan^{-1}\left(\frac{\cos\delta F(1-a)}{\lambda_{r,i}}\right)$

4.1.3.4. Calculate angle of attack $\alpha_i = \varphi_i - \beta_{0,i} - pitch + \Delta\alpha_c$;

$$\Delta\alpha_c = \frac{B\cos\varphi_0 A_a}{2\pi r_i c_i} + \frac{1}{4}\left\{\tan^{-1}\frac{(1-a)r_i}{(1+2a')R} - \tan^{-1}\frac{(1-a)r_i}{R}\right\};$$

$$A_a = 0.68 c_i t_{\max,i}$$

4.1.3.5. Use α_i read off life and drag coefficients from tables: $C_{L,i}$ and $C_{D,i}$

Algorithm2.2-BEMT calculator-Continue

4.1.3.6. Calculate thrust coefficient at zero lift:

$$C_{T_0} = \frac{\sigma_{r,i}\cos^2\delta(1-a)^2 C_{L,i}\cos\varphi_i}{\sin^2\varphi_i}$$

4.1.3.7. Calculate a_{new}. If $C_{T_0} > 0.96F$:

$a_{new} = \left(-B_1 + \sqrt{B_1^2 - 4B_0(B_2 - C_{T_0})}\right)\Big/2B_0$, otherwise

$a_{new} = \left(1 - \sqrt{1 - C_{T_0}/F}\right)\Big/2$; $(B_0 = 2/(1-a_c)^2 - 4F$;

$B_1 = -4a_c/(1-a_c)^2 + 4F$; $B_2 = 2 + (4a_c - 2)/(1-a_c)^2$; $a_c = 0.4$).

4.1.3.8. Calculate $a'_{new} = a_{new}\tan\varphi_i/\lambda_{r,i}\cos\delta$

4.1.3.9. If $\left(|a - a_{new}| \le \varepsilon_a \wedge |a' - a'_{new}| \le \varepsilon_{a'}\right)$: $converged \leftarrow true$; Else:

$a \leftarrow a_{new}$, $a' \leftarrow a'_{new}$.

4.1.4. Calculate

$$V_{rel,i} = \sqrt{\left(V_{i,j}\cos\gamma\cos\delta(1-a)\right)^2 + \left(V_{i,j}\sin\gamma\cos\delta\sin\psi_j - r_i\Omega(1+a')\right)^2}$$

4.1.5. Calculate $\Delta M_i = \frac{1}{2}\rho V_{rel,i}^2 B c_i \left(C_{L,i}\sin\varphi_i - C_{D,i}\cos\varphi_i\right) r_i \Delta r\cos\delta$

4.2. Calculate $P_j = \Omega\sum_{i=1}^{n_{seg}}\Delta M_i$

Step 5- Calculate $P = \frac{1}{n_{\text{sec}}}\sum_{j=1}^{n_{\text{sec}}} P_j$

2.5 Validation

AWTSim has been validated against the latest version of WTPerf (Buhl, 2005) using the test wind turbine AWT-27. WTPerf is an accredited code developed and in use in the National Renewable Energy Laboratories, NREL, USA. AWT-27 is a 2-bladed wind turbine, one of the very few wind turbines with known specifications to public. AWT-27 is taken as the case for study all through this project. Table (2.4) gives AWT-27 specifications. In order to compare the results obtained by AWTSim with those of WTPerf, the input data files of a typical test run of WTPerf (obtained from the NREL website) have been downloaded and used to generate the input data files of Tables (2.1) and (2.2) as required by AWTSim. The design pitch angle for AWT-27 is 1.2° to stall (-1.2). However, in order to compare the results with available results, pitch angles 0, 1 and 2 degrees to stall are considered for simulation. Figures (2.12) and (2.13) show the power curves and thrust curves for this wind turbine obtained by WTPerf and AWTSim.

It can be observed that the difference between the predicted mechanical power and thrust by two codes is very small. The reason for this difference can be explained as follows. The blade aerodynamic loading and therefore the rotor mechanical power are very sensitive to the accuracy of the predicted angle of attack. The more the number of segments, more accurately the angle of attack is calculated. WTPerf is using 17 unequal segments in this run while AWTSim has divided the blade into 20 equal segments.

Table 2.4-AWT-27 wind turbine

Rotor diameter	27.514 m
Hub height	30 m
Cone angle	7°
No. of blades	2
Aerofoils	S800 Series
Original constant rotor speed	53.3 rpm
Rated power	300 kW
Design blade pitch angle	1.2° (to stall)
Hub radius	1.184 m
Yaw angle	0°
Tilt angle	0°

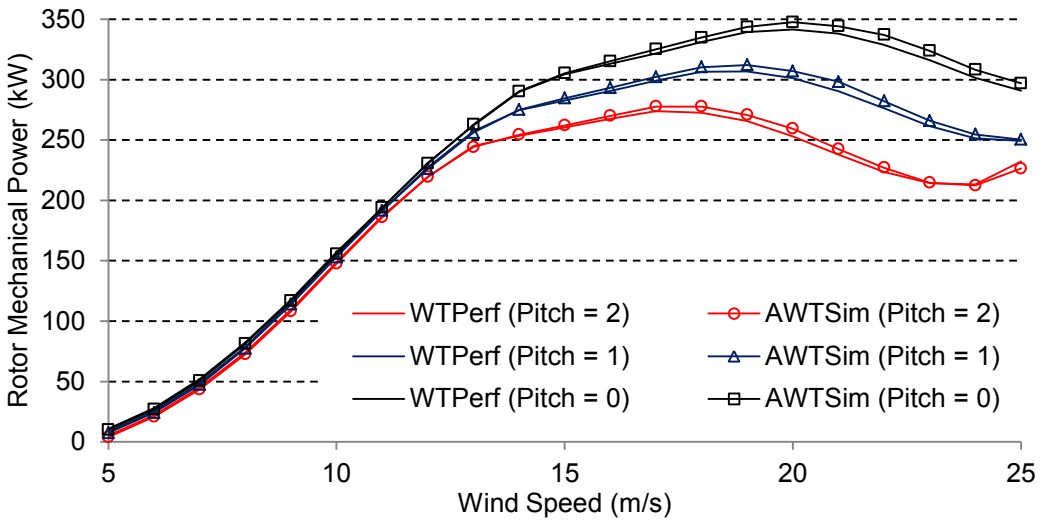

Figure 2.12-AWTSim versus WTPerf (Buhl, 2004)-Power curves at different pitch angles

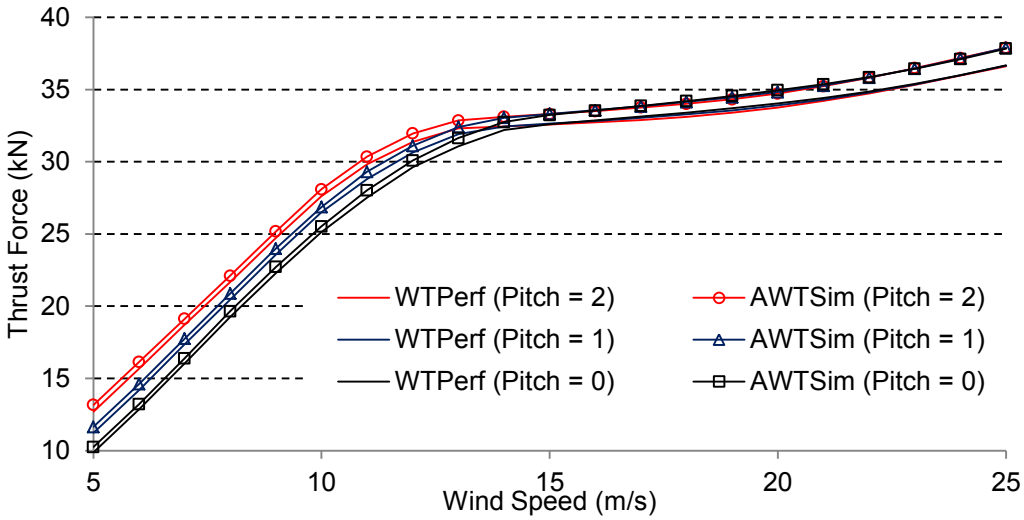

Figure 2.13-AWTSim versus WTPerf (Buhl, 2004)-Thrust force at different pitch angles

2.6 Summary

In this chapter the theory behind AWTSim, a software tool developed for the aerodynamic analysis of stall-regulated wind turbines was explained. AWTSim is based on BEMT method. The main modules of AWTSim, the blade discretiser and the BEMT calculator, were also explained. At the end of the chapter, it was shown that AWTSim produces accurate results while compared with the accredited code WTPerf.

To this end, AWTSim is only capable of simulating constant speed stall-regulated wind turbines which do not utilise any active control systems. In Chapter 3, the modifications required making AWTSim applicable for variable speed rotors and blades with active control systems are explained.

3 Aerodynamic Performance Analysis of Wind Turbines Utilising Aerodynamic Control Systems

3.1 Introduction

In Chapter 2, the theory behind the aerodynamic performance analysis tool was explained. It was also shown that how the software tool can be used for simulation of a constant-speed stall-regulated wind turbine. In this chapter, first power and load control systems will be classified based on their effect and types and then the controller simulation method is explained. It is followed by details on further development of the software tool developed in Chapter 2 towards making it suitable for analysis of both constant speed and variable speed rotors utilising blades with variable pitch, flap, microtab and variable length blades. For each type a case study is run to evaluate the performance of the software. Finally, a preliminary comparison of different types of control systems is carried out and reported.

3.2 Power and Blade Load Control

Wind turbine rotor mechanical power and blade aerodynamic loading depend on wind speed. Wind speed is a stochastic parameter which can be represented by

$$V = \overline{V} + \hat{V} \tag{3.1}$$

in which, V is the instantaneous wind speed, $\overline{V}$ is the mean value and $\hat{V}$ is the turbulence. Wind turbulence spectrum includes variations with time scales from a fraction of seconds to several seconds.

Wind turbines utilise power and load control systems in order to:

1. increase extracted wind power at low wind speeds,
2. regulate the rotor power at its rated value rated value preventing the generator from overloading at high wind speeds,
3. alleviate the steady and quasi-steady aerodynamic loads on blades (e.g. due to a gradual rise in wind speed, or variations of aerodynamic load as the blade passes through wind shear for wind turbines with lower rotor speeds), and
4. damp and alleviate the fluctuating behaviour of aerodynamic loads, mainly produced by wind turbulence and ground shear for wind turbines with high rotor speeds.

While the first two functions above are very important for all wind turbines irrespective of their type and size, the third and fourth functions of a control system are of prime

importance in larger wind turbines, in which the long blades experience massive loads. Since the present study is mainly focused on improving the energy capture capability of smaller wind turbines, the first two functions are of prime interest here.

3.2.1 Power and Blade Load Control Systems via Blade

Power and blade load control can be carried out either through devices installed on blades (or blade itself), or via mechanism affecting the rotor as a whole.

Figure (3.1) shows different conventional and nonconventional power and load control mechanisms affecting the blade performance. Some of these control systems respond only to wind variations with large time scales, while some other have shorter response time and therefore can be used for controlling the effect of wind variations with smaller time-scales.

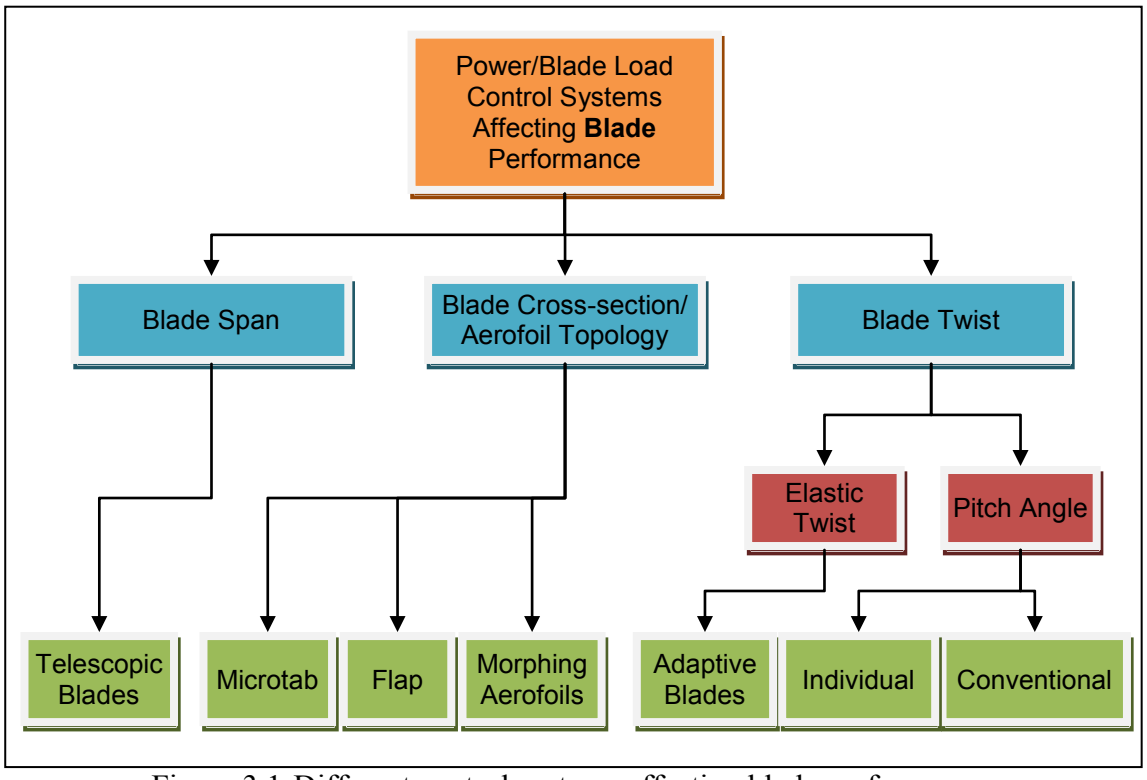

Figure 3.1-Different control systems affecting blade performance

According to this figure, control systems can be categorised based on the controlling parameters affecting the blade span, blade cross-section (aerofoil) and blade twist.

Figure (3.2) shows a two-dimensional flow kinematic diagram around the blade at span location r .

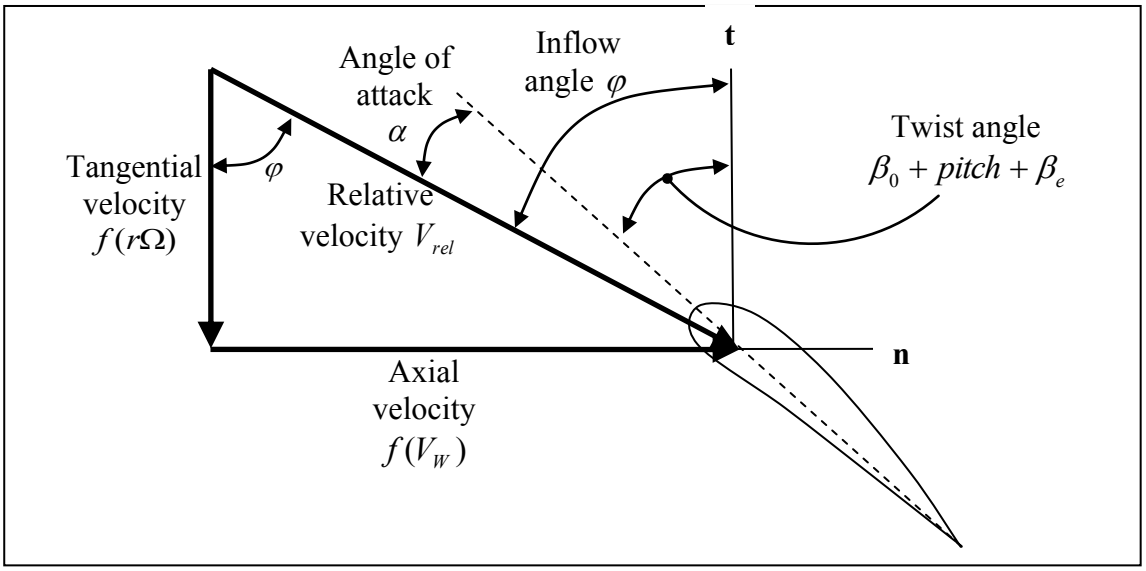

Figure 3.2- Flow kinematic diagram at span location r

All control systems above, besides the telescopic blades, change the wind turbine performance via imposing a change in the angle of attack α. The angle of attack is related to inflow angle φ and the blade twist angle (elastic twist β_e, pretwist β_0 and pitch angle *pitch*) via Equation (3.2).

$$\alpha = \varphi - \beta_e - \beta_0 - pitch \tag{3.2}$$

Conventional and individual pitch control systems use the blade pitch angle *pitch* as the controlling parameter. Adaptive blades control the performance via elastic twist angle β_e produced as a result of elastic coupling in the material of the blade. Stall-regulated rotors rely on the influence of the inflow angle φ (as a non-independent controlling parameter) on the angle of attack and consequently the rotor output power.

3.2.2 Power and Blade Load Control Systems via Rotor

Referring to Equations (2.11), (2.12), (2.45) and (2.51) evidently yaw angle γ and rotor speed Ω have influence on both rotor mechanical power and blade loading and therefore can be used as controlling parameters. Another parameter (not discussed in Chapter 2) is the rotor tilt angle and that can be also used for affecting the flow kinematics around the entire of the rotor. Both yaw and tilt control systems need heavy mechanical systems to change the direction of the rotor. This makes these systems highly sluggish and therefore unsuitable for accurate power and load control. Controlling power through yaw or tilt angle also produce various complications such as

unbalance rotor loading and consequently increasing fatigue loading on blades and other components. Both systems are rarely used in modern wind turbines. On the other hand rotor speed can be easily controlled via changing the electrical load (generator output). Variable speed rotors are very popular, in particular for smaller wind turbines.

3.2.3 Active Control versus Passive Control

In view of the above discussion the control systems can be also categorised as either active or passive. In an active control, the controlling parameter is independent of the wind turbine operating condition (state) and is adjusted through commands from controller. It provides a *full control* on rotor power and/or blade loading. These controllers influence the flow kinematics around a portion of the blade (i.e. flap, microtab, morphing aerofoil, telescopic blades), the entire of the blade (i.e. conventional and individual pitch control systems), or the entire of the rotor (i.e. yaw, tilt and rotor speed).

In passive control, the controlling parameter depends on wind turbine operating condition. In fact, no separate controller is in place and the blade itself acts as a controller. A change in wind turbine operating condition (e.g. wind speed) affects the flow kinematics around the entire of the blade either via changes in inflow angle (i.e. in case of stall-regulated blades), or via changes in both inflow angle and blade elastic twist (i.e. adaptive blades). A change in wind turbine operating condition leads to a *partial control* on rotor power and/or blade loading

In case of adaptive and telescopic blades as well as blades utilising flaps, microtabs and morphing aerofoils, corrections are required to be applied to the baseline blade topology and/or geometry and/or aerodynamic characteristics.

3.3 Simulation of Controller

The aerodynamic performance of a wind turbine depends on the characteristics of the control system in place (type, response time, controlling parameter, controllable parameter, etc) as well as the wind turbine rotor characteristics (e.g. blade topology and size, number of blades and rotor angular speed) and the operating condition (e.g. mean wind speed at hub elevation, wind direction and turbulence level). Therefore, to be able to simulate a wind turbine, the behaviour of the control system is also to be simulated along with the aerodynamic behaviour of the wind turbine. This, however, is not

practical as it requires having the control system designed prior to the blade. An alternative solution to this is to assume that the controller is capable of delivering the expected functions perfectly. This implies that the controlling parameter is always adjusted at its best possible value which leads to the best (goal) performance. Adapting this approach, the optimum (best possible) controlling parameter, which optimises the performance measure(s) can be found via solving an optimisation problem.

In case of variable speed rotors, the rotor speed is also required to be known. Two approaches can be adopted to find the rotor speed. In the first approach, the rotor speed is found such that the tip speed ratio is retained constant at its design value, where the power coefficient C_P has its maximum value. This approach serves well for conventional blades. In the second approach, the rotor speed is found along with the main controlling parameter (if there is any) via an optimisation procedure. For example, in case of a variable speed pitch-controlled wind turbine, both rotor speed and the blade pitch angle are to be found via solving an optimisation problem, with the controllable parameter as variables to be found. In this case, control laws may also apply. For example: the rotor power is controlled via changing rotor speed for $\Omega \le \Omega_c$, and via changing the pitch angle for $\Omega > \Omega_c$ (Ω_c is a constraint on the rotor speed); or: the blade load is controlled via changing the pitch angle only, while the rotor power is controlled via changing both rotor speed and pitch angle. The advantage of the second approach is that it does not require the design tip speed ratio (in fact, it can be used to find the design tip speed ratio), and that it is a general method applicable to all types of control systems and allows implementing control laws.

In this project, all of controlling parameters (including rotor speed) are obtained via solving an optimisation problem, which can formulated as follows:

$$\max \quad P(q_i);\ i = \{1,2,...,n_q\} \tag{3.3.a}$$

subject to

$$P \le P_{rated} \tag{3.3.b}$$

$$q_{i,l} \le q_i \le q_{i,u}\ ;\ i = \{1,2,...,n_q\} \tag{3.3.c}$$

In Equation (3.3), P is the rotor mechanical power at a given wind speed, q_i stands for the i-th controlling parameter limited to the interval $[q_{i,l}, q_{i,u}]$. Number of independent controlling parameters, n_q depends on the type of the blade and the rotor (constant speed or variable speed). Table (3.1) shows the number of controlling parameters for the blades studied in this project.

Table 3.1-Number of independent controlling parameters

	Number of independent controlling parameters	
	Constant speed rotor	Variable speed rotor
Conventional blades-stall regulated	0 (passive control)	1
Conventional blades-pitch controlled	1	2
Blades utilising flap	1	2
Telescopic blades	1	2
Blades utilising microtab	N_{MT} (No. of microtabs)	$N_{MT}+1$
Adaptive blades	0 (passive control)	1

Optimisation methods can be classified in many different ways, including:

- Gradient-based versus derivative free methods. Gradient based methods needs an explicit form of objective function correlating the objective to variables. Derivative-free methods, on the other hand, do not require a known objective function and can be applied to problems in which the objective or constraints are calculated through numerical analysis (e.g. CFD, finite element analysis, BEMT)
- Global versus local search methods. Global search methods find the global optimum irrespective of the number of local optima, whilst local search methods only find local optima in the neighbourhood of the search initial point (or points).
- Constrained versus unconstrained methods. Some optimisation methods are applicable to unconstrained problems only, while some other methods can handle both equality and inequality constraints.

In order to select the best optimisation method for optimisation problem of Equation (3.3), we need to identify the type of this problem first. Obviously, this is a constrained problem and therefore we need an optimisation method capable of dealing with constrained problems. As explained in Chapter 2, the rotor power can be calculated only via a numerical iterative procedure (Algorithm (2.2)-BEMT Calculation). Since there is

no explicit correlation between the power and controlling parameters, gradient-based optimisation methods cannot be used for this optimisation problem. This leaves us with derivative free optimisation methods. Figure (3.3) shows three possible behaviour of objective P with respect to a typical controlling parameter q_i. Figure (3.3.a) shows a case where there is only one optimum. In the second case, Figure (3.3.b), there are multiple local optimum points. In the third case, Figure (3.3.c), there are multiple local optima and multiple global optima. In view of this figure, a global optimisation method should be employed to solve this problem as employing a local optimisation method will lead to a local optimum point, unless the initial point is located within interval Q (see Figure (3.3)).

Since this is a constrained problem with no known explicit correlation between the objective and variables, and that the solution space may have multiple local/global optimum points, meta-heuristic optimisation methods such as genetic algorithm (GA) seem to be the natural choice for solving this problem. Meta-heuristic methods are derivative-free global optimisation methods applicable to constrained problems. These methods, however, need significant computational time to find the global optimum.

Hill-climbing and pattern search methods, on the other hand, find a local optimum in the neighbourhood of the initial point. If the initial point is selected wisely (within the interval Q), a hill-climbing search finds the global optima. Hill-climbing and pattern search methods are very efficient for problems with small number of variables. Referring to Table (3.1), it can be observed that except one case the number of independent controlling parameters is limited to 2, making hill-climbing and pattern search alternative solutions subject to the condition of starting with a suitable initial point.

Tables (3.2) and (3.3) summarise different types of blades which have been investigated in this project. Depending on the type of the control system in use and the corresponding controlling parameter(s) different optimisation methods are employed. The rest of this chapter elaborates on these optimisation methods and the corrections which are required to be applied to the BEMT calculator and the baseline blade topology/ geometry/ aerodynamic characteristics.

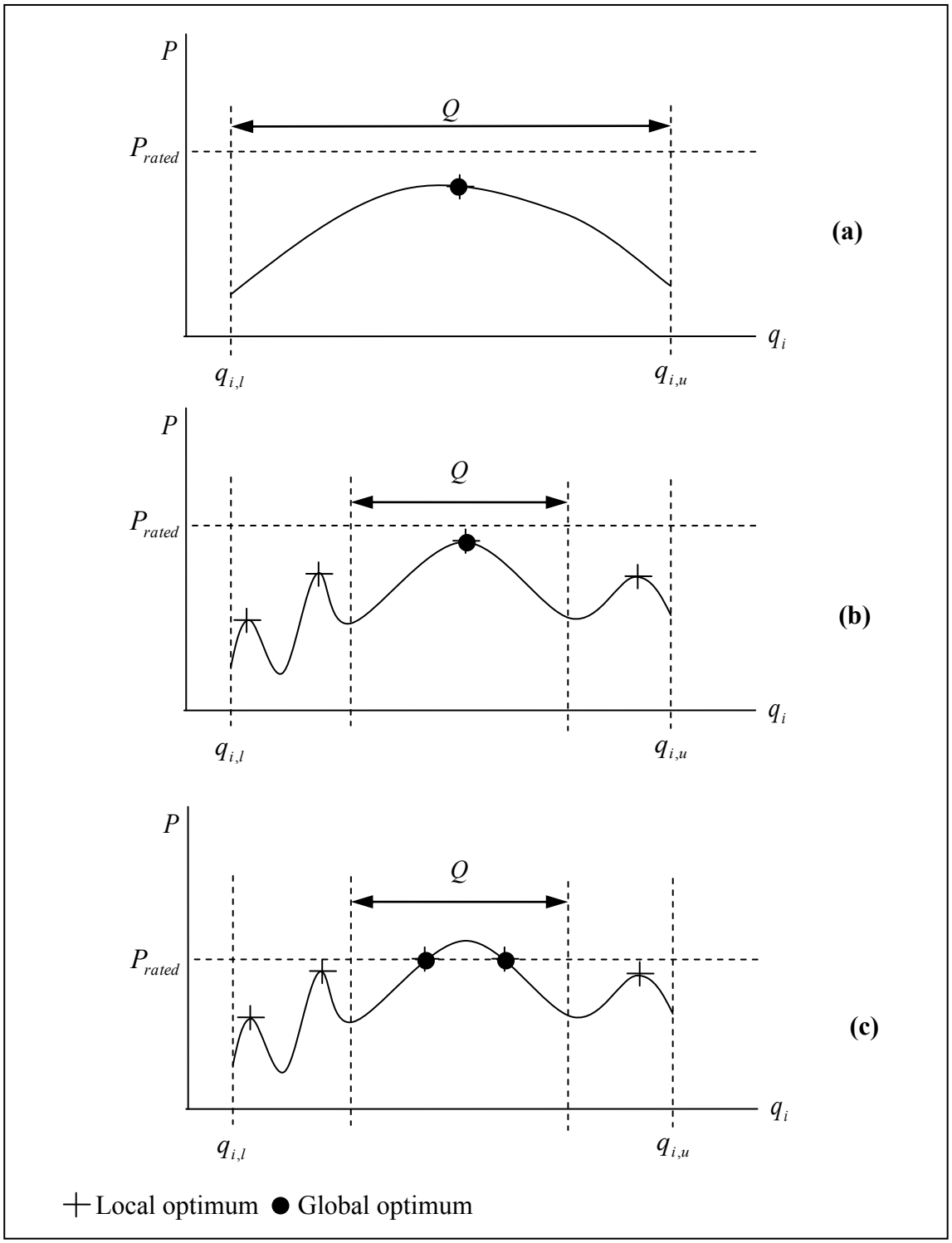

Figure 3.3- Three possible behaviour of objective P with respect to controlling parameters q_i.

Table 3.2-Simulation of *constant-speed* wind turbines with different types of blades

Blade type {parameters defining blade}	Independent controlling parameters	Type of control on power or steady load	Optimisation method for finding controlling parameters	Corrections applicable to blade topology/ geometry	Corrections applicable to blade aerodynamic characteristics
Conventional blade-stall regulated $\{R, c, \beta_0, AF, t_{\max}\}$	N/A	Partial-Passive	N/A	N/A	N/A
Conventional blade-pitch controlled $\{R, c, \beta_0, AF, t_{\max}\}$	pitch angle $pitch_s \le pitch \le pitch_e$	Full-Active	Hill climbing	N/A	N/A
Blade utilising flap $\{R, c, \beta_0, AF, t_{\max}, R_{F,s}, R_{F,e}, d_F\}$	Flap deployment angle $\delta_{F,s} \le \delta_F \le \delta_{F,e}$	Full-Active	Hill climbing	N/A	$\{C_L, C_D\}$
Telescopic blade $\{R, c, \beta_0, AF, t_{\max}, R_{T,s}, R_{T,e}\}$	Blade deployment length $R_{T,s} \le R_T \le R_{T,e}$	Full-Active	Hill climbing	$\{R, c, \beta_0, AF, t_{\max}\}$	N/A
Blade utilising microtab $\{R, c, \beta_0, AF, t_{\max}, R_{MT,s}, R_{MT,e}, N_{MT}\}$	N_{MT} microtab states $mt_i \in \{-1, 0, +1\}$	Full-Active	GA search	N/A	$\{C_L, C_D\}$

Table 3.3-Simulation of *variable-speed* wind turbines with different types of blades

Blade type {parameters defining blade}	Independent controlling parameters	Type of control on power or steady load	Optimisation method for finding controlling parameters	Corrections applicable to blade topology/ geometry	Corrections applicable to blade aerodynamic characteristics
Conventional blade-stall regulated $\{R, c, \beta_0, AF, t_{\max}\}$	rotor speed $\Omega_s \le \Omega \le \Omega_e$	Full-Active	Hill climbing	N/A	N/A
Conventional blade-pitch controlled $\{R, c, \beta_0, AF, t_{\max}\}$	rotor speed and pitch angle $\Omega_s \le \Omega \le \Omega_e$ $pitch_s \le pitch \le pitch_e$	Full-Active	Pattern search	N/A	N/A
Blade utilising flap $\{R, c, \beta_0, AF, t_{\max}, R_{F,s}, R_{F,e}, d_F\}$	rotor speed and flap deployment angle $\Omega_s \le \Omega \le \Omega_e$ $\delta_{F,s} \le \delta_F \le \delta_{F,e}$	Full-Active	Pattern search	N/A	$\{C_L, C_D\}$
Telescopic blade $\{R, c, \beta_0, AF, t_{\max}, R_{T,s}, R_{T,e}\}$	rotor speed and blade deployment length $\Omega_s \le \Omega \le \Omega_e$ $R_{T,s} \le R_T \le R_{T,e}$	Full-Active	Pattern search	$\{R, c, \beta_0, AF, t_{\max}\}$	N/A
Blade utilising microtab $\{R, c, \beta_0, AF, t_{\max}, R_{MT,s}, R_{MT,e}, N_{MT}\}$	rotor speed $\Omega_s \le \Omega \le \Omega_e$ and N_{MT} microtab states $mt_i \in \{-1,0,+1\}$	Full-Active	GA search	N/A	$\{C_L, C_D\}$

3.4 Aerodynamic Performance of Stall Regulated Wind Turbines

The same code as explained in Chapter 2 without any further modifications serves well for simulation of constant speed stall regulated wind turbines. However, in case of variable speed stall regulated wind turbines, the rotor speed is a controlling parameter and needs to be determined.

3.4.1 Control Simulation of Variable Speed Stall Regulated Wind Turbines

Simulating AWT-27 wind turbine for various rotor speeds, the effect of rotor speed on the rotor mechanical power can be observed. Figure (3.4) shows four distinct behaviours of rotor power with respect to rotor speed at different wind speeds:

Case 1- $V_W = 8m/s$: One feasible local/global optimum ($P_{\max} < P_{rated} = 300kW$)

Case 2- $V_W = 11m/s$: One feasible local/global optimum at a boundary ($P_{\max} < P_{rated}$)

Case 3- $V_W = 13m/s$: Infeasible optimum at boundary; one feasible optimum ($P_{\max} = P_{rated}$)

Case 4- $V_W = 25m/s$: Multiple feasible local optima; global optima ($P_{\max} = P_{rated}$)

It can be seen that in all cases, if the initial point in a hill-climbing algorithm is taken as the upper limit $\Omega_0 = \Omega_u$ with a negative search direction (from right to left), the algorithm will find the feasible global optima without getting trapped in a local optima (if there is one).

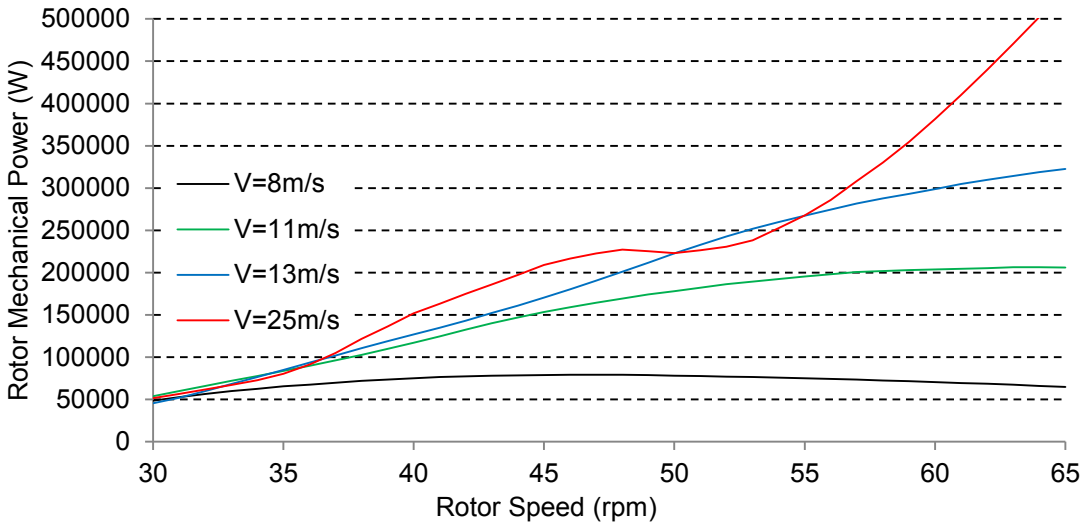

Figure 3.4-Diffrent distinct behaviours of $P-\Omega$ curve

Starting with $\Omega = \Omega_u$ as the initial point and searching from right to left, the hill-climbing Algorithm (3.1) finds the global solution for optimisation problem (3.3) for all four behaviours of $P-\Omega$, as explained below:

- Case (1): The search continues from right to left until the optimum point is passed and the power at new iteration ($k+1$) becomes less than the power at the previous iteration $P^{k+1} < P^k$. At this point the search algorithm goes back to the previous point (k) and recalculates P^{k+1} by a new step size: $step_{new} = step_{old}/2$. This processes repeats until the step size becomes less than or equal to a predefined tolerance ($step \le \varepsilon_\Omega$).
- Case (2): The first iteration leads to $P^{k+1} < P^k$ and therefore the search algorithm goes back to the initial point and recalculates P^{k+1} by a new step size: $step_{new} = step_{old}/2$. The second iteration also leads to $P^{k+1} < P^k$ and consequently restarting from initial point with a smaller step size. This processes repeats until the step size becomes less than or equal to a predefined tolerance ($step \le \varepsilon_\Omega$).
- Cases (3) and (4): The first iteration leads to $P^{k+1} < P^k$ but since $P^{k+1} > P_{rated}$ the search algorithm continues in the same direction with the same step size until $P^{k+1} < P_{rated}$. A this point the algorithm goes back to the previous point and recalculates P^{k+1} by a smaller step: $step_{new} = step_{old}/2$. This processes repeats until either the step size becomes less than or equal to a predefined tolerance ($step \le \varepsilon_\Omega$) or power lies between the tolerated margin $\left|P^{k+1} - P_{rated}\right| \le \varepsilon_P$.

Algorithm 3.1-Hill climbing search for finding optimum rotor speed for variable speed stall regulated WT

Given:

- $step_\Omega, \varepsilon_\Omega, \Omega_l, \Omega_u, \varepsilon_P$
- All parameters required for running Algorithm 2.2 except Ω

Step 1- Initialise: $\Omega_0 \leftarrow \Omega_u$

Step 2- Start with $\Omega \leftarrow \Omega_0$ and simulate wind turbine to find P (Algorithm 2.2);
$P_0 \leftarrow P$.

Step 3- While $(step_\Omega > \varepsilon_\Omega) \wedge \left|P - P_{rated}\right| > \varepsilon_P$ do:

3.1. $\Omega \leftarrow \Omega_0 - step_\Omega$ simulate wind turbine to find P

3.2. If $(P > P_0 \wedge P < P_{rated}) \vee (P < P_0 \wedge P > P_{rated}) \vee (P > P_0 \wedge P_0 > P_{rated})$, then $\Omega_0 \leftarrow \Omega_0 - step_\Omega, P_0 \leftarrow P$; Else: Half the step: $step_\Omega = 0.5 step_\Omega$

To show the performance of this algorithm, AWT-27 wind turbine is simulated as a variable speed wind turbine with the following search parameters:

- Rotor speed limits: $\Omega_l = 30rpm$ and $\Omega_u = 65rpm$
- Initial step size: $step = (\Omega_u - \Omega_l)/10 = 3.5rpm$
- Power tolerance: $\varepsilon_P = 0.01P_{rated} = 3kW$
- Rotor speed tolerance: $\varepsilon_\Omega = 0.1rpm$

Figure (3.5) shows the iteration points when using the hill-climbing method of Algorithm (3.1) for four typical wind speeds. Figure (3.6) shows the number of iterations for each wind speeds. It should be noted that an exhaustive search with a grid of size of $\varepsilon_\Omega = 0.1rpm$ requires $(\Omega_u - \Omega_l)/\varepsilon_\Omega + 1 = 351$ points (iterations). This is 35 times more than the average number of iterations when using the hill-climbing algorithm.

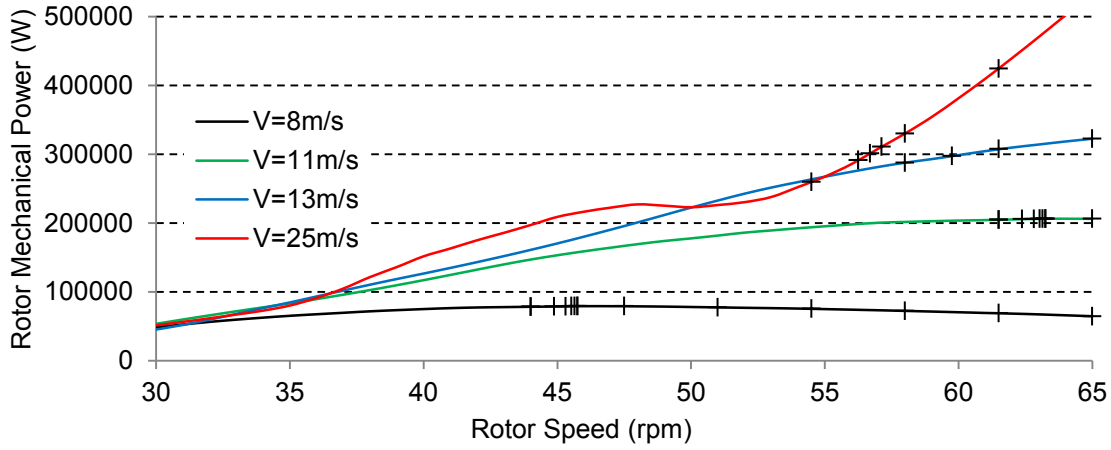

Figure 3.5-Iteration points in hill-climbing method of Algorithm (3.1)

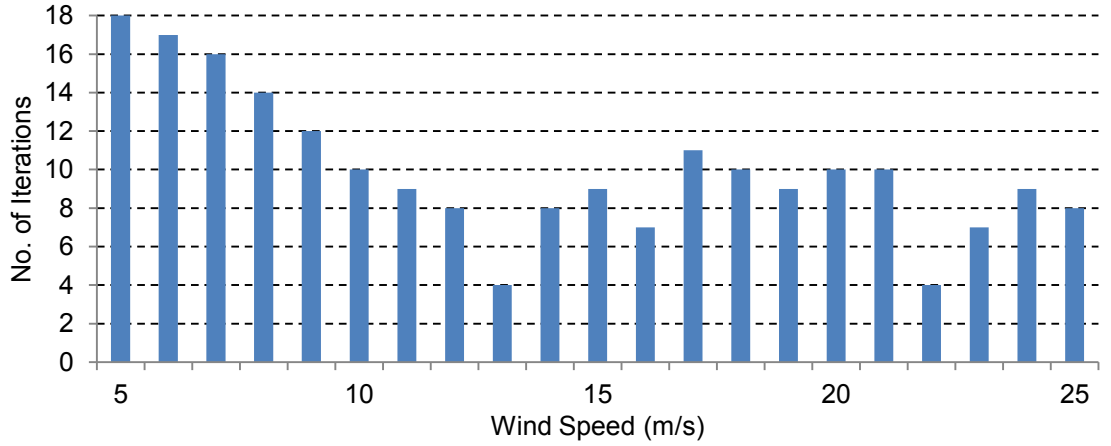

Figure 3.6-Number of iterations against wind speed using hill-climbing method of Algorithm (3.1)

Figure (3.7) shows the results of this simulation.

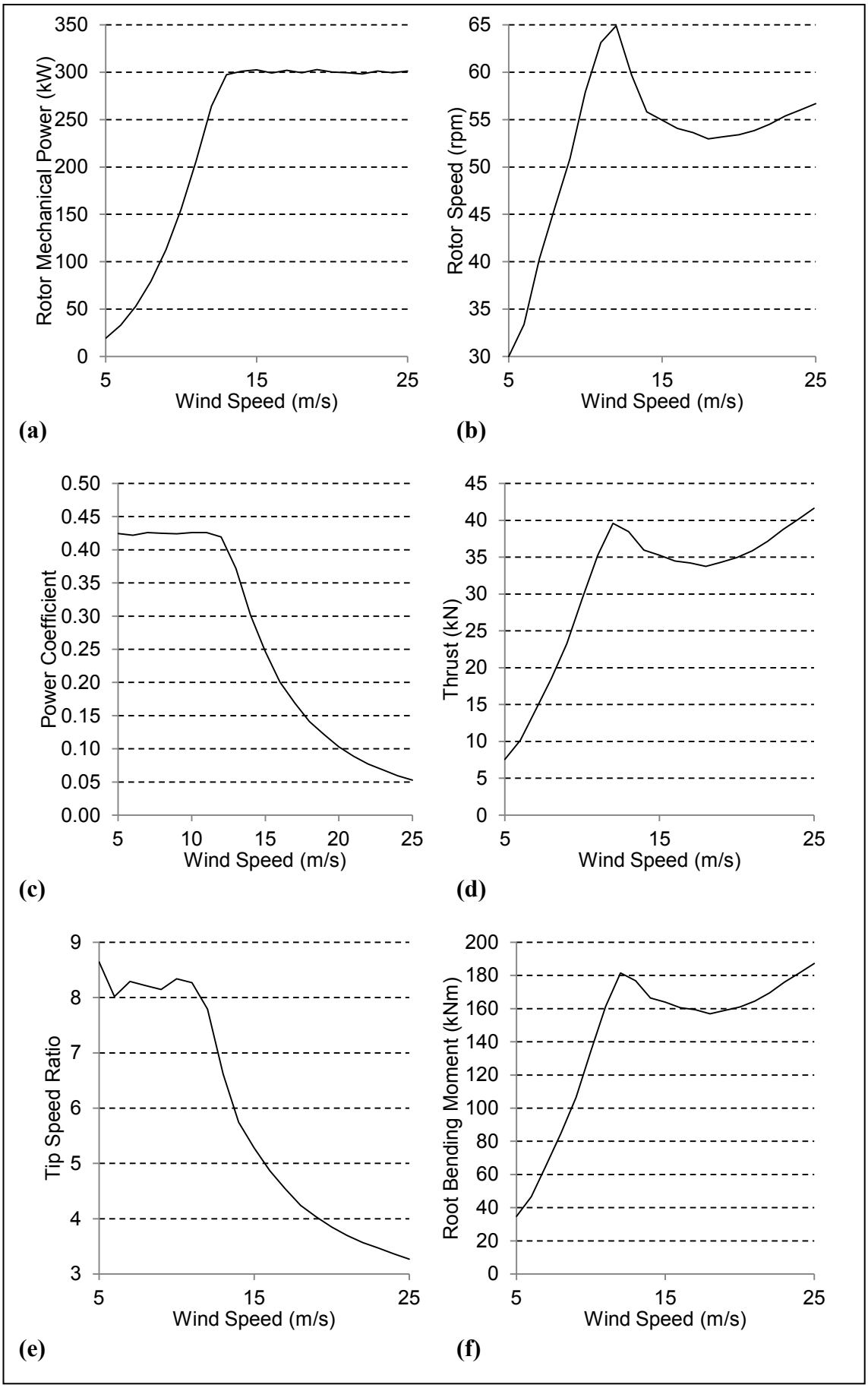

Figure 3.7-Results of simulation of variable-speed stall-regulated AWT-27

Figure (3.7.a) shows that the power curve reaches its rated value (300kW) at about a wind speed of 12 m/s and remains constant (within the tolerated margin of $P_{rated} \pm \varepsilon_P$) at higher wind speeds. This confirms that the control simulation of Algorithm (3.1) successfully finds the rotor speed which is required to maintain the power at its rated value.

The power coefficient curve of Figure (3.7.c), as expected, is horizontal at lower wind speeds having its highest value achievable by this wind turbine. The power coefficient decreases as the power remains constant at higher wind speeds.

The rotor speed as shown in Figure (3.7.b), as expected, increases with wind speed at lower wind speeds until it reaches its upper bound (here 65 rpm). The concave shape of the second part of the curve is due to the fact that the baseline wind turbine is stall-regulated and its original power curve is below the rated power at high wind speeds (see Figure (2.12)), hence the rotor speed increases at higher wind speeds to shift the power curve up to its rated value.

The form of the tip speed ratio curve, as shown in Figure (3.7.e) is a very interesting result. It can be observed that the tip speed ratio is not constant at low wind as it is normally expected. As explained earlier in Section (3.3), two approaches can be adopted to find the rotor speed. In the traditional approach, the rotor speed is found such that the tip speed ratio is retained constant at its design value, while in the second approach, as proposed and used in this study, the rotor speed is found via an optimisation procedure. This figure confirms that the second approach is superior to the first one, as a constant tip speed ratio will lead to a fluctuating power coefficient which is obviously not optimum.

Finally, comparing the rotor thrust force, shown in Figure (3.7.d), and the root bending moment curves, shown in Figure (3.7.f), it can be observed that, as expected, these curves have almost identical forms.

3.5 Aerodynamic Performance of Pitch Controlled Wind Turbines

The BEMT-Calculator of Algorithm (2.2), without any modifications, can be used for simulation of pitch controlled wind turbines. In case of constant speed rotor, blade pitch angle and in case of variable speed rotor blade pitch angle and rotor speed are the controlling parameters that need to be determined by solving optimisation problem of Equation (3.3).

3.5.1 Control Simulation of Constant Speed Pitch Controlled Rotors

Simulating AWT-27 wind turbine for various blade pitch angle, the effect of blade pitch angle on the rotor mechanical power can be observed. Figure (3.8) shows five distinct behaviours of rotor power with respect to blade pitch angle at different wind speeds:

Case 1- $V_W = 10m/s$: One feasible optimum ($P_{\max} < P_{rated}$)

Case 2- $V_W = 14m/s$: Multiple feasible global optimum points ($P_{\max} = P_{rated}$)

Case 3- $V_W = 15m/s$: One infeasible local optimum; one feasible global optimum ($P_{\max} = P_{rated}$)

Case 4- $V_W = 19m/s$: One infeasible local optimum at boundary; one feasible global optimum ($P_{\max} = P_{rated}$)

Case 5- $V_W = 24m/s$: Multiple local optima (feasible and infeasible); one feasible global optima ($P_{\max} = P_{rated}$)

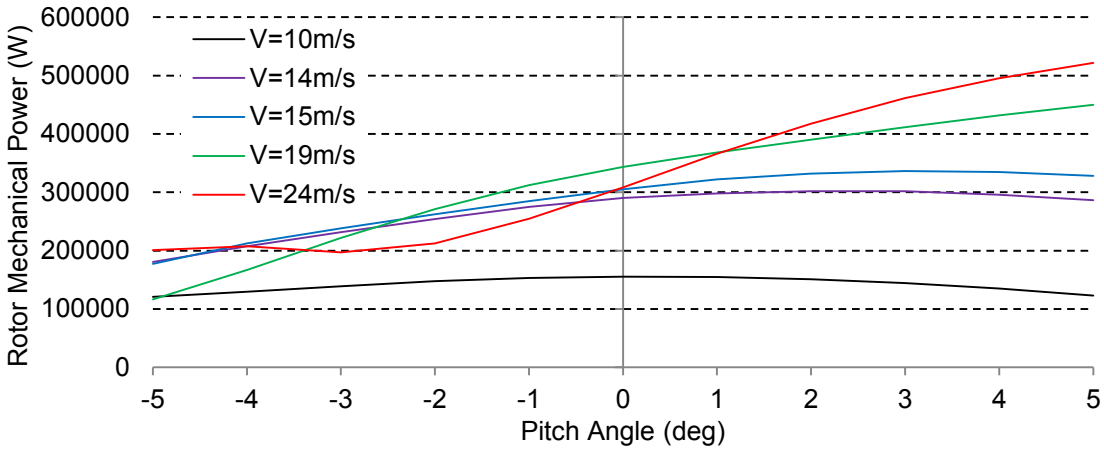

Figure 3.8-Diffrent distinct behaviours of $P - pitch$ curve

It can be seen that in all cases, if the initial point in a hill-climbing algorithm is taken as the upper limit $pitch_0 = pitch_u$ with a search direction from right to left, the algorithm

will find the feasible global optima without getting trapped in a local optima (if there is one). In Case 2 with multiple global optimum points, since the search direction is from right to left, optimum point closer to the upper limit $pitch_u$ is selected as the solution. Replacing Ω with $pitch$ in Algorithm (3.1), this algorithm can be used to find the optimum pitch angle at each wind speed for a constant speed pitch controlled wind turbine.

To show the performance of this algorithm, AWT-27 wind turbine is simulated as a pitch controlled wind turbine with the following search parameters:

- Pitch limits: $pitch_l = -5^\circ$ and $pitch_u = 5^\circ$
- Initial step: $step = (pitch_u - pitch_l)/10 = 1^\circ$
- Power tolerance: $\varepsilon_P = 0.01 P_{rated} = 3kW$
- Pitch tolerance: $\varepsilon_{pitch} = 0.1^\circ$

Figure (3.9) shows the results of this simulation. Referring to this figure, it can be observed that the power curve reaches its rated value at about a wind speed of 12 m/s and remains constant at higher wind speeds. This confirms that replacing Ω by $pitch$ in Algorithm (3.1), this algorithm successfully finds the suitable blade pitch angle to retain the rotor power at its rated value at higher wind speeds. The power coefficient, as shown in Figure (3.9.c), reaches a maximum value of 0.45 which is higher than the maximum power coefficient of the previous simulation shown in Figure (3.7.c) (about 0.42). This confirms that this algorithm also successfully finds the optimum blade pitch angle which increases the rotor power at lower wind speeds.

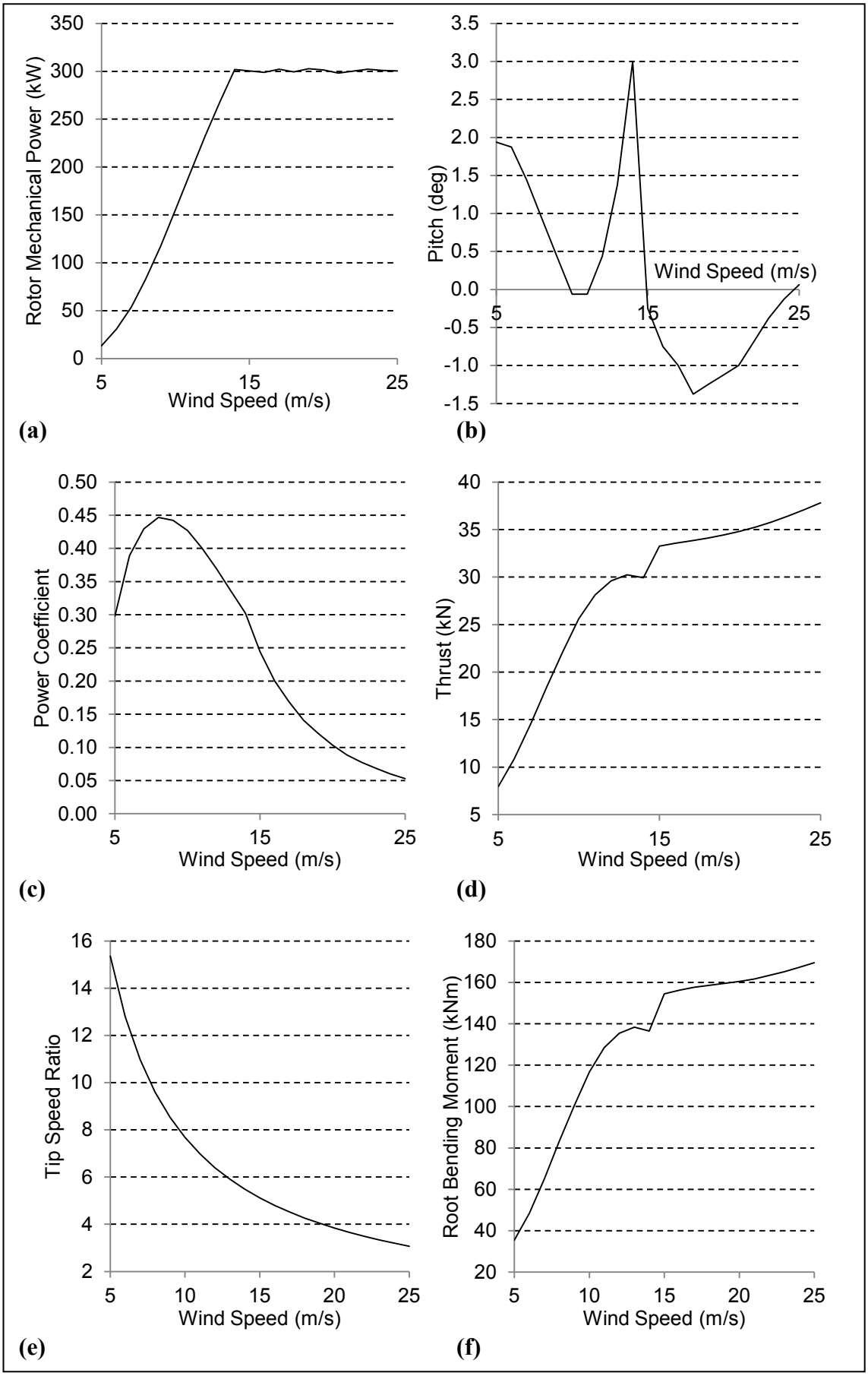

Figure 3.9- Results of simulation of constant-speed pitch-controlled AWT-27

3.5.2 Control Simulation of Variable Speed Pitch Controlled Rotors

For this type of wind turbine, the rotor speed and blade pitch angle are the controlling parameters to be determined via solving optimisation problem of Equation (3.3). Simulating AWT-27 wind turbine over a 2-dimensional grid on rotor speed and blade pitch angle, the effect of these parameters on the rotor mechanical power can be observed. Figure (3.10) shows four typical distinct behaviours for rotor power with respect to blade pitch angle and rotor speed at different wind speeds. To produce these figures the following data was used:

- Pitch limits: $pitch_l = -5^\circ$ and $pitch_u = 5^\circ$
- Rotor speed limits: $\Omega_l = 30rpm$ and $\Omega_u = 65rpm$
- Grid size in pitch-direction: 1°
- Grid size in rotor speed-direction: $3.5rpm$

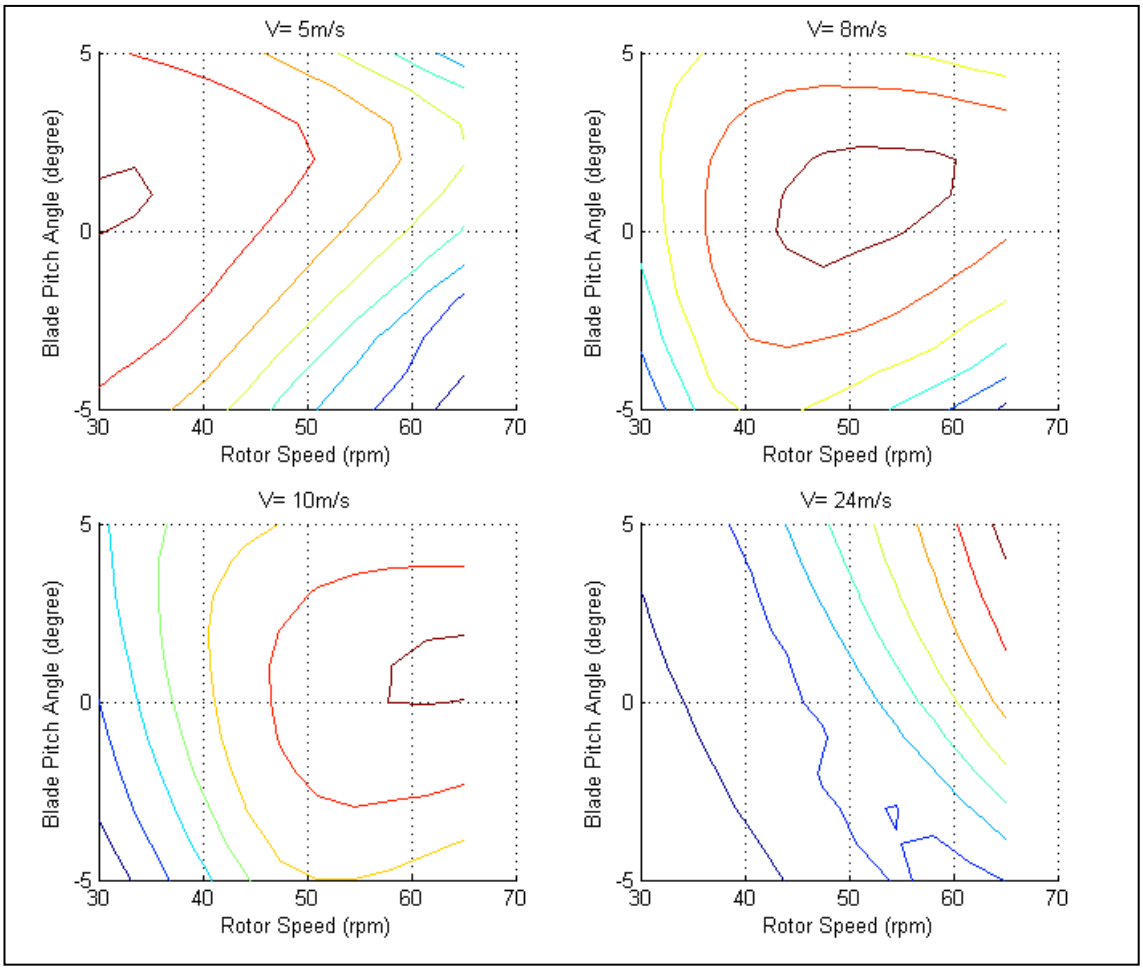

Figure 3.10-Rotor power versus rotor speed and blade pitch angle at various wind speeds

It can be seen that for all cases a pattern search method can be used to find the global optima (located inside the inner contour) if point $(pitch_u, \Omega_u)$ is taken as the initial point. Algorithm (3.2) details the pattern search used for this purpose. The search algorithm terminates when either of the termination criteria: $step_{pitch} \le \varepsilon_{pitch}$, $step_\Omega \le \varepsilon_\Omega$ and $|P - P_{rated}| \le \varepsilon_P$ is satisfied.

Algorithm 3.2-Pattern search method for finding optimum rotor speed and pitch angle for variable speed pitch controlled wind turbines

Given:

- $step_{pitch}, \varepsilon_{pitch}, pitch_l, pitch_u, step_\Omega, \varepsilon_\Omega, \Omega_l, \Omega_u, \varepsilon_P$
- All parameters required for running Algorithm 2.2 except Ω and $pitch$

Step 1- Initialise: $(pitch_0, \Omega_0) \leftarrow (pitch_u, \Omega_u)$

Step 2- Start with $(pitch_0, \Omega_0)$ and simulate wind turbine to find P (Algorithm 2.2); $P_0 \leftarrow P$.

Step 3- While $(step_{pitch} > \varepsilon_{pitch}) \wedge (step_\Omega > \varepsilon_\Omega) \wedge |P - P_{rated}| > \varepsilon_P$ do:

3.1. Initialise $move_1 = 0$, $move_2 = 0$

3.2. Move in Ω-direction: For $(pitch_0, \Omega_0 - step_\Omega)$ simulate wind turbine to find P

3.3. If $(P > P_0 \wedge P < P_{rated}) \vee (P < P_0 \wedge P > P_{rated}) \vee (P > P_0 \wedge P_0 > P_{rated})$, then $move_1 = 1$, $\Omega_0 \leftarrow \Omega_0 - step_\Omega, P_0 \leftarrow P$

3.4. Move in $pitch$-direction: For $(pitch_0 - step_{pitch}, \Omega_0)$ simulate wind turbine to find P

3.5. If $(P > P_0 \wedge P < P_{rated}) \vee (P < P_0 \wedge P > P_{rated}) \vee (P > P_0 \wedge P_0 > P_{rated})$, then $move_2 = 1$, $pitch_0 \leftarrow pitch_0 - step_{pitch}, P_0 \leftarrow P$

3.6. If $move_1 = 0 \wedge move_2 = 0$ then half the steps: $step_{pitch} = 0.5 step_{pitch}$, $step_\Omega = 0.5 step_\Omega$

To show the performance of this algorithm, AWT-27 wind turbine is simulated as a variable speed pitch controlled wind turbine with the following search parameters:

- Pitch: $pitch_l = -5^\circ$, $pitch_u = 5^\circ, step_{pitch} = (pitch_u - pitch_l)/10 = 1^\circ$, $\varepsilon_{pitch} = 0.1^\circ$
- Rotor speed: $\Omega_l = 30rpm, \Omega_u = 65rpm, step_\Omega = (\Omega_u - \Omega_l)/10 = 3.5rpm$, $\varepsilon_\Omega = 0.1rpm$
- Power tolerance: $\varepsilon_P = 0.01 P_{rated} = 3kW$

Figure (3.11) shows the iteration points when using the pattern search method of Algorithm (3.2) for four wind speeds shown in Figure (3.10). Red markers in Figure (3.11) ($V_W = 24m/s$) correspond to infeasible solutions for which $P > P_{rated}(1 + \varepsilon_P)$.

Figure (3.12) shows the number of iterations for each wind speeds. It should be noted that an exhaustive search with a grid of size of $\varepsilon_{\Omega} = 0.1rpm$ and $\varepsilon_{pitch} = 0.1^{\circ}$ requires $35451(\left(\Omega_u - \Omega_l\right)/\varepsilon_{\Omega} + 1 = 351$ by $\left(pitch_u - pitch_l\right)/\varepsilon_{pitch} + 1 = 101)$ simulation points. This is 2100 times more than the average number of iterations when using the pattern search algorithm.

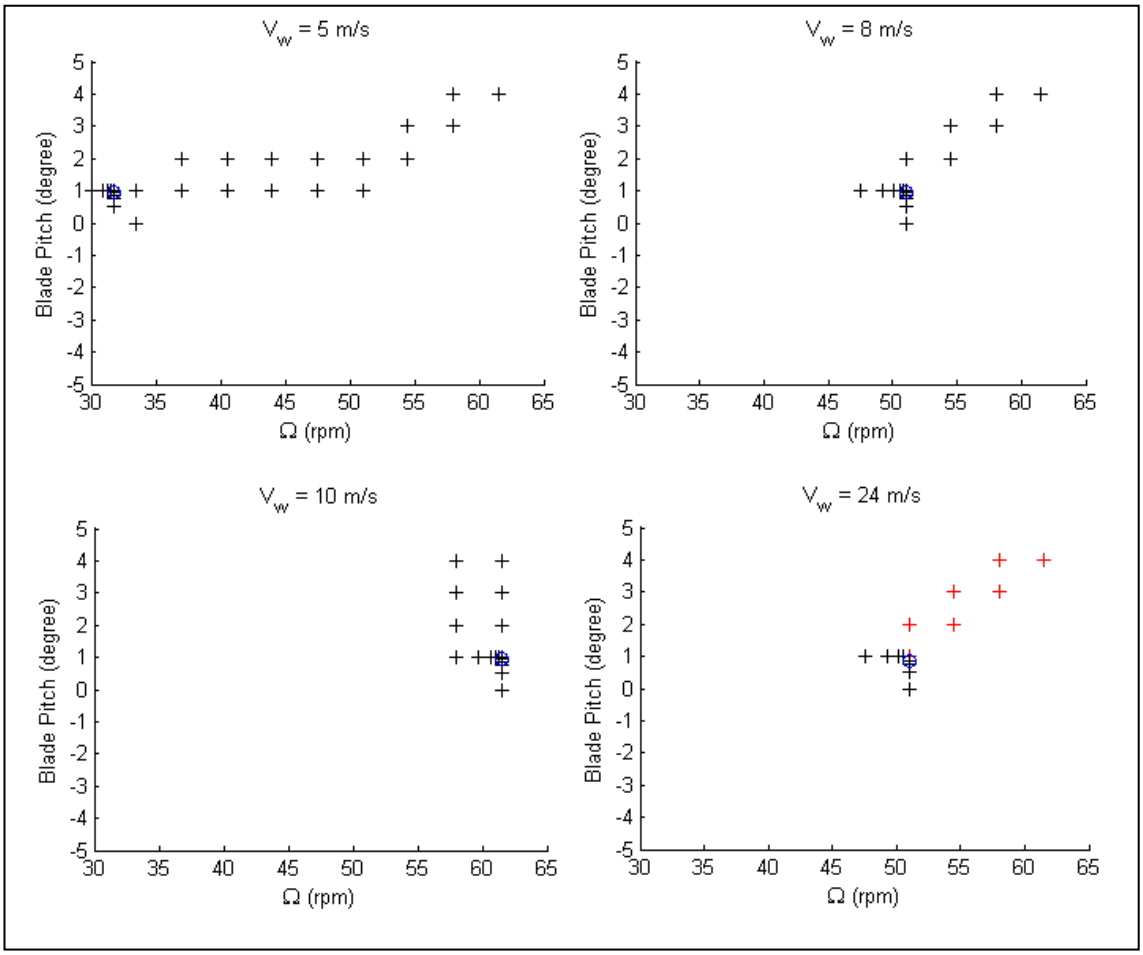

Figure 3.11- Iteration points in pattern search method of Algorithm (3.2)

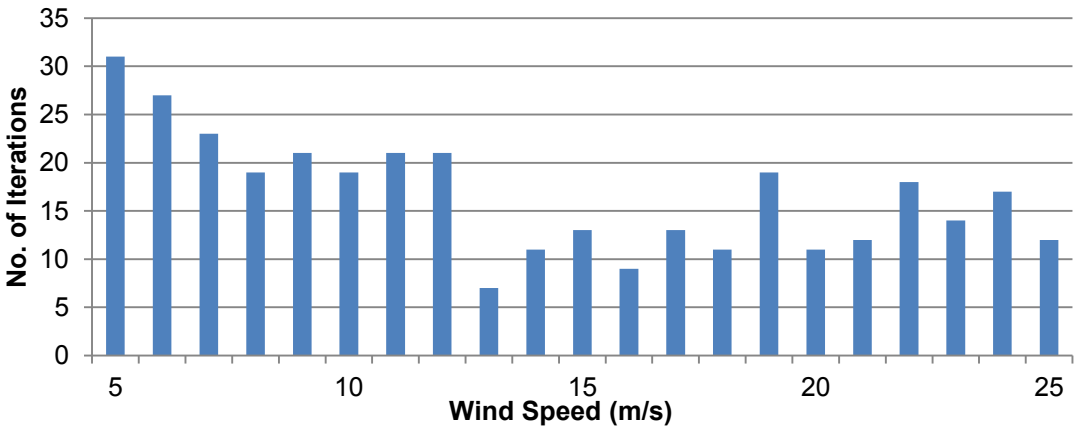

Figure 3.12- Number of iterations against wind speed using pattern search method of Algorithm (3.2)

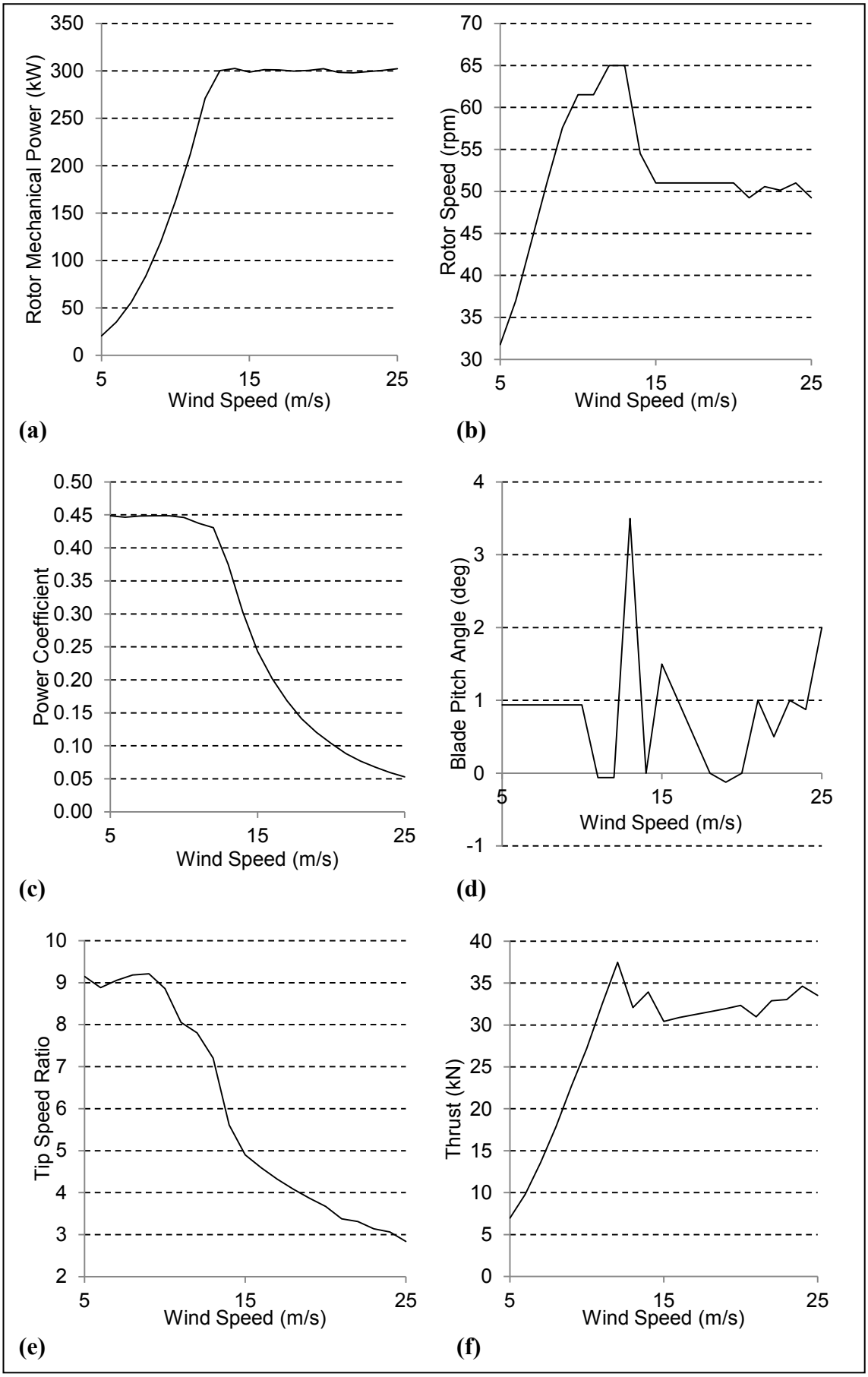

Figure 3.13- Results of simulation of variable-speed pitch-controlled AWT-27

Figure (3.13) shows the results of this simulation. Referring to Figure (3.13.c), it can be observed that the power coefficient curve, as expected, is horizontal at lower wind speeds and decreases as the power remains constant at higher wind speeds. The rotor speed shown in Figure (3.13.b), as expected, increases with wind speed at lower wind speeds until it reaches its upper bound (here 65 rpm). The second part of the rotor speed curve at higher wind speeds indicates that the rotor speed does not vary significantly as the wind speed changes. This behaviour is different from that of the variable speed stall regulated (see Figure (3.7.b)). This is mainly due to having two controls (rotor speed and blade pitch angle) and that rotor power is more sensitive to the blade pitch angle rather than the rotor speed in this region.

The form of the tip speed ratio curve shown in Figure (3.13.e) is also different from that of variable speed stall regulated wind turbine. It can be observed that the tip speed ratio reduces from about 9 for wind speeds up to 10m/s to about 8 at wind speed of about 12 m/s, while the power coefficient remains constant for wind speeds up to about 12 m/s. This figure confirms that the traditional method of finding rotor speed, in which the rotor speed is found such that the tip speed ratio is retained constant at its design value, is not valid for variable speed rotors which utilise an additional control system.

3.6 Aerodynamic Performance of Wind Turbines with Blades Utilising Flap

In case of blades utilising flap, in addition to the parameters defining the topology and geometry of the blade $\{R, c, \beta_0, AF, t_{\max}\}$, three more parameters are also required to define the location and size of the flap:

- Inboard radial location $R_{F,s}$
- Outboard radial location $R_{F,e}$
- Width of the flap as a fraction of the chord length at the centre of the flap $d_F^* = \frac{d_F}{c_F}$.

These parameters are shown in Figure (3.14).

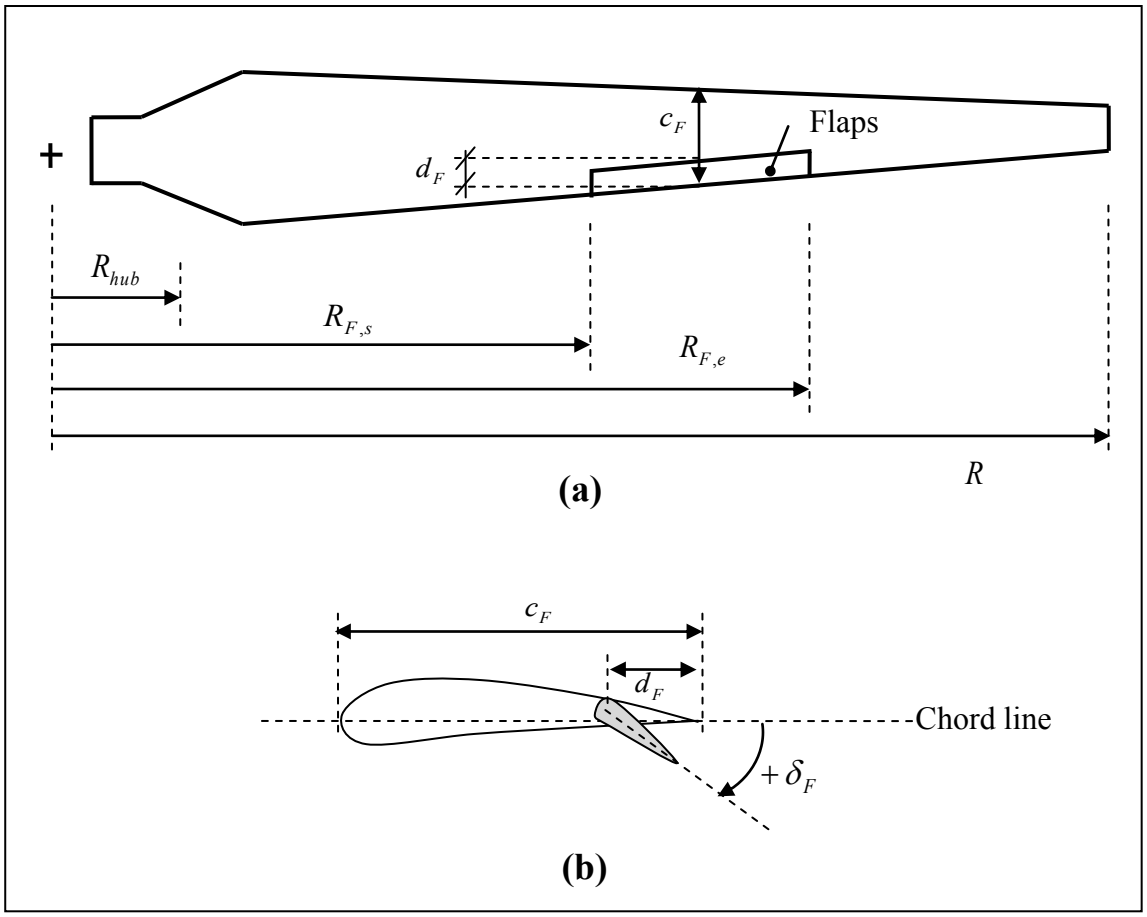

Figure 3.14-(a) Parameters defining location and size of flap, (b) Flap deployment angle sign convention

3.6.1 Modifications Applicable to the Aerodynamic Performance Calculator

A deployed flap changes lift and drag coefficients. These changes can be presented as:

$$\Delta C_L|_{\delta_F} = C_L|_{\delta_F} - C_L|_{\delta_F=0} \tag{3.4}$$

$$\Delta C_D|_{\delta_F} = C_D|_{\delta_F} - C_D|_{\delta_F=0} \tag{3.5}$$

in which, respectively, $\Delta C_L|_{\delta_F}$ and $\Delta C_D|_{\delta_F}$ are changes in lift and drag coefficients due to a deployment of δ_F, $C_L|_{\delta_F}$ and $C_D|_{\delta_F}$ are the lift and drag coefficients at that deployment angle, and $C_L|_{\delta_F=0}$ and $C_D|_{\delta_F=0}$ are the original lift and drag coefficients (as there is no flap or no flap deployment $\delta_F = 0$). All these parameters depend on the aerofoil angle of attack α as well. Figures (3.15) and (3.16) show two dimensional (infinite length) ΔC_L and ΔC_D as functions of angle of attack, α and flap deployment angle, δ_F. These results are obtained for aerofoil S808 with a flap width of 10% of chord length ($d_F^* = d_F/c_F = 0.1$) by running software XFOIL (Drela 1987, 1988, 1989a, 1989b, 1989c, 1990, 1998, 2008) as reported by Macquart (2012).

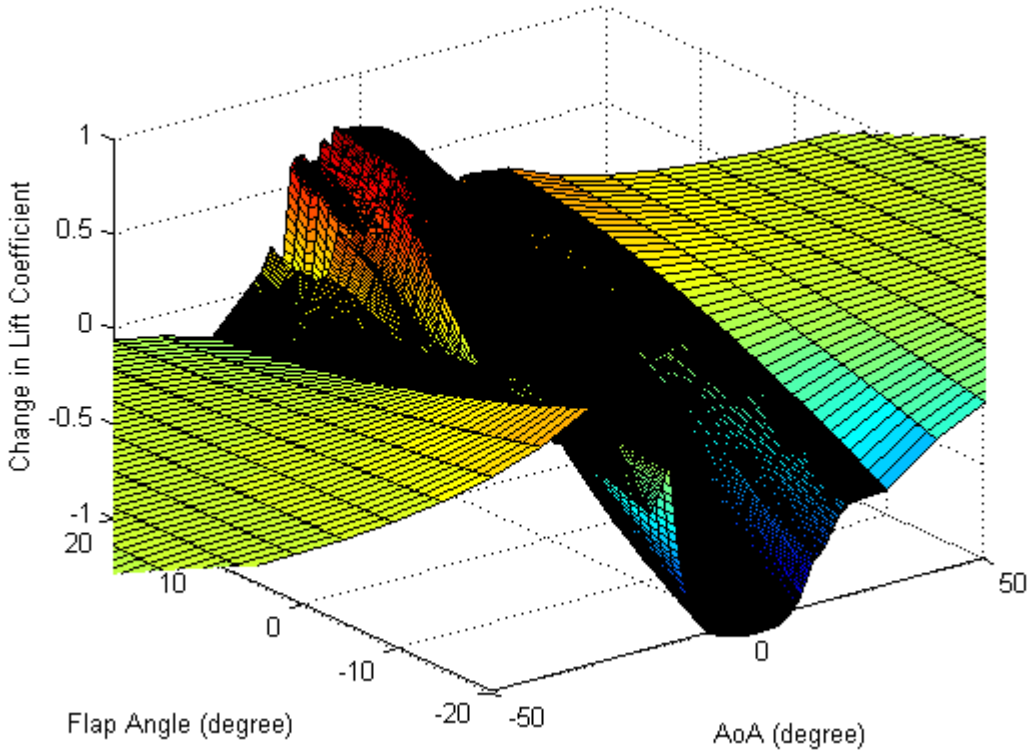

Figure 3.15- ΔC_L variation against angle of attack, α and flap deployment angle, δ_F

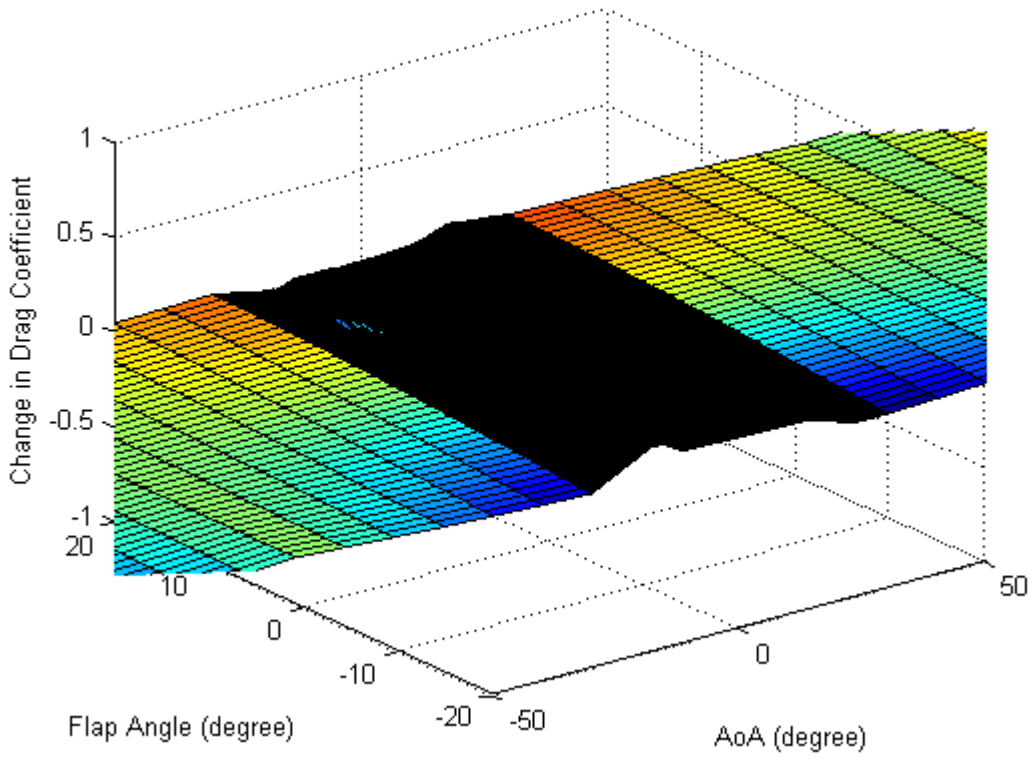

Figure 3.16- ΔC_D variation against angle of attack, α and flap deployment angle, δ_F

Since tabulated data $\Delta C_L(\alpha, \delta_F)$ and $\Delta C_D(\alpha, \delta_F)$ are three dimensional, reading off data from these tables requires interpolations in two dimensions as explained in Algorithm (3.3).

Algorithm 3.3-Reading $\Delta C_L(\alpha, \delta_F)$ and $\Delta C_D(\alpha, \delta_F)$ from 3-D tabulated data

Given:

- Aerofoils angle of attack α and flap deployment angle δ_F
- $\Delta C_L(\alpha, \delta_F)$ and $\Delta C_D(\alpha, \delta_F)$ tabulated data

Step 1- Find δ_F^- and δ_F^+, the closest flap angles in the data file to δ_F and α^- and α^+, the closest angles of attack to α.

Step 2- Using linear interpolation between $\Delta C_L(\alpha^-, \delta_F^-)$ and $\Delta C_L(\alpha^-, \delta_F^+)$ find $\Delta C_L(\alpha^-, \delta_F)$

Step 3- Using linear interpolation between $\Delta C_L(\alpha^+, \delta_F^-)$ and $\Delta C_L(\alpha^+, \delta_F^+)$ find $\Delta C_L(\alpha^+, \delta_F)$

Step 4- Using linear interpolation between $\Delta C_L(\alpha^-, \delta_F)$ and $\Delta C_L(\alpha^+, \delta_F)$ find $\Delta C_L(\alpha, \delta_F)$

Step 5- Repeat Step 2 to 4 for ΔC_D

In order to analyse the aerodynamic performance of a wind turbine with blades utilising flaps, the BEMT calculator of Algorithm (2.2) requires some modification as shown by red boxes in Algorithm (3.4).

Algorithm 3.4-Modified BEMT calculator for blades utilising flap

Given:

- …
- $\{R^*_{F,s}, R^*_{F,e}, d^*_F\}$ and δ_F

Step 5- …

Step 6- Dimensionalise … $R_{F,s}$, $R_{F,e}$

…

4.1.3.5 Use α_i read off life and drag coefficients from tables: $C_{L,i}$ and $C_{D,i}$

4.1.3.6 If $R_{F,s} \le r_i \le R_{F,e}$: Using δ_F and α_i read off lift and drag coefficient corrections (ΔC_L and ΔC_D) from the table corresponding to d^*_F (Algorithm 3.3); $C_{L,i} \leftarrow C_{L,i} + \Delta C_L$ and $C_{D,i} \leftarrow C_{D,i} + \Delta C_D$

4.1.3.7 Calculate thrust coefficient at zero lift:

$$C_{T_0} = \frac{\sigma_{r,i} \cos^2 \delta (1-a)^2 C_{L,i} \cos \varphi_i}{\sin^2 \varphi_i}$$

…

3.6.2 Control Simulation of Constant Speed Rotors with Blades Utilising Flap

Here, the flap deployment angle is the controlling parameter to be found by solving the optimisation problem of Equation (3.3). In order to observe the effect of the flap deployment angles on the rotor mechanical power, it is assumed that the blades of the baseline AWT-27 wind turbine are utilised by flaps with relative depth of $d^*_F = 0.1$ extended from $R^*_{F,s} = R_{F,s}/R = 0.6$ to $R^*_{F,e} = R_{F,e}/R = 0.65$. Simulating the wind turbine for various flap deployment angles $-20^\circ \le \delta_F \le 20^\circ$, the rotor power at different wind speeds is obtained and shown in Figure (3.17). According to this figure, one can observe that at different wind speeds the $P - \delta_F$ curves have one optimum point only. It can be seen that in all cases, if the initial point in a hill-climbing algorithm is taken as the upper limit $\delta_{F,0} = \delta_{F,u}$ with a search direction from right to left, the algorithm will find the feasible global optima. Hence, a similar hill-climbing method as in Algorithm (3.1), in which Ω is replaced by δ_F, can be used to find the optimum flap deployment angle at each wind speed. In order to examine the performance of this algorithm, using an initial $step = (\delta_{F,u} - \delta_{F,l})/10 = 4^\circ$, a power tolerance

$\varepsilon_P = 0.01P_{rated} = 3kW$ and a flap deployment angle tolerance of $\varepsilon_{\delta_F} = 0.1^\circ$ simulation of AWT-27 with blades utilising flaps is carried out. In this simulation flap deployment angle is limited to the lower and upper bound $\delta_{F,l} = -20^\circ$ and $\delta_{F,u} = 20^\circ$ respectively. Figure (3.18) shows the results of this simulation.

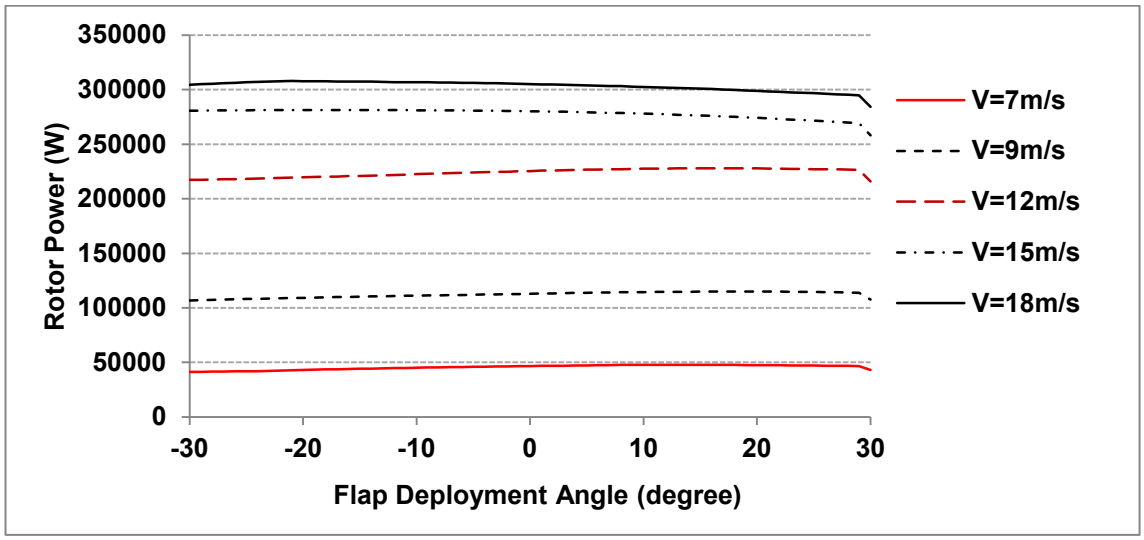

Figure 3.17-Power-flap deployment ($P - \delta_F$) curves at different wind speeds

Referring to Figure (3.18.a), it can be observed that the power curve at high wind speeds does not remain horizontal. In fact it is very similar to that of the baseline constant speed stall regulated wind turbine (see Figure 2.12). This indicated that the flap used in this simulation is not aerodynamically efficient enough. This is in agreement with the $P - \delta_F$ curves shown in Figure (3.17) showing that rotor power has little sensitivity to the variation of flap deployment angle δ_F .

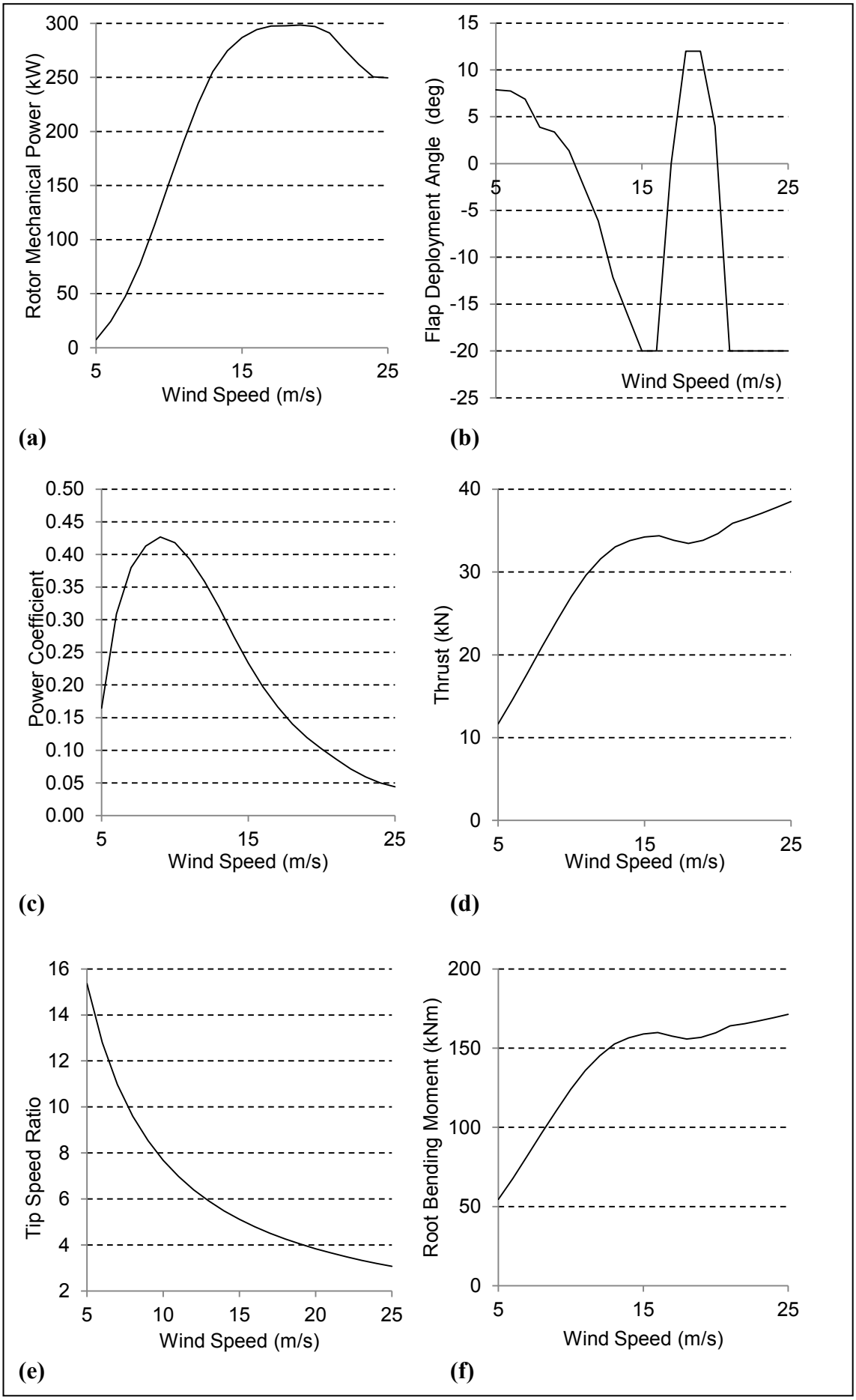

Figure 3.18- Results of simulation of constant-speed flap-controlled AWT-27

3.6.3 Control Simulation of Variable Speed Rotors with Blades Utilising Flap

Similar to the case of variable-speed pitch-controlled blades, here first an exhaustive search is carried out to observe the behaviour of the output power as a function of the controlling parameters rotor speed and flap deployment angle. Figure (3.19) shows the results for four typical wind speeds. To generate this figure the following data was used: flap extended between $R^*_{F,s} = 0.6$ and $R^*_{F,e} = 0.65$ of blade span with a relative depth of $d^*_F = 0.1$, flap deployment angle lower and upper limits $\delta_{F,l} = -20^\circ$ and $\delta_{F,u} = 20^\circ$; rotor speed lower and upper limits $\Omega_l = 30rpm$ and $\Omega_u = 65rpm$; 4° grid size in δ_F-direction and $3.5rpm$ in rotor speed-direction.

Comparing Figure (3.19) to Figure (3.10) (variable speed pitch controlled) one can observed that the contours in Figure (3.19) are very close to vertical lines, showing that the power is more sensitive to the rotor speed rather than the flap deployment angle. Nevertheless, the same pattern search method as in Algorithm (3.2) can be used for finding the optimum rotor speed and flap angle when *pitch* is replaced with δ_F.

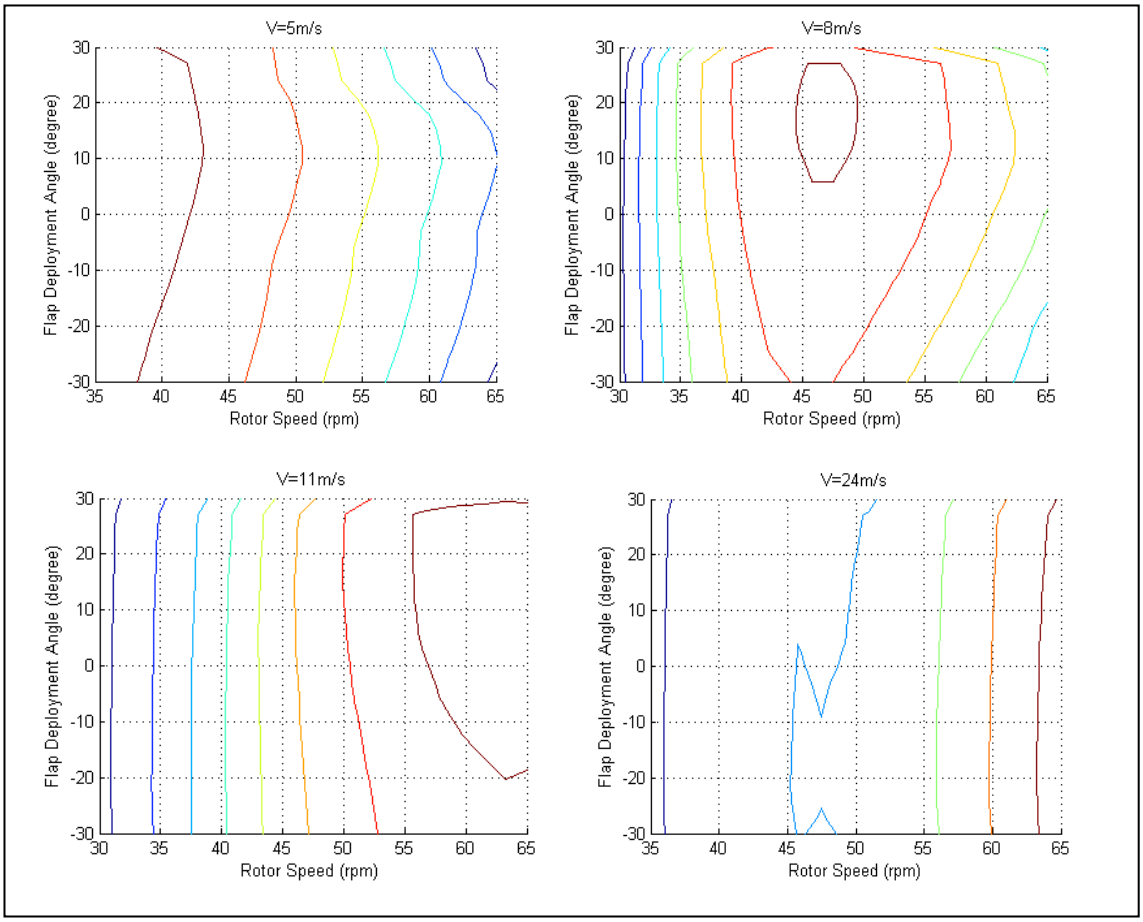

Figure 3.19-Rotor power versus rotor speed and flap deployment angle at various wind speeds

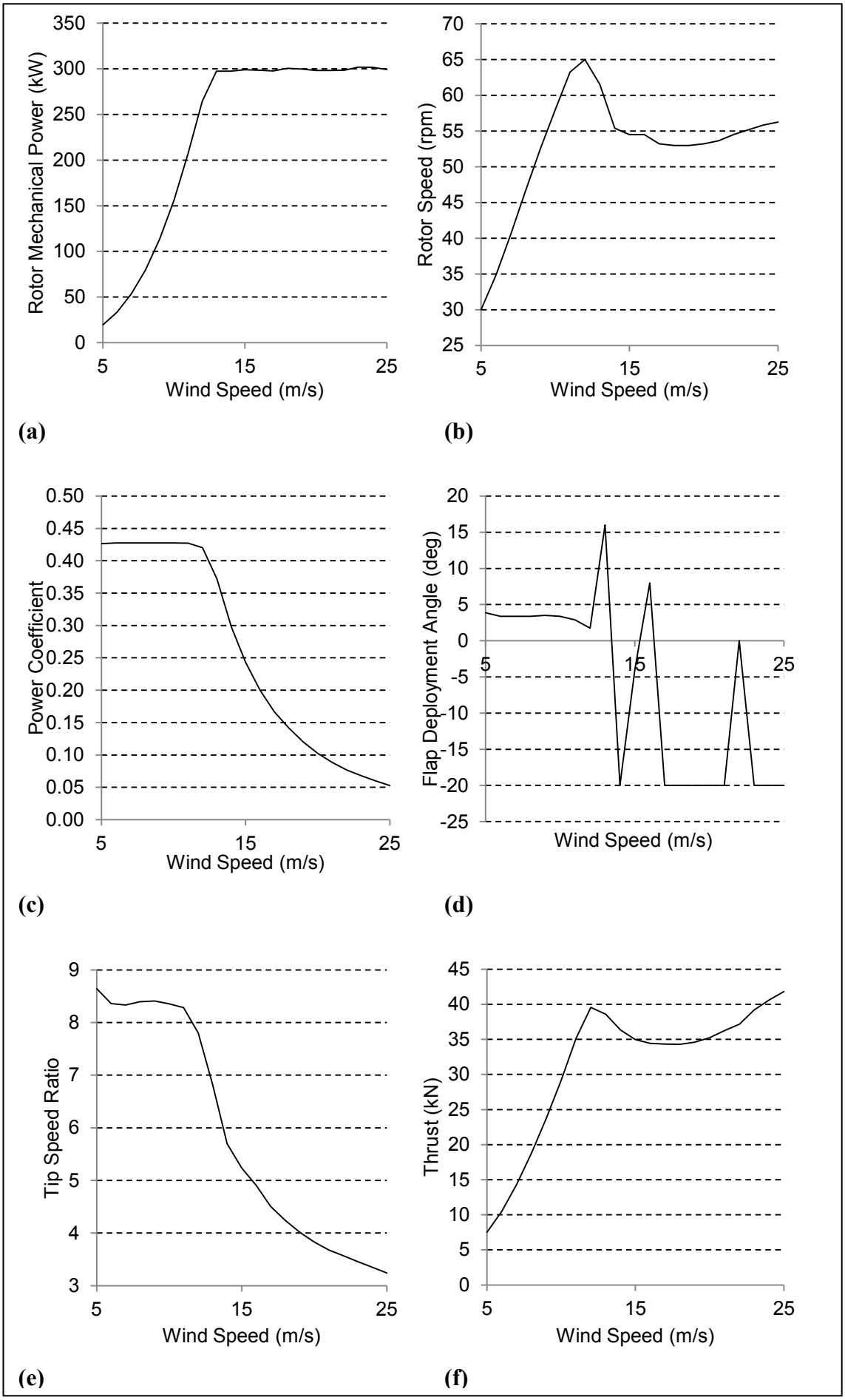

Figure 3.20- Result of simulation of variable-speed flap-controlled AWT-27

Simulation of AWT-27 wind turbine as a variable speed flap controlled wind turbine with the following search parameters leads to the results shown in Figure (3.20).

- Flap: $\delta_{F,l} = -20^\circ, \delta_{F,u} = 20^\circ, step_{\delta_F} = (\delta_{F,u} - \delta_{F,l})/10 = 4^\circ$, $\varepsilon_{\delta_F} = 0.1^\circ$
- Rotor speed: $\Omega_l = 30rpm, \Omega_u = 65rpm, step_\Omega = (\Omega_u - \Omega_l)/10 = 3.5rpm$, $\varepsilon_\Omega = 0.1rpm$
- Power tolerance: $\varepsilon_P = 0.01P_{rated} = 3kW$

Comparing the power coefficient curve of this wind turbine shown in Figure (3.20.a) (with a maximum value of about 0.427) with that of variable speed pitch controlled shown in Figure (3.13.a) (with a maximum value of about 0.45), it can be observed that pitch control is generally more efficient than flap control.

Figure (3.21) compares the power curve of the variable speed flap controlled wind turbine with variable speed stall regulated wind turbine. These two wind turbines are the same except the former is also equipped with flaps. One can observe that the power curves are almost identical (slight difference in the horizontal section is due to using a tolerance of $\varepsilon_P = 3kW$ for the power rather than different performances). This leads one to conclude that once flaps are used in conjunction with another controlling system, such as rotor speed, the accompanied controlling system dominates the control process. In other words, there is no advantage of using flaps on variable speed wind turbines for the purpose of power enhancement.

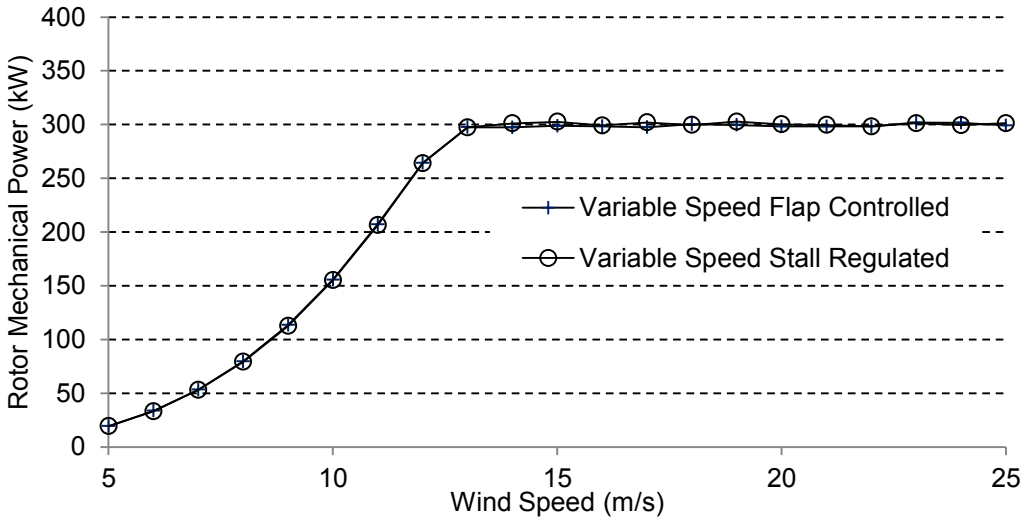

Figure 3.21-Comparison of power curves for variable speed flap controlled and variable speed stall regulated wind turbines

3.7 Aerodynamic Performance of Wind Turbines with Telescopic Blades

Figure (3.22) shows the concept of a telescopic blade. A telescopic blade has a fixed part attached to the hub and an extendable part. Rotor radius R_T is variable. It is limited between $R_{T,s}$ the span of the fixed part of the blade, Figure (3.22.b), and $R_{T,e}$ when the telescopic part is fully deployed, Figure (3.22.c). While the fixed part of the blade, like conventional wind turbine blades, can have variable chord length and pretwist distributions and can be made of several aerofoils, the telescopic part is not pretwisted; it has a constant chord length (c_T),) and is made of one single aerofoil which is the same as the aerofoil of the fixed part at span location $r = R_{T,s}$.

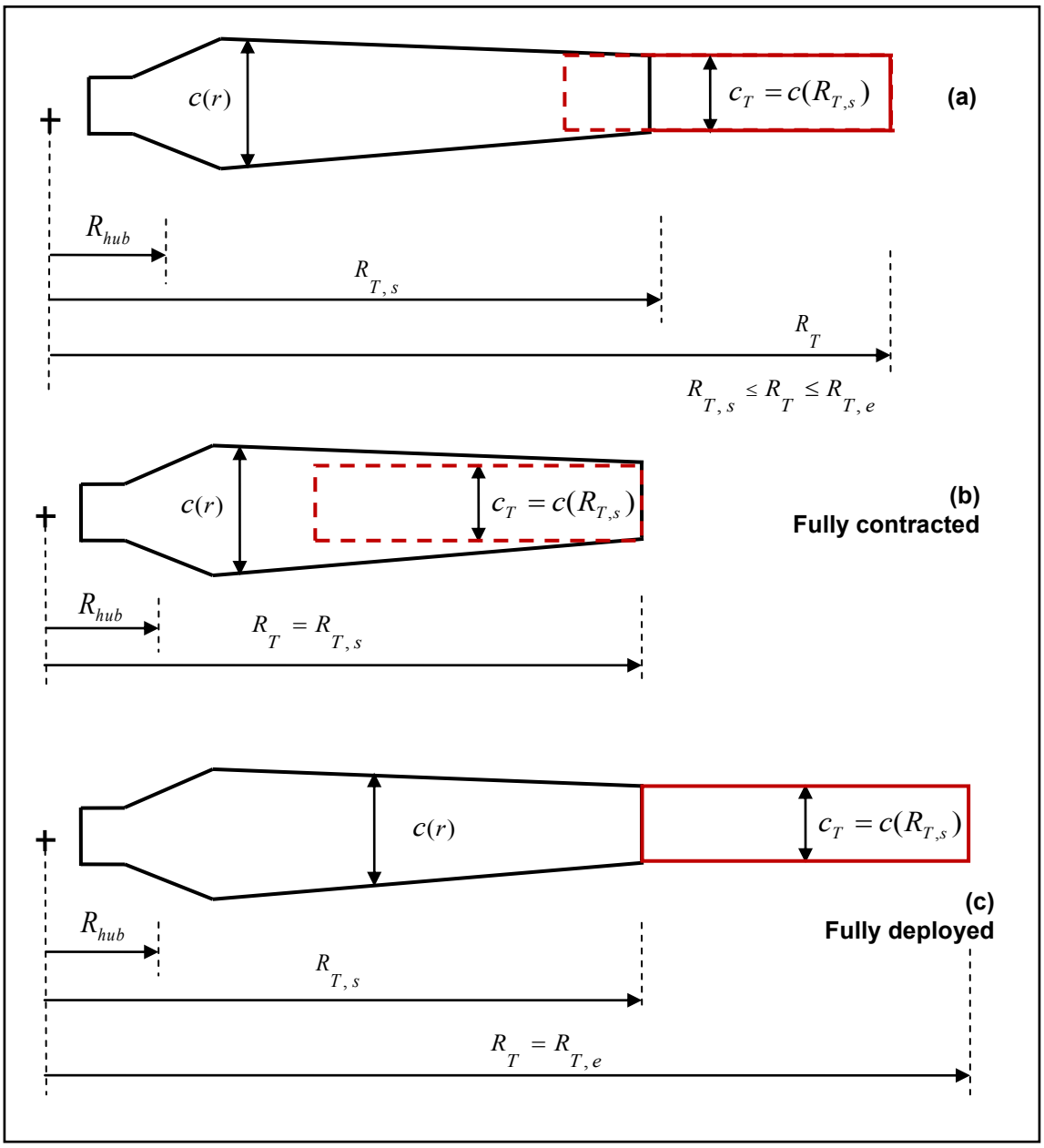

Figure 3.22-Telescopic blade definition

3.7.1 Modifications Applicable to the Aerodynamic Performance Calculator

In order to simulation a wind turbine with telescopic blades it is required to apply some modifications to the data file of the baseline blade. The telescopic blade data file is the same as the data file of the baseline blade for $r \le R_{T,s}$. For $r > R_{T,s}$ (the telescopic section) the aerofoil is $AF\left(R_{T,s}\right)$ and the chord length and pretwist distributions remain constant with values $c\left(R_{T,s}\right)$ and $\beta_0\left(R_{T,s}\right)$, respectively. It should be noted that the topology of the blade is defined against span location normalised rotor radius (R for baseline blade and R_T for telescopic). Therefore, the span location normalised by the rotor radius R, $r^* = r/R$ in the baseline data file should be converted to $r^* = r/R_T$ in the telescopic blade file. Algorithm (3.5) details steps for making telescopic blade data file based on a baseline blade data file.

Algorithm 3.5-Modification of the data file of the baseline blade for a telescopic blade

Given:

- Original blade data file $\{R, R^*_{hub}, c^*(r^*), \beta_0(r^*), AF(r^*)$ and $t^*_{\max}(r^*)\}$
- $R^*_{T,s}$ and R^*_T; $(R^*_{T,s} \le R^*_T \le R^*_{T,e})$

Step 1- Find $c^*(R^*_{T,s}), \beta_0(R^*_{T,s}), AF(R^*_{T,s})$ and $t^*_{\max}(R^*_{T,s})$

Step 2- In the original blade file, remove all data for $r^* > R^*_{T,s}$ and replace them with values calculated in Step 1 at $r^* = R^*_{T,s}$ and $r^* = R^*_{T,e}$:

$r^* = \frac{r}{R}$	$c^*(r^*) = \frac{c(r^*)}{R}$	$\beta_0(r^*)$	$AF(r^*)$	$t^*_{\max}(r^*) = \frac{t_{\max}(r^*)}{c}$
…	….	…	…	…
$R^*_{T,s}$	$c^*(R^*_{T,s})$	$\beta_0(R^*_{T,s})$	$AF(R^*_{T,s})$	$t^*_{\max}(R^*_{T,s})$
R^*_T	$c^*(R^*_{T,s})$	$\beta_0(R^*_{T,s})$	$AF(R^*_{T,s})$	$t^*_{\max}(R^*_{T,s})$

Step 3- Normalise the radial location in the new table by $R_T = R^*_T R$:

$r^* = \frac{r}{R_T}$	$c^*(r^*) = \frac{c(r^*)}{R_T}$	$\beta_0(r^*)$	$AF(r^*)$	$t^*_{\max}(r^*) = \frac{t_{\max}(r^*)}{c}$
…	….	…	…	…
$R^*_{T,s}\frac{R}{R_T}$	$c^*(R^*_{T,s})\frac{R}{R_T}$	$\beta_0(R^*_{T,s})$	$AF(R^*_{T,s})$	$t^*_{\max}(R^*_{T,s})$
$R^*_T\frac{R}{R_T} = 1$	$c^*(R^*_{T,s})\frac{R}{R_T}$	$\beta_0(R^*_{T,s})$	$AF(R^*_{T,s})$	$t^*_{\max}(R^*_{T,s})$

Step 4- $R^*_{hub} \leftarrow R^*_{hub}\frac{R_T}{R}$ and $R \leftarrow R_T$; save telescopic blade data file $\{R, R^*_{hub}, c^*(r^*), \beta_0(r^*), AF(r^*)$ and $t^*_{\max}(r^*)\}$

Table (3.4) (repeated Table (2.1)) contains the first part of the blade data file of AWT-27 wind turbine blade as the baseline. Tables (3.5) and (3.6) show the results of Steps 2 and 3 of Algorithm (3.5) applied to this blade for $R^*_{T,s} = 0.7$ and $R^*_T = 1.1$. Normalised chord distribution and pretwist distribution are shown in Figure (3.23).

Table 3.4-Baseline blade data

r^*	$c^*(r^*)$	$\beta_0(r^*)$
0.086	0.053	6.270
0.109	0.056	6.100
0.155	0.063	5.764
0.223	0.070	5.470
0.269	0.075	5.233
0.315	0.081	4.996
0.360	0.082	4.602
0.406	0.083	4.208
0.452	0.081	3.689
0.497	0.079	3.172
0.543	0.076	2.628
0.589	0.074	2.086
0.634	0.071	1.601
0.680	0.068	1.117
0.726	0.064	0.770
0.772	0.060	0.424
0.806	0.056	0.273
0.840	0.052	0.122
0.863	0.049	0.099
0.886	0.047	0.076
0.918	0.042	0.048
0.936	0.039	0.041
0.954	0.036	0.033
0.963	0.035	0.028
0.973	0.033	0.023
0.986	0.030	0.012
0.995	0.029	0.006
1.000	0.028	0.000

$r^* = r/R, c^* = c/R$

Table 3.5-Data at the end of Step 2 of Algorithm (3.5)

r^*	$c^*(r^*)$	$\beta_0(r^*)$
0.086	0.053	6.270
0.109	0.056	6.100
0.155	0.063	5.764
0.223	0.070	5.470
0.269	0.075	5.233
0.315	0.081	4.996
0.360	0.082	4.602
0.406	0.083	4.208
0.452	0.081	3.689
0.497	0.079	3.172
0.543	0.076	2.628
0.589	0.074	2.086
0.634	0.071	1.601
0.680	0.068	1.117
0.700	0.066	0.966
1.100	0.066	0.966

$r^* = r/R, c^* = c/R$

Table 3.6-Telescopic blade data file (at the end of Step 3 of Algorithm (3.5))

r^*	$c^*(r^*)$	$\beta_0(r^*)$
0.078	0.048	6.270
0.099	0.051	6.100
0.141	0.057	5.764
0.203	0.064	5.470
0.244	0.068	5.233
0.286	0.073	4.996
0.328	0.075	4.602
0.369	0.076	4.208
0.411	0.074	3.689
0.452	0.072	3.172
0.494	0.070	2.628
0.535	0.067	2.086
0.577	0.064	1.601
0.618	0.062	1.117
0.636	0.060	0.966
1.000	0.060	0.966

$r^* = r/R_T, c^* = c/R_T$

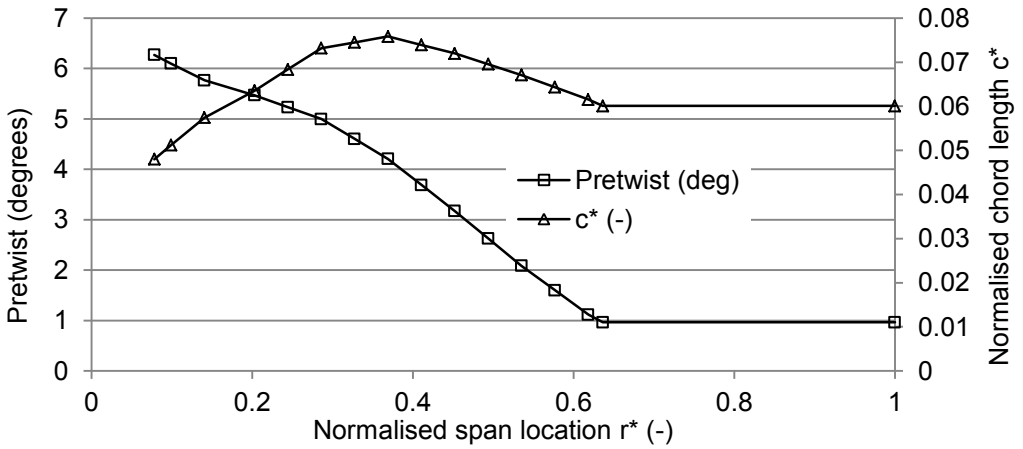

Figure 3.23-Telescopic blade chord and pretwist distribution ($r^* = r/R_T, c^* = c/R_T$).

3.7.2 Control Simulation for Constant Speed Rotors with Telescopic Blades

Here, the rotor radius R_T is the only controlling parameter. The same hill climbing search method as explained in Algorithm (3.1), can be used to find the optimum value of R_T. For each examined R_T within the search, the blade topology changes. Hence it is required to modify the blade data file and discretise the blade for each examined R_T. Algorithm (3.6) details the modified hill climbing method for control simulation of constant speed wind turbines with telescopic blades.

Algorithm 3.6- Hill climbing search for finding optimum rotor radius (R_T) for constant speed telescopic blade wind turbines

Given:

- $step_{R_T^*}, \varepsilon_{R_T^*}, R_{T,s}^*, R_{T,e}^*, \varepsilon_P$
- All parameters required for running Algorithm 2.2

Step 1- Initialise: $R_{T,0}^* \leftarrow R_{T,e}^*$

Step 2- Start with $R_T^* \leftarrow R_{T,0}^*$

2.1. produce telescopic blade data file (Algorithm 3.5)
2.2. discretise the blade (Algorithm 2.1)
2.3. simulate wind turbine to find P (Algorithm 2.2); $P_0 \leftarrow P$.

Step 3- While $\left(step_{R_T^*} > \varepsilon_{R_T^*}\right) \wedge \left|P - P_{rated}\right| > \varepsilon_P$ do:

3.1. $R_T^* \leftarrow R_{T,o}^* - step_{R_T^*}$

3.1.1. produce telescopic blade data file (Algorithm 3.5).
3.1.2. discretise the blade (Algorithm 2.1)
3.1.3. simulate wind turbine to find P (Algorithm 2.2)

3.2. If $\left(P > P_0 \wedge P < P_{rated}\right) \vee \left(P < P_0 \wedge P > P_{rated}\right) \vee \left(P > P_0 \wedge P_0 > P_{rated}\right)$, then $R_{T,0}^* \leftarrow R_{T,0}^* - step_{R_T^*}, P_0 \leftarrow P$; Else: Half the step: $step_{R_T^*} = 0.5 step_{R_T^*}$

Figure (3.24) shows the results of simulating AWT-27 wind turbine with telescopic blades using the following data: $step_{R_T^*} = 0.1, \varepsilon_{R_T^*} = 0.001, R_{T,s}^* = 0.7, R_{T,e}^* = 1.1$ and $\varepsilon_P = 3kW$.

Referring to Figure (3.24.b), it can be observed that, as expected, at higher wind speeds (14m/s and above) the blade is contracted to maintain the rotor power at its rated value by reducing the rotor area. Interestingly, at wind speeds of 5 and 6 m/s the telescopic blade is not fully extended as opposed to what is expected. The reason for this can be explained by referring to Figure (3.25).

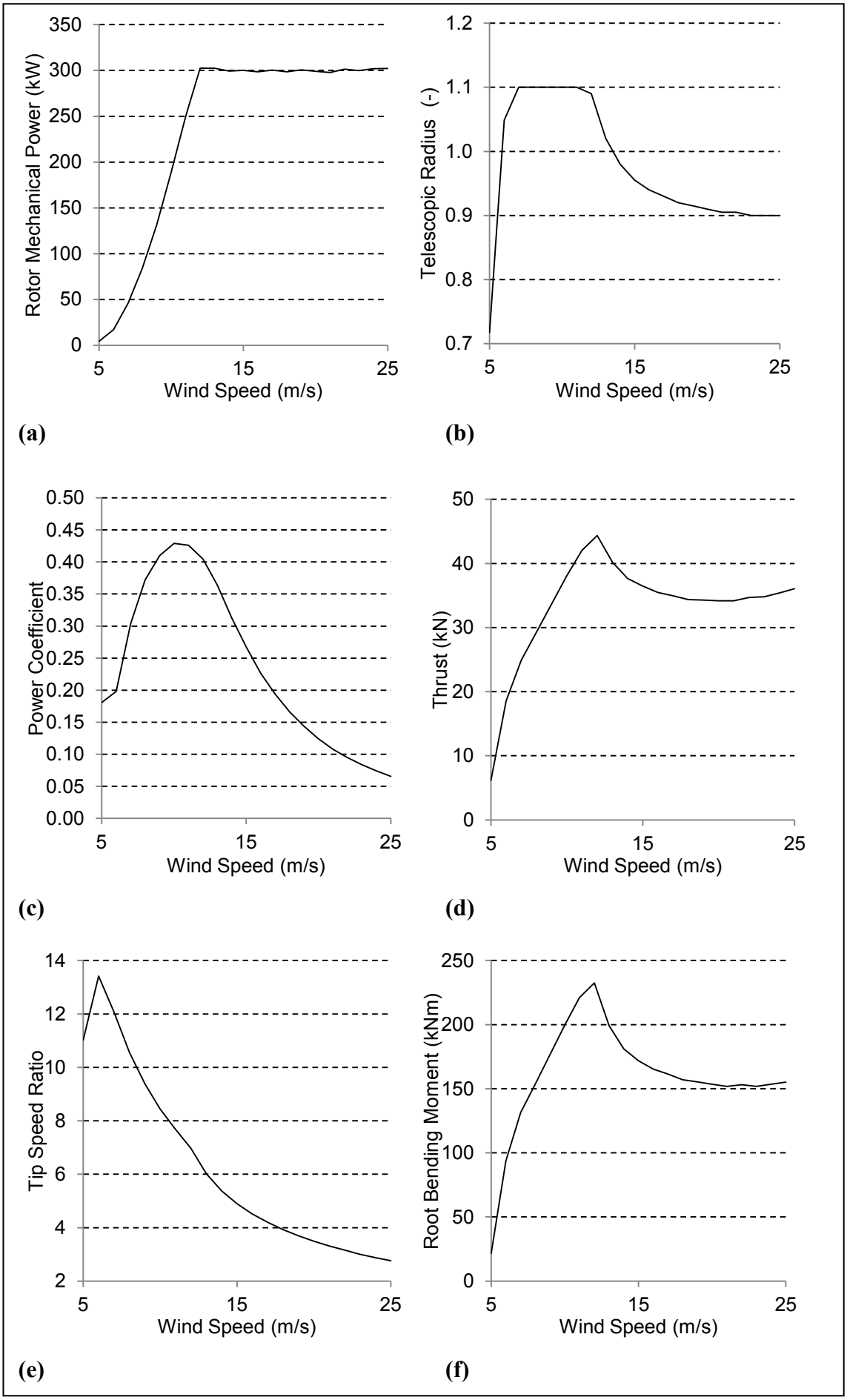

Figure 3.24- Result of simulation of constant-speed telescopic blade AWT-27

In Figure (3.25) the torque produced by each blade segment at wind speed 5m/s is plotted against the radial location of that segment. It can be seen that at rotor span locations above 0.73R, the produced torque by each segment is negative. This is due to the fact that the telescopic part of the blade is not pretwisted and consequently the flow kinematics is not optimised (also, see Equation (2.45)).

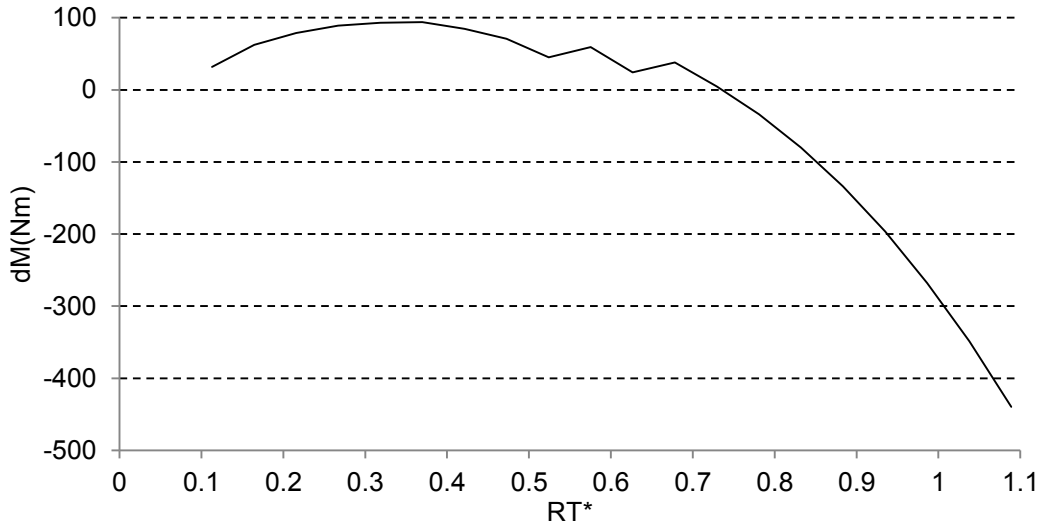

Figure 3.25- Torque produced by each blade segment at wind speed 5m/s against the radial location

Comparing the thrust curve of Figure (3.24.d) with the thrust curves of Figures (3.7.d), (3.9.d), (3.13.f), (3.18.d) and (3.20.f), it can be observed that the maximum thrust force for wind turbines utilising telescopic blades is higher than other types of wind turbines. This is due to utilising larger blades.

3.7.3 Control Simulation for Variable Speed Rotors with Telescopic Blades

Having two controlling parameters, namely, the rotor radius R_T and the rotor speed Ω, the same pattern search method as explained in Algorithm (3.2), can be used to find the optimum values of R_T and Ω. Similar to constant speed telescopic blades for each examined R_T within the search, the blade data file should be created and the blade should be discretised. Algorithm (3.7) details the modified pattern search method for control simulation of variable speed wind turbines with telescopic blades.

Figure (3.26) shows the results of simulating AWT-27 wind turbine with telescopic blades and a variable speed rotor using the following data: $step_{R_T^*} = 0.1, \varepsilon_{R_T^*} = 0.001$,

$R^*_{T,s} = 0.7$, $R^*_{T,e} = 1.1$, $\Omega_l = 30rpm$, $\Omega_u = 65rpm$, $step_\Omega = 3.5rpm$, $\varepsilon_\Omega = 0.1rpm$ and $\varepsilon_P = 3kW$.

Comparing the variation of the telescopic blade radius of variable speed (Figure (3.26.d)) with that of constant speed (Figure (3.24.b)), it can be observed that while for the case of constant speed, the span of the telescopic blade is gradually decreases with wind speed, in case of variable speed the span is fluctuating. This is due to the fact that the blade span becomes the dominant controlling parameter because the rotor mechanical power is more sensitive to the rotor diameter ($P \propto D^3$) rather than rotor speed ($P \propto \Omega$).

Algorithm 3.7-Pattern search method for finding optimum rotor speed and rotor radius for variable speed telescopic blade

Given:

- $step_{R^*_T}, \varepsilon_{R^*_T}, R^*_{T,s}, R^*_{T,e}, step_\Omega, \varepsilon_\Omega, \Omega_l, \Omega_u, \varepsilon_P$
- All parameters required for running Algorithm 2.2 except Ω

Step 1- Initialise: $\left(R^*_{T,0}, \Omega_0\right) \leftarrow \left(R^*_{T,0}, \Omega_u\right)$

Step 2- Start with $\left(R^*_{T,0}, \Omega_0\right)$

2.1. produce telescopic blade data file (Algorithm 3.5)
2.2. discretise the blade (Algorithm 2.1)
2.3. simulate wind turbine to find P (Algorithm 2.2); $P_0 \leftarrow P$.

Step 3- While $\left(step_{R^*_T} > \varepsilon_{R^*_T}\right) \wedge \left(step_\Omega > \varepsilon_\Omega\right) \wedge \left|P - P_{rated}\right| > \varepsilon_P$ do:

3.1. Initialise $move_1 = 0$, $move_2 = 0$
3.2. Move in Ω-direction: For $\left(R^*_{T,0}, \Omega_0 - step_\Omega\right)$ simulate wind turbine to find P
3.3. If $\left(P > P_0 \wedge P < P_{rated}\right) \vee \left(P < P_0 \wedge P > P_{rated}\right) \vee \left(P > P_0 \wedge P_0 > P_{rated}\right)$, then $move_1 = 1$, $\Omega_0 \leftarrow \Omega_0 - step_\Omega$, $P_0 \leftarrow P$
3.4. Move in R^*_T-direction: For $\left(R^*_{T,0} - step_{R^*_T}, \Omega_0\right)$
  3.4.1. produce telescopic blade data file (Algorithm 3.5)
  3.4.2. discretise the blade (Algorithm 2.1)
  3.4.3. simulate wind turbine to find P (Algorithm 2.2)
3.5. If $\left(P > P_0 \wedge P < P_{rated}\right) \vee \left(P < P_0 \wedge P > P_{rated}\right) \vee \left(P > P_0 \wedge P_0 > P_{rated}\right)$, then $move_2 = 1$, $R^*_{T,0} \leftarrow R^*_{T,0} - step_{R^*_T}$, $P_0 \leftarrow P$
3.6. If $move_1 = 0 \wedge move_2 = 0$ then half the steps: $step_{R^*_T} = 0.5 step_{R^*_T}$, $step_\Omega = 0.5 step_\Omega$

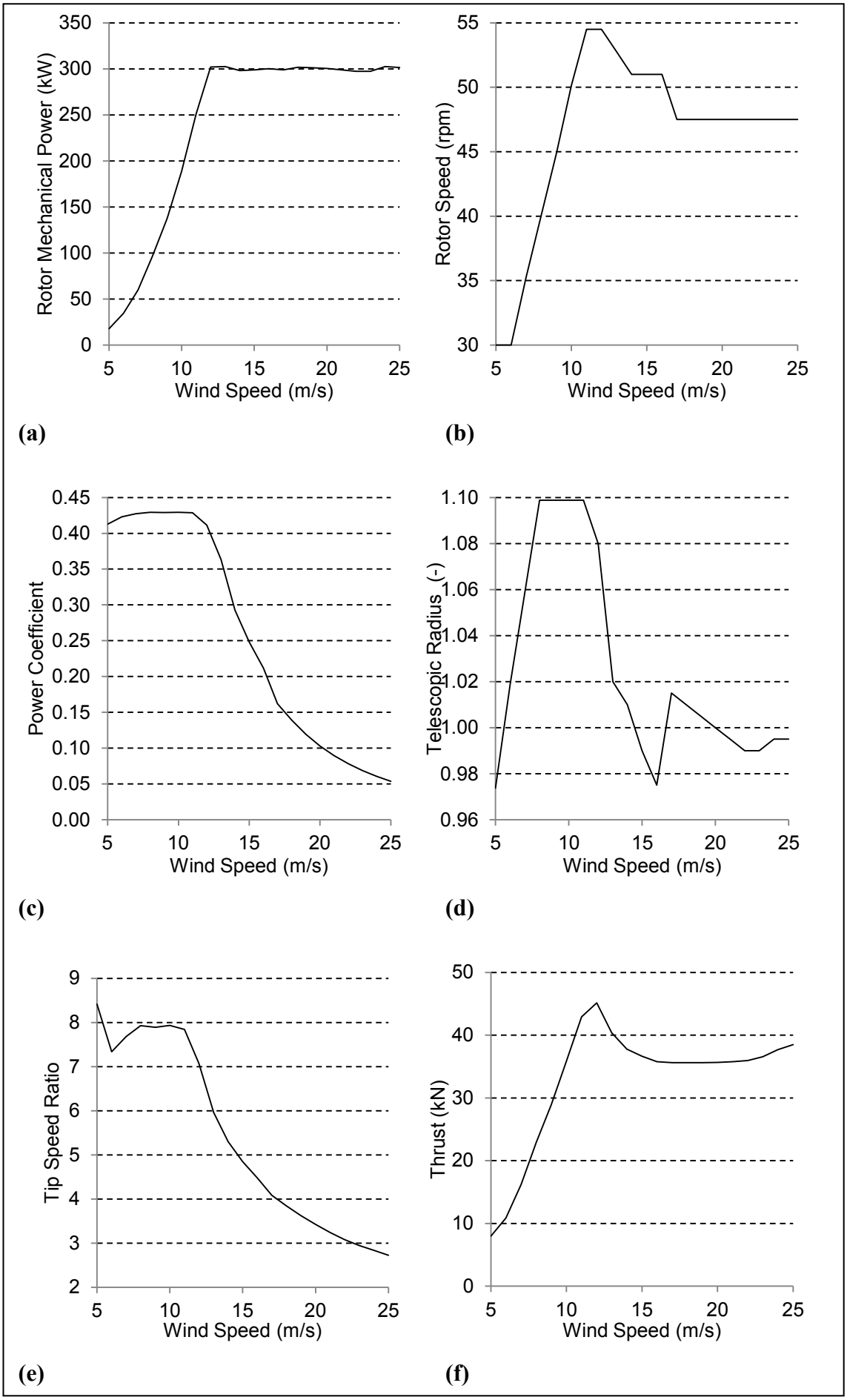

Figure 3.26- Result of simulation of variable-speed telescopic blade AWT-27

3.8 Aerodynamic Performance of Wind Turbines with Blades Utilising Microtabs

In addition to the parameters defining the topology and geometry of the blade $\{R, c, \beta_0, AF, t_{\max}\}$, the following parameters are also required to define a string of microtabs:

- Inboard radial location of string of microtabs $R_{MT,s}$
- Outboard radial location of string of microtabs $R_{MT,e}$
- Microtab distance from leading edge $d_{MT}^* = \dfrac{d_{MT}}{c_{MT}}$, in which c_{MT} is the chord length at the centre of microtab
- Microtab length s_{MT}
- Microtab actuation height $h_{MT}^* = \dfrac{h_{MT}}{c_{MT}}$

These parameters are shown in Figure (3.27).

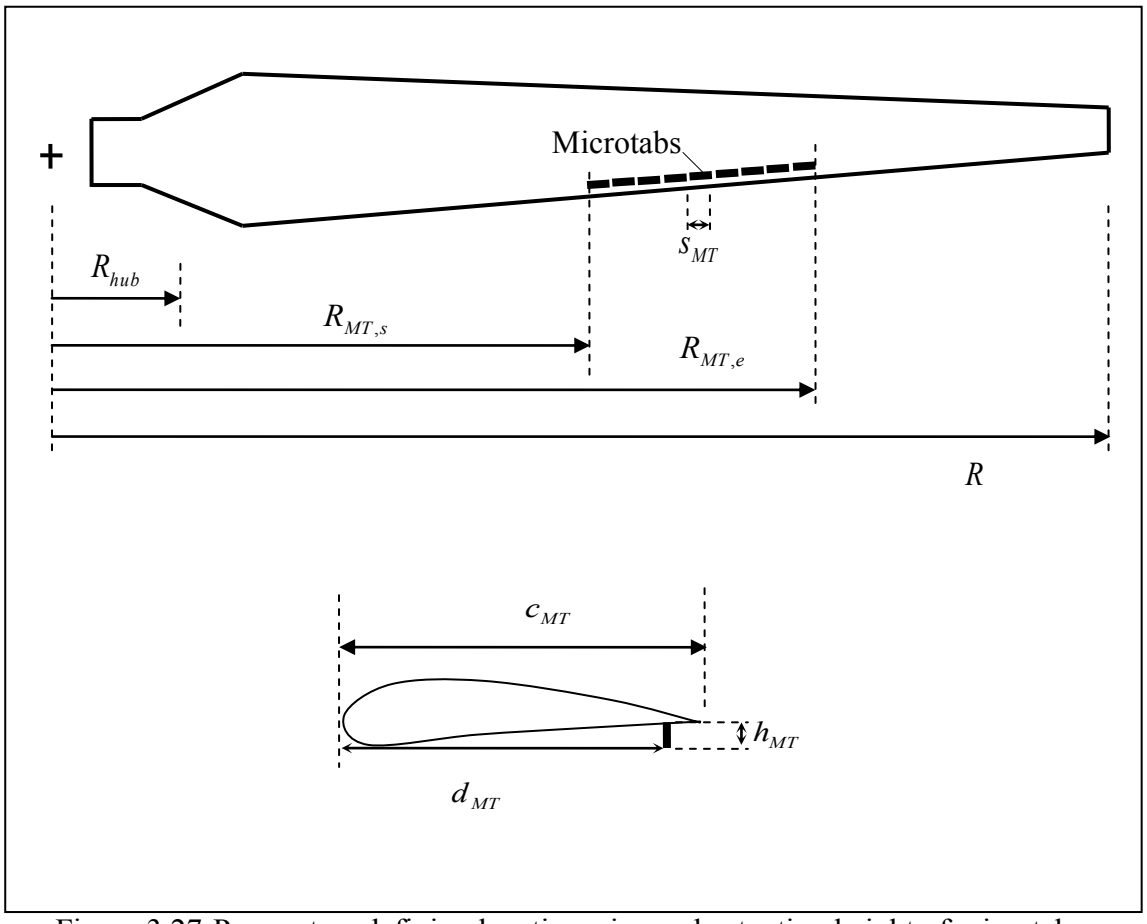

Figure 3.27-Parameters defining location, size and actuation height of microtabs

3.8.1 Modifications Applicable to the Aerodynamic Performance Calculator

A microtab can have three states, namely, deployed upward (on the suction side of the aerofoil), deployed downward (on the pressure side of the aerofoil), and neutral (not deployed). These states are coded by -1, +1 and 0 respectively. A deployed microtab changes lift and drag coefficients. These changes can be presented as:

$$\Delta C_L|_{MT} = C_L|_{MT} - C_L|_{MT=0} \;;\; MT \in \{-1,+1\} \tag{3.6}$$

$$\Delta C_D|_{MT} = C_D|_{MT} - C_D|_{MT=0} \;;\; MT \in \{-1,+1\} \tag{3.7}$$

in which, respectively, $\Delta C_L|_{MT}$ and $\Delta C_D|_{MT}$ are changes in lift and drag coefficients due to deployment of a microtab upward ($MT = -1$) or downward ($MT = +1$), $C_L|_{MT}$ and $C_D|_{MT}$ are the actual lift and drag coefficients due to the presence of the microtab angle, and $C_L|_{MT=0}$ and $C_D|_{MT=0}$ are the original lift and drag coefficients (as there is no microtab or the microtab is in neutral state $MT = 0$). All these parameters depend on the aerofoil angle of attack α as well. Figures (3.28) through (3.31) show ΔC_L and ΔC_D as functions of angle of attack, α, microtab distance from leading edge d^*_{MT}, and microtab actuation height h^*_{MT}. These results are obtained for aerofoil S808 by CFD analysis as reported by Hella (2012).

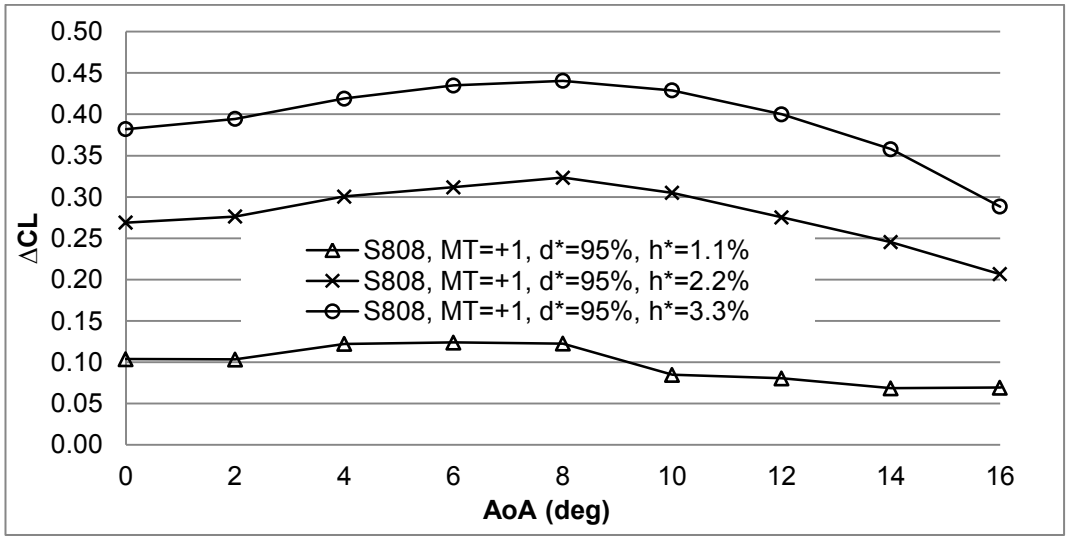

Figure 3.28- ΔC_L variation against angle of attack, microtab deployed downward

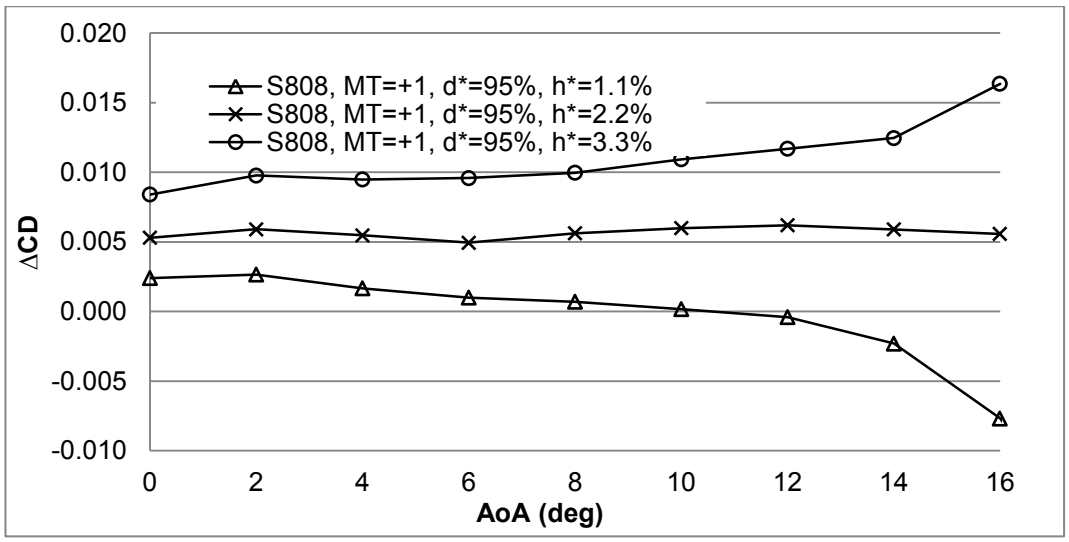

Figure 3.29- ΔC_D variation against angle of attack, microtab deployed downward

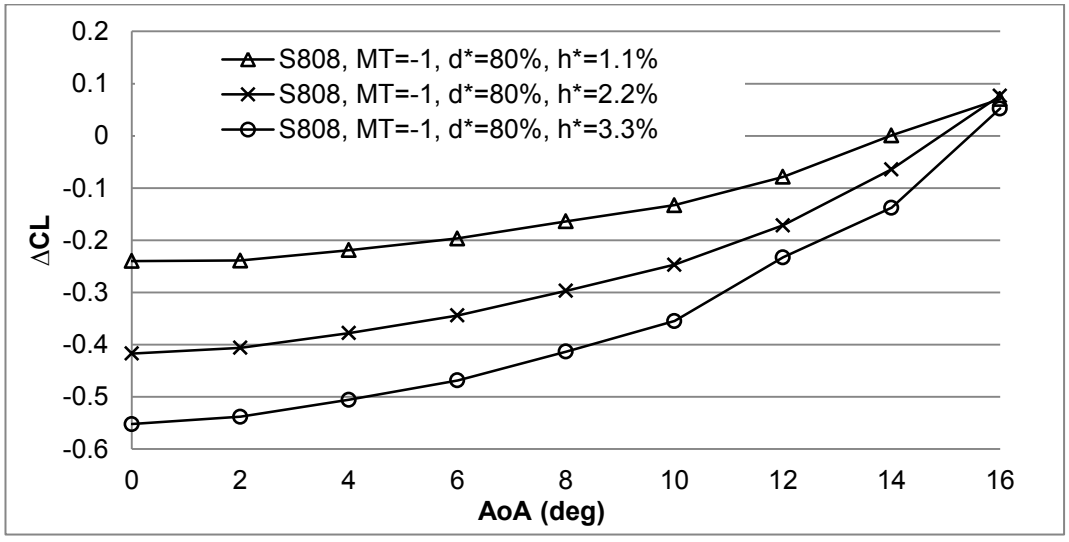

Figure 3.30- ΔC_L variation against angle of attack, microtab deployed upward

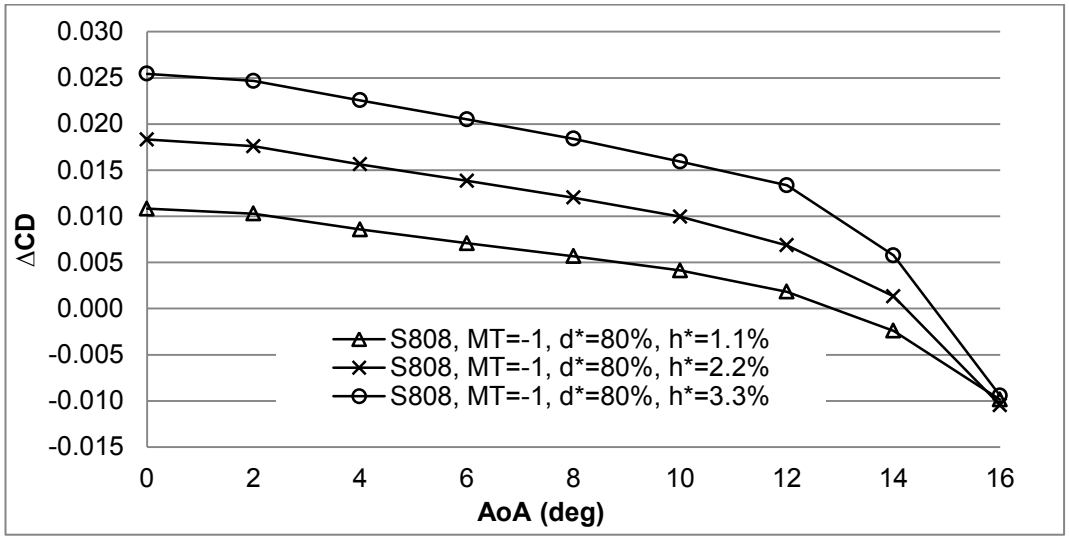

Figure 3.31- ΔC_D variation against angle of attack, microtab deployed upward

In order to analyse the aerodynamic performance of a wind turbine with blades utilising microtabs, the BEMT calculator of Algorithm (2.2) requires some modification as shown by red boxes in Algorithm (3.8). Moreover, in discretisation of the blade (Algorithm (2.1)), the number of segments (n_{seg}) should be selected such that segment length (Δr) is equal to the length of microtabs (s_{MT}). By doing this the number of microtabs (N_{MT}) distributed between the inboard and outboard radial locations $R_{MT,s}$ and $R_{MT,e}$ will b the same as the number of segments between these two span locations.

Algorithm 3.8-Modified BEMT calculator for blades equipped with microtabs

Given:

- …
- $\left\{R^*_{MT,s}, R^*_{MT,e}, d^*_{MT}, h^*_{MT}, s_{MT}\right\}$ and the state of each microtab $MT_j \in \{-1,,0,+1\}$; $j = 1,2,...,N_{MT}$

Step 1- …

Step 2- Dimensionalise … $R_{MT,s}$, $R_{MT,e}$.

…

4.1.3.5 Use α_i read off lift and drag coefficients from tables: $C_{L,i}$ and $C_{D,i}$

4.1.3.6 If $R_{F,s} \le r_i \le R_{F,e}$: Using MT_j and α_i read off life and drag coefficient corrections (ΔC_L and ΔC_D) from the table corresponding to d^*_{MT} and h^*_{MT} ; $C_{L,i} \leftarrow C_{L,i} + \Delta C_L$ and $C_{D,i} \leftarrow C_{D,i} + \Delta C_D$

4.1.3.7 Calculate thrust coefficient at zero lift:

$$C_{T_0} = \frac{\sigma_{r,i} \cos^2 \delta (1-a)^2 C_{L,i} \cos \varphi_i}{\sin^2 \varphi_i}$$

3.8.2 Control Simulation of Constant Speed Rotors with Blades Equipped with Microtabs

Here, each of N_{MT} microtabs distributed between $R_{MT,s}$ and $R_{MT,e}$ acts as a controlling device and the state of each microtab $\{-1,0,+1\}$ becomes a controlling parameter which needs to be determined via solving the optimisation problem of Equation (3.3). In other words, we are dealing with N_{MT} controlling parameters. Since the length of each microtab (s_{MT}) is much smaller than the length of the portion of the blade equipped with microtabs, the number of microtabs can be large. This makes exhaustive search impractical as the total number of examined points in an exhaustive search is $3^{N_{MT}}$ (3 is the number microtab states). For example, for the case of $N_{MT} = 20$ Algorithm (3.8) is required to run about 3.5×10^9 times for each single wind speed. An N_{MT}-dimensional

pattern search is also highly inefficient. Genetic algorithms (GA), on the other hand, perform efficiently compared to other methods when dealing with large number of variables.

Algorithm (3.9) details the GA used for finding the optimum state of each microtab. In this algorithm, n_{pop}, n_{gen}, p_c and p_m are, respectively, number of population, number of generations, probability of crossover and probability of mutation. In this algorithm the fitness is defined as the rotor mechanical power ($fit = P$), parent selections for both crossover and mutation is a random process, and the constraint handling is based on rejection strategy (rejecting individuals contradicting the constraint $P \le P_{rated} + \varepsilon_P$).

Using this GA with the GA parameters $n_{pop} = 20$, $n_{gen} = 50$, $p_c = 0.3$ and $p_m = 0.2$, AWT-27 wind turbine with blades equipped with microtabs between $R^*_{MT,s} = 0.6$ and $R^*_{MT,e} = 0.9$ (where the blade is made of aerofoil S808) is simulated. Using 20segments for discretising the blade, a string of 7 microtabs will be in the range of $R^*_{MT,s} = 0.6$ to $R^*_{MT,e} = 0.9$. The microtabs used for this simulation are located at $d^*_{MT} = 80\%$ and $d^*_{MT} = 95\%$ of the chord from the leading edge on upper and lower surface respectively, with an actuation height of $h^*_{MT} = 3.3\%$ of the chord length.

Results of this simulation are shown in Figures (3.32) and (3.33). The power curve of Figure (3.32) shows that although microtab can be used to regulate the power (the horizontal section of the curve wind speeds between 14 to 21 m/s), comparing to other controlling systems this device is not efficient enough to keep the curve horizontal at lower or higher wind speeds (e.g. compared to variable speed pitch controlled wind turbine of Figure (3.13), for which the power curve remains horizontal over the wind speeds of 13 to 25 m/s). Figure (3.33) shows the optimum state of the string of microtabs at each wind speed.

Referring to the power curve of Figure (3.32.a) showing that microtabs are not efficient enough to keep the power curve horizontal, and recalling the discussion at the end of Section 3.4.3, one can conclude that microtabs, like flaps, when used in conjunction with another controlling system (e.g. rotor speed), the accompanied controlling system

dominates the control process. That is, there is no advantage in using microtabs on variable speed wind turbines.

Algorithm 3.9-GA for finding optimum state of microtabs

Given:

- n_{pop}, n_{gen}, p_c and p_m
- ε_P
- N_{MT}
- All parameters required for running Algorithm (3.8) except the state of microtabs $MT_j \in \{-1,0,+1\}$; $j = 1,2,...,N_{MT}$

Step 1- Initialise: $MT_i = 0$, $i = 1,2,...,n_{seg}$

Step 2- Prdocude an initial poulation of n_{pop} individuals:

2.1. $i_{pop} = 0$

2.2. While $i_{pop} < n_{pop}$ do:

2.2.1. Genrate a string of size N_{MT} with values randomly selected from $\{-1,0,+1\}$, representing the states of microtabs.

2.2.2. Using Algorithm (3.8), calculate rotor mechanical power P for this individual; If $P \le P_{rated} + \varepsilon_P : i_{pop} = i_{pop} + 1$, add this individual to the population; Else: Reject this individual as infeasible solution

Step 3- For $i_{gen} = 1$ to n_{gen}

3.1. Crossover (co): For $i_{co} = 1 : p_c n_{pop}$

3.1.1. Randomly select two individuals (parents)

3.1.2. Randomly select a cut point (I_{cut}), an integer number between 1 and N_{MT}.

3.1.3. Creat a new child with microtab states similar to those of the first parent for microtabs 1 to I_{cut} and microtab states the same as those of the second parent for microtabs $I_{cut} + 1$ to N_{MT}

3.1.4. Using Algorithm (3.8), calculate rotor mechanical power P for the produced child; If $P > P_{rated} + \varepsilon_P$ reject this child as infeasible solution; otherwise add this child to the population

3.2. Mutation: For $i_{mute} = 1 : p_m n_{pop}$

3.2.1. Randomly select an individual (parent)

3.2.2. Randomly select a microtab (I_{mute}), an integer number between 1 and N_{MT}.

3.2.3. Change the current value to a different value, randomly taken from $\{-1,0,+1\}$ to create a new child

3.2.4. Using Algorithm (3.8), calculate rotor mechanical power P for the produced child; If $P > P_{rated} + \varepsilon_P$ reject this child as infeasible solution; otherwise add this child to the population

3.3. Regeneration: Keep the first n_{pop} individuals with heighest fitness (P) and discard the rest of individuals.

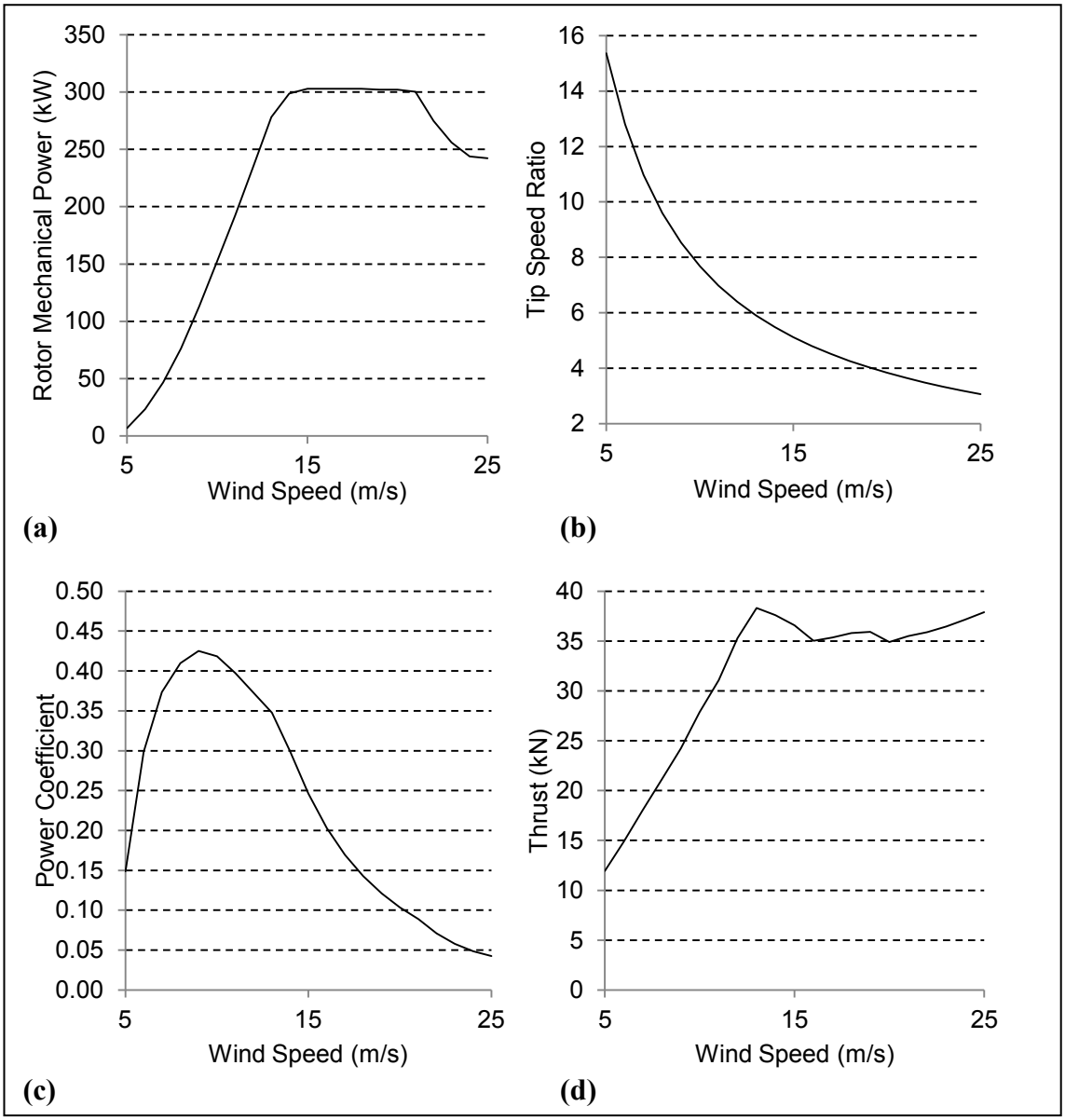

Figure 3.32- Results of simulation of constant-speed AWT-27 equipped with microtabs

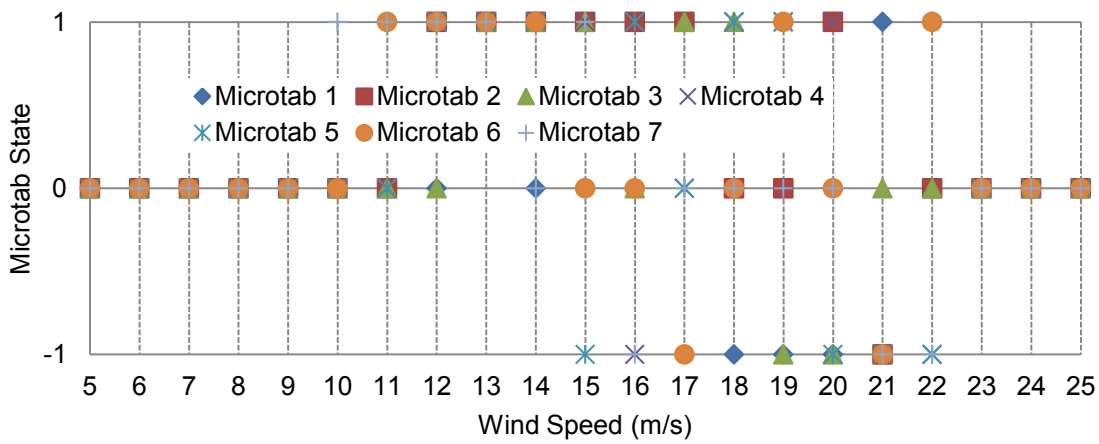

Figure 3.33- Results of simulation of constant-speed AWT-27 equipped with microtabs- The states of the microtabs

3.9 A Preliminary Comparison of Different Types of Control Systems

The comparison of the power, power coefficient, bending moment at the root of the blade and the rotor speed for different types of wind turbines simulated in this chapter are shown in Figures (3.34) to (3.40).

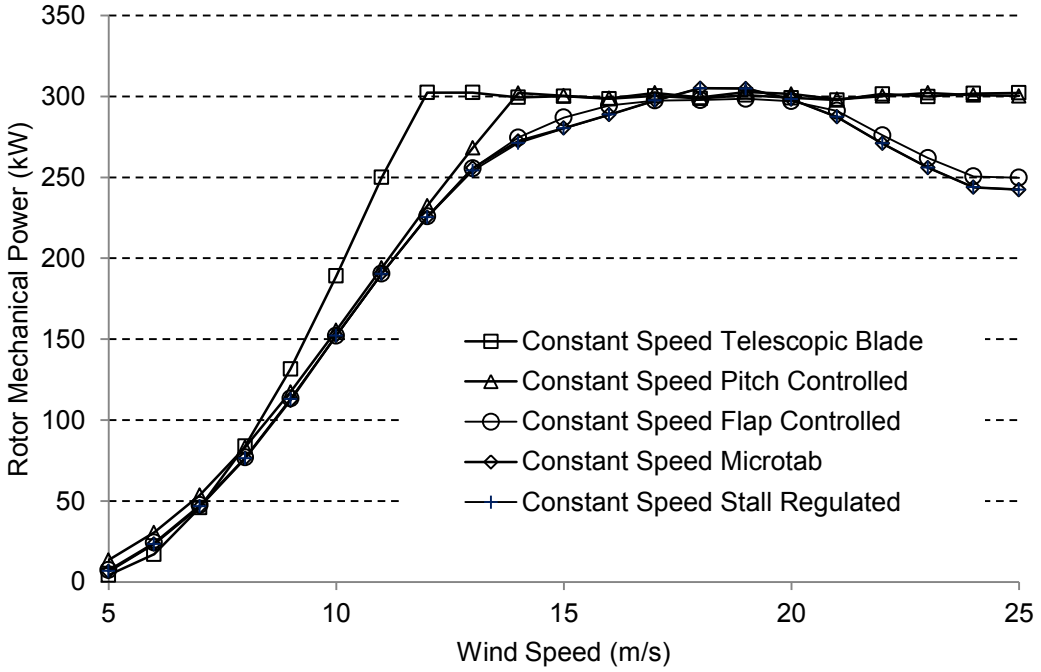

Figure 3.34- Comparison of the power curves of different types of constant speed wind turbines

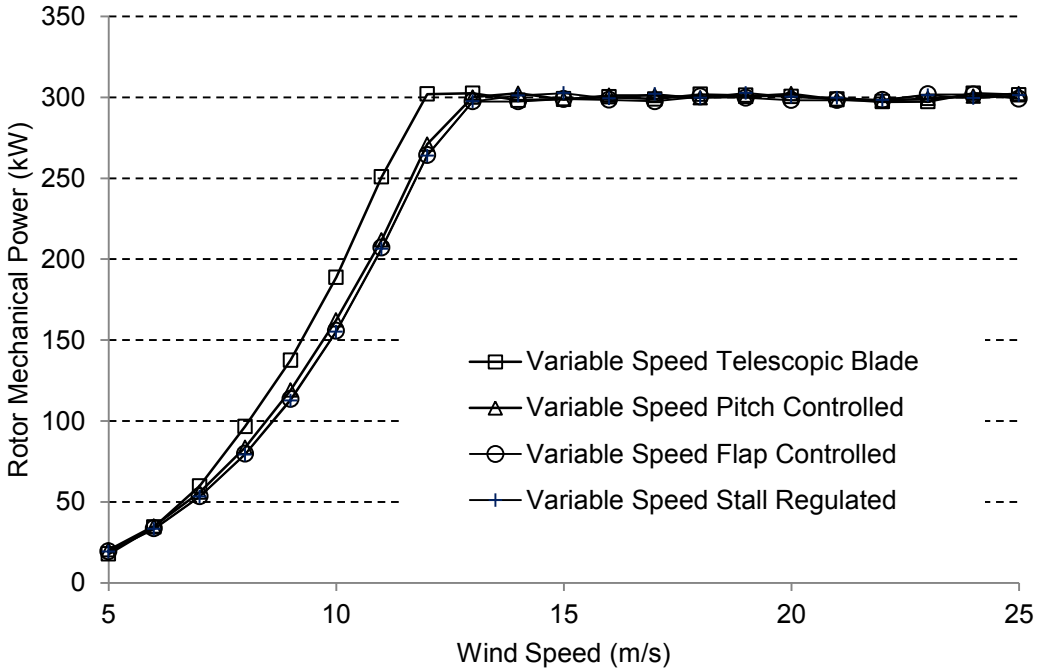

Figure 3.35- Comparison of the power curves of different types of variable speed wind turbines

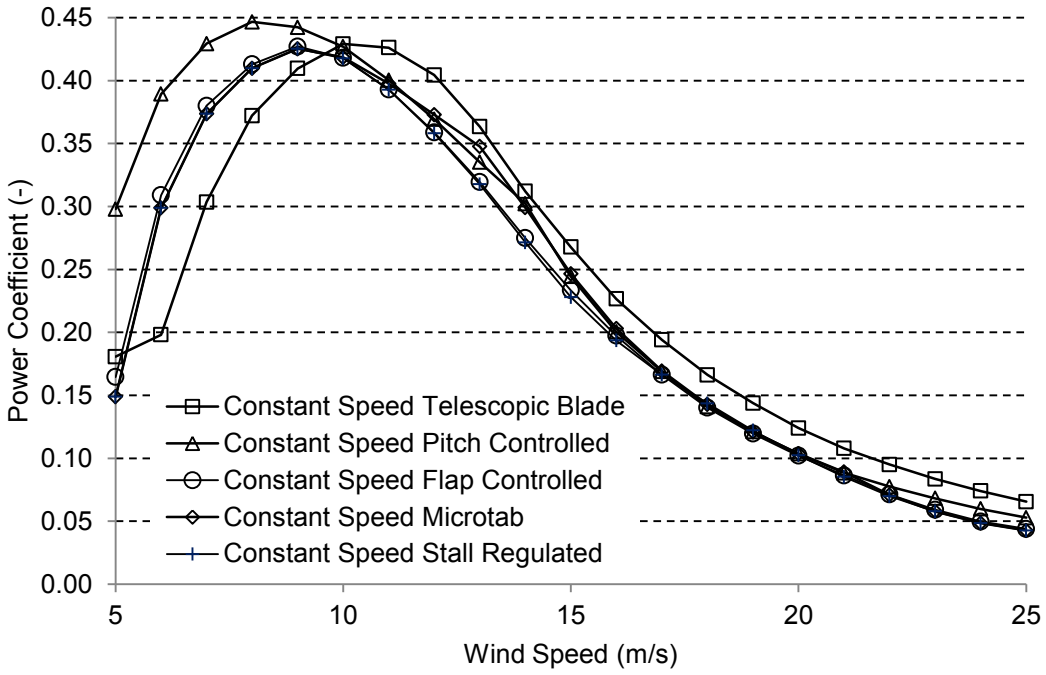

Figure 3.36- Comparison of the power coefficient of different types of constant speed wind turbines

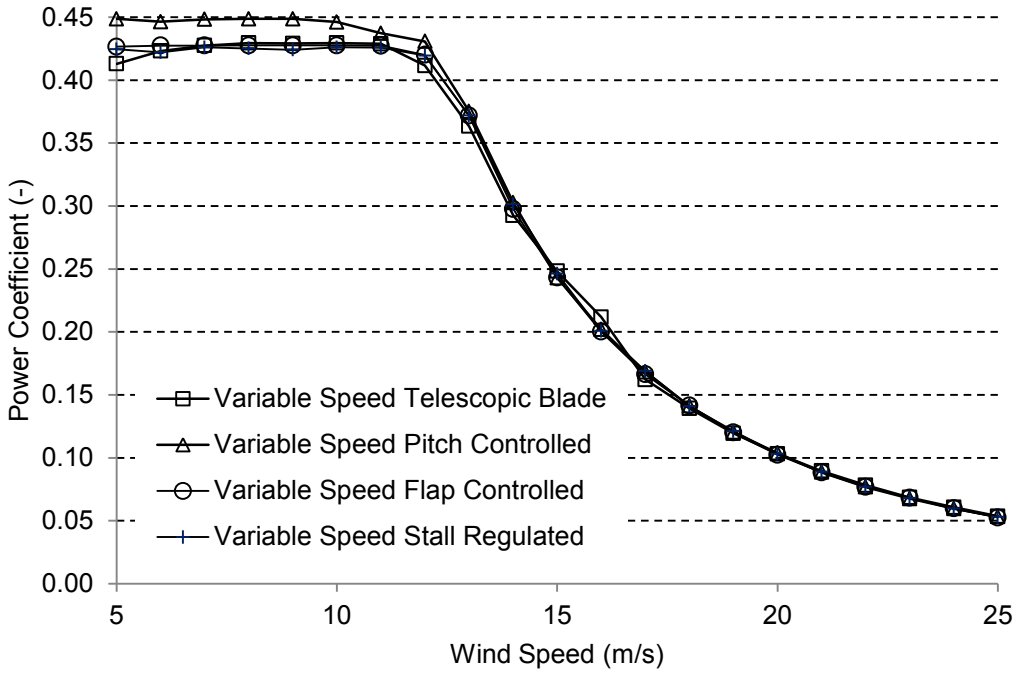

Figure 3.37- Comparison of the power coefficient of different types of variable speed wind turbines

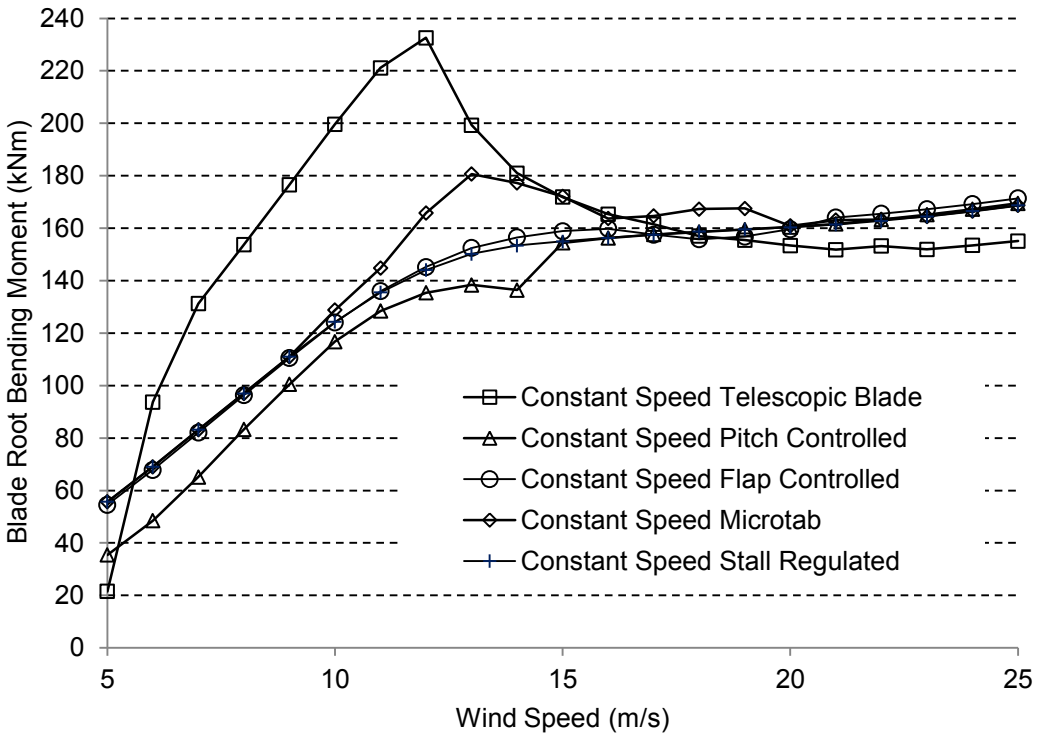

Figure 3.38- Comparison of the blade root bending moment of different types of constant speed wind turbines

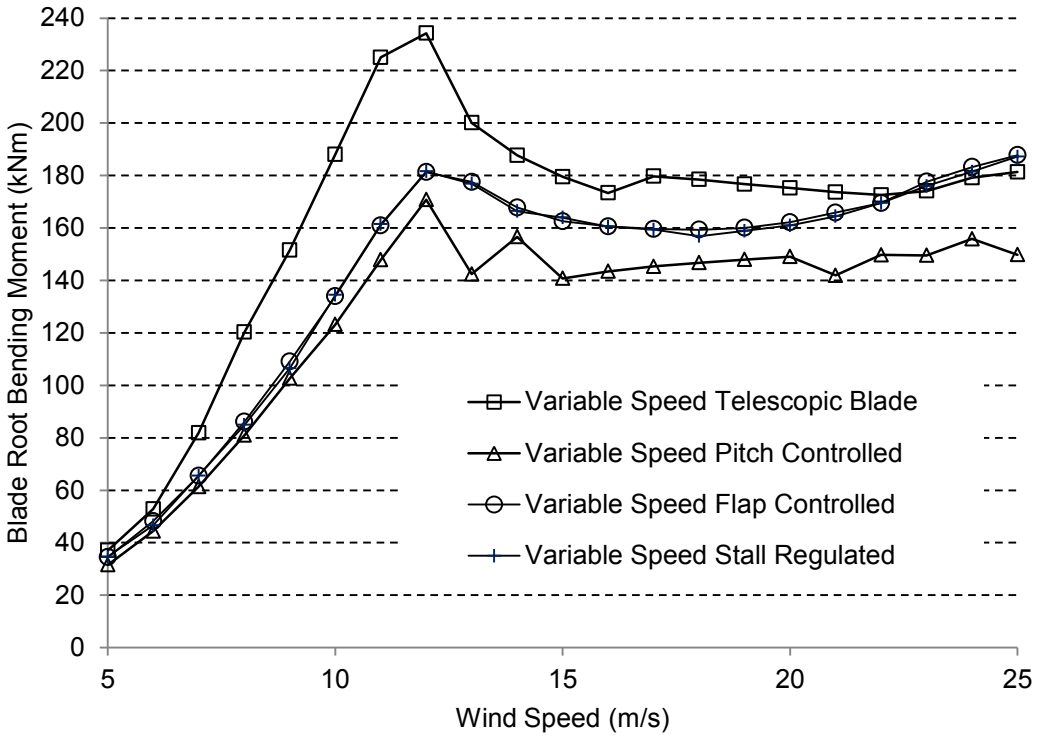

Figure 3.39- Comparison of the blade root bending moment of different types of variable speed wind turbines

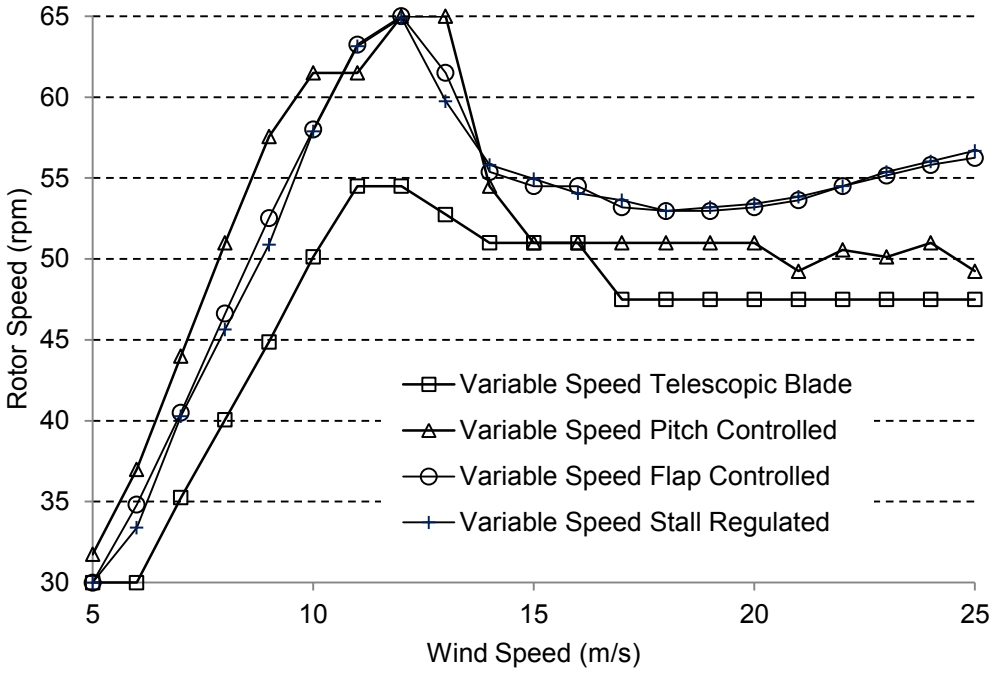

Figure 3.40- Comparison of rotor speed variation for different types of variable speed wind turbines

With reference to these figures the following conclusions can be drawn.

- Using telescopic blades enhances the power capture capability significantly at lower wind speeds for both constant speed and variable speed rotors (Figures (3.34) and (3.35)).
- Telescopic blades provide a full (Figure (3.34)) and smooth (Figure (3.24.b)) control.
- Pitch control is the most efficient control system having the highest power coefficient in both constant and variable speed rotors (Figures (3.36) and (3.37)).
- While variable speed stall regulated, variable speed pitch controlled and variable speed flap controlled wind turbines tend to operate at maximum possible rotor speed at some points, the variable speed telescopic wind turbines operate at lower rotor speeds (Figure (3.40)).
- The bending moment at the root of the blade increases significantly by using telescopic blades (Figures (3.38) and (3.39)).
- Although microtab is not as efficient as flap or pitch control systems, it increases the load on blades significantly when used for power enhancement (Figures (3.38)).
- Pitch control system produces minimal blade root bending moment for both constant speed and variable speed rotors, particularly variable speed (Figures (3.38) and (3.39)).

- Microtab and flap have been initially developed for load alleviation purposes. These controlling devices, however, can be used to regulate and enhance the rotor mechanical power to some extent (Figure (3.34)).
- Microtab and flap slightly improve the rotor power extraction efficiency (power coefficient) (Figure (3.36)).
- Flaps, when used in conjunction with another controlling system such as rotor speed, the accompanied controlling system dominates the control process (Figure (3.21)). This conclusion can be extended to microtabs by observing similar effect of both controlling systems on the power curve (Figure (3.34)).

It should be noted that since none of the above wind turbines (except the baseline constant speed stall regulated) has been optimised to operate optimally, some of these conclusions might not be valid for optimally designed blades. Chapter 4 elaborates on the optimisation methodology for each wind turbine blade utilising the above controlling systems.

3.10 Summary

In this chapter different types of aerodynamic control systems for constant and variable speed rotors were explained and classified. It was also explained that assuming the controller performs perfectly, solving an optimisation problem leads to quantifying the controlling parameters making simulation of wind turbines utilising control systems possible. Three methods of optimisation, namely, hill climbing, pattern search and genetic algorithm were developed and used to solve the optimisation problem. The performance of the hill climbing and pattern search methods was evaluated and reported.

The wind turbine simulator developed in Chapter 2 is only capable of simulating constant speed stall regulated wind turbines which do not utilise any active control systems. In this chapter the capabilities of this software was expanded via implementing necessary modifications for simulating the following eight different types of wind turbines.

1. Variable speed stall regulated rotors
2. Constant speed pitch controlled rotors
3. Variable speed pitch controlled rotors
4. Constant speed flap controlled rotors

5. Variable speed flap controlled rotors
6. Constant speed rotor with telescopic blades
7. Variable speed rotors with telescopic blades
8. Constant speed rotors with blades equipped with microtab

For each type a case study was carried out to demonstrate the capability and the performance of the developed wind turbine simulator. It should be noted that, none of the wind turbine simulators reported in open literature is capable of simulating wind turbines of types 4 to 8 above. Moreover, they use inefficient exhaustive search methods for simulating wind turbines of type 2 and 3, and wind turbine type 1 is simulated by assuming that the tip speed ratio must be kept constant at its design value, an assumption challenged in this Chapter.

Through a preliminary study, the performance of different types of wind turbines was compared.

It was found that:

- Telescopic blades provide a full and smooth control and enhance the power capture capability significantly. However, this enhancement comes with the price of a significant increase in bending moment at the root of blade.
- Pitch control is the most efficient control system having the highest power coefficient and minimal blade root bending moment for both constant speed and variable speed rotors.
- While variable speed stall regulated, variable speed pitch controlled and variable speed flap controlled wind turbines tend to operate at maximum possible rotor speed at some points, the variable speed telescopic wind turbines operate at lower rotor speeds.
- Microtab and flap have been initially developed for load alleviation purposes. These controlling devices, however, can be used to regulate and enhance the rotor mechanical power to some extent. Microtab is not as efficient as flap control systems.

4 AWTSimD, an Optimisation Tool for Wind Turbine Blades Equipped with Nonconventional Aerodynamic Control Systems

4.1 Introduction

In this chapter, first design phases of a wind turbine blade are explained. It is followed by explaining and classifying different design variables involved in each design phase. Focusing on the aerodynamic design phase of wind turbine blade, two design methods applicable to the aerodynamic design of wind turbine blades are explained, followed by formulation of the design problem in the standard format of an optimisation problem. In Section 4.3, the developed genetic algorithm optimisation method is explained in details. Section 4.4 details the implementation of the optimisation tool and the wind turbine simulation tool developed in Chapter 3.

4.2 Aerodynamic Design of Wind Turbine Blades

Wind turbine blades are designed in three consecutive phases, namely, conceptual, aerodynamic and structural. Parameters defining a blade are as follows:

- Span (rotor radius)
- Aerofoil distribution
- Chord length distribution
- Pretwist distribution
- Material and structural features (including shell material and thickness distribution, number and location of webs)

The rotor size (diameter) is a design parameter which is obtained at the conceptual design phase of wind turbines alongside with the number of blades, hub height, generator type (constant speed or variable speed), generator size (wind turbine rated power), type of the control system, rated wind speed and rated rotor speed. Once the rotor diameter is decided the span of the blade is fixed.

In the aerodynamic phase, the aerofoil, chord length and pretwist distributions are obtained. Material and structural features of the blade are designed in the structural design phase.

4.2.1 Classification of Design Variables

Design variables defining wind turbine blades can be classified into singular and distributed groups:

- Singular: design variable is defined with one single value such as rotor radius and the number of webs

- Distributed: design variables are distributed along the span of the blade, such as chord length, pretwist, aerofoil index, material, shell thickness, web thickness. In a design process each of these design variables is presented by n_{dp} values at n_{dp} span locations. Here, n_{dp} is called the number of design points (not to be confused with design variables). For example, using $n_{dp} = 5$ design points, the blade chord length distribution is presented as $c(r): \{c_1, c_2, c_3, c_4, c_5\}@\{r_1, r_2, r_3, r_4, r_5\}$, where c_i stands for the chord length corresponding to the span location r_i. For design variables with sharp variations more design points are required to capture the best distribution.

Design variables can be also classified based on their types as follows:

- Real number, such as rotor radius, chord length, pretwist, shell thickness, web thickness and location
- Integer number, such as number of webs and blades
- Indexed or coded, such as aerofoil index (e.g. S814, NACA6430, …) and material type (e.g. glass fibre, carbon fibre, …)

4.2.2 Direct versus Inverse Design Methods

In a direct design approach, first the designer selects the design parameters and then evaluates the design candidate based on a series of assessment criteria, including constraints. A direct design method is iterative. Selection of design variables and evaluation of design candidate repeats until all evaluation criteria are satisfied. This method is the common practice and dominant in most of engineering design problems.

In cases for which the number of explicit analytical equations governing the problem is the same as the number of design variables, an inverse design method can be adopted. In an inverse design method, the designer sets some target values and then solve the equations for the design variables leading to those target values. This method can be applied to very simple cases with simple equations and small number of design variables. Figure (4.1) compares these two design methods.

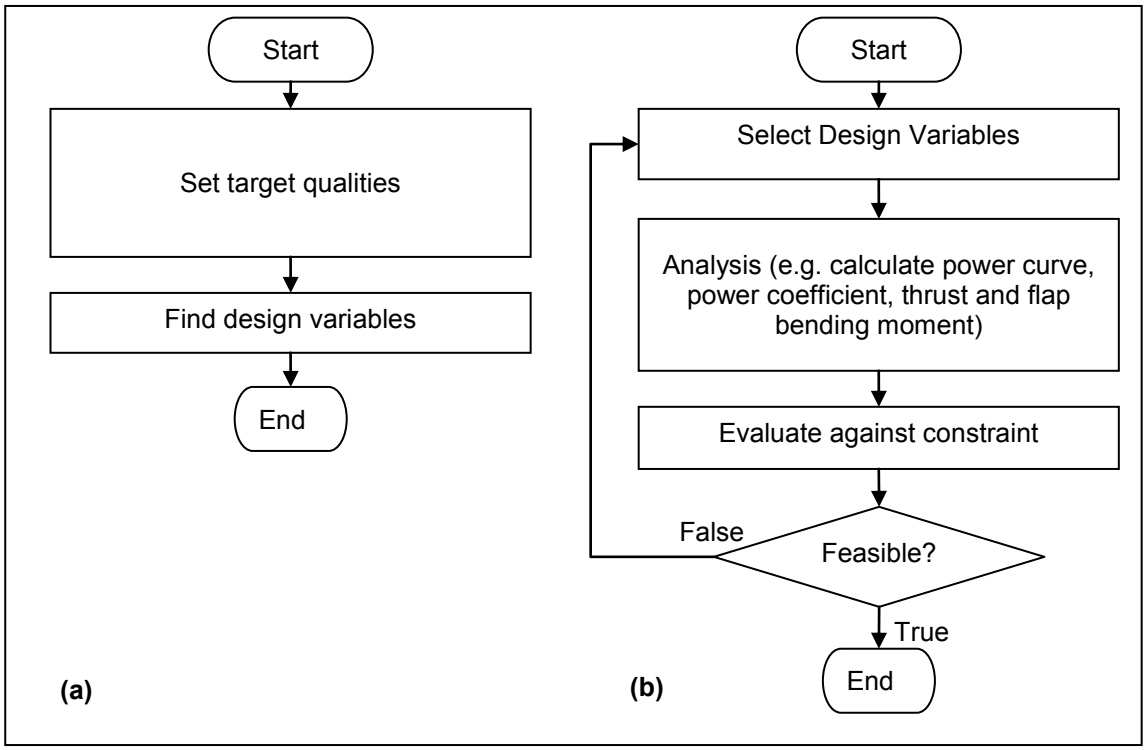

Figure 4.1- (a) Inverse and (b) Direct Design

4.2.3 Inverse Design

Although the aerodynamics of wind turbine blades is very complicated, an inverse design method can be applied for chord and pretwist design of blades installed on variable speed rotors. The inverse design method determines directly the blade geometry that will achieve certain desired aerodynamic performance. Normally, the geometry is then modified to account for structural and other considerations.

Having decided the rotor size, and hence the blade span, in conceptual design phase, the aerofoil, pretwist and chord distributions are to be determined in blade aerodynamic design phase. Referring the BEMT of Chapter 2, for a variable speed rotor with constant tip speed ratio $\lambda = \frac{R\Omega}{V}$, the maximum extracted energy from wind corresponds to the following values of the axial and rotational induction factors (Burton, 2001):

$$a = 1/3 \tag{4.1}$$

$$a' = \frac{2}{9\lambda^2 \mu^2} \tag{4.2}$$

where, $\mu = r/R$ is the normalised span location, R is the rotor radius. Substituting these values in the BEMT equations the optimum chord and pretwist distributions can be found as (Burton, 2001):

$$c = \frac{16\pi R}{9B\lambda C_{L,opt}\sqrt{\frac{4}{9}+\lambda^2\mu^2\left[1+\frac{2}{9\lambda^2\mu^2}\right]^2}} \tag{4.3}$$

$$\tan\varphi = \frac{2}{3\lambda\mu\left(1+\frac{2}{3\lambda^2\mu^2}\right)} \tag{4.4}$$

$$\beta_0 = \varphi - \alpha_{opt} \tag{4.5}$$

In the above equations, $C_{L,opt}$ is the lift coefficient at optimum angle of attack α_{opt}, the optimum angle of attack is the angle of attack at which C_L/C_D is maximum, φ stands for inflow angle, β_0 is the pretwist and c is the chord length.

The chord length obtained from Equation (4.3) is normally linearised for blade manufacturing considerations. Often, the chord is linearised to produce a simpler blade that is easier to manufacture. A straight line drawn through the 70% and 90% span point not only simplifies the plan-form of blade design but also removes a lot of material close to the root (Burton 2001 and Drew 2011).

4.2.4 Performance of Inverse Design

Although the inverse design method above is based on some optimality condition (maximum energy extraction for case of $a = 1/3$ and $a' = 2/9\lambda^2\mu^2$), in practice these conditions will not completely satisfy. This affects the performance of this method in design of blades. As a case study, the blade of AWT-27 is redesigned for a variable speed rotor, assuming the same rotor radius (R=13.75m) but with aerofoil S809 ($\alpha_{opt} = 14.2^\circ$) all through the blade. Results are shown in Figures (4.2) and (4.3). Figure (4.2) shows both chord distribution obtained by Equation (4.3) and its linearised form.

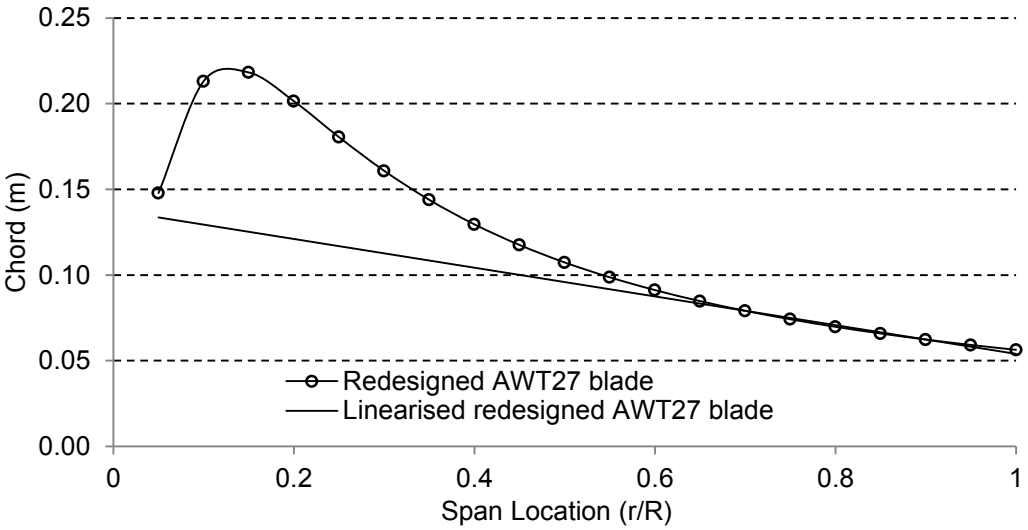

Figure 4.2-Redesigned chord of AWT-27 blade for variable speed rotor using inverse method

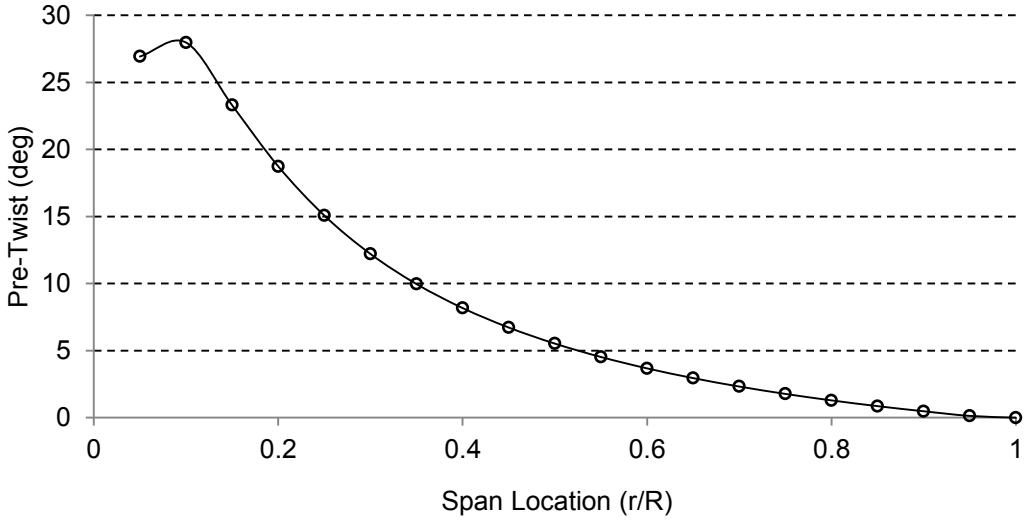

Figure 4.3- Redesigned pretwist of AWT-27 blade for variable speed rotor using inverse method

It should be noted that the original blade is not designed based on an inverse method, but has been designed using a direct search-based method as explained in the next section. Figures (4.4) and (4.5) show the results of simulation of a variable speed AWT-27 wind turbine once using the design blade using inverse method (results shown in Figures (4.2) and (4.3)), and once using its original blade. Table (4.1) summarises the results of the simulation of variable speed AWT-27 with original and redesigned blades. It is evident that the inverse design method does not produce optimum solutions. The blade designed using the inverse method produces less power while subjected to higher loads.

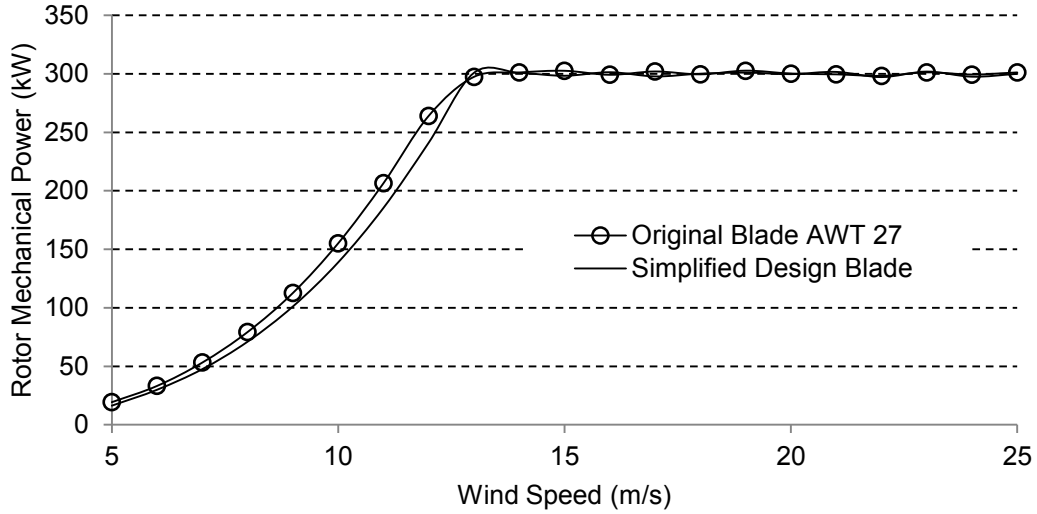

Figure 4.4-Power curve: Variable speed AWT-27 with original and redesigned blades

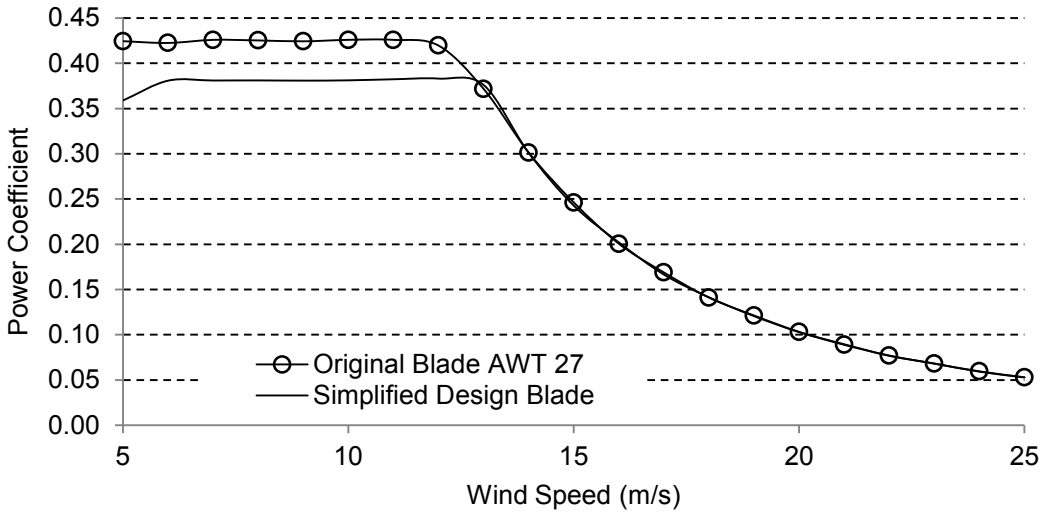

Figure 4.5-Power coefficient: Variable speed AWT-27 with original and redesigned blades

In calculating the annual average power a site average wind speed of 5.7 m/s with a Rayleigh PDF is used.

Table 4.1- Results of the simulation of variable speed AWT-27 with original and redesigned blades using inverse method

	Average Power (kW)	Maximum Power (kW)	Max Power Coefficient	Max Thrust (kN)	Max Root Bending Moment (kNm)
Original Blade AWT-27	49.6	302.7	0.426	41.6	187.2
Simplified Design Blade AWT-27	45.2	301.9	0.383	53.4	234.6

4.3 Optimal Aerodynamic Design of Wind Turbine Blades

As explained in previous section, inverse methods of blade aerodynamic design are typically based on some optimality assumptions imposed on the blade angle of attack distribution and/or tip speed ratio and/or axial and rotational induction factors. These methods normally provide closed formed design equations for pretwist and chord distributions. These methods are easy to use and give acceptable but not optimal results. Assuming blade has a fixed topology and aerodynamic characteristics, these design methods theoretically give the optimal topology of the blade. These design methods, however, fail in optimal design of blades equipped with controlling aerodynamic devices which actively affect the aerodynamic characteristics of blade. For such cases optimal aerodynamic design is achievable by employing a direct search-based design method, as shown in Figure (4.6).

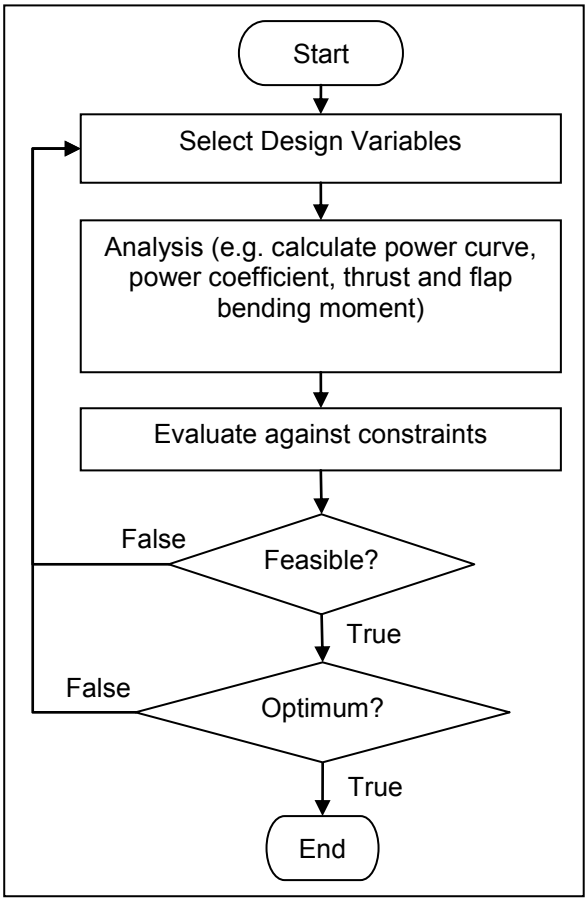

Figure 4.6-Search-based design (Direct design optimisation)

In a search-based design the objective of the optimisation is normally to maximise the annual energy production rather than, for example, maximising the power coefficient at a certain wind speed. The annual energy production of a wind turbine is influenced by

the wind characteristics of the site at which the unit is installed as well as the wind turbine capability of generating power. Wind density probability function is a model giving information on the magnitude and likelihood of wind in a site. Power curve, on the other hand, provides information on the capability of a wind turbine in producing power at various wind speeds. Annual average power, P_{av}, is defined as:

$$P_{av} = \int_{V_i}^{V_0} P(V)R(V)dV \tag{4.6}$$

where, $R(V)$ is wind speed probability density function (PDF), P is the wind turbine power and V_i and V_o are the cut-in and cut-out velocities, respectively. In this study, a Rayleigh PDF represented by:

$$R(V) = \frac{2}{V}\frac{\pi}{4}\left(\frac{V}{V_{av}}\right)^2 \exp\left[-\frac{\pi}{4}\left(\frac{V}{V_{av}}\right)^2\right] \tag{4.7}$$

has been used to calculate average power. Parameter V_{av} stands for the site average wind speed.

The optimisation problem, therefore, can be summarised as

maximise P_{av}

subject to main constraint

$$P \le P_{rated} \tag{4.8}$$

and possibly other constraints on, for example, blade maximum bending moment, weight of the blade, etc.

4.4 Genetic Algorithm Optimisation Method

Genetic algorithm is a well known optimisation technique applicable to all kind of optimisation problems, including constrained/unconstrained, linear/nonlinear, real/integer/mixed value, concave/convex and continuous/discrete domains. Many text

books can be found on the fundamentals and application of genetic algorithm. For instance, see Holland (1975), Michalewicz (1992) and Baeck (2010).

For the optimisation problem at hand, solutions (also called individuals and design candidates) are wind turbine blade. The following sections elaborate on the developed GA with the following order: chromosome representation of solutions (wind turbine blades), initial population generation, crossover operator, mutation operator, fitness definition, parent selection, regeneration, constraint handling and termination criteria.

4.4.1 Chromosome Representation

A real number encoding is used. Depending on the number of design points (n_{dp}) considered for distributed design variables and the number of design variables included in the optimisation problem, the maximum length of the chromosome (for three distributed and one singular design variables) is $3n_{dp}+1$ as shown in Figure (4.7)

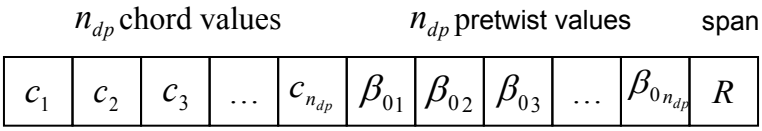

Figure 4.7-Wind turbine blade chromosome

In the developed optimisation code in MATLAB, the user sets n_{dp} and selects the design variables to be included in the optimisation problem from the set of $\{c, \beta_0, R\}$. For each design variable selected for optimisation a realistic range is also required to be set. For those design parameters not selected for optimisation, a fixed value or distribution is considered. For example, to optimise the AWT-27 blade for pretwist, the pretwist is selected as design variable while the original chord and rotor radius are used. Other required parameters are n_{dp} and the lower and upper limits for the pretwist: $\beta_{0,l}, \beta_{0,u}$

4.4.2 Initial Population Generation

The initial population in most of GAs is generated randomly. A random initial population generation method can generate both feasible and infeasible solutions. In highly constrained problems and problems in which the constraints are very sensitive to

the design variables, generating feasible initial population can be very time consuming due to high number of failed attempts.

In our case here, the output power (constraint of Equation (4.8)), is highly sensitive to the blade pretwist and chord length distribution as well as the rotor radius. Particularly, random generation of initial population becomes very time consuming when all these design variables are included in the optimisation process. To overcome this problem, two approaches have been adopted as explained below.

4.4.2.1 Randomly Generated

Depending on whether the design variable included in the optimisation is singular or distributed, each individual in initial population is generated as follows:

For each singular design variable included in the optimisation, a random number between the identified limits is assigned to that design variable. The limits are set based on realistic values.

For each distributed design variable included in the optimisation there are n_{dp} design points. Each design point of each distributed design variable is assigned a random value between the limits. It is possible to implement some heuristics when generating these random numbers to reduce the chance of producing infeasible and unrealistic solutions. For example, chord has a decreasing trend from hub to tip and pretwist has a concave trend. Generally, five possible trends that can be selected for each real number distributed design variable are shown in Figure (4.8).

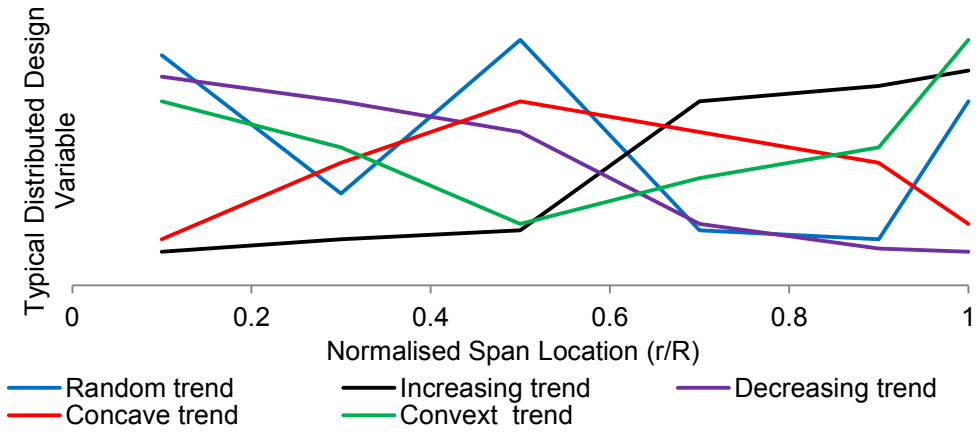

Figure 4.8- Randomly generated distribution for a typical real-number distributed design variable

4.4.2.2 Perturbation of the Baseline Design

In this method, a new design candidate is produced by a random deviation of an initial design rather than a randomly generated blade from scratch. This method is applicable when the design variable is distributed (i.e. pretwist and chord). In this method, one of the design points is randomly selected and the rest have the same value as the baseline design. Figures (4.9) and (4.10) illustrate this method, assuming the design variables are pretwist and chord and the baseline is AWT-27 wind turbine blade. In this example the number of design points, n_{dp}, is 6. A random number between 1 and 6 has been selected (here 5). For design point number 5, the chord and pretwist are assigned new "randomly" selected values (between identified limits).

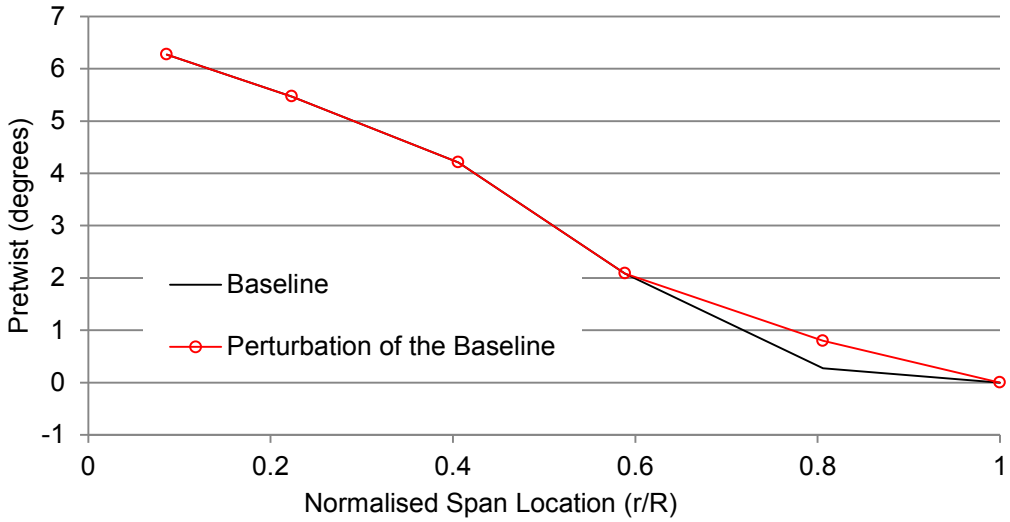

Figure 4.9- Initial population generation using perturbation of an initial design candidate: Blade pretwist

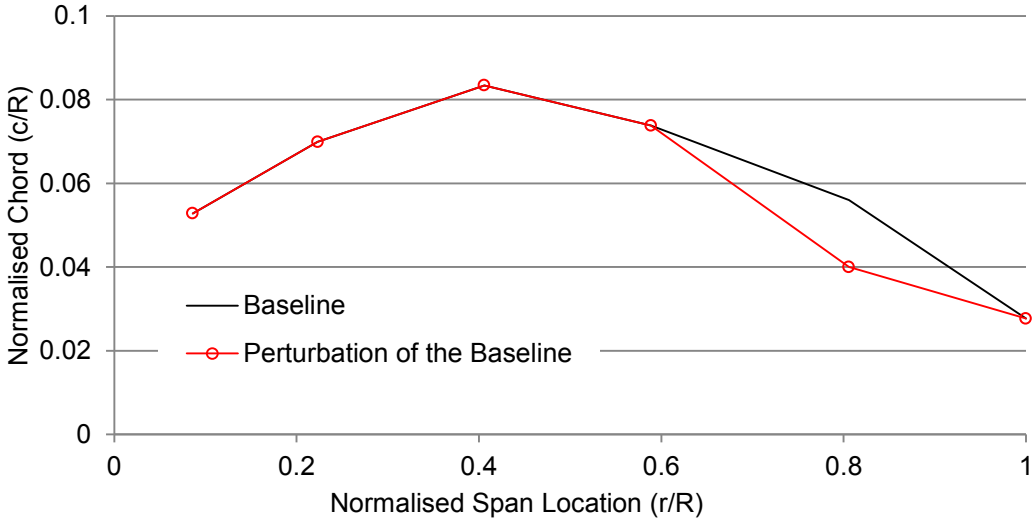

Figure 4.10- Initial population generation using perturbation of an initial design candidate: Blade chord

In the developed software tool the initial population generation is a hybrid of both approaches. That is, x_{ip} fraction of the initial population is produced using perturbation method and the remaining $(1\text{-}x_{ip})$ fraction is produced using random method. Therefore, the following parameters are required to be set by the user:

- Population size, n_{pop}
- Lower and upper limits for each design variable considered for optimisation
- Fraction of initial population to be generated based on perturbation method, x_{ip}
- In case of $x_{ip} \neq 1$, the trend of randomly generated distributed design variables: $t_{ip,rand}$ =1, 2, 3, 4, 5, respectively, for random, increasing, decreasing, concave and convex.

4.4.3 Crossover

The purpose of the crossover operation is to exploit the search area via creating new solutions from existing solutions in the current population. Two types of crossover has been coded and implemented in the optimisation module. The first type is classical arithmetic or weighted average crossover. The second type is the geometric crossover recently proposed by Maheri et al (2012).

4.4.3.1 Arithmetic Crossover

In an arithmetic crossover, each gene in the chromosome of a child is a weighted average of the corresponding genes of its parents as given by:

$$\varphi_{child} = \lambda\varphi_{parent_1} + (1-\lambda)\varphi_{parent_2} \tag{4.9}$$

In the above equation φ represents any gene of the chord, pretwist or rotor radius section of the chromosome and $\lambda \in (0,1)$ is a random number. Figure (4.11) illustrates arithmetic crossover (curves show typical parents and child chord distribution).

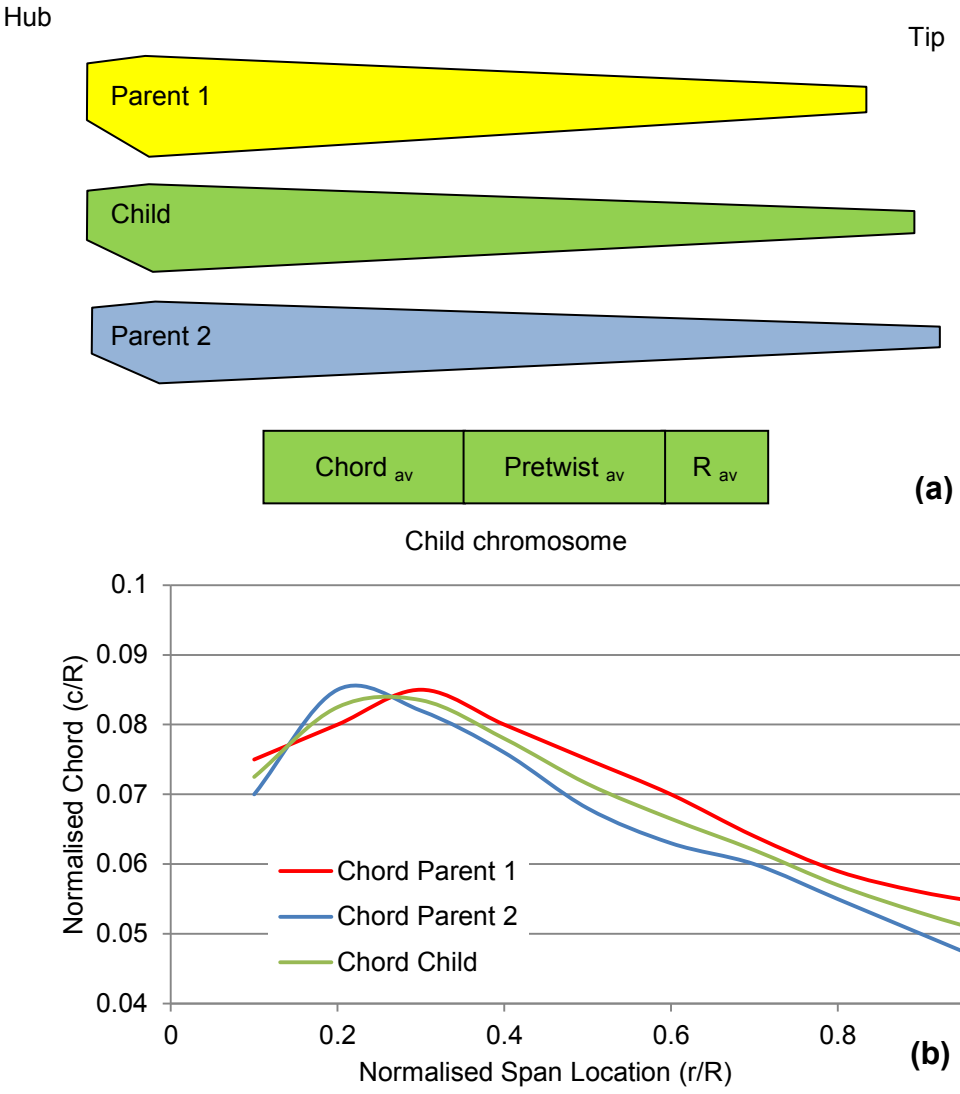

Figure 4.11-Arithmetic (weighted average) crossover

4.4.3.2 Geometric Crossover

This section explains the geometric crossover proposed by Maheri et al (2012). In a geometric crossover, two parents are cut at a random span location and the child is formed by swapping sections of parents as shown in Figure (4.12).

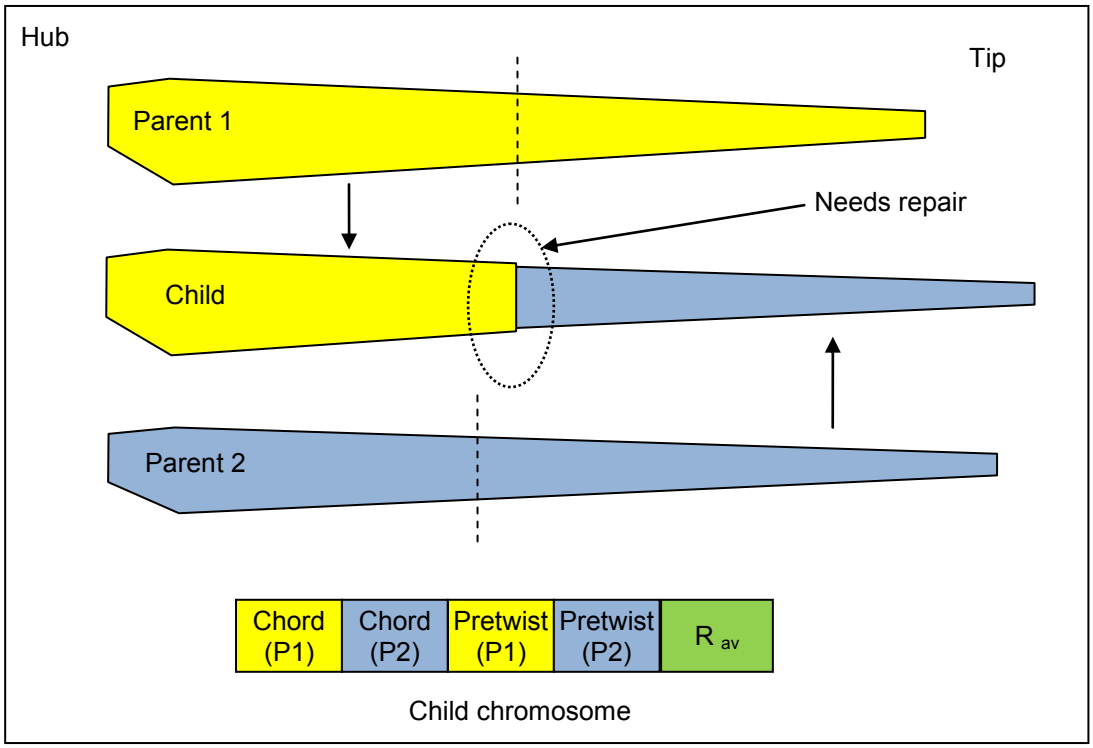

Figure 4.12-Geometric crossover

Having the radial coordinate normalised by span length ($r^* = r/span$), the cut point is a randomly selected design point r_c^*. The cut divides each parent blade into two parts. The distributed design variables of the child blades are formed by those of the left and right hand sides of each parent blade. A repair operation is also required to retain the continuity of the distributed design variable (Maheri, 2012).

Figure (4.13) illustrates the process of forming a distributed design variable (here the pretwist distribution β_0) of a child from a pair of parents. The repaired pretwist is obtained by multiplying the unrepaired pretwist by the left and right multipliers $M_L(r^*)$ and $M_R(r^*)$.

$$\left[\beta_0(r^*)\right]_{C_1,R} = \begin{cases} \left[\beta_0(r^*)\right]_{P_1} M_L(r^*) & if \quad 0 \le r^* \le r_c^* \\ \left[\beta_0(r^*)\right]_{P_2} M_R(r^*) & if \quad r_c^* < r^* \le 1 \end{cases} \tag{4.10}$$

where, subscripts C_1, P_1, P_2 and R stand for child 1, parent 1, parent 2 and repaired, respectively. $M_L(r^*)$ and $M_R(r^*)$ are the left and right segments of a multiplier curve.

The multiplier curve for child 1 is a linear curve between 1 at $r^* = 0$ and $\frac{\lfloor \beta_{0,c} \rfloor_{C_1,R}}{\lfloor \beta_{0,c} \rfloor_{P_1}}$ at the cut point; and $\frac{\lfloor \beta_{0,c} \rfloor_{C_1,R}}{\lfloor \beta_{0,c} \rfloor_{P_2}}$ at the cut point r_c^* and 1 at $r^* = 1$ as shown in Figure (4.13.c).

The pretwist at the cut point r_c^* is denoted by $\beta_{0,c}$. The repaired pretwist at the cut point is a combination of the left and right values proportional to the length of the left and right segments respectively. That is, the repair process has less effect on the segment with longer length.

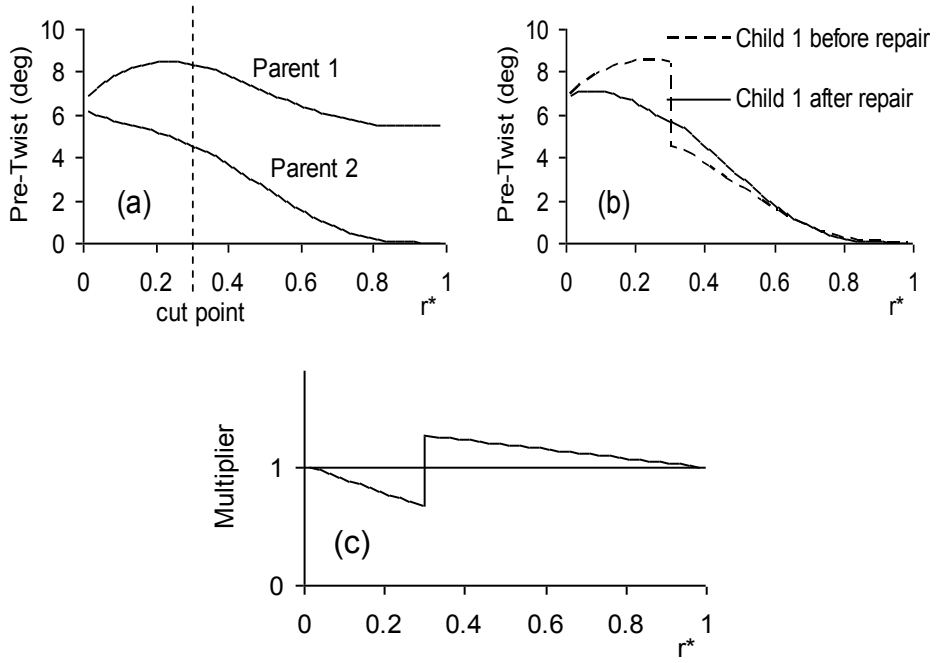

Figure 4.13- Pretwist formation of a child blade; child is formed based on the left segment of parent 1and the right segment of parent 2 (Maheri, 2012).

The blade span of child 1, R, is the combination of those of parent blades in a weighting sense (Maheri, 2012).

$$R_{child} = r_c^* R_{parent1} + (1 - r_c^*) R_{parent2} \tag{4.11}$$

Similar to initial population generation, in the developed optimisation module, the crossover operation is a hybrid of both methods. That is, x_{CO} fraction of the total crossover operations in each generation ($n_{CO} = n_{pop} \times p_c$) is carried out using arithmetic

method and the remaining (1-x_{CO}) fraction is carried out using geometric method. Therefore, the following parameters are required to be set by the user:

- Population size, n_{pop}
- Probability of crossover, p_c
- Fraction of total crossover to be carried out using arithmetic method, x_{CO}

It should be noted that geometric crossover can be applied only if distributed design variables are included in the optimisation.

In both arithmetic and geometric crossover, a roulette wheel based on the fitness is used to select the parents.

The fitness is defined as the average power:

$$fitness = P_{av} \tag{4.12}$$

4.4.4 Mutation

Mutation is a random operation. A random gene in the chromosome of a randomly selected individual is selected for mutation. This gene will be replaced by a randomly selected new value within the range of the corresponding design variable. In the optimisation module, the following parameters are required to be set by the user:

- Population size, n_{pop}
- Probability of mutation, p_m
- Lower and upper limits for each design variable in the optimisation

4.4.5 Constraint Handling

After each crossover or mutation operator the feasibility of the offspring is checked. If all constraints are satisfied, the offspring is added to the population. Infeasible solutions will be discarded.

4.4.6 Regeneration

At the end of each generation, after $n_{CO} = n_{pop} \times p_c$ crossover and $n_{Mute} = n_{pop} \times p_m$ mutation, the population size increase from n_{pop} to a maximum of $n_{pop} + n_{CO} + n_{Mute}$. At

this point, all individuals will be sorted based on their fitness. The first fittest n_{pop} individuals are passed to the next generation.

4.4.7 Termination

Genetic algorithm continues until the generation number reaches the set maximum number of generations, n_{gen} or when the maximum fitness in a generation becomes the same as the average fitness (converged solution).

4.5 AWTSimD, Advanced Wind Turbine Simulation and Design

AWTSim developed in Chapters 2 and 3 now can be integrated with the GA optimisation module as its evaluator to form the blade design optimisation tool AWTSimD. That is, each produced design candidate at the stage of initial population generation or as a result of crossover and mutation operations is evaluated using AWTSim, as shown in Algorithm (4.1). AWTSim calculates the wind turbine aerodynamic performance (blade and rotor loads and rotor mechanical power) between cut-in and cut-out velocities and using a Rayleigh PDF and finds the average annual power P_{av} at a given site average wind speed V_{av}.

In this algorithm, the data required for evaluation of each design candidate (blade) depends on the type of the blade (telescopic, equipped with microtab, equipped with flap, equipped with pitch, with no active control) under optimisation and the rotor speed (constant or variable). The required data are as explained in Algorithm (2.2) and Algorithms (3.1) through (3.9), except the design variables.

As explained in Step 1 of the algorithm, the initial population generation is carried out in two parts, namely, random generation and perturbation of a baseline design. Crossover is also performed in two parts (Steps 2.2.1 and 2.2.2), one arithmetic and one geometric.

Algorithm 4.1- AWTSimD: Optimisation of wind turbine blades utilising active control systems

Given:

- All data required for wind turbine simulation as identified in
  - Algorithm 2.2 for constant speed stall-regulated
  - Algorithm 3.1 for variable speed stall-regulated
  - modified Algorithm 3.1 for constant speed pitch controlled (Ω in Algorithm 3.1 replaced by $pitch$)
  - Algorithm 3.2 for variable speed pitch controlled wind turbines
  - Algorithms 3.3 and 3.4 as well as modified Algorithm 3.1 (in which Ω is replaced by δ_F) for constant speed flap controlled wind turbines
  - Algorithms 3.3 and 3.4 as well as modified Algorithm 3.2 (in which $pitch$ is replaced by δ_F) for variable speed flap controlled wind turbines
  - Algorithms 3.5 and 3.6 for constant speed wind turbines with telescopic blades
  - Algorithms 3.5 and 3.7 for variable speed wind turbines with telescopic blades
  - Algorithms 3.8 and 3.9 for constant speed wind turbines with microtab-equipped blades

  except those blade topology data selected as design variables (c, β_0, R)
- Selected design variables from the set of $\{c, \beta_0, R\}$, for each selected design variable the upper and lower bounds
- n_{dp} in case of selecting distributed parameters c and β_0
- Site average wind speed V_{av}
- Cut-in and cut-out velocities (V_i and V_o) and wind speed increment ΔV
- Constraints on maximum power P_{rated} and allowable root bending moment $M_{root,\max}$
- GA parameters: $n_{gen}, n_{pop}, p_c, p_m, x_{ip}, x_{co}$ and $t_{ip,rand}$ in case of $x_{ip} \neq 1$
- An initial design candidate in case of $x_{ip} \neq 0$

Step 1- Initial population generation:

1.1. $i_{pop} = 0$

1.2. While $i_{pop} < n_{pop} x_{ip}$

  1.2.1. Generate a design candidate using the method of perturbation of a baseline design

  1.2.2. Evaluate; If feasible: add to the population; $i_{pop} = i_{pop} + 1$.

1.3. While $i_{pop} < n_{pop}$

  1.3.1. Randomly generate a design candidate

  1.3.2. Evaluate; If feasible: add to the population; $i_{pop} = i_{pop} + 1$.

1.4. Construct the roulette wheel based on the fitness of individuals

1.5. Find the highest fitness in the initial population $fit_{\max}$ and calculate the initial population average fitness fit_{av}

1.6. $i_{gen} = 0$

Algorithm 4.1- AWTSimD: Optimisation of wind turbine blades utilising active control systems-continue

Step 2- Reproduction: While $(i_{gen} \le n_{gen}) \vee (fit_{\max} = fit_{av})$

2.1. For $i_{CO} = 1 : n_{pop} p_c x_{CO}$

2.1.1. Using the roulette wheel select two parents

2.1.2. Perform arithmetic crossover to form a child

2.1.3. Evaluate; If feasible add to the population.

2.2. For $i_{CO} = n_{pop} p_c x_{CO} + 1 : n_{pop} p_c$

2.2.1. Using the roulette wheel select two parents

2.2.2. Perform geometric crossover to form a child

2.2.3. Evaluate; If feasible add to the population.

2.3. For $i_{Mute} = 1 : n_{pop} p_m$

2.3.1. Randomly select an individual

2.3.2. For selected individual, randomly select a gene

2.3.3. For selected gene, randomly change the value within the limits

2.3.4. Evaluate; If feasible add to the population.

2.4. Sort extended population based on the fitness

2.5. Trim the sorted extended population to the size of n_{pop}

2.6. Find the highest fitness in the population $fit_{\max}$ and calculate the population average fitness fit_{av}

2.7. Construct a new roulette wheel

2.8. $i_{gen} = i_{gen} + 1$

Evaluate:

Step 1- Using suitable BEMT algorithm, find the power curve for the generated design candidate

Step 2- If $P_{\max} \le P_{rated}$ and other constraints are satisfied: feasible = true; calculate average power and fitness: $fitness = P_{av}$

4.6 A Case Study: Blade Optimisation for Modified Pitch Controlled AWT-27 Wind Turbine

In Chapter 3, the blade of AWT-27 wind turbine was equipped with various active control systems and was analysed for constant and variable speed rotors. Results of modified constant speed AWT-7 with pitch control system were shown in Figure (3.9). In these analyses the following search parameters for the control system were used:

- Pitch: $pitch_l = -5^\circ$, $pitch_u = 5^\circ$, $step_{pitch} = (pitch_u - pitch_l)/10 = 1^\circ$, $\varepsilon_{pitch} = 0.1^\circ$
- Power tolerance: $\varepsilon_P = 0.01 P_{rated} = 3kW$

Using the same set of search parameters as used in Chapter 3 for simulation of the pitch control, together with the following design/optimisation parameters the optimisation code AWTSimD is used to optimise the baseline blade of AWT-27 for constant speed pitch controlled scenario.

- Design variable: pretwist β_0
- Number of design points: $n_{dp} = 5$
- Constraints on maximum power $P_{\max} \le P_{rated} = 300kW$
- GA parameters: $n_{gen} = 40$, $n_{pop} = 20$, $p_c = 0.3$, $p_m = 0.1$, $x_{ip} = 0.5$, $x_{co} = 0.5$, $t_{ip,rand} = 3$ (decreasing)
- Site average wind speed $V_{av} = 5.7m/s$; Cut-in and cut-out velocities $V_i = 5m/s$, $V_o = 25m/s$ and wind speed increment $\Delta V = 1m/s$

Results of design optimisation are shown in Figures (4.14) and (4.15). Figure (4.14) shows the pretwist distribution of the optimised blade. As it can be seen the optimised pretwist has a sharper slope compared to the initial pretwist. A sharper behaviour was excepted as by adding a pitch control system, the blade pitch angle varies as blade tends to enter deep stall due to its sharper pretwist variation.

Figure (4.15) compares the power coefficients of the baseline stall regulated, baseline wind turbine with added pitch control system and optimised wind turbine with added pitch control system. As expected, the power coefficient improves due to optimisation of the blade pretwist. Figure (4.16) shows the optimisation search history. Rapid growth of the population average fitness shown in this figure indicates the robustness of the

crossover operator used in the optimisation algorithm. On the other hand, gradual improvement of the fitness of the best design candidate in the population to the latest generations indicates the diversity of the population and the effectiveness of the mutation operator.

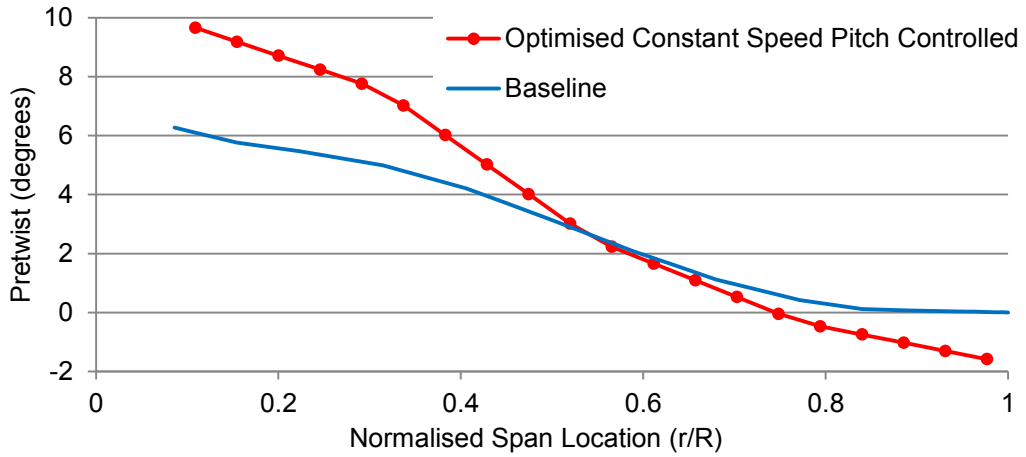

Figure 4.14-Optimised blade pretwist for modified pitch controlled AWT-27

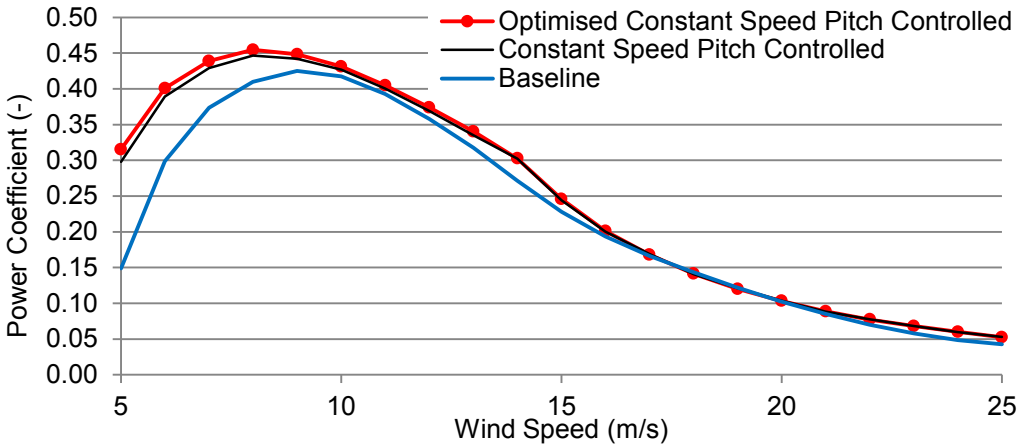

Figure 4.15-Optimum power coefficient of modified pitch controlled AWT-27

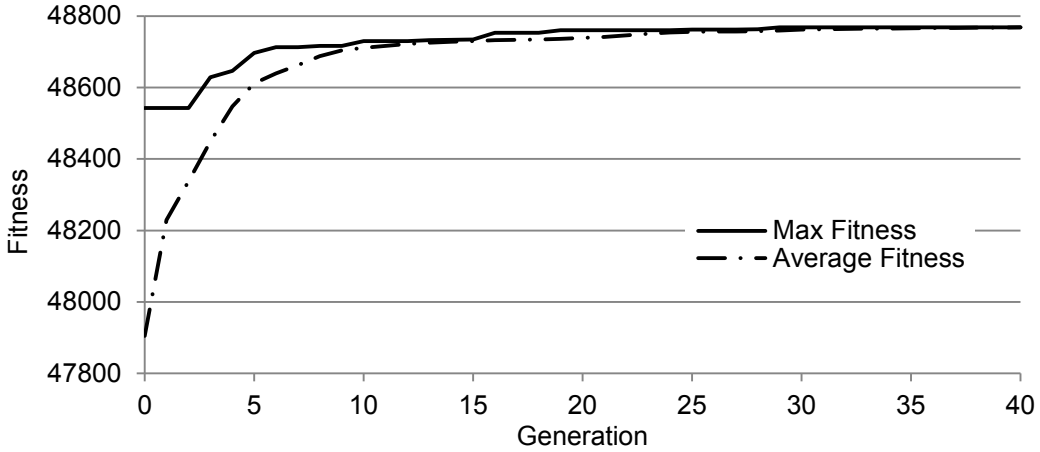

Figure 4.16-Search history for optimisation of the pretwist for modified AWT-27 constant speed pitch controlled blade

4.7 Summary

In this chapter first three phases of design of wind turbine blades were explained. Elaborating on the direct and inverse design methods, an inverse design method for design of variable speed wind turbine blades, taken from literature, was explained. Applying the inverse design method to redesign the blade of AWT-27, it was shown that the inverse design methods do not perform well in optimisation of blades topology. Adopting a direct, also called search-base, design optimisation method, the aerodynamic design of blades was formulated as a standard optimisation problem in which the objective is to maximise the annual average power subject to constraints on maximum power and blade loading.

The second part of this chapter details the genetic algorithm-based optimisation module with some advanced features designed particularly for wind turbine blade optimisation application.

The final part of this chapter elaborates on integration of AWTSim simulation tool and the GA optimisation module towards creating AWTSimD, a design optimisation tool for wind turbine blades equipped with nonconventional control systems. The performance of the tool was demonstrated by performing a design optimisation case study.

5 Design Optimisation of Wind Turbine Blades Equipped with Nonconventional Aerodynamic Control Systems

5.1 Introduction

In Chapter 3, Section 3.9 (A preliminary comparison of different types of control systems) different control systems were compared against each other and some preliminary conclusions were drawn. It was mentioned that since none of the blades had been optimised to operate optimally, some of the conclusions might not be valid for optimally designed blades. In this chapter, employing the optimisation tool AWTSimD, the potentials of flap trailing edge, microtab and telescopic blades in enhancing energy capture capability of blades are investigated. In all cases only the pretwist is considered for optimisation to keep the optimised blade structurally as close as the baseline blade, making comparison possible. In the case of trailing edge flaps and telescopic blades both constant speed and variable speed rotors are investigated. In the case of microtab, only constant speed rotor is considered. Sample simulation and design optimisation input files are given in Appendix A.

5.2 Potentials of Trailing Edge Flaps in Power Extraction Enhancement: Constant Speed Rotors

In design optimisation of blades equipped with trailing edge flap three parameters, namely, blade pretwist, flap length and flap location, are considered as design variables. Referring to Figure (3.14), parameter $\left(R_{F,e}-R_{F,s}\right)$ stands for the flap length and $0.5\left(R_{F,e}+R_{F,s}\right)$, the radial location of the centre of the flap, represents the flap location. In all cases the width of the flap d_F is considered as 10% of the local chord C_F ($d_F=0.1C_F$), where $C_F=chord@r=0.5\left(R_{F,e}+R_{F,s}\right)$. In simulating the flap control system the following data are used: $\delta_{F,l}=-20^\circ, \delta_{F,u}=20^\circ, step_{\delta_F}=4^\circ$, $\varepsilon_{\delta_F}=0.1^\circ$ and $\varepsilon_P=3kW$.

Table (5.1) shows the examined flap lengths and flap locations for this study. For each case shown in this table, using AWTSimD, the pretwist is optimised. For optimisation module the following data were used:

- Design variable: pretwist β_0
- Number of design points: $n_{dp}=5$
- Constraints on maximum power $P_{\max}\le P_{rated}=300kW$
- GA parameters: $n_{gen}=40$, $n_{pop}=20$, $p_c=0.3$, $p_m=0.1$, $x_{ip}=0.5$, $x_{co}=0.5$, $t_{ip,rand}=3$ (decreasing)

- Site average wind speed $V_{av} = 5.7 m/s$; cut-in and cut-out velocities $V_i = 5 m/s$, $V_o = 25 m/s$ and wind speed increment $\Delta V = 1 m/s$

Table 5.1- Examined flap lengths and flap locations (all values in % of R)

Case	$R_{F,s}$	$R_{F,e}$	Flap location $0.5(R_{F,e} + R_{F,s})$	Flap length $R_{F,e} - R_{F,s}$
1	60	65	62.5	5
2	65	70	67.5	5
3	70	75	72.5	5
4	75	80	77.5	5
5	80	85	82.5	5
6	85	90	87.5	5
7	90	95	92.5	5
8	60	70	65	10
9	60	75	67.5	15
10	60	80	70	20
11	60	85	72.5	25

Figure (5.1) shows the results for Case 1. The pretwist of the baseline AWT-27 and the optimised pretwist are shown in Figure (5.1.a). Figures (5.1.b) through (5.1.d) show the performance of wind turbine for three cases: (i) original AWT-27 without installing flap, (ii) original AWT-27 blades equipped with flap (with original pretwist), and (iii) optimised AWT-27 blades equipped with flap. Comparing the results of the optimised blade with original blade, it can be observed that: the blade equipped with flap produces more energy (Figures (5.1.b) and (5.1.c)) without increasing blade loading (Figure (5.1.d)). Appendix C contains the results for other cases.

The amount of enhancement in the average power due to equipping blades with flap for each case of Table (5.1) is shown in Figures (5.2) and (5.3). The calculations for the average power are based on a site average wind speed of 5.7m/s and Rayleigh probability density function. In this figure, results are shown for original blades without flap, original blades with flap and optimised blades with flap.

Using the data shown in Figure (5.3), share of installing flap and optimisation in the power enhancement are shown separately in Figure (5.4). Figure (5.5) shows the effect of the flap size on the power enhancement.

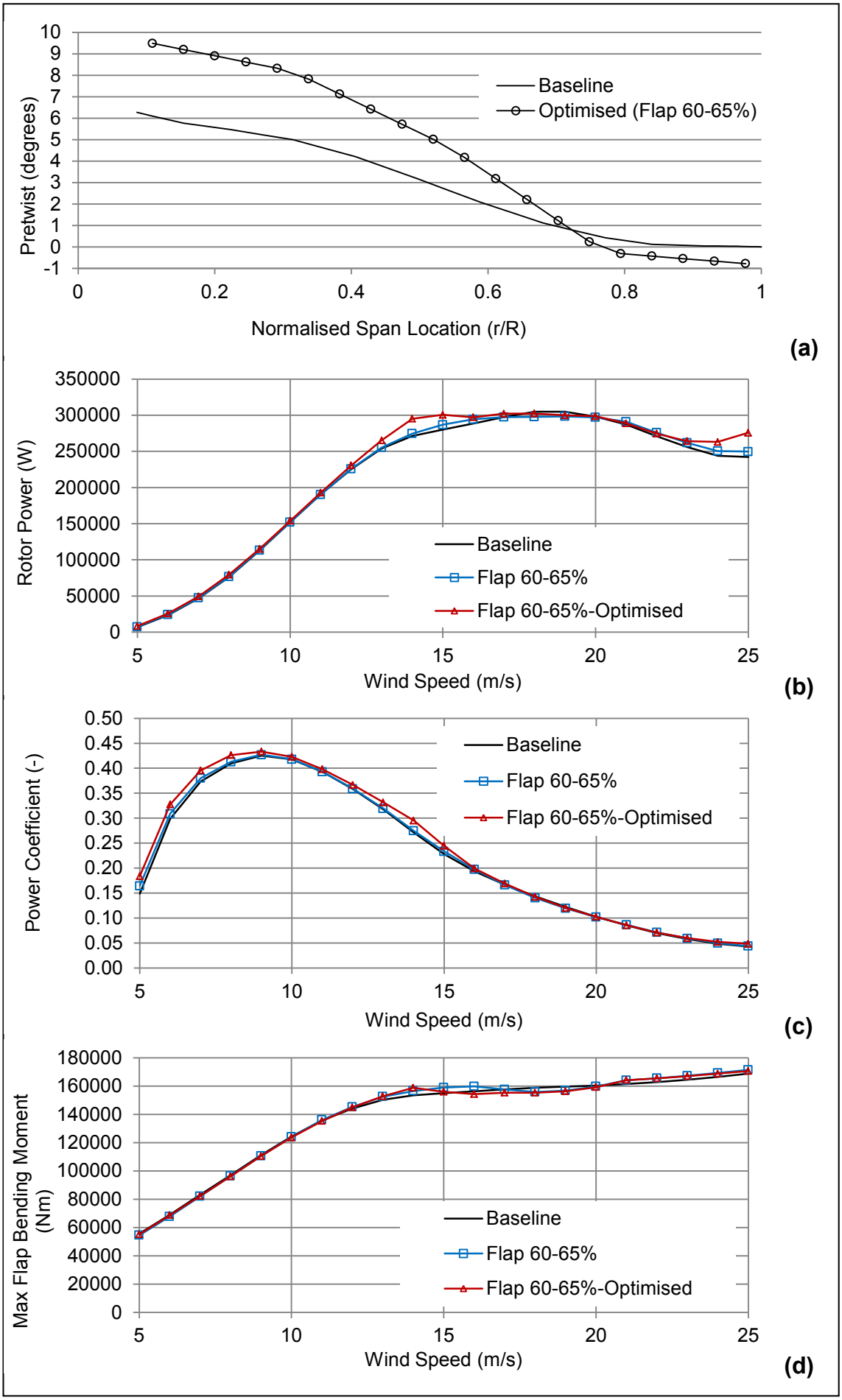

Figure 5.1-Flap 60-65%-constant speed rotor

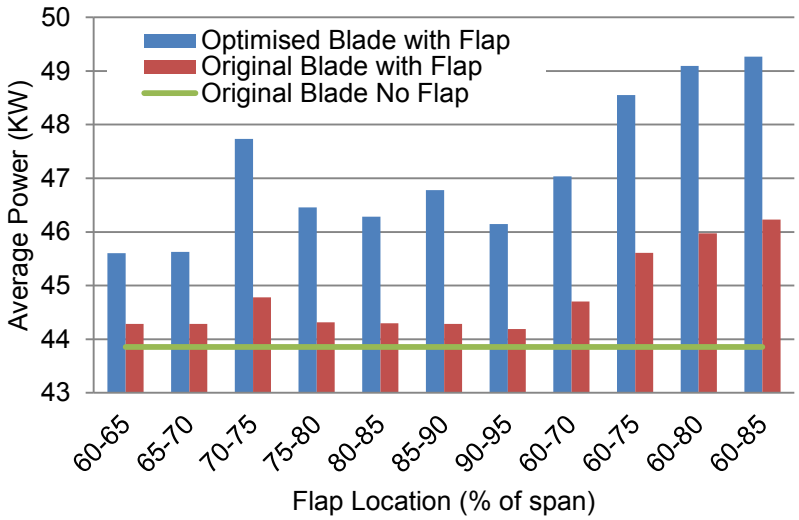

Figure 5.2-Effect of flap size and location on power enhancement-constant speed rotor

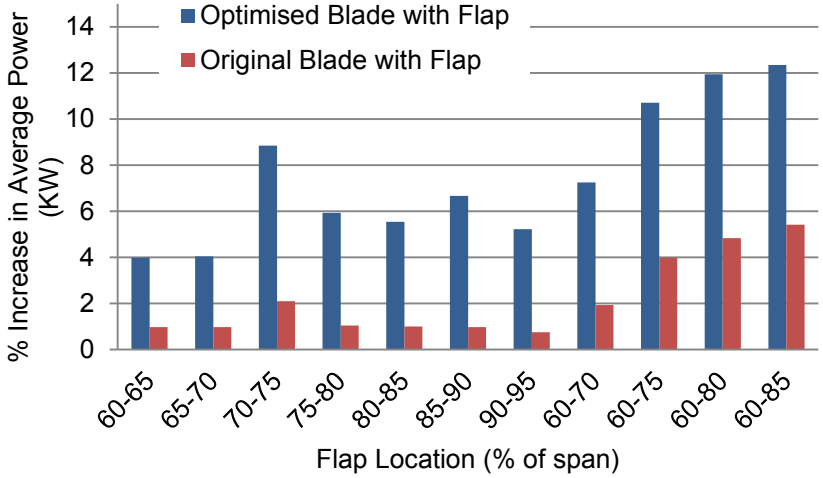

Figure 5.3-Percent increase in the average power versus flap size and location-constant speed rotor

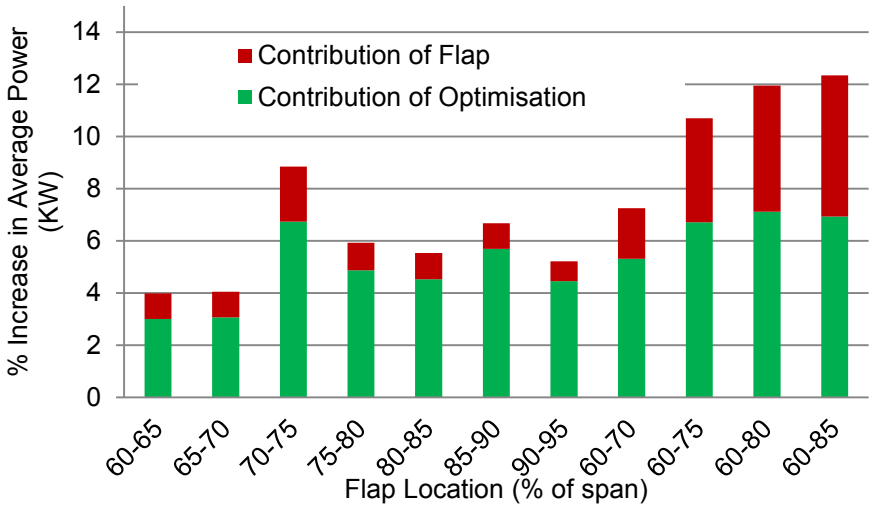

Figure 5.4-Percent improvement in the average power due to blade optimisation-constant speed rotor

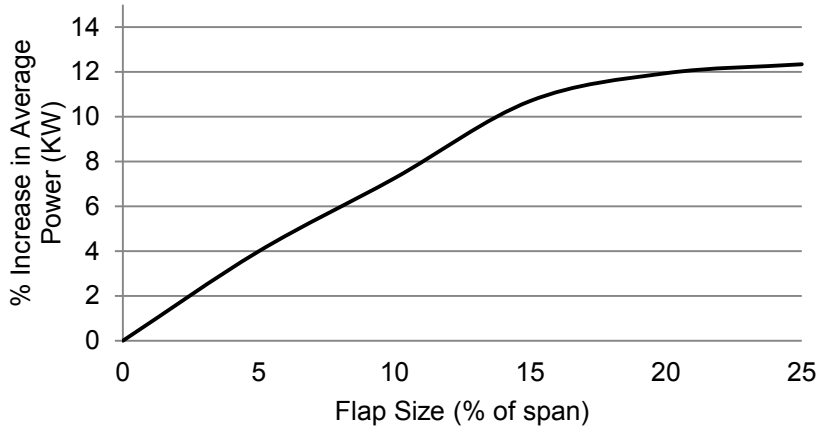

Figure 5.5-Effect of flap size on the power extraction enhancement-constant speed rotor

Figures (5.6) through (5.8) show the power curves, power coefficient and maximum flap bending moment for all 11 examined cases for which the blade has been optimised.

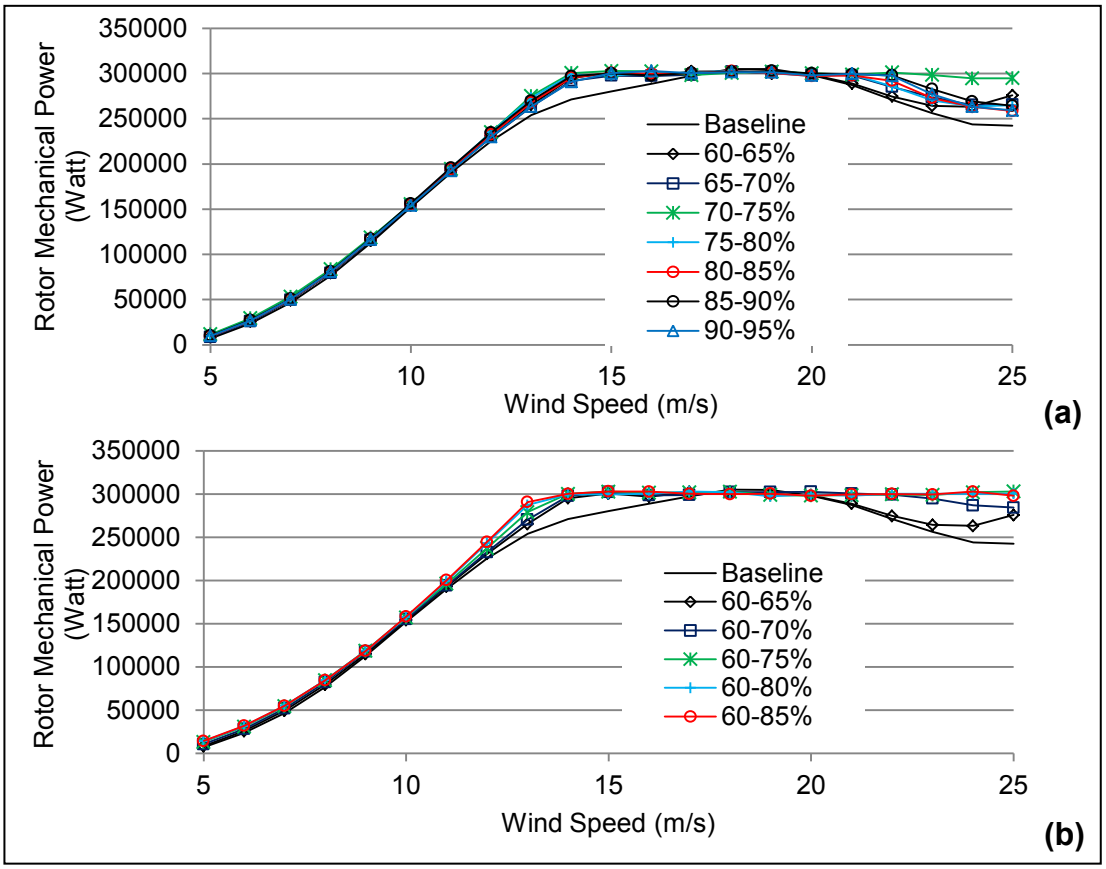

Figure 5.6-Power produced by constant speed rotors utilising blades equipped with flap

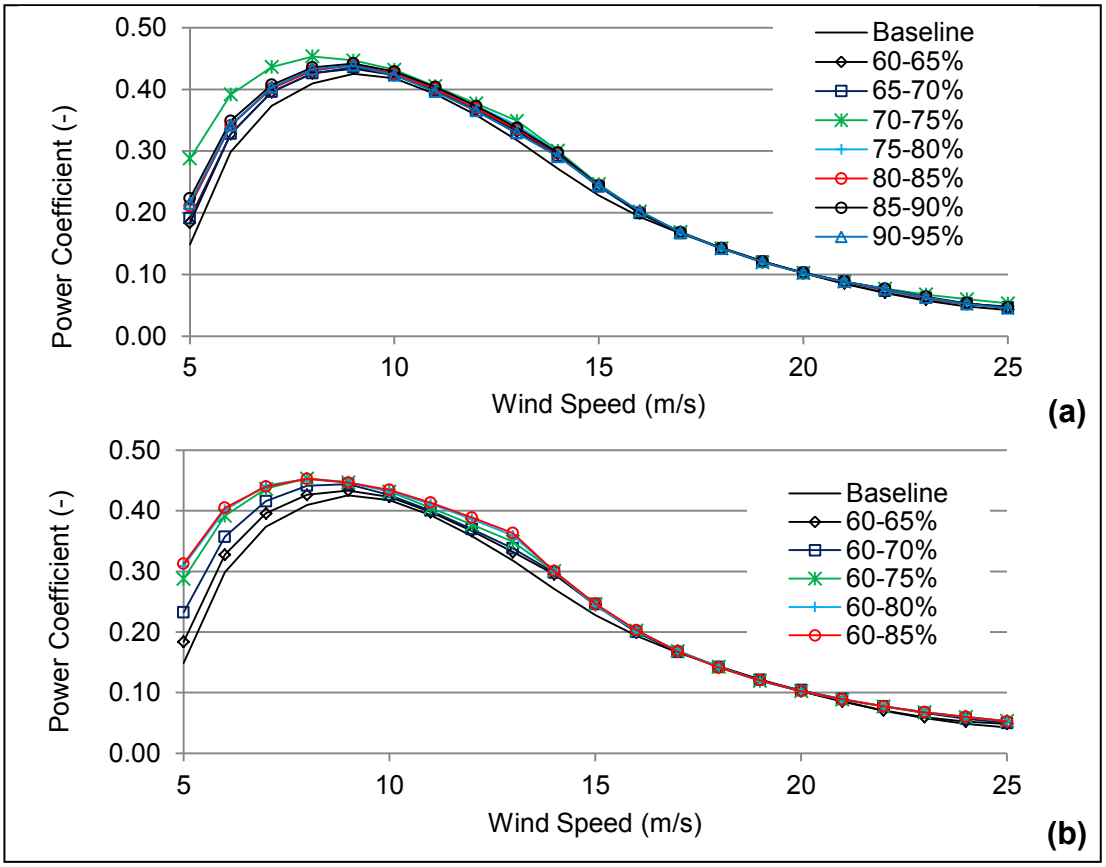

Figure 5.7-Power coefficient of constant speed rotors utilising blades equipped with flap

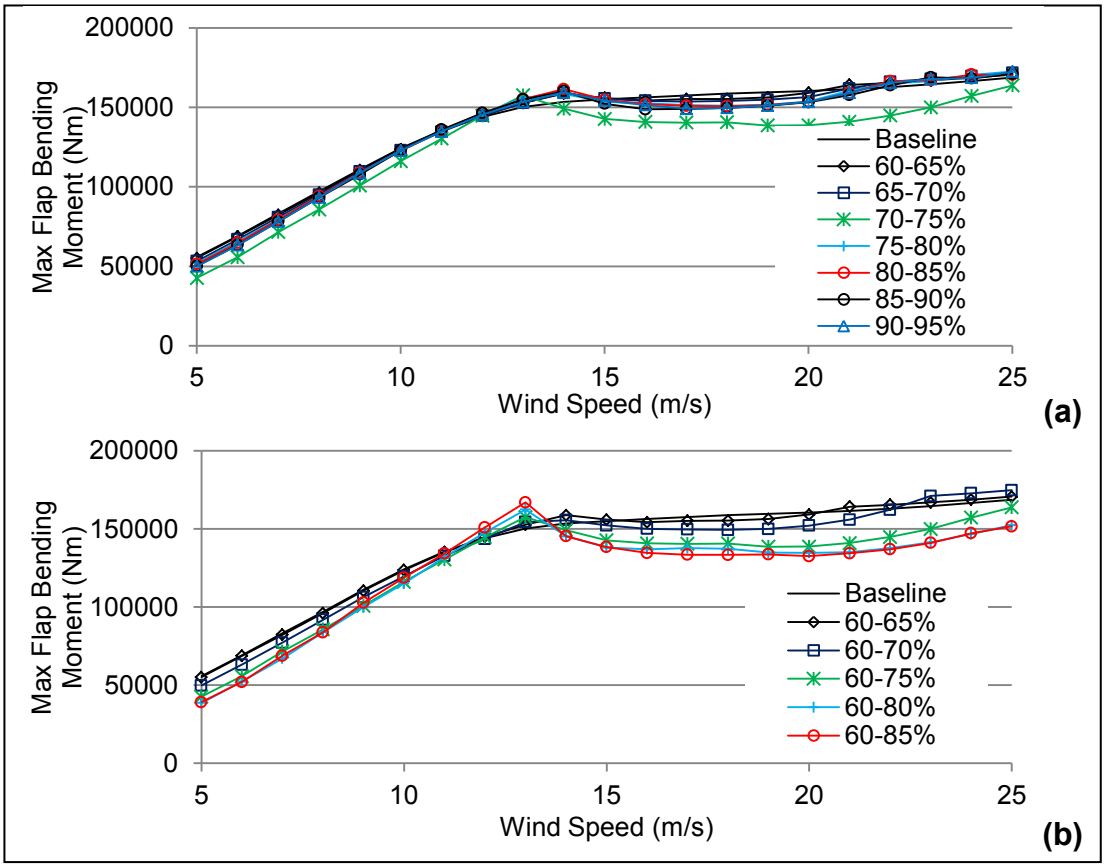

Figure 5.8- Maximum flap bending moment in blades equipped with flap-constant speed rotor

According to the above figures the following conclusion can be drawn:

- Adding flap without optimisation improve the power extraction capability as high as of about 5% for the case of flap located between 60-85% of span. However, optimisation of the blade is required to obtain the highest power improvement (Figure (5.4)). Improvement as a result of optimisation can be as high as 7% (for case of 60-80%). The overall improvement can be reached as high as 12%.
- Location of flap is a key parameter influencing the amount of improvement in the power extraction (Figures (5.2.a) and (5.3.a)). The best location for placing a flap is at about 70% of the blade span from the root of the blade.
- The size of the flap has also significant effect on the amount of enhancement in the average power. This effect, however, reduces dramatically as the size increases (Figure (5.5)).

5.3 Potentials of Trailing Edge Flaps in Power Extraction Enhancement: Variable Speed Rotors

Using the same set of data, blades of a variable speed AWT-27 are optimised for all 11 cases of Table (5.1). For these optimisation case studies it is assumed that $\Omega_l = 30rpm$, $\Omega_u = 65rpm$, $step_\Omega = (\Omega_u - \Omega_l)/10 = 3.5rpm$, $\varepsilon_\Omega = 0.1rpm$, as used in Chapter3.

Figure (5.9) shows the results for Case 1. Appendix C contains the results for other cases. Similar to Section 5.2, here for the variable speed rotor, the average power and the enhancement in the average power for all 11 cases of Table (5.1) is calculated and shown in Figures (5.10) through (5.13). Figures (5.14) through (5.16) show the power curves, power coefficient and maximum flap bending moment for all 11 examined cases for which the blade has been optimised.

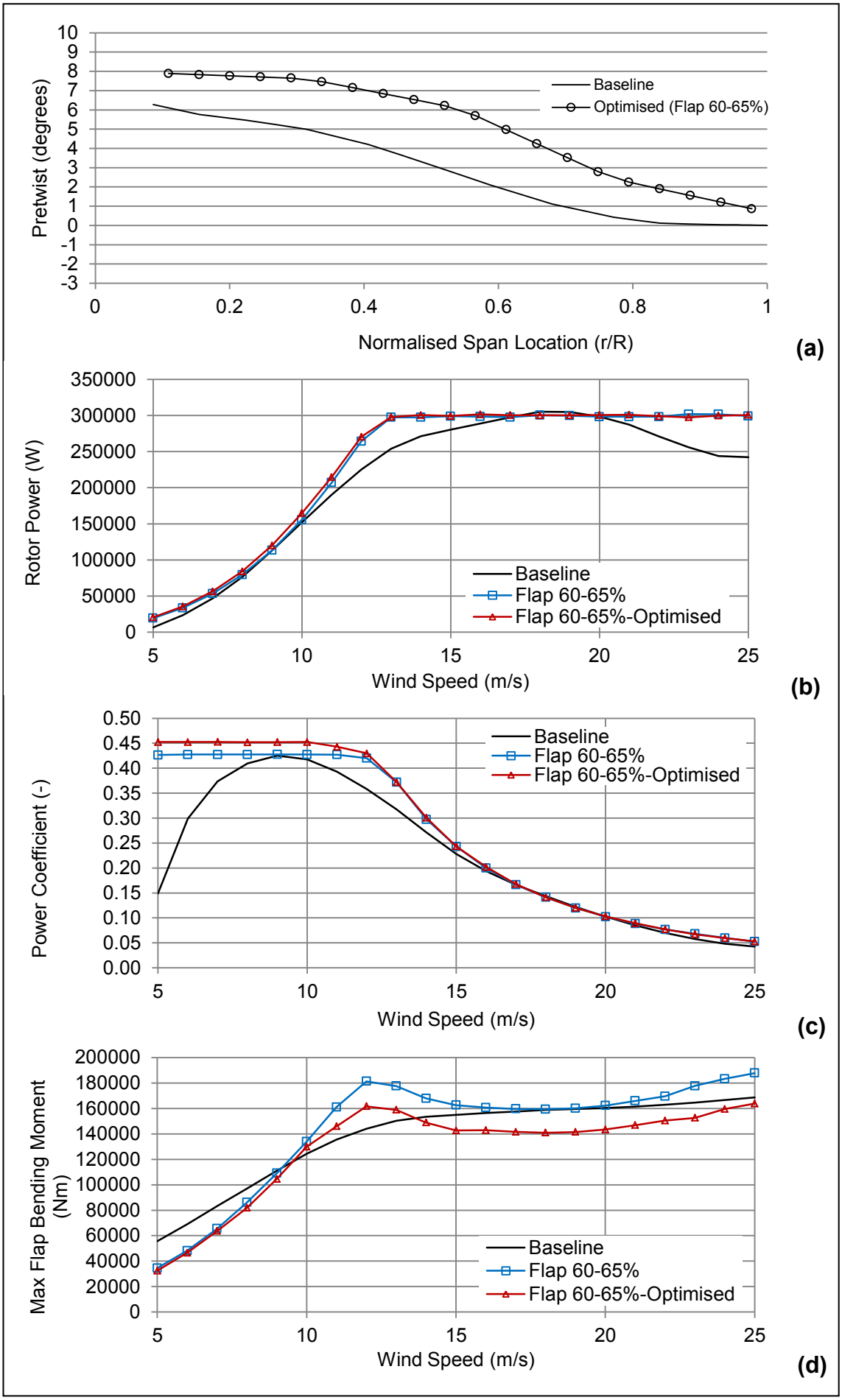

Figure 5.9-Flap 60-65%-variable speed rotor

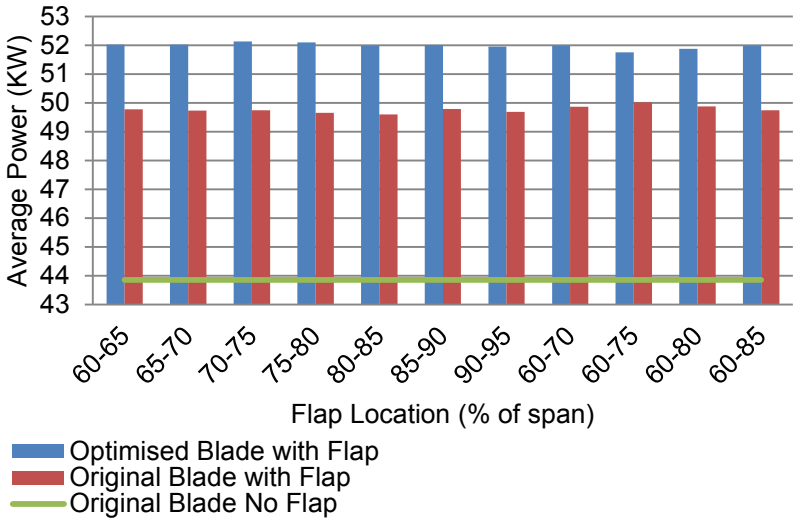

Figure 5.10-Effect of flap size and location on power enhancement-variable speed rotor

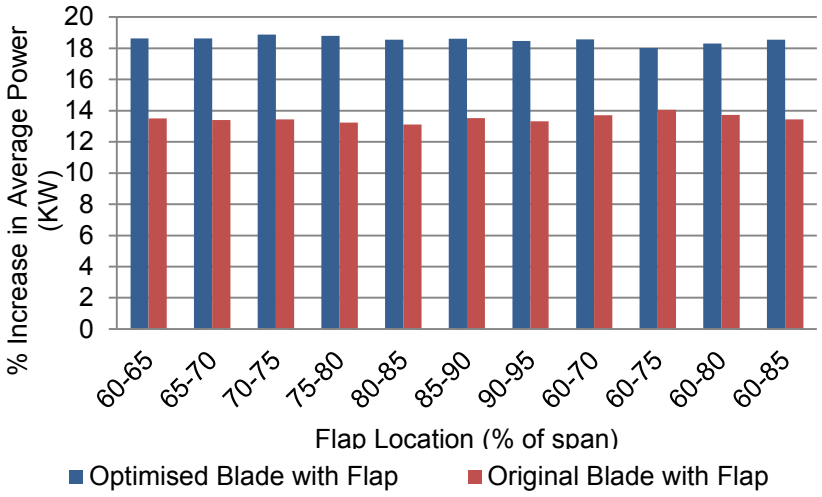

Figure 5.11-Percent increase in the average power versus flap size and location-variable speed rotor

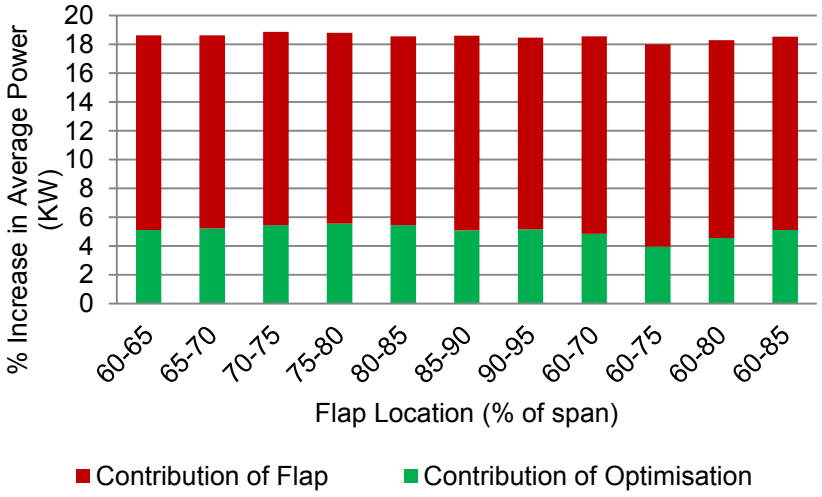

Figure 5.12-Percent improvement in the average power due to blade optimisation-variable speed rotor

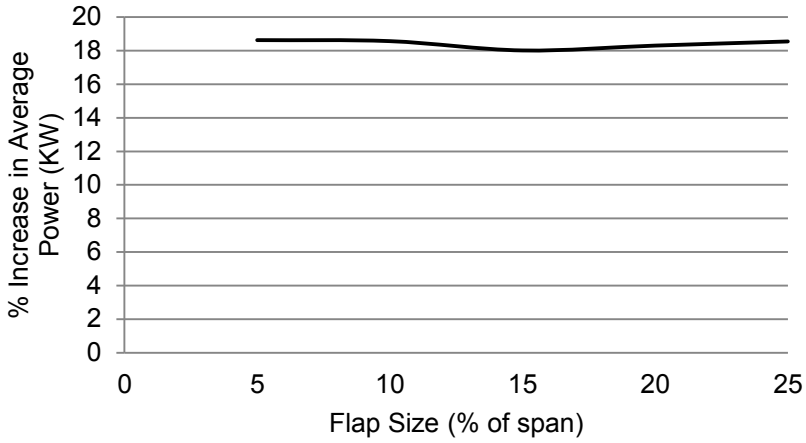

Figure 5.13-Effect of flap size on the power extraction enhancement-variable speed rotor

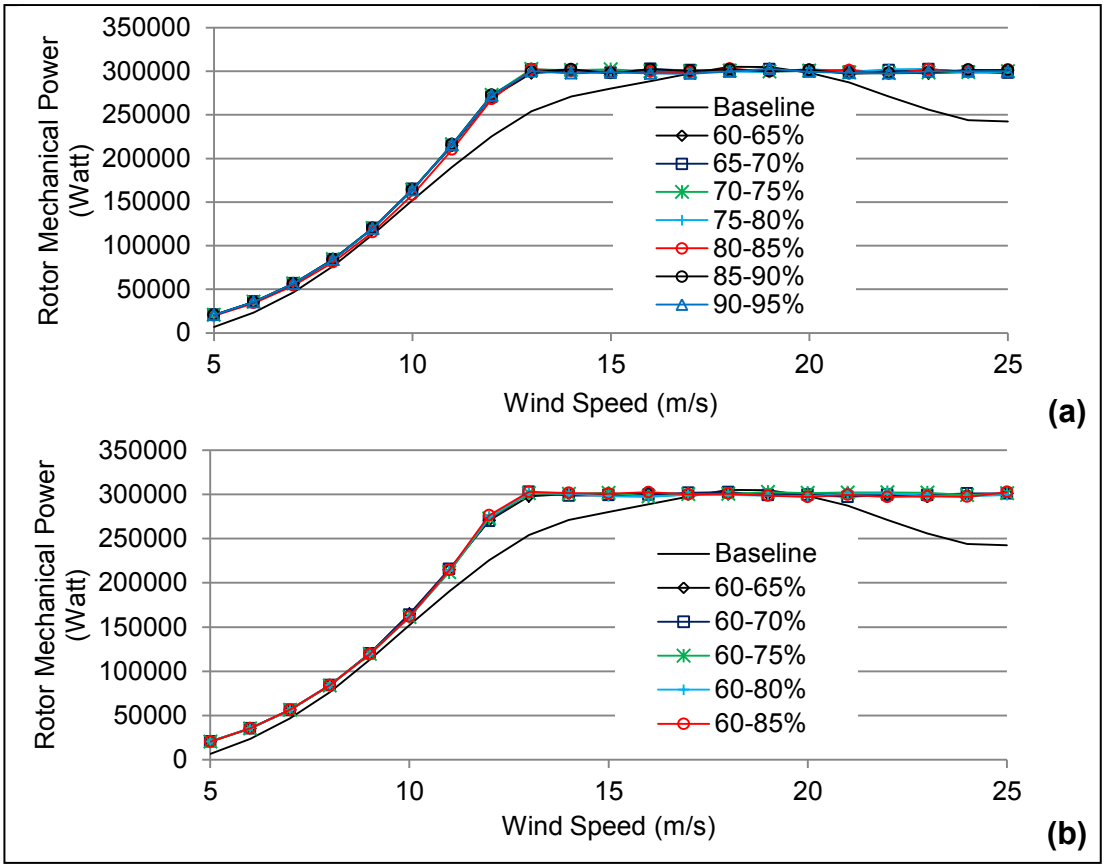

Figure 5.14-Power produced by variable speed rotors utilising blades equipped with flap

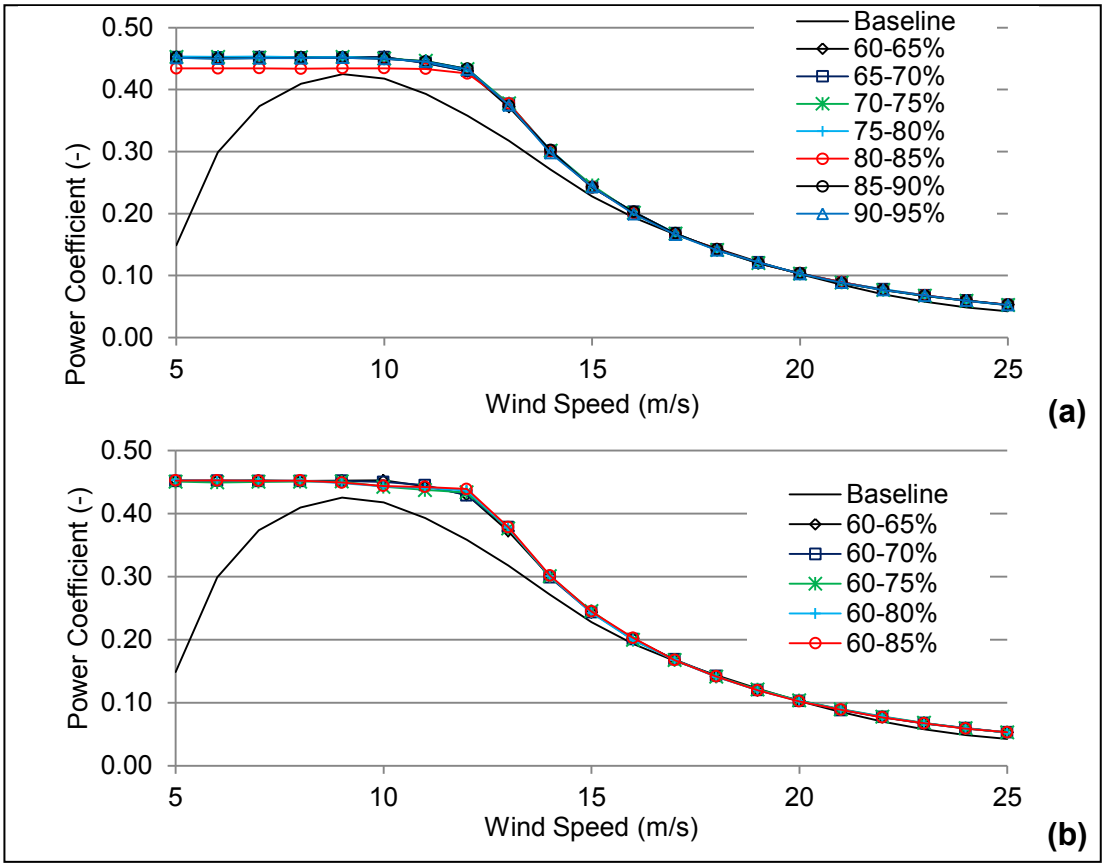

Figure 5.15-Power coefficient of variable speed rotors utilising blades equipped with flap

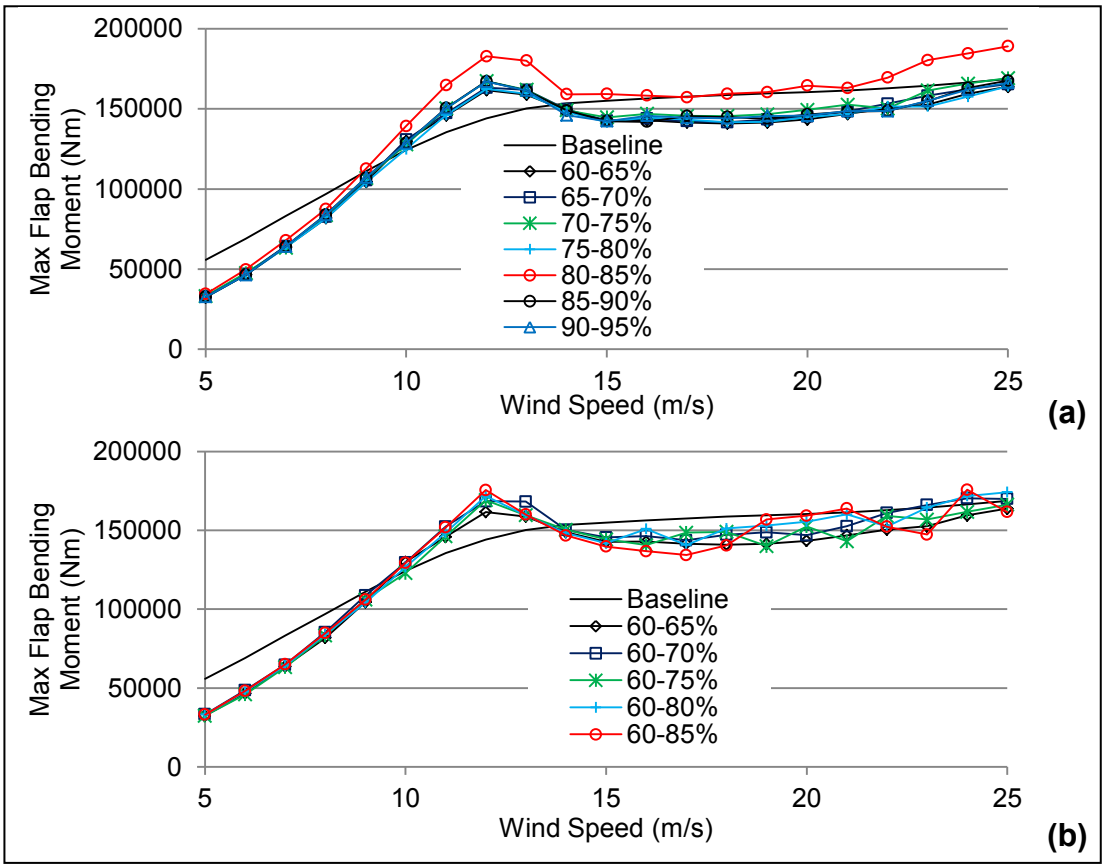

Figure 5.16-Maximum flap bending moment in blades equipped with flap-variable speed rotor

According to the above figures the following conclusion can be drawn:

- Comparing the results of the optimised blade with original blade, it can be observed that using flaps on variable speed rotors can have a twofold effect. Firstly, blades equipped with flap produce more energy (Figure (5.14) and (5.15)). Secondly, for some cases, flap causes a reduction of the blade loading (see V=25 m/s in Figure (5.16)).
- Adding flap without optimisation improve the power extraction capability as high as of about 14% for case of flap located between 60-75% of span (Figure (5.11)). In contrary to the constant speed rotor, the effect of optimisation is less and is limited to only 6% (Figure (5.12)). The overall improvement can be reached as high as 18%.
- In contrary to constant speed rotors, neither the location of flap nor the size of the flap affects the performance significantly. This is mainly due to having rotor speed as the dominant controlling system in place(Figures (5.11) and (5.13)).

5.4 Potentials of Telescopic Blades in Power Extraction Enhancement

Following the same approach as taken in Sections 5.2 and 5.3, for two cases of Table (5.2) the telescopic blades are optimised and compared with the original blades and telescopic blades without optimisation. All simulation, design and optimisation parameters are as given in Sections 5.2 and 5.3. Results are shown in Figures (5.17) and (5.18) for constant speed rotors and Figures (5.19) and (5.20) for variable speed rotors.

Table 5.2- Examined telescopic ranges (all values in % of R)

Case	$R_{T,s}$	$R_{T,e}$
1	80	105
2	80	110

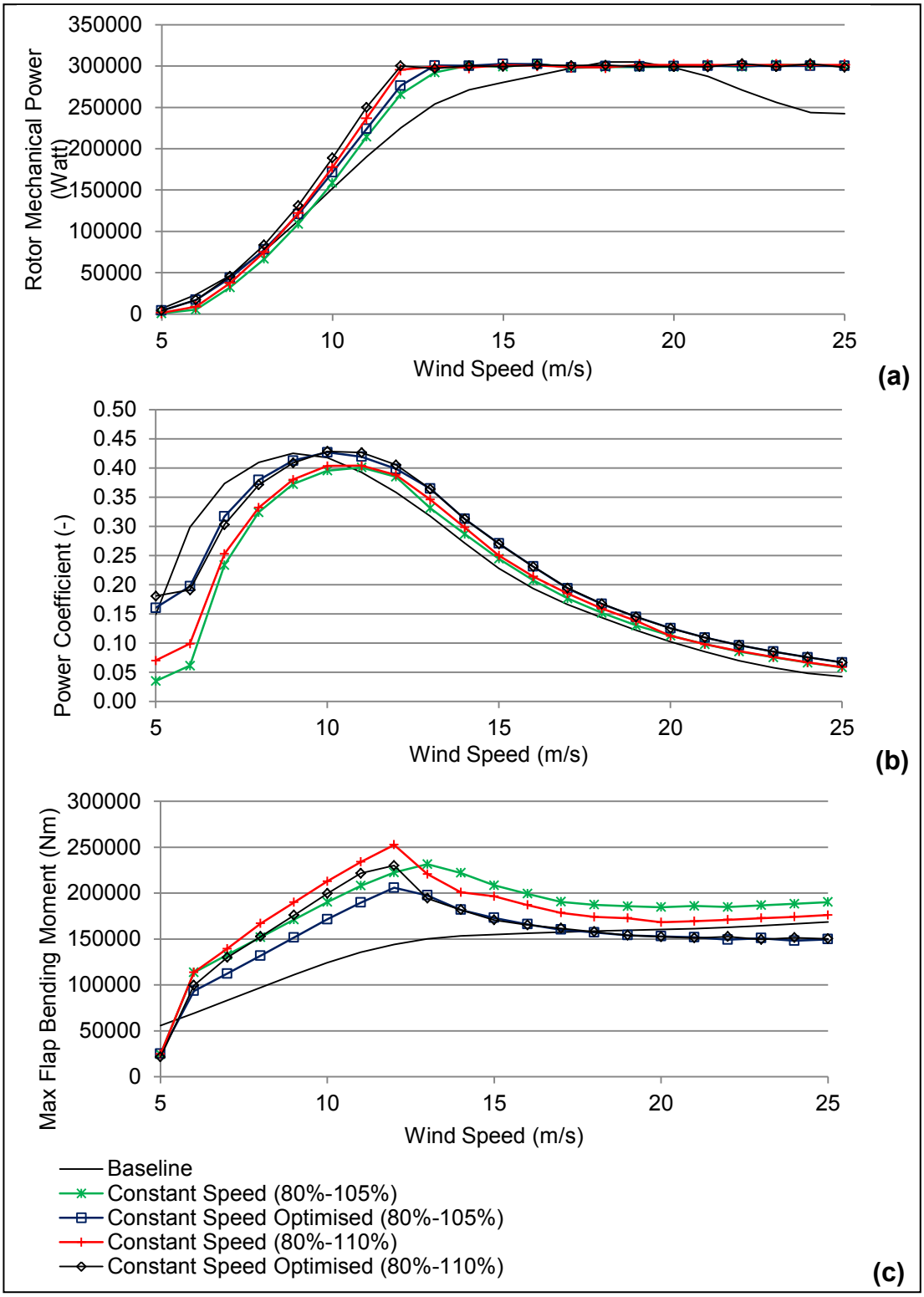

Figure 5.17-Optimised telescopic blade-constant speed rotor

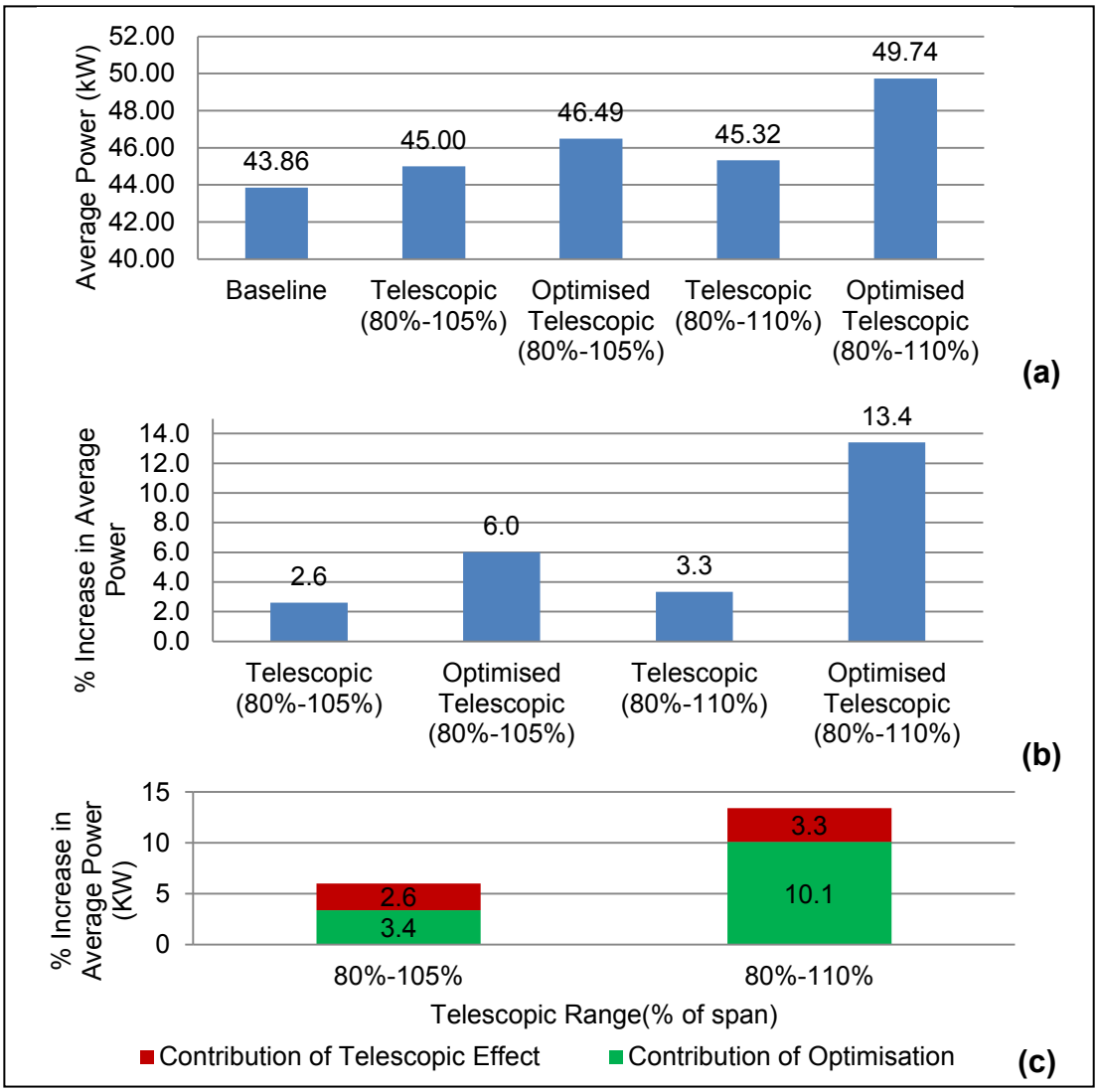

Figure 5.18-Power enhancement via utilising telescopic blades-constant speed rotor

In view of Figures (5.17) and (5.18) the following conclusions can be drawn:

- For constant speed rotors, as expected, utilising telescopic blades improves the amount of the power extraction (Figure (5.17.a)). This amount slightly increases when the telescopic part of the blade is allowed to expand more (2.6% versus 3.3% in Figure (5.18.b)). This difference become significant when the blades are optimised (6% versus 13.4% in Figure (5.18.b)).
- For constant speed rotors, the power coefficient improves only for higher wind speeds above 10 m/s (Figure (5.17.b)). Recalling that the power coefficient is the ratio of the extracted power by the rotor and the available wind power over the rotor area, increase in power coefficient in higher wind speeds is partly due to higher extracted power and partly due to blade contraction. On the other hand, the power coefficient at lower wind speeds is significantly less than the baseline AWT-27 wind turbines. Drop in the power coefficient in low winds, despite extracting more power, is due to blade extension and consequently an increase in the rotor area.

- The maximum flap bending moment in the blades significantly increases with the maximum length of the telescopic blades (Figure (5.17.c)). Optimisation of the blade pretwist reduces the added blade loading significantly.
- Similar to blades equipped with flap, for constant speed rotors the effect of blade optimisation on the power enhancement is significant. The power enhancement is mainly due to the optimisation (Figure (5.18.c)).

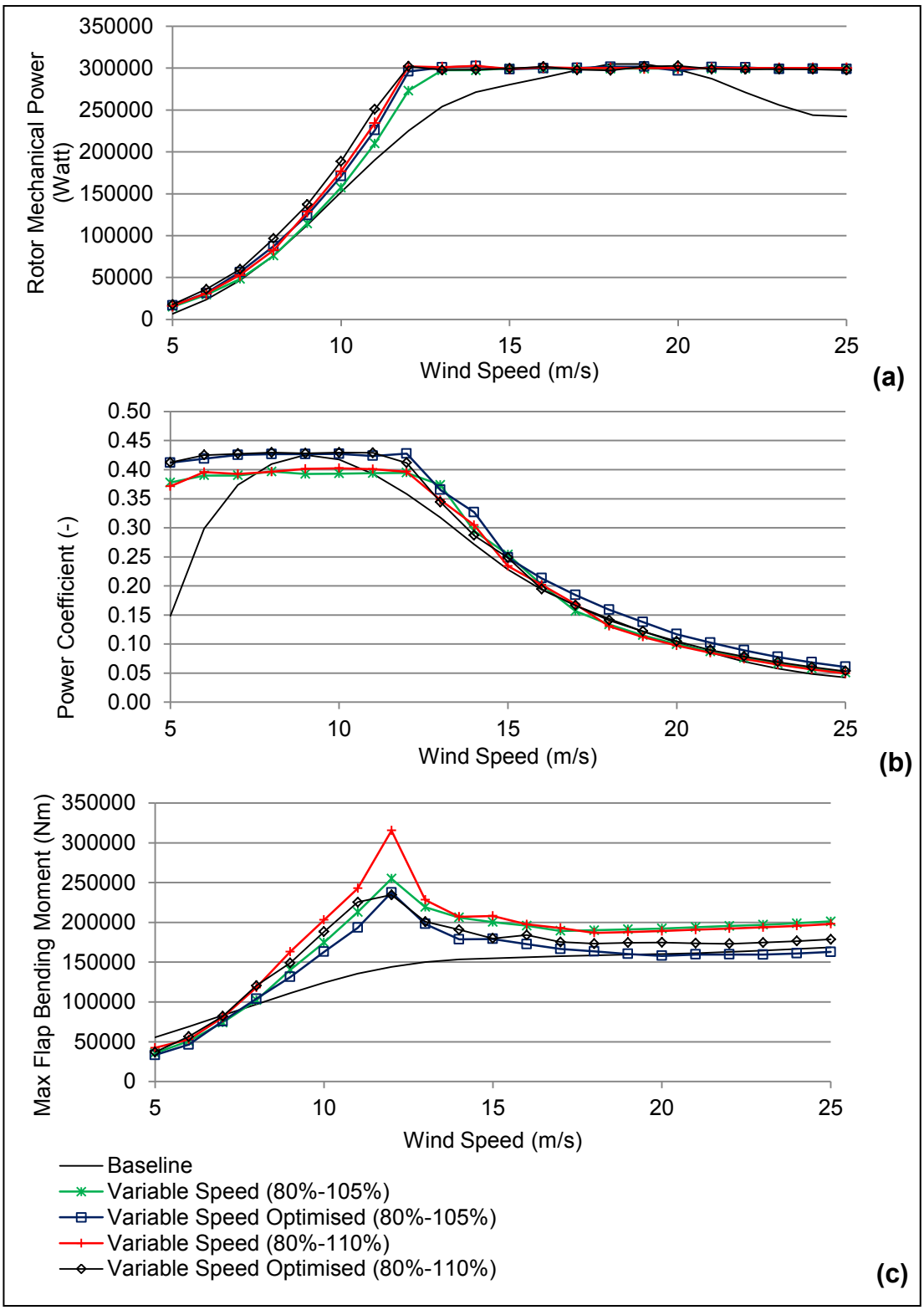

Figure 5.19-Optimised telescopic blade-variable speed rotor

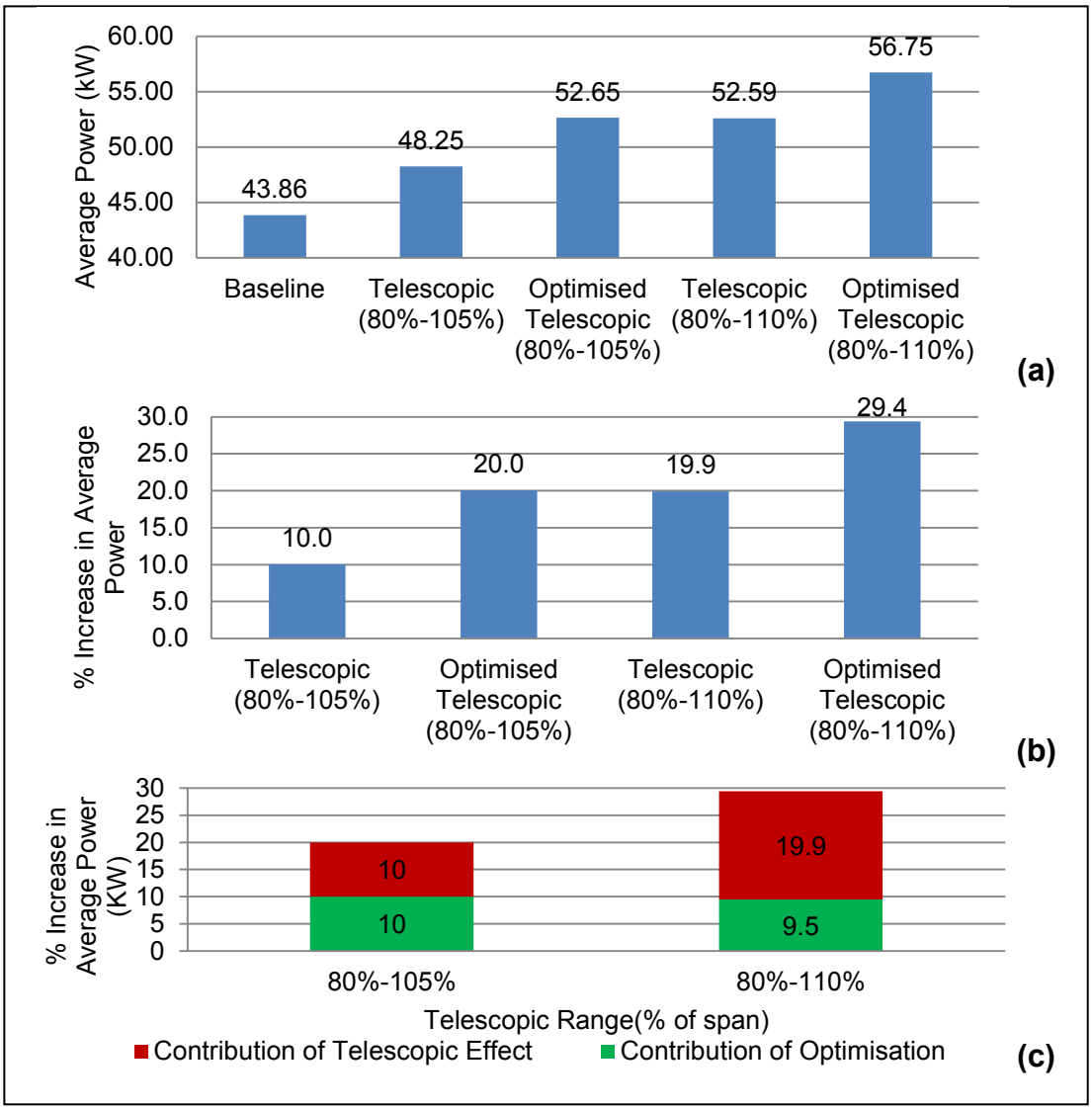

Figure 5.20-Power enhancement via utilising telescopic blades-variable speed rotor

According to Figures (5.19) and (5.20) the following conclusions can be drawn:

- For variable speed rotors, utilising telescopic blades improves the amount of the power extraction (Figure (5.19.a)). This amount increases as the telescopic part of the blade is allowed to expand more (10% versus 19.9% in Figure (5.20.b)). This difference remains significant when the blades are optimised (20% versus 29.4% in Figure (5.18.b)).
- For variable speed rotors, the power coefficient improves for both low wind and high wind regions. This is mainly due to having two controlling parameters (blade span and rotor speed).
- The maximum flap bending moment in the blades significantly increases with the maximum length of the telescopic blades (Figure (5.19.c)). Optimum blades have significantly less maximum flap bending moments.

5.5 Potentials of Microtabs in Power Extraction Enhancement

In Section 3.8 it was shown that unlike other controlling devices, microtab has little effect on the power extraction enhancement when installed on the blade. In this section, adopting the same case study as in Section 3.8 ($R^*_{MT,s}=0.6$ to $R^*_{MT,e}=0.9$, $d^*_{MT}=80\%$ and $d^*_{MT}=95\%$ of the chord from the leading edge on the upper and lower surface respectively, with an actuation height of $h^*_{MT}=3.3\%$ of the chord length), the blades are also optimised for pretwist. Results are shown in Figures (5.21) and (5.22).

According to Figures (5.21), (5.22.b) and (5.22.c), it is evident that pretwist optimisation has significant influence on the extracted power. The baseline blades extract more or less the same amount of power, with or without microtab, unless the pretwist is optimised.

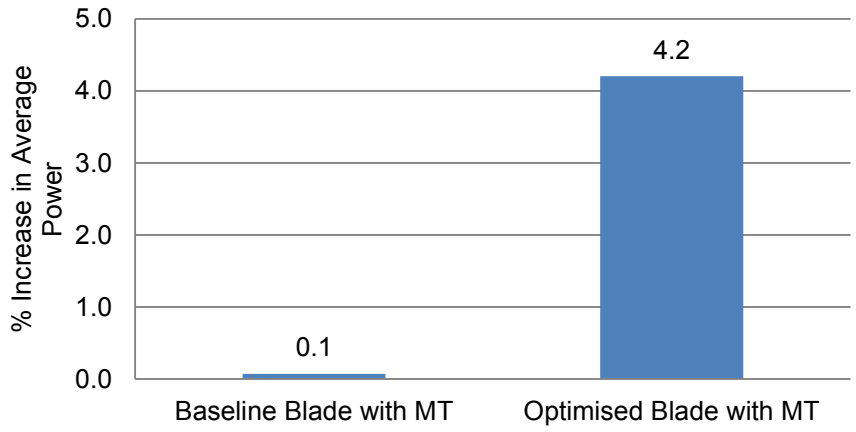

Figure 5.21-Microtab on optimised blades-power enhancement

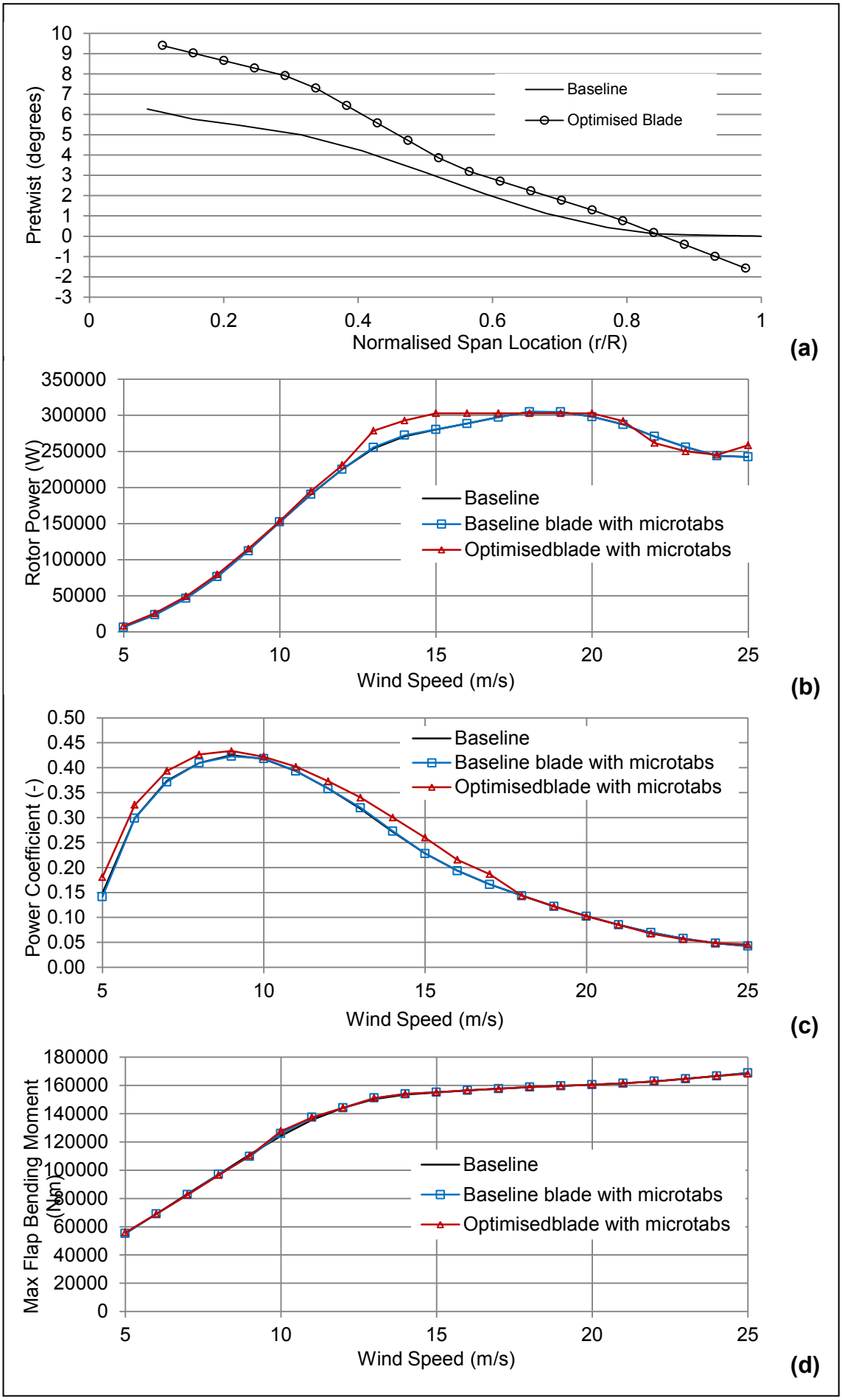

Figure 5.22-Microtab on optimised blades

5.6 Summary

In this chapter, employing the optimisation tool AWTSimD, the potentials of flap trailing edge, microtab and telescopic blades in enhancing energy capture capability of blades were investigated. In all cases only the pretwist was considered for optimisation keeping the optimised blade structurally as close as possible to the baseline blade. In case of trailing edge flaps the effect of size and location of the flap was also investigated. In all cases the amount of enhancement in power production was broken down into two parts, namely, contribution of the controlling device (flap, microtab and telescopic blade) and the contribution of the optimisation. It was shown that optimisation of the blade plays a major role in enhancing the power capture capability for constant speed rotors.

6 Summary and Conclusion

6.1 Summary of Work, Achievements and Contribution

To meet the overall goal of this research: "investigation of the potentials of nonconventional control systems which have been initially developed for load control in energy capture capability enhancement", a design optimisation code, capable of simulating wind turbines with constant and variable speed rotors utilising telescopic blades as well as blades equipped with microtab and trailing edge flaps was developed.

The aerodynamic analysis module of the code is based on the well-established method of BEMT. A software tool, called AWTSim, was developed for aerodynamic analysis of wind turbines. Using a stall-regulated constant speed test wind turbine, the performance of AWTSim was validated against WTPerf, a simulation code accredited by NREL. Further necessary enhancements to AWTSim were applied to make it capable of simulating wind turbines with nonconventional control systems.

Analysis of the controlling system is based on a realistic assumption: the actual controllers perform perfectly in finding and adjusting the controlling parameters to their best (optimum) values. This assumption was then used to transform "simulation of the controlling system" to "solving an optimisation problem". It was shown that this method performs well with sufficient accuracy and robustness as required for the aerodynamic analysis of nonconventional blades. In solving the corresponding optimisation problem, three methods of optimisation, namely, hill climbing, pattern search and genetic algorithm were tailored and used to solve the optimisation problem. The performance of the hill climbing and pattern search methods was evaluated and reported.

AWTSim is a unique simulation tool capable of simulating the following types of wind turbines:

1. Constant speed stall regulated rotors
2. Variable speed stall regulated rotors
3. Constant speed pitch controlled rotors
4. Variable speed pitch controlled rotors
5. Constant speed flap controlled rotors
6. Variable speed flap controlled rotors

7. Constant speed rotor with telescopic blades
8. Variable speed rotors with telescopic blades
9. Constant speed rotors with blades equipped with microtab

For each type a case study was carried out to demonstrate the capability and the performance of the developed wind turbine simulator. It should be noted that, none of the wind turbine simulators reported in open literature is capable of simulating wind turbines of types 5 to 9 above.

For the optimiser module of the code, a robust genetic algorithm, with some advanced features such as geometric crossover and initial population generation based on perturbation of an existing design candidate, was developed. Integration simulation tool AWTSim into the optimiser module constructs the design optimisation code AWTSimD.

Employing AWTSim and AWTSimD and investigating three nonconventional control systems, microtab, trailing edge flap and telescopic blades led to the following results.

Trailing edge flaps

- Adding flap without optimisation improves the power extraction capability as high as of about 5% and 14% for constant speed and variable speed rotors, respectively. Significant further improvement as a result of optimisation can be achieved (up to 7%) for constant speed rotors, while the effect of optimisation is less and limited to only 6% for variable speed rotors. The overall improvement in the produced power can be reached as high as 12% and 18% for constant speed and variable speed rotors respectively.
- For constant speed rotors, the location of flap is a key parameter influencing the amount of improvement in the power extraction. The best location for placing a flap is at about 70% of the blade span from the rotor centre. The size of the flap has also significant effect on the amount of enhancement in the average power. This effect, however, reduces dramatically as the size increases. For variable speed rotors, neither the location of flap nor its size affects the performance significantly.
- Flaps, when used in conjunction with another controlling system such as rotor speed, the accompanied controlling system dominates the control process.

Telescopic blades

- Telescopic blades provide a full and smooth power control.
- Utilising telescopic blades in both constant and variable speed rotors improves the amount of the power extraction. Power extraction enhancement is higher in variable speed rotors. However, this enhancement comes with the price of a significant increase in bending moment at the root of blade.
- In constant speed rotors, the improvement in the power extraction slightly increases with the fully extended length of the blade (2.6% for permissible extended length of 105% versus 3.3% for permissible extended length of 110% of the baseline rotor radius). This difference becomes significant when the blades are optimised (6% versus 13.4% respectively). For variable speed rotors, the enhancement in the produced power is more significant and sensitive to the permissible extended length (10% for permissible extended length of 105% versus 19.9% for permissible extended length of 110%). This difference remains significant when the blades are optimised (20% versus 29.4%).
- For constant speed rotors, the power coefficient improves only for higher wind speeds, while at lower wind speeds it is significantly less than the baseline wind turbines. Drop in the power coefficient in low winds, despite extracting more power, is due to blade extension and consequently increase in the rotor area. In case of variable speed rotors, the power coefficient improves for both low wind and high wind regions. This is mainly due to having both blade span and rotor speed as controlling parameters.
- In both constant and variable speed rotors, the maximum flap bending moment in the blades significantly increases with the maximum length of the telescopic blades, unless the blades are optimised.

Microtabs:

- The baseline blades extract more or less the same amount of power, with or without microtab, unless the pretwist is optimised.
- Microtabs on optimised blades can improve the produced power by up to 4%.

Also, it was shown that pitch control is the most efficient control system having the highest power coefficient and minimal blade root bending moment for both constant speed and variable speed rotors. For constant speed rotors, optimised telescopic blades are more effective than flaps in power enhancement. However, in comparison with flap,

telescopic blades have two disadvantages: (i) complexity in telescopic mechanism and the added weight and (ii) increased blade loading.

These results, together with the tools developed as part of this project can be used in design of more efficient wind turbines.

6.2 Critical Appraisal and Future Work

Optimisation of blades equipped with microtabs is highly time-consuming. Each optimisation run takes 20 hours on university work stations. This is due to the fact that each design candidate evaluation as part of the blade optimisation includes a full optimisation process by itself for the purpose of controller simulation (to obtain the best microtab states). As a result of this the effect of the location of microtabs was not investigated in this study.

In investigating the effect of microtabs, only deployment height of 3.3% was studied. This deployment height has the maximum effect on the lift and drag coefficients.

In investigating the effect of flaps, only the case of flap width of 10% chord and deployment angle limited to -20 to +20 degrees was investigated. This was mainly due to lack of available data for other flap widths.

A continuation to the presented research, after addressing above shortcomings, can be followed by:

- Design of blades from scratch with rotor radius, chord and aerofoil distributions as design variables in addition to the pretwist.
- Investigating the full potentials of new devices will be completed by performing cost analysis for each device. Cost analysis should include initial, operating and maintenance cost.

References

Ashwill, T. & Laird, D. (2007) Concepts to facilitate very large blades. *In: Proceedings of ASME/AIAA Wind Energy Symposium*, Reno, NV. 2007.

Andersen P. B., Gaunaa . M., et al. (2006) Load alleviation on wind turbine blades using variable airfoil geometry. *In: Proceedings of European Wind Energy Conference and Exhibition2006, Athens*.

Baeck, T., Fogel, D. B. & Michalewicz, Z. (2010) *Handbook of Evolutionary Computation*. Taylor & Francis.

Baker, J. P., Standish, K. J. & van Dam, C. P. (2005) Two-dimensional wind tunnel and computational investigation of a microtab modified S809 airfoil, *AIAA 2005-1186. In: Proceedings of the 43rd AIAA/ASME*, *Reno, NV, USA*.

Barlas, T. & Van Kuik, G. M. (2010) Review of state of the art in smart rotor control research for wind turbines. *Aerospace Sciences*, 46, 1-27.

Bossanyi, E. A. (2000) The design of closed loop controllers for wind turbines. *Wind Energy*, 3.

Bossanyi, E. A. (2003) Individual blade pitch control for load reduction. *Wind Energy*, 6, 119-128.

Bottrell, G. W. (1981) Passive cyclic pitch control for horizontal axis wind turbines. In: *Proceedings of Wind Turbine Dynamics*, *NASA Conference Pub. 2185,DOE Pub. CONF-810226, Cleveland, OH*.

BTM Consult ApS, (2005) *Ten Year Review of the International Wind Power Industry 1995-2004*.

Burton, T., Sharpe, D., Jenkins, N. & Bossanyi, E. *Wind energy handbook*. John Wiley & Son Inc.

Buhl, T. & Gaunaa, M., et al. (2005) Potential load reduction using airfoils with variable trailing edge geometry. *Journal of Solar Energy Engineering*, 127, 503-516.

Buhl, Jr., M. L.(2004) *NWTC Design Codes, 2004. WT_Perf Version 3.1*. [Online]. Available from: http://wind.nrel.gov/ designcodes/ simulators/wtperf/ [Accessed 28 Aug. 2012].

Buhl, Jr, M. L. (2005) *A new empirical relationship between thrust coefficient and induction factor for the turbulent windmill state*. National Renewable Energy Laboratory, Technical report NREL/TP-500-36834.

Currin, H. (1981) North wind 4kW 'Passive Control System Design, In: *Proceedings Wind Turbine Dynamics*, *NASA Pub. 2185, DOE Pub. CONF-810226, Cleveland, OH*.

Cheney, M. C. & Speirings, P. S. M. (1978) Self regulating composite bearing less wind turbine. *Solar Energy*, 20.

Caselitz, P., Kleinkauf, W., Kruger, T., Petschenka, J., Reichardt, M. & Storzel, K. (1997) Reduction of fatigue loads on wind energy converters by advanced control methods. *In: Proceedings of the European Wind Energy Conference*, *Dublin*, pp.555–558.

Chow, R. & van Dam, C.P. (2007) Computational investigations of deploying load control microtabs on a wind turbine airfoil. *AIAA-2007-1018. In: Proceedings of the 45th AIAA/ASME*, *Reno, NV, USA*.

Crespo, A., Hernández, J. & Frandsen, S. (1999) Survey of modelling methods for wind turbine wakes and wind farms. *Wind Energy*, vol.2, 1–24.

Corbet, D. C. & Morgan, C. A. (1992) *Report on the passive control of horizontal axis wind turbines*. Garrad Hassan and Partners, Bristol, UK, ETSU WN 6043.

DOE. (2005) *Variable length wind turbine blade*. DE-FG36-03GO13171.

Hella, D. (2012) *Producing reliable aerodynamic lookup tables for microtabs installed on wind turbine blades made of S800 series aerofoils*. Northumbria University, MSc Dissertation.

Drela, M. & Giles, M. B.(1987) Viscous-inviscid analysis of transonic and low Reynolds Number airfoils. *AIAA Journal*, 25(10), 1347-1355.

Drela, M. (1988) Low-Reynolds Number airfoils design for the MIT daedalus prototype: a case study. *Journal of Aircraft*, 25(8), 724-732.

Drela, M. (1989) XFOIL: An analysis and design system for low Reynolds Number airfoils. *In: Proceedings Conference on Low Reynolds Number Airfoil Aerodynamics, University of Notre Dame*.

Drela, M. (1989) *Low Reynolds Number aerodynamics*. T.J. Mueller (Editor), [Lecture] Lecture Notes in Engineering #54, Springer Verlag, 1989.

Drela, M. (1989) Integral boundary layer formulation for blunt trailing edges. *AIAA-89-2166*.

Drela, M. (1990) Elements of airfoil design methodology, applied computational aerodynamics. *In: Henne, P. (Editor) AIAA Progress in Aeronautics and Astronautics*, 125.

Drela, M. (1998) *Pros and Cons of Airfoil Optimization, Chapter in Frontiers of Computational Fluid Dynamics.* Caughey, D. A., Hafez, M. M. Eds. World Scientific.

Drela, M. (2008) *XFOIL Subsonic Airfoil Development System, 2008*. [Online] Available from: http://web.mit.edu/drela/Public/web/xfoil/ [Accessed 28 August 2011].

Du, Z. & Selig, M. S. (1998) A 3-D stall-delay model for horizontal axis wind turbine performance prediction. *In: Proceedings of the 1998 ASME Wind Energy Symposium*, Reno, NV ,pp. 9–19.

Enenkl, B., Klopper, V., et al., (2002) Full scale rotor with piezoelectric actuated blade flaps. *28th European Rotorcraft Forum*.

Farhan, G. & Phuriwat, A. I. (2008) Skin design studies for variable camber morphing airfoils. *IOPP'S Journal*.

GE Wind Energy LLC (2006) *Advanced wind turbine program next generation turbine development project*, NREL laboratory, Report NREL/SR-5000-38752.

Global Wind Energy Council (2011) *Global wind statistic 2010*.

Herbert, G. M. J., Iniyan, S., Sreevalsan, E. & Rajapandian, S. (2007) A review of wind turbine technologies. *Renewable and Sustainable Energy Reviews*,11.

Hohenemser, K. H. & Swift, A. H. P. (1981) Dynamics of an experimental two bladed horizontal axis wind turbine with blade cyclic pitch variation. NASA, Report NASA 82N23716.

Holland, J. H. (1975) *Adaptation in Natural and Artificial Systems* . MIT Press, Cambridge, MA.

Johnson, S. J., van Dame, C.P. & Berg, D.E. (2008) *Active load control techniques for wind turbines*. SANDIA, Report SAND2008-4809.

Jureczko, M., Palwak, M. & Mężyk, A. (2005) Optimisation of wind turbine blade. *Materials Processing Technology*, 167, 463-471.

Johnson, W. (1982) *Self-Tuning Regulators for Multicyclic Control of Helicopter Vibration*, NASA, Report NASA.

Jonkman, J. M. (2003) Modelling of the UAE wind turbine for refinement of FAST AD. National Renewable Energy Laboratory, Technical Report NREL/TP-500-34755.

Karaolis, N. M. (1989) The design of fibre reinforced composite blades for passive and active wind turbine aerodynamic control. Dissertation University of Reading.

Kooijiman, H. J. T. (1996) Smart rotor, feasibility study for a passive pitch regulation of a wind turbine rotor blade. ECN, Report Petten ECN-I-96-0011 ECN.

Larsen, T., Madson, H. & Thomson, K. (2005) Active load reduction using individual pitch, based on local blade flow measurements. *Wind Energy*, 8, 67–80.

Leishman, G. (2000) *Principles of helicopter aerodynamic.* Cambridge Univ. Press, Cambridge.

Lobitz, D. W., Veers, P. S., Laino, D. J., Migliore, P. G. & Bir, G. (2001) *The use of twist-coupled blades to enhance the performance of horizontal axis wind turbine*. Sandia National Laboratories, Report SAND2001-1003.

Lovera, Colaneri, M. P., Malpica, C. & Celi, R. (2003) Closed-loop stability analysis of HHC and IBC, with application to a hinge less rotor helicopter. *In: Proceedings 29th European Rotorcraft Forum*.

Macquart, T. (2012) *Flap data generation using XFOIL*. Internal Report, Northumbria University.

Madsen, H. A. (1996) A CFD analysis for the actuator disc flow compared with momentum theory results. In: *Proceedings 10th IEA Symp. Aerodyn. Wind Turbines*, *Tech. Univ. Denmark, Lyngby, Denmark*, pp. 109–24.

Madsen, H. A. & Rasmussen, F. (2004) A near wake model for trailing vorticity compared with the blade element momentum theory. *Wind Energy*, 7, 325-34.

Maheri, A. (2006) *Aero-structure simulation and aerodynamic design of wind turbines utilising adaptive blades*. University of West England-Bristol, PhD Thesis.

Maheri, A., Noroozi, S., Toomer, C. & Vinney, J. (2006a) Single step versus coupled aero-structure simulation of a wind turbine with bend-twist adaptive blades. *European Wind Energy Conference EWEC 2006*, *27 February-2 March 2006,Athens, Greece*.

Maheri, A., Noroozi, S., Toomer, C. & Vinney, J. (2006b) A Simple algorithm to modify an ordinary wind turbine blade to an adaptive one. *European Wind Energy Conference EWEC 2006*, *27 February-2 March 2006,Athens, Greece*.

Maheri, A., Noroozi, S. & Vinney, J. (2007a) Application of combined analytical/FEA coupled-aero-structure simulation in design of wind turbine adaptive blades. *Renewable Energy*, 32(12), 2011-2018.

Maheri, A., Noroozi, S. & Vinney, J. (2007b) Decoupled design of wind turbine adaptive blades. *Renewable Energy*, 32(10), 1753-1767.

Maheri, A. & Isikveren, A. T. (2008) Variable-state design parameters in design of aero-structures made of intrinsically smart materials. *High Performance Structures and Materials IV*. Editors de Wilde, W. P. & Brebbia, C.A., WIT Press, pp. 421-430.

Maheri, A. & Isikveren, A. T.(2008) Facilitating meta-design techniques for multi-disciplinary conceptual design. *Adaptive Computing in Design and Manufacture, Bristol,UK*.

Maheri, A. & Isikveren, A.T.(2009a) Design of wind turbine passive smart blades. *European Wind Energy Conference EWEC 2009*, *Marseille, France*.

Maheri, A. & Isikveren, A. T. (2009b) A parallel genetic algorithm for optimal synthesis of a morphing aerofoil. In: Topping, B.H.V. & Ivanyi, P. (Editors) *In : Proceedings of the First International Conference on Parallel, Distributed and Grid Computing for Engineering.* Civil-Comp Press, Stirlingshire, UK, Paper 9.

Maheri, A. & Isikveren, A. T. (2010) Performance prediction of wind turbines utilising passive smart blades: approaches and evaluation. *Wind Energy*, 3, 255-265.

Maheri, A., Macquart, T., Safari, D. & Maheri, M. R. (2012) Phenotype Building Blocks and Geometric Crossover in Structural Optimisation. In: Topping, B.H.V. (Editors) *In: Proceedings of the Eighth International Conference on Engineering Computational Technology.* Civil-Comp Press, Stirlingshire, UK, Paper 5.

Mayda, E. A., van Dam, C. P., & Nakafuji, D. Y. (2005) Computational investigation of finite width microtabs for aerodynamic load control. *AIAA-2005-1185. In: Proceedings of the 43th AIAA/ASME*, *Reno, NV*.

Mēndez, J. & Greiner, D. (2006) Wind blade chord and twist angle optimization using genetic algorithms. *In: Proceedings of the Fifth International Conference on Engineering Computational Technology*.

Migliore, P. G., Quandt, G. A., et al. (1995) *Wind turbine trailing edge aerodynamic brakes*. National Renewable Energy Laboratory ,Technical Report NREL/TP-441-7805.

Michalewicz, Z. (1992) *Genetic Algorithms + Data Structures = Evolution Program* . Springer Verlag.

Moriarty, P. J., & Hansen, A. C. (2005) *AeroDyn theory manual*. National Renewable Energy Laboratory, Technical report NREL/TP-500-3688.

Nijssen, R. P. L. (2006) Fatigue life prediction and strength degradation of wind turbine rotor blade composites. *Knowledge Centre Wind Turbine Materials and Constructions (KC-WMC)*, Netherland.

Nakafuji, D. T. Y., van Dam, C. P., Michel, J. & Morrison, P. (2002) Load control for wind turbines - a non-traditional microtab approach. *AIAA2002-0054.In: Proceedings of the 40th AIAA/ASME*, *Reno, NV, USA*.

Pasupulati, S. V., Wallace, J. & Dawson, M. (2005) *Variable Length Blades Wind Turbine.* Energy Unlimited Inc.

Robert, G. & Jochen, T. (2011) *Wind power plants fundamentals, design, construction and operation*.Springer.

Sanderse, B., van der Pijl, S. P. & Koren, B. (2011) Review of computational fluid dynamics for wind turbine wake aerodynamics. *Wind Energy*, 14, 799-819.

Sanderse, B. (2009) *Aerodynamics of wind turbine wakes Literature review*. ECN, Report ECN-E-09-016.

Seki, K., Shimizu, Y. & Zhu, K. (1996) A design strategy for the improvement of an existing 300kW WTGs rotor blade. *Renewable Energy*, 9, 858-86.

Shrama, R. N. & Madawala, U. (2007) The concepts of a smart wind turbine system. *In: Proceeding* of *16th Australian Fluid Mechanics Conference*, *Australia*.

Snel, H. & Schepers, J. G. (1995) Joint investigation of dynamic inflow effects and implementation of an engineering method, ECN, Report Petten ECN-C-94-107.

Snel, H. (1998) Review of the present status of rotor aerodynamics, *Wind Energy*, 1, 46–69.

Snel, H. (2003) Review of aerodynamics for wind turbines, *Wind Energy*, 6, 203–211.

Stuart, J. G., Wright, A. D. & Butterfield, C. P. (1996) Considerations for an integrated wind turbine controls capability at the national wind technology centre: an aileron control case study for power regulation and load mitigation. National Renewable Energy Laboratory, Technical Report NREL/TP-440-21335.

Spera, D. A. (1994) *Wind Turbine Technology, Fundamental Concepts of Wind Turbine Engineering.* American Society of Mechanical Engineers.

Stuart, J. G., Wright, A. D., et al. (1997) Wind turbine control systems: dynamic model development using system identification and the fast structural dynamics code. *In: Proceedings 35th AIAA/ASME*.

Tangler, J. L. (2002) The nebulous art of using wind-tunnel airfoil data for predicting rotor performance. National Renewable Energy Laboratory, Report NREL/CP-500-31243.

Tangler, J. L. (2002) The nebulous art of using wind tunnel aerofoil data for predicting rotor performance. *Wind Energy*, 5,245–257.

Tangler, J. L. & Kocurek, J. D. (2004) Wind turbine post-stall airfoil performance characteristics guidelines for blade element momentum methods. National Renewable Energy Laboratory, Report NREL/CP-500-36900.

Troldborg, N. (2005) Computational study of the risø-b1-18 airfoil with a hinged flap providing variable trailing edge geometry. *Wind Engineering*, 29(2), 89-113.

Van der Hooft, E. L., Schaak, P. & Van Engelen, T. G. (2003) Wind turbine control algorithms. ECN, Report ECN-C-03-111.

Van Engelen, T. & Van der Hooft, E. (2003) *Individual pitch control inventory*. ECN, Report ECN-C–03-138.

Vermeer, L. J., Sørensen, J. N. & Crespo, A. (2003) Wind turbine wake aerodynamics. *Progress in Aerospace Sciences*,39, 467–510.

Wind Turbine Dynamics, (1985) NASA Pub. 2185, DOE Pub. CONF-810226, Cleveland, OH.

Wright, A. & Barlas, M. (2002) Design of State-Space-Based Control Algorithms for Wind Turbine Speed Regulation. In : *Proceeding of the 2002 ASME Wind Energy Symposium*, *Reno, Nevada.* pp. 299-309.

Yen, D. T., van Dam, C. P., Smith, R. L. & Collins, S. D. (2001) Active load control for wind turbine blades using MEM translational tabs, *AIAA-2001-0031.In: Proceedings of the 39th AIAA/ASME*, *Reno , NV , USA*.

Appendix A-Sample Simulation and Design Input Files

```
%====================
wttype=3;
%====================
vw_s=5;
vw_i=1;
vw_e=25;
%====================
rpm=53.3;
pitch=-1.2;
flap_s=-20;flap_i=.1;flap_e=20;
rflap1=.6;rflap2=.65;
r_telescop=1;
rmt1=0;rmt2=0;
%====================
yaw=0;
b=2;
d=27.514;
cone=7;
h=30;
prated=300000;
tolprated=.01;
z0=0.025;
vav=5.7;
dens=1.225;
ip=5;
%====================
sim_results_1_par='vw,rpm,pitch,tsr,p,cp,thrust,mroot_maxvw,beta(nseg),flap
,r_telescop,{azimuth_mroot}';
sim_results_2_par='pav,pmax,cpmax,thrustmax,mrootmax';

nseg=20;nsec=1;rx=0.5;
```

Figure A1-Sample simulation file for constant speed rotor with flap control

```
%====================
wttype=3;
%====================
vw_s=5;
vw_i=1;
vw_e=25;
%====================
rpm_s=30;rpm_i=.1;rpm_e=65;
pitch=-1.2;
flap_s=-20;flap_i=.1;flap_e=20;
rflap1=.6;rflap2=.65;
r_telescop=1;
rmt1=0;rmt2=0;
%====================
yaw=0;
b=2;
d=27.514;
cone=7;
h=30;
prated=300000;
tolprated=.01;
z0=0.025;
vav=5.7;
dens=1.225;
ip=5;
%====================
sim_results_1_par='vw,rpm,pitch,tsr,p,cp,thrust,mroot_maxvw,beta(nseg),flap
,r_telescop,{azimuth_mroot}';
sim_results_2_par='pav,pmax,cpmax,thrustmax,mrootmax';

nseg=20;nsec=1;rx=0.5;
```

Figure A2-Sample simulation file for variable speed rotor with flap control

```
%====================
wttype=4;
%====================
vw_s=5;
vw_i=1;
vw_e=25;
%====================
rpm=53.3;
pitch=-1.2;
flap=0;rflap1=0;rflap2=0;
rtelescop1=.7;rtelescop_i=.001;rtelescop2=1.1;
rmt1=0;rmt2=0;
%====================
yaw=0;
b=2;
d=27.514;
cone=7;
h=30;
prated=300000;
tolprated=.01;
z0=0.025;
vav=5.7;
dens=1.225;
ip=5;
%====================
sim_results_1_par='vw,rpm,pitch,tsr,p,cp,thrust,mroot_maxvw,beta(nseg),flap
,r_telescop,{azimuth_mroot}';
sim_results_2_par='pav,pmax,cpmax,thrustmax,mrootmax';

nseg=20;nsec=1;rx=0.5;
```

Figure A3- Sample simulation file for constant speed rotor with telescopic blades

```
%====================
wttype=10;
%====================
vw_s=5;
vw_i=1;
vw_e=25;
%====================
rpm_s=30;rpm_i=.1;rpm_e=65;
pitch=-1.2;
flap=0;rflap1=0;rflap2=0;
rtelescop1=.7;rtelescop_i=.001;rtelescop2=1.1;
rmt1=0;rmt2=0;
%====================
yaw=0;
b=2;
d=27.514;
cone=7;
h=30;
prated=300000;
tolprated=.01;
z0=0.025;
vav=5.7;
dens=1.225;
ip=5;
%====================
sim_results_1_par='vw,rpm,pitch,tsr,p,cp,thrust,mroot_maxvw,beta(nseg),flap
,r_telescop,{azimuth_mroot}';
sim_results_2_par='pav,pmax,cpmax,thrustmax,mrootmax';

nseg=20;nsec=1;rx=0.5;
```

Figure A4-Sample simulation file for variable speed rotor with telescopic blades

```
%====================
wttype=2;
%====================
vw_s=5;
vw_i=1;
vw_e=25;
%====================
rpm=53.3;
pitch_s=-5;pitch_i=0.05;pitch_e=5;
flap=0;rflap1=0;rflap2=0;
r_telescop=1;
rmt1=0;rmt2=0;
%====================
yaw=0;
b=2;
d=27.514;
cone=7;
h=30;
prated=300000;
tolprated=.01;
z0=0.025;
vav=5.7;
dens=1.225;
ip=5;
%====================
sim_results_1_par='vw,rpm,pitch,tsr,p,cp,thrust,mroot_maxvw,beta(nseg),flap
,r_telescop,{azimuth_mroot}';
sim_results_2_par='pav,pmax,cpmax,thrustmax,mrootmax';

nseg=20;nsec=1;rx=0.5;
```

Figure A5- Sample simulation file for constant speed rotor with pitch control

```
%====================
wttype=8;
%====================
vw_s=5;
vw_i=1;
vw_e=25;
%====================
rpm_s=30;rpm_i=.1;rpm_e=65;
pitch_s=-5;pitch_i=0.05;pitch_e=5;
flap=0;rflap1=0;rflap2=0;
r_telescop=1;
rmt1=0;rmt2=0;
%====================
yaw=0;
b=2;
d=27.514;
cone=7;
h=30;
prated=300000;
tolprated=.01;
z0=0.025;
vav=5.7;
dens=1.225;
ip=5;
%====================
sim_results_1_par='vw,rpm,pitch,tsr,p,cp,thrust,mroot_maxvw,beta(nseg),flap
,r_telescop,{azimuth_mroot}';
sim_results_2_par='pav,pmax,cpmax,thrustmax,mrootmax';

nseg=20;nsec=1;rx=0.5;
```

Figure A6-Sample simulation file for variable speed rotor with pitch control

```
%====================
wttype=1;
%====================
vw_s=5;
vw_i=1;
vw_e=25;
%====================
rpm=53.3;
pitch=-1.2;
flap=0;rflap1=0;rflap2=0;
r_telescop=1;
rmt1=0;rmt2=0;
%====================
yaw=0;
b=2;
d=27.514;
cone=7;
h=30;
prated=300000;
tolprated=.01;
z0=0.025;
vav=5.7;
dens=1.225;
ip=5;
%====================
sim_results_1_par='vw,rpm,pitch,tsr,p,cp,thrust,mroot_maxvw,beta(nseg),flap
,r_telescop,{azimuth_mroot}';
sim_results_2_par='pav,pmax,cpmax,thrustmax,mrootmax';

nseg=20;nsec=1;rx=0.5;
```

Figure A7- Sample simulation file for stall regulated constant speed rotor

```
%====================
wttype=5;
%====================
vw_s=5;
vw_i=1;
vw_e=25;
%====================
rpm=53.3;
pitch=-1.2;
flap=0;rflap1=0;rflap2=0;
r_telescop=1;
rmt1=.6;rmt2=.9;
%====================
yaw=0;
b=2;
d=27.514;
cone=7;
h=30;
prated=300000;
tolprated=.01;
z0=0.025;
vav=5.7;
dens=1.225;
ip=5;
%====================
sim_results_1_par='vw,rpm,pitch,tsr,p,cp,thrust,mroot_maxvw,beta(nseg),flap
,r_telescop,{azimuth_mroot}';
sim_results_2_par='pav,pmax,cpmax,thrustmax,mrootmax';

nseg=20;nsec=1;rx=0.5;
```

Figure A8-Sample simulation file for constant speed rotor with microtab

```
%====================
wttype=10;
%====================
vw_s=5;
vw_i=1;
vw_e=25;
%====================
rpm_s=30;rpm_i=.1;rpm_e=65;
pitch=-1.2;
flap=0;rflap1=0;rflap2=0;
rtelescop1=.7;rtelescop_i=.001;rtelescop2=1.1;
rmt1=0;rmt2=0;
%====================
yaw=0;
b=2;
d=27.514;
cone=7;
h=30;
prated=300000;
tolprated=.01;
z0=0.025;
vav=5.7;
dens=1.225;
ip=5;
%====================
sim_results_1_par='vw,rpm,pitch,tsr,p,cp,thrust,mroot_maxvw,beta(nseg),flap
,r_telescop,{azimuth_mroot}';
sim_results_2_par='pav,pmax,cpmax,thrustmax,mrootmax';


nseg=20;nsec=1;rx=0.5;


x_par={'pretwist'};
x_type=[1]; %1-3: distributed real/integer/indexed, 4-6:singular
real/integer/indexed
x_npoint=[5];
x_limit_batch={[-3,10]};
x_dist_limit={[rhub_r,1]};
x_co=[1]; % fraction of total CO in the form of arithmetic/integer
arithmatic CO (the rest geometric/exchange)
x_pattern=[3]; %1:random, 2:increasing, 3:decresing,4:concave, 5:convex
%-------------------------
parent_select=.5; %fraction of total selection randomly (the rest roulette-
wheel selection)
inipop_dev=0; %fraction of total initial population generated based on
deviation from baseline (the rest generated randomly)
%-------------------------
popsize=20;
popsize_u=20;
pc=0.3;
pm=0.1;
ngen=40;
%-------------------------
mutemethod=1;
comethod=1;
fitscalemethod=1;
termmethod=1;
%-------------------------

fitness=pav;
const=[pmax,0,305000];
```

Figure A9-Sample design optimisation file for variable speed rotor with telescopic blades

Appendix B-Microtab Data

The lift and drag coefficients obtained using CFD analysis with ANSYS package (Hella, 2012).

Table C1-Lift and drag coefficients for different microtab actuation heights on the lower surface

	S808 Aerofoil		**S808 Lower TL =95%, TH=1.1%**		**S808 Lower TL =95%, TH=2.2%**		**S808 Lower TL=95%, TH=3.3%**	
α	C_L	C_D	C_L	C_D	C_L	C_D	C_L	C_D
0	3.36E-01	1.17E-02	4.40E-01	1.41E-02	6.05E-01	1.70E-02	7.18E-01	2.01E-02
2	5.58E-01	1.29E-02	6.61E-01	1.56E-02	8.34E-01	1.88E-02	9.52E-01	2.27E-02
4	7.59E-01	1.59E-02	8.81E-01	1.76E-02	1.059	2.14E-02	1.1776	2.54E-02
6	9.47E-01	1.92E-02	1.0707	2.02E-02	1.2586	2.42E-02	1.3818	2.88E-02
8	1.1116	0.023195	1.234	2.39E-02	1.435	2.88E-02	1.5522	3.32E-02
10	1.259	0.028135	1.3437	2.83E-02	1.564	3.41E-02	1.688	3.91E-02
12	1.3596	0.035096	1.44	3.47E-02	1.6349	4.13E-02	1.7597	4.68E-02
14	1.3982	0.046187	1.4665	4.39E-02	1.6434	5.21E-02	1.7561	5.87E-02
16	1.3583	0.069745	1.4274	6.21E-02	1.5648	7.53E-02	1.6466	8.61E-02
18	1.13E+00	1.19E-01	1.2187	0.10036	1.2949	1.27E-01		

Table C2-Lift and drag coefficients for different microtab actuation heights on the upper surface

	S808 Aerofoil		**S808 Upper TL =80%, TH=1.1%**		**S808 Upper TL=80%, TH=2.2%**		**S808 Upper TL =80%, TH=3.3%**	
α	C_L	C_D	C_L	C_D	C_L	C_D	C_L	C_D
0	3.36E-01	1.17E-02	9.61E-02	2.25E-02	-8.09E-02	3.00E-02	-2.16E-01	3.71E-02
2	5.58E-01	1.29E-02	3.19E-01	2.32E-02	1.52E-01	3.05E-02	1.96E-02	3.76E-02
4	7.59E-01	1.59E-02	5.40E-01	2.45E-02	3.81E-01	3.15E-02	2.53E-01	3.85E-02
6	9.47E-01	1.92E-02	7.50E-01	2.63E-02	6.03E-01	3.31E-02	4.79E-01	3.97E-02
8	1.1116	0.023195	9.48E-01	2.89E-02	8.15E-01	3.52E-02	6.98E-01	4.16E-02
10	1.259	0.028135	1.1263	3.23E-02	1.012	3.81E-02	9.04E-01	4.41E-02
12	1.3596	0.035096	1.281	3.69E-02	1.1883	4.20E-02	1.127	4.85E-02
14	1.3982	0.046187	1.399	4.38E-02	1.334	4.75E-02	1.2605	5.19E-02
16	1.3583	0.069745	1.4288	5.99E-02	1.4352	5.93E-02	1.4106	6.03E-02

Table C3-Changes in lift and drag coefficients for different microtab actuation heights on the lower surface

	S808 Lower TL =95%, TH=1.1%		**S808 Lower TL =95%, TH=2.2%**		**S808 Lower TL =95%, TH=3.3%**	
α	ΔC_L	ΔC_D	ΔC_L	ΔC_D	ΔC_L	ΔC_D
0	1.04E-01	2.41E-03	2.69E-01	5.31E-03	3.82E-01	8.40E-03
2	1.03E-01	2.66E-03	2.76E-01	5.91E-03	3.95E-01	9.77E-03
4	1.22E-01	1.67E-03	3.00E-01	5.48E-03	4.19E-01	9.49E-03
6	1.24E-01	1.01E-03	3.12E-01	4.94E-03	4.35E-01	9.59E-03
8	1.22E-01	7.05E-04	3.23E-01	5.63E-03	4.41E-01	9.97E-03
10	8.47E-02	1.76E-04	3.05E-01	5.99E-03	4.29E-01	1.09E-02
12	8.04E-02	-3.98E-04	2.75E-01	6.20E-03	4.00E-01	1.17E-02
14	6.83E-02	-2.29E-03	2.45E-01	5.90E-03	3.58E-01	1.25E-02
16	6.91E-02	-7.68E-03	2.07E-01	5.58E-03	2.88E-01	1.64E-02
18	9.16E-02	-1.90E-02	1.68E-01	7.17E-03		-1.19E-01

Table C4-Changes in lift and drag coefficients for different microtab actuation heights on the upper surface

	S808 Upper TL =80%, TH=1.1%		**S808 Upper TL =80%, TH=2.2%**		**S808 Upper TL =80%, TH=3.3%**	
α	ΔC_L	ΔC_D	ΔC_L	ΔC_D	ΔC_L	ΔC_D
0	-2.40E-01	1.08E-02	-4.17E-01	1.83E-02	-5.52E-01	2.54E-02
2	-2.39E-01	1.03E-02	-4.06E-01	1.76E-02	-5.38E-01	2.47E-02
4	-2.19E-01	8.57E-03	-3.78E-01	1.56E-02	-5.06E-01	2.26E-02
6	-1.96E-01	7.09E-03	-3.44E-01	1.38E-02	-4.68E-01	2.05E-02
8	-1.64E-01	5.68E-03	-2.97E-01	1.20E-02	-4.13E-01	1.84E-02
10	-1.33E-01	4.14E-03	-2.47E-01	9.96E-03	-3.55E-01	1.59E-02
12	-7.86E-02	1.82E-03	-1.71E-01	6.86E-03	-2.33E-01	1.34E-02
14	8.00E-04	-2.40E-03	-6.42E-02	1.32E-03	-1.38E-01	5.76E-03
16	7.05E-02	-9.86E-03	7.69E-02	-1.05E-02	5.23E-02	-9.44E-03

Appendix C-Design Optimisation Results

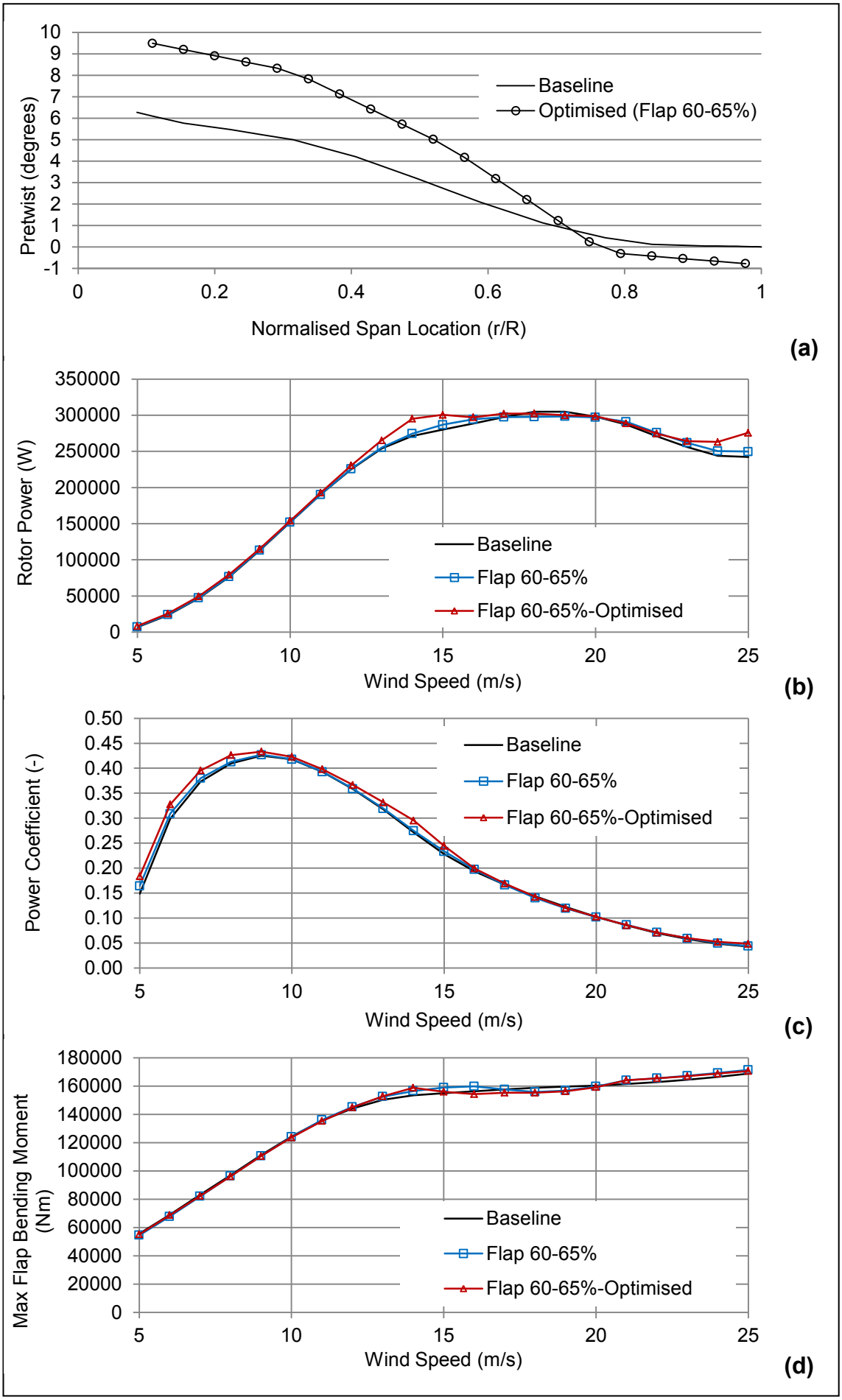

Figure C1-Flap 60-65%- constant speed

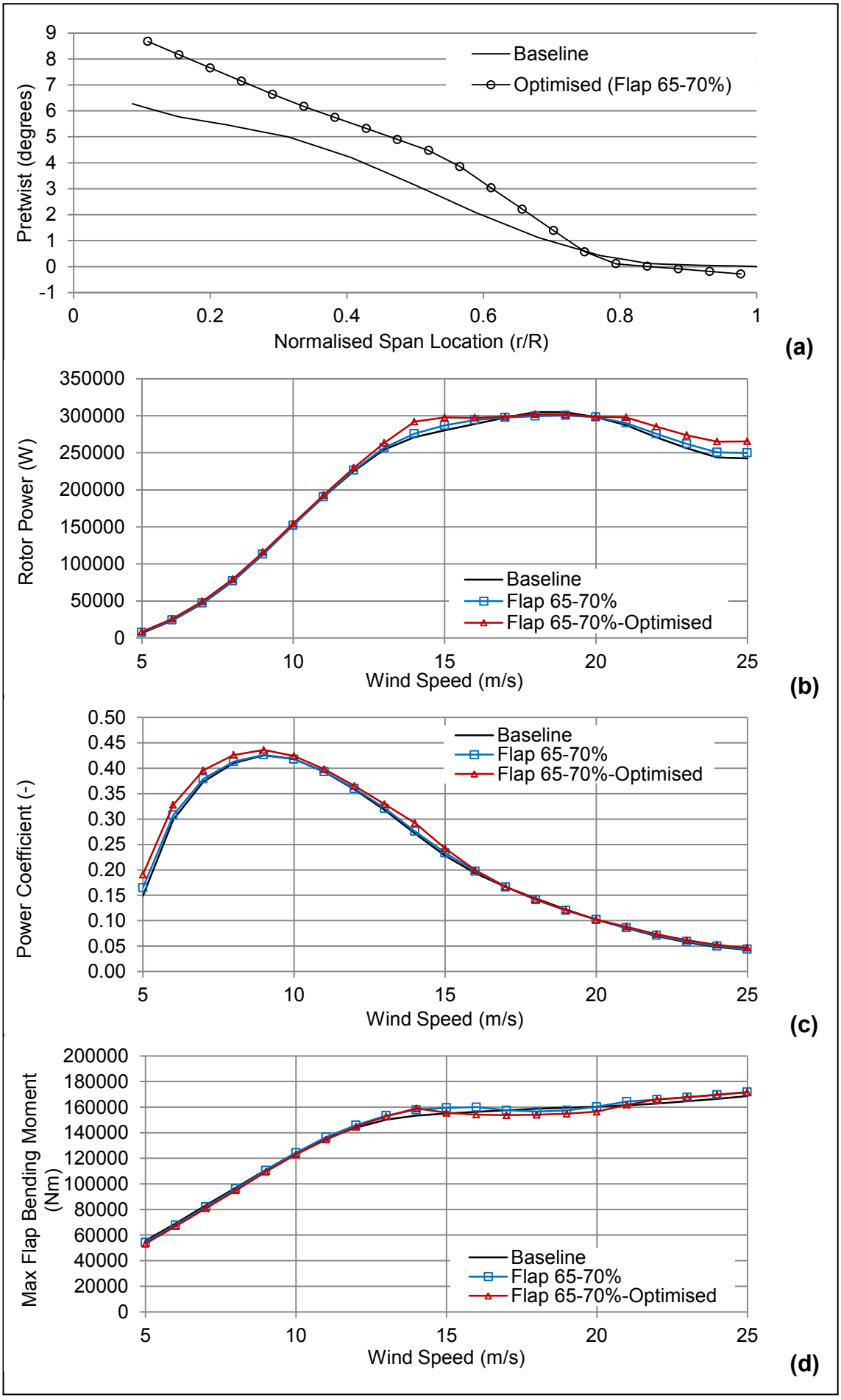

Figure C2-Flap 65-70%- constant speed

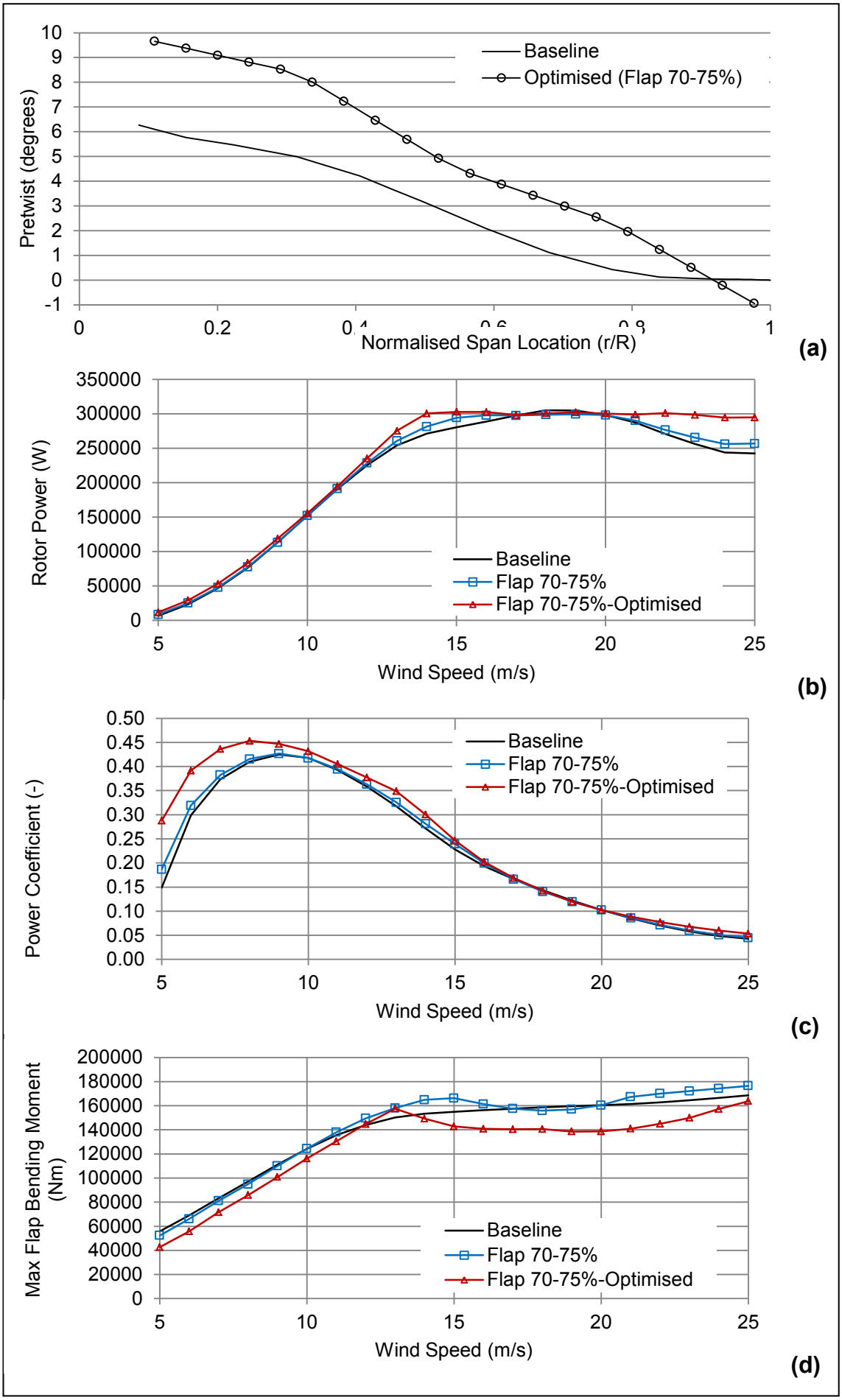

Figure C3-Flap 70-75%- constant speed

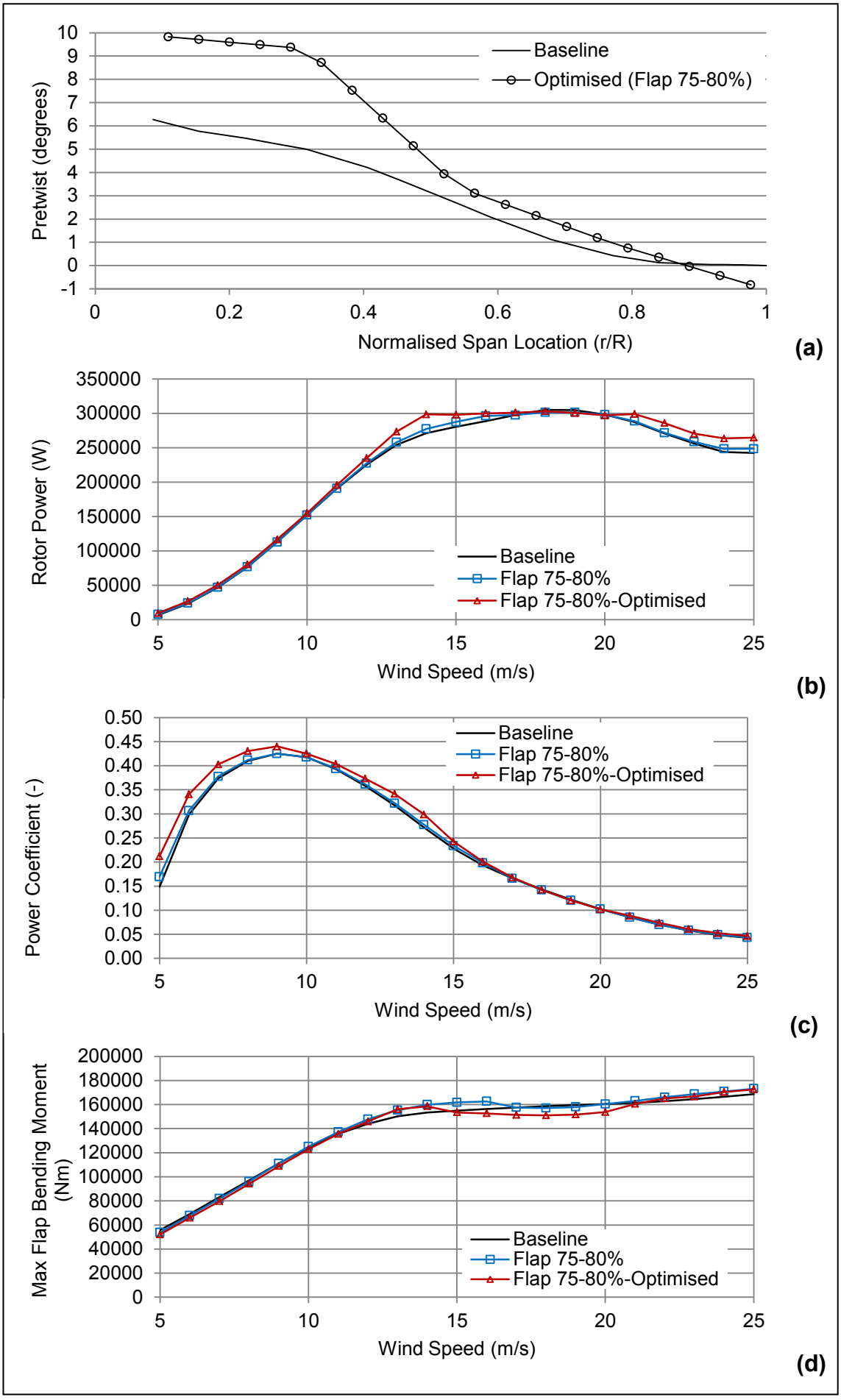

Figure C4-Flap 75-80%- constant speed

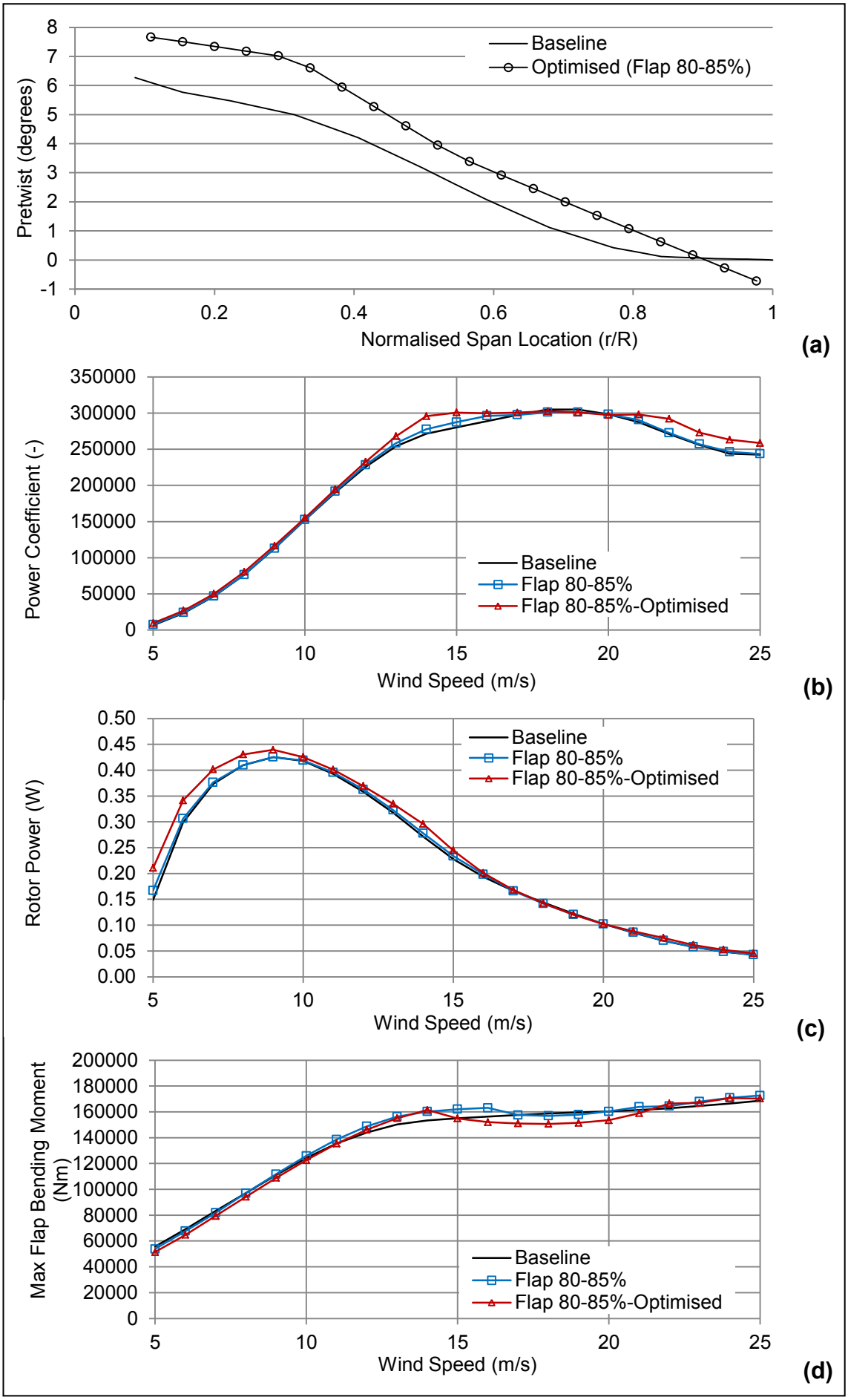

Figure C5-Flap 80-85%- constant speed

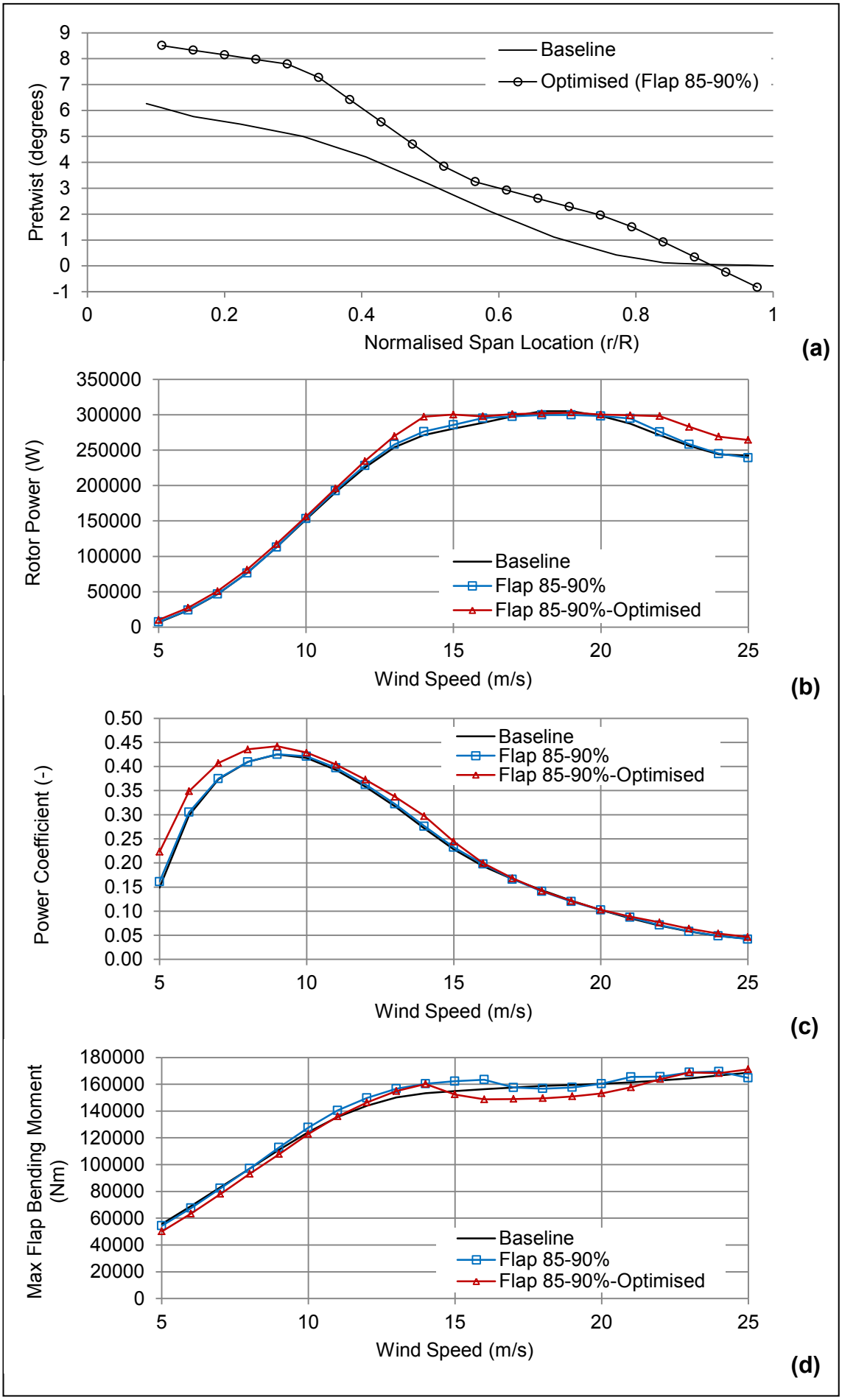

Figure C6-Flap 85-90%- constant speed

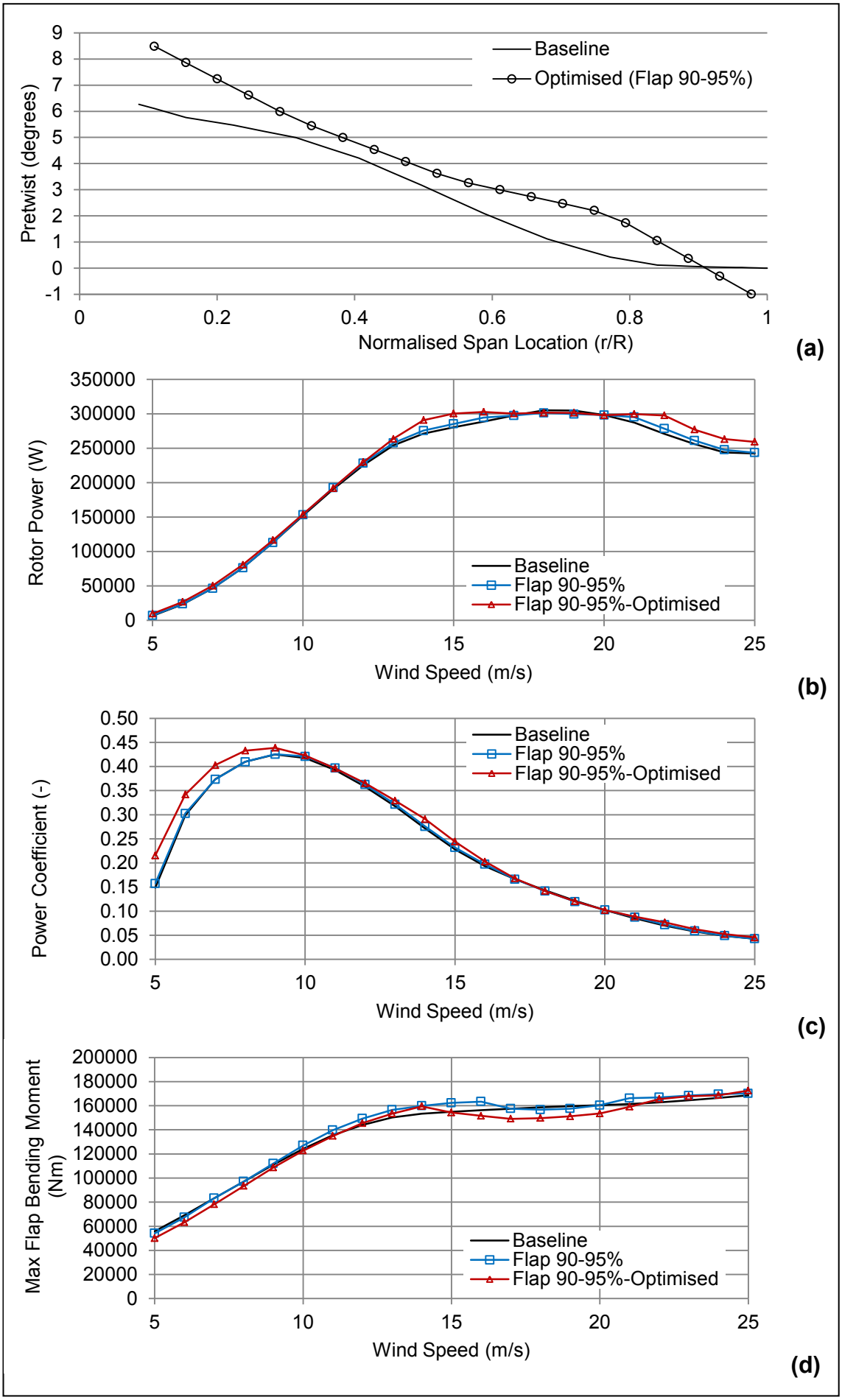

Figure C7-Flap 90-95%- constant speed

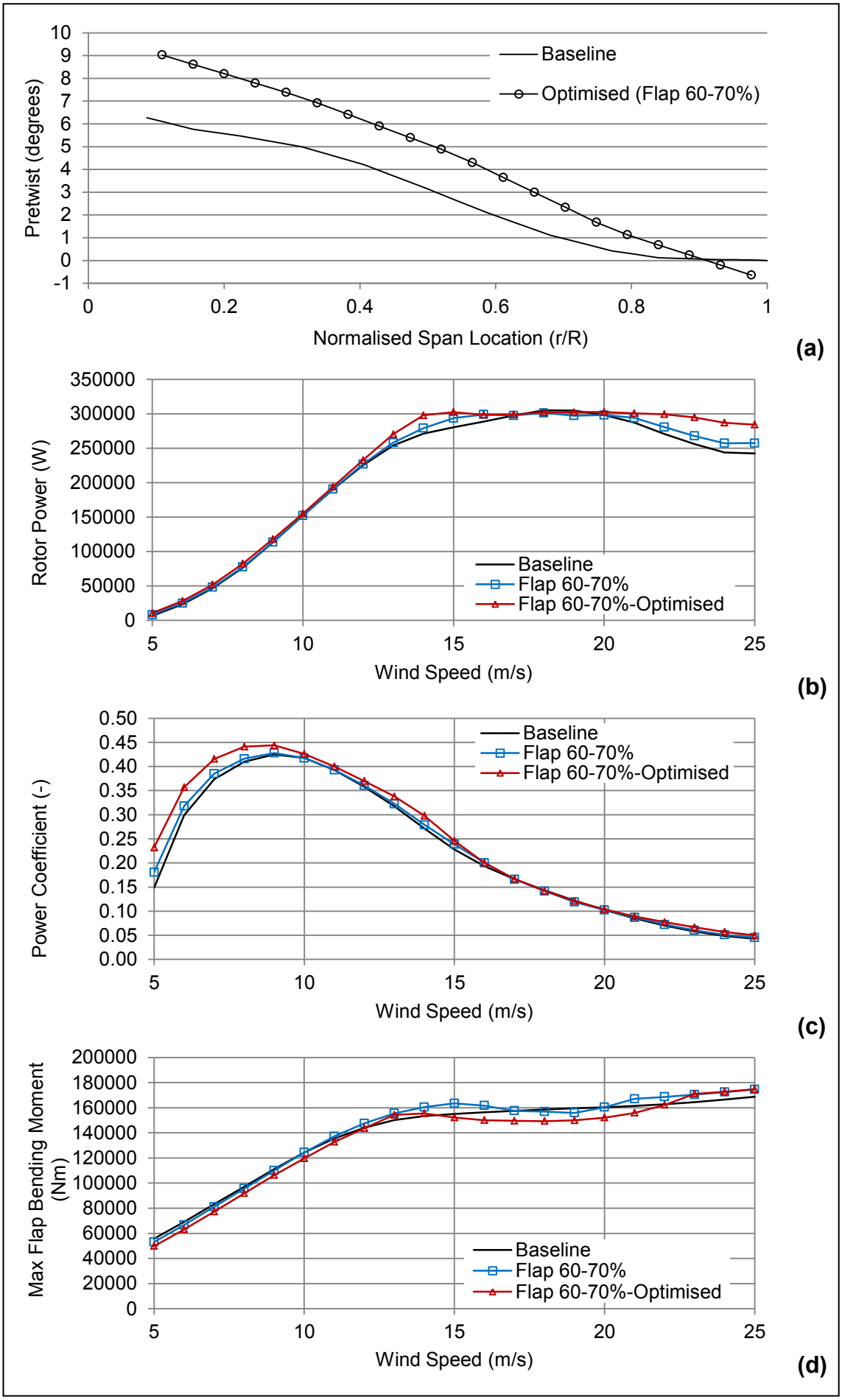

Figure C8-Flap 60-70%- constant speed

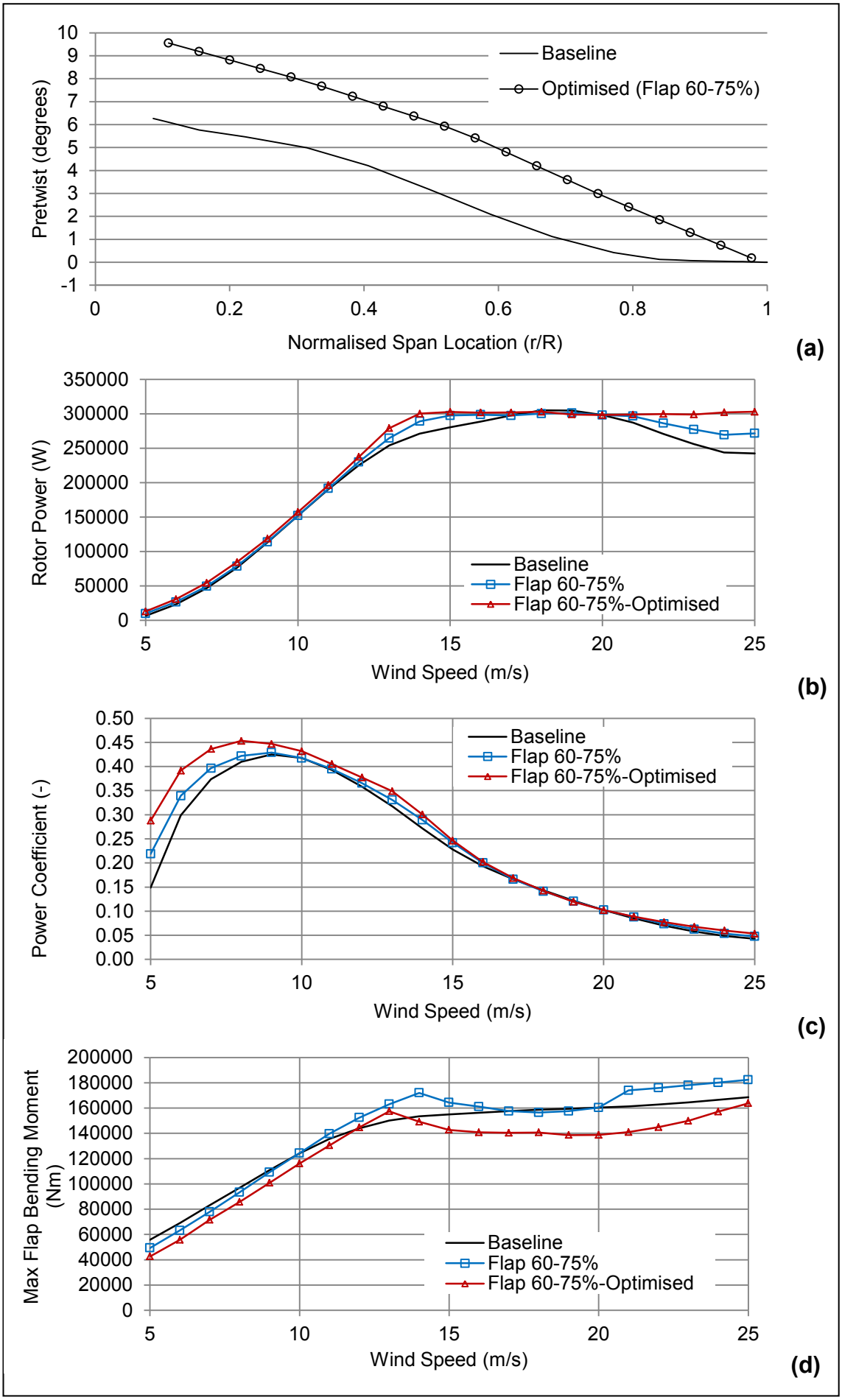

Figure C9-Flap 60-75%- constant speed

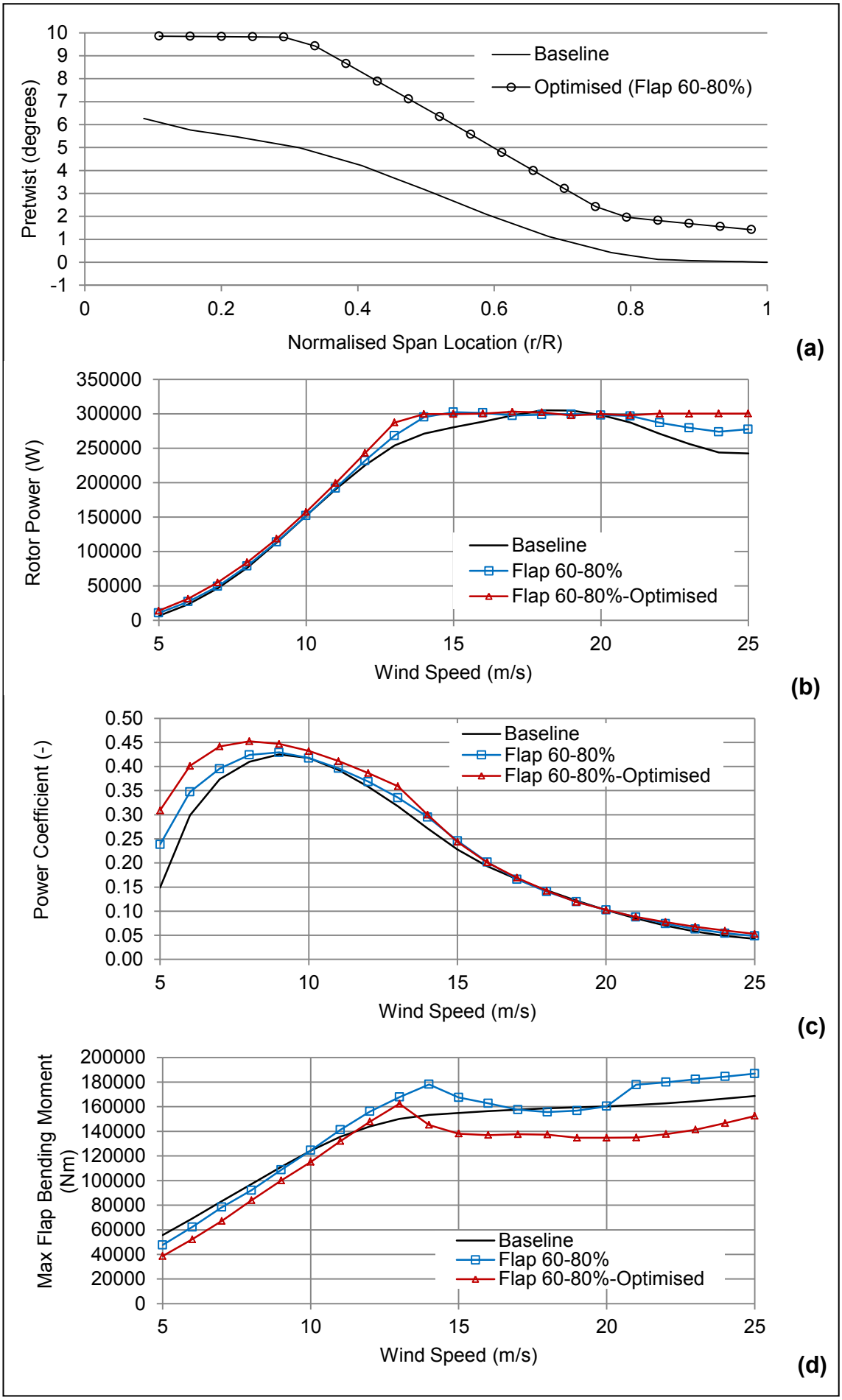

Figure C10-Flap 60-80%- constant speed

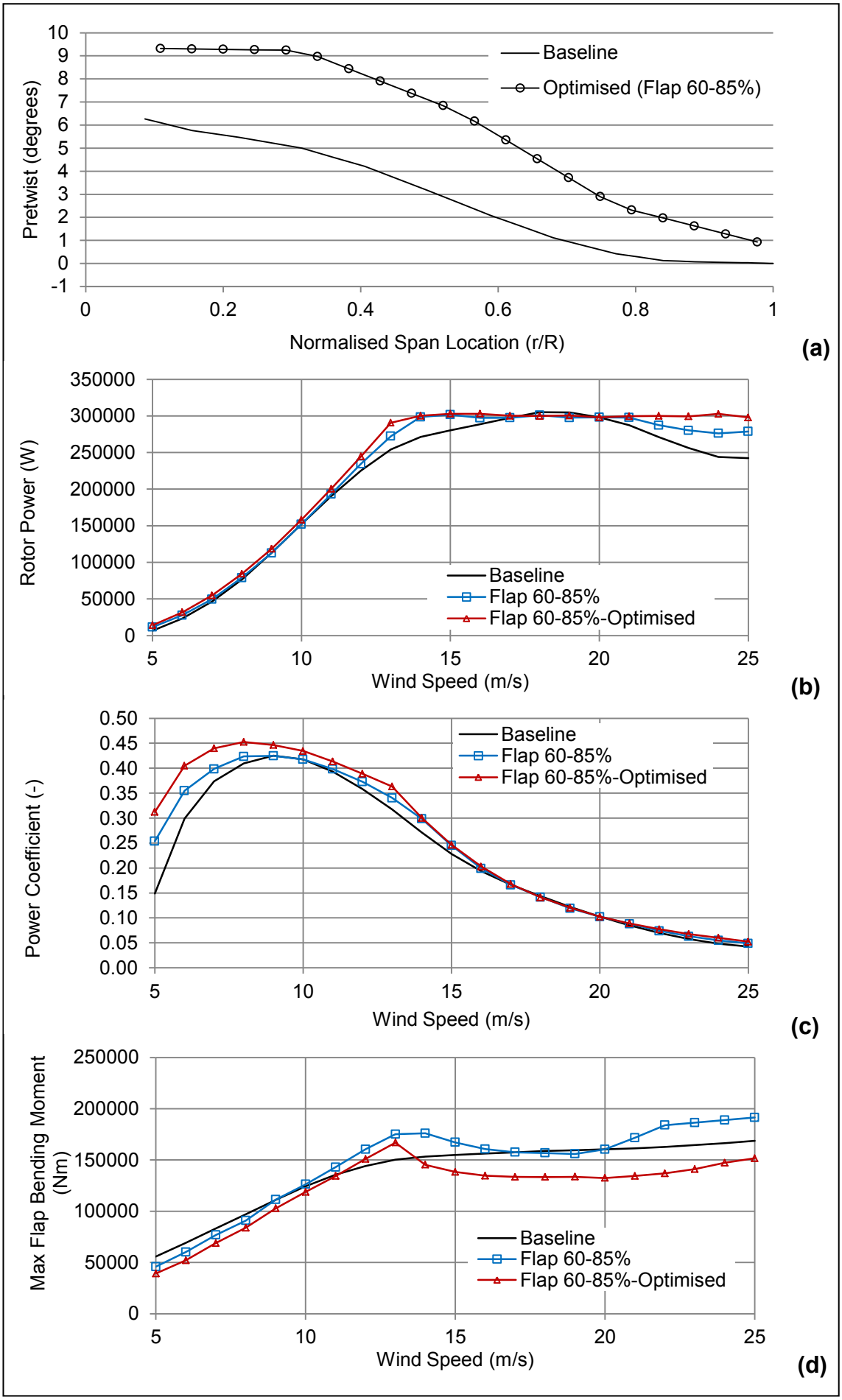

Figure C11-Flap 60-85%- constant speed

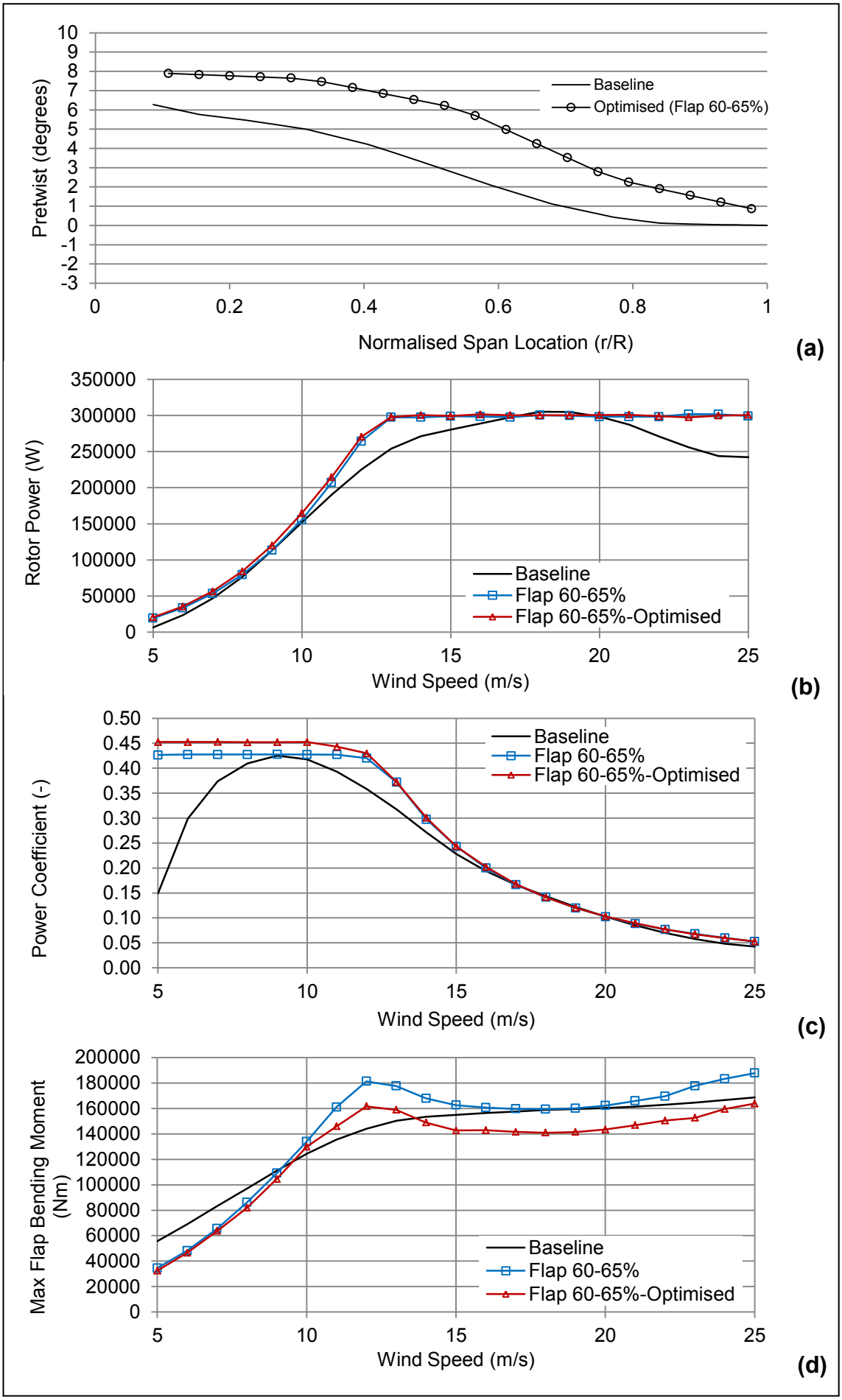

Figure C12-Flap 60-65%- variable speed

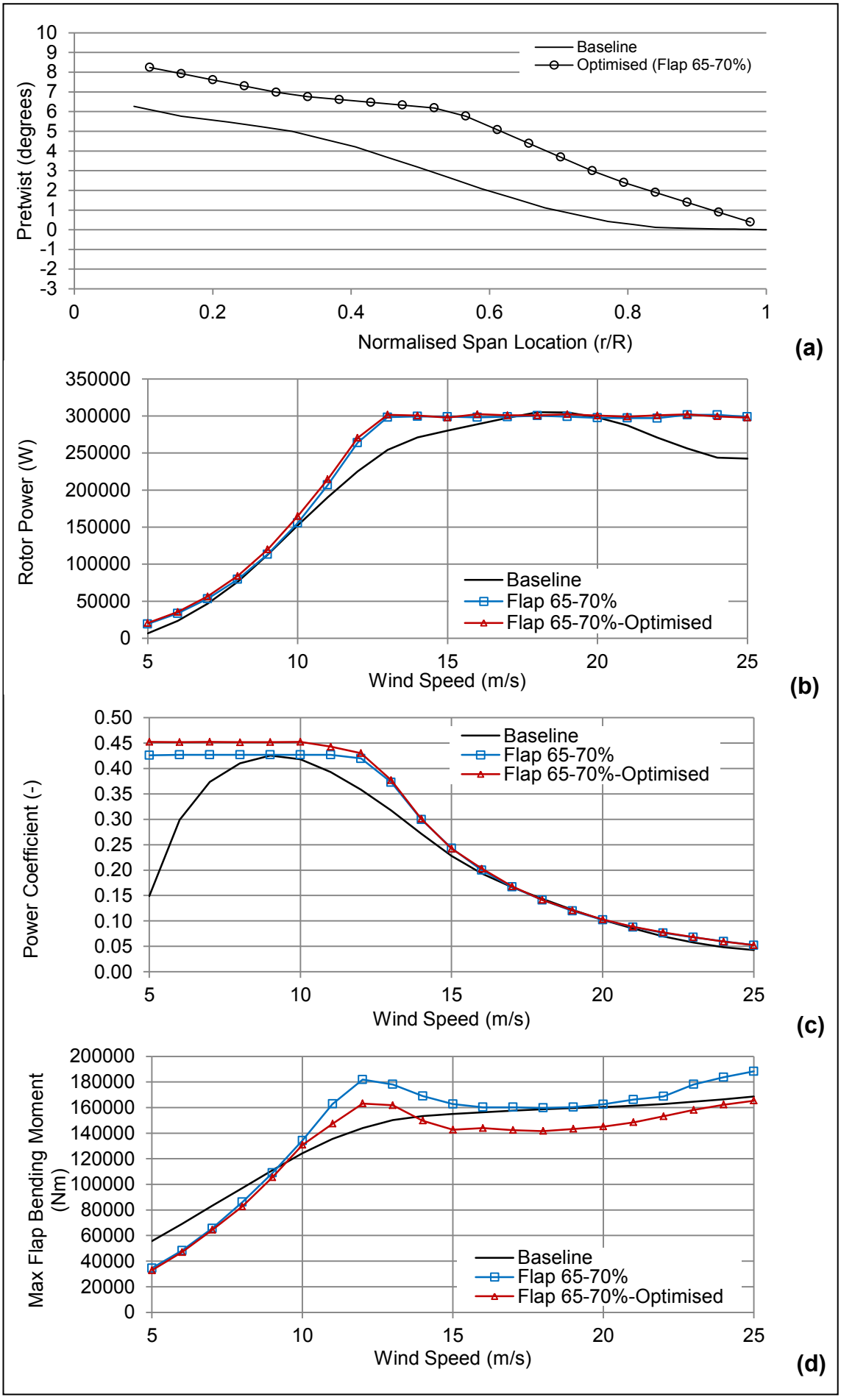

Figure C13-Flap 60-70%- variable speed

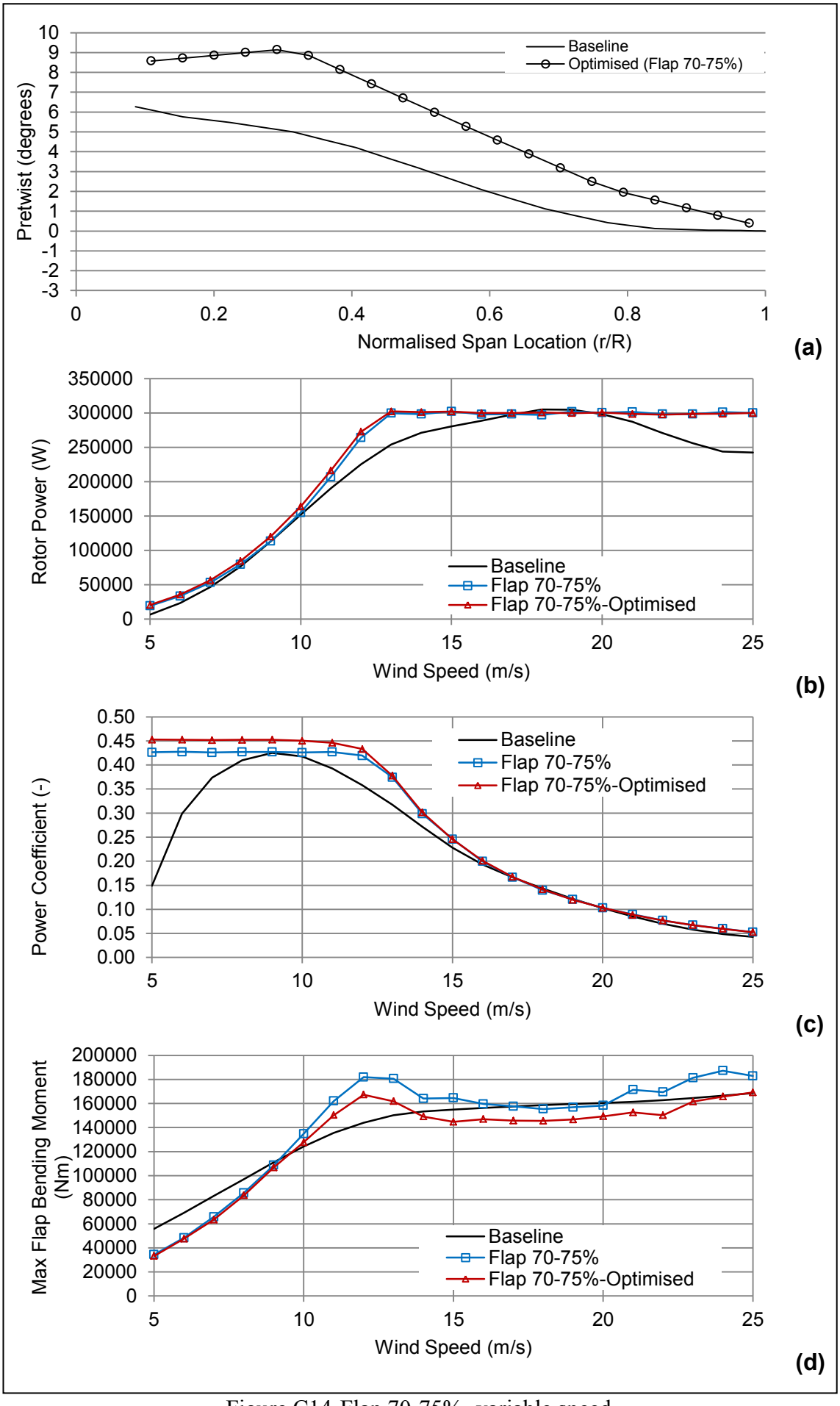

Figure C14-Flap 70-75%- variable speed

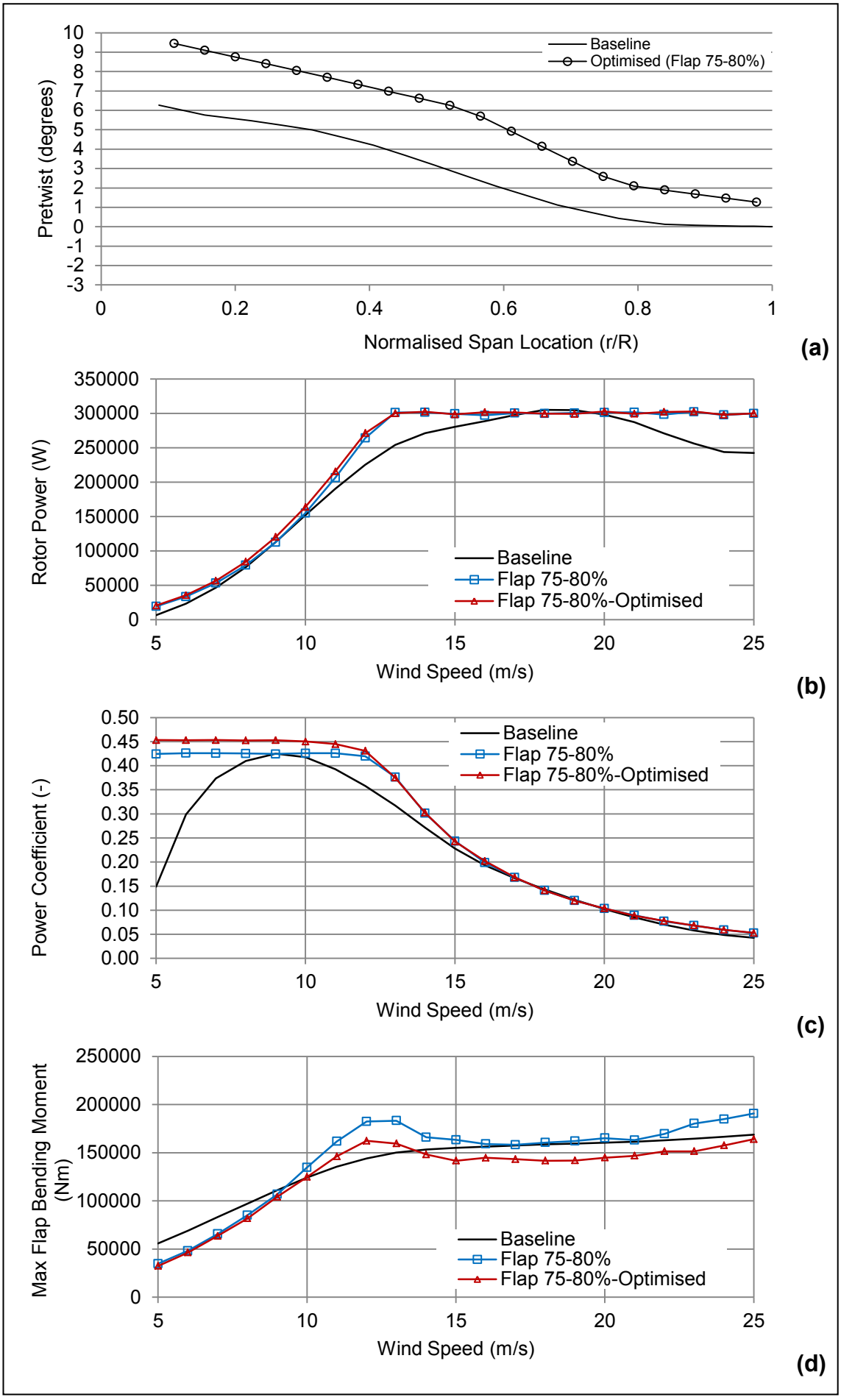

Figure C15-Flap 75-80%- variable speed

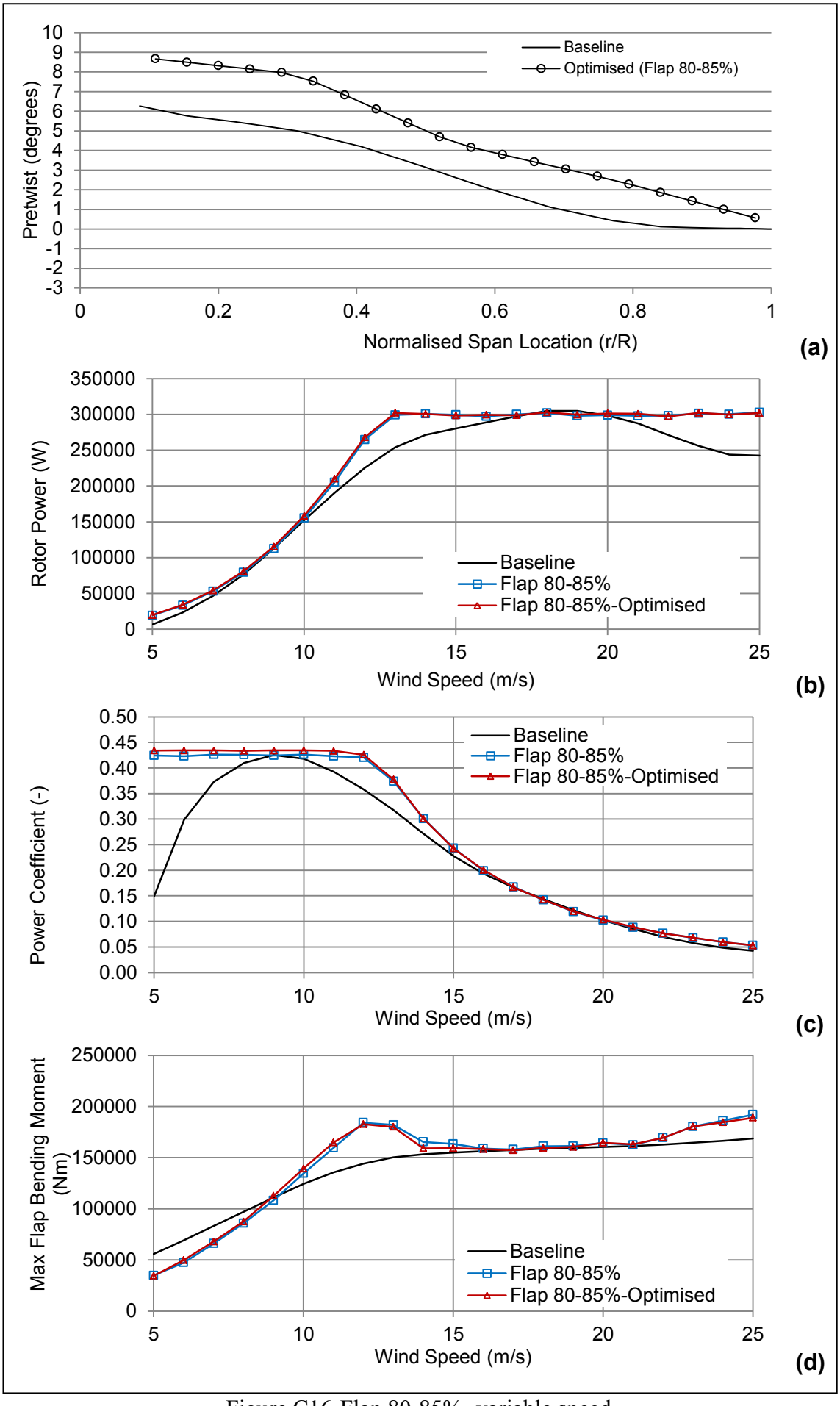

Figure C16-Flap 80-85%- variable speed

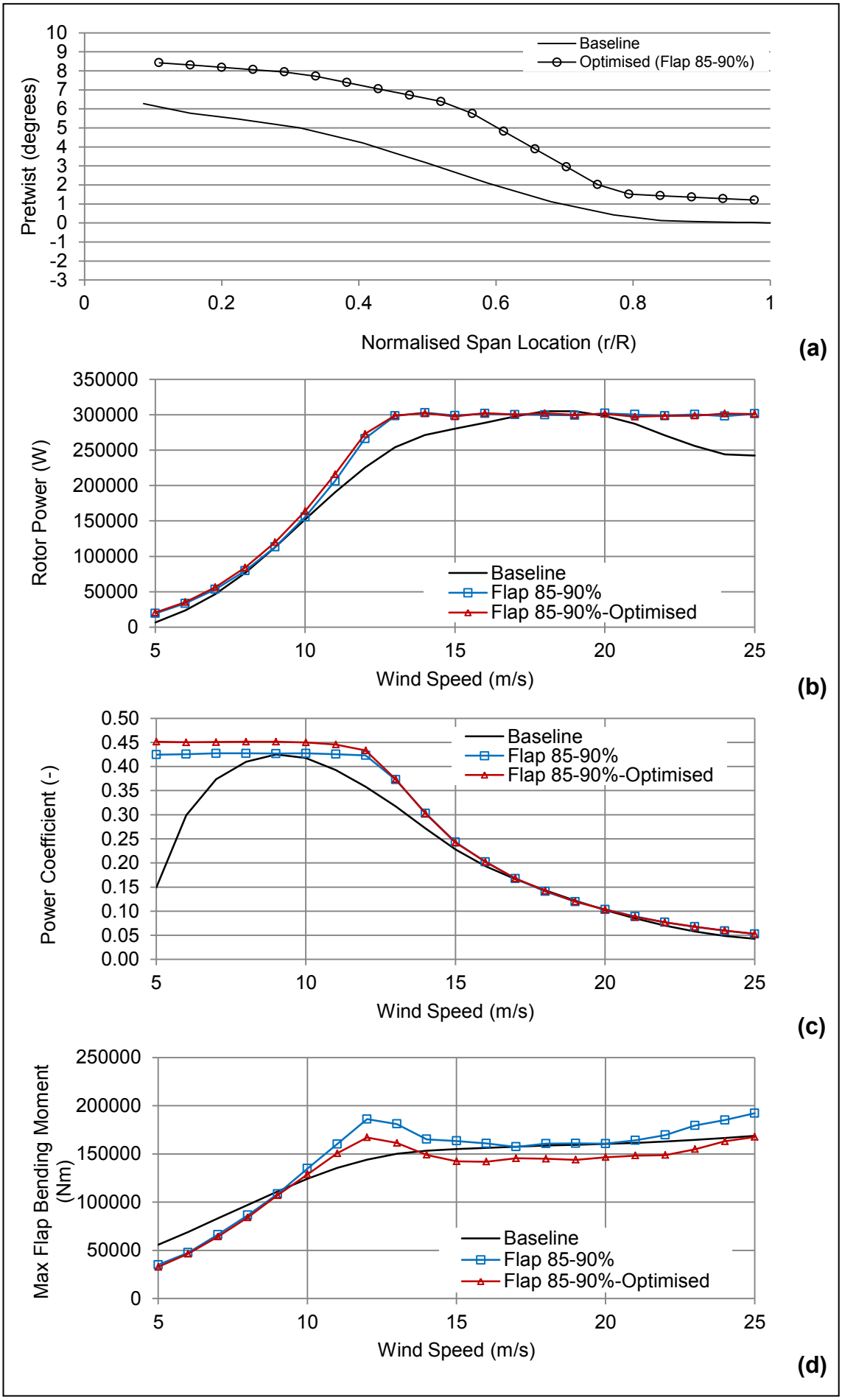

Figure C17-Flap 85-90%- variable speed

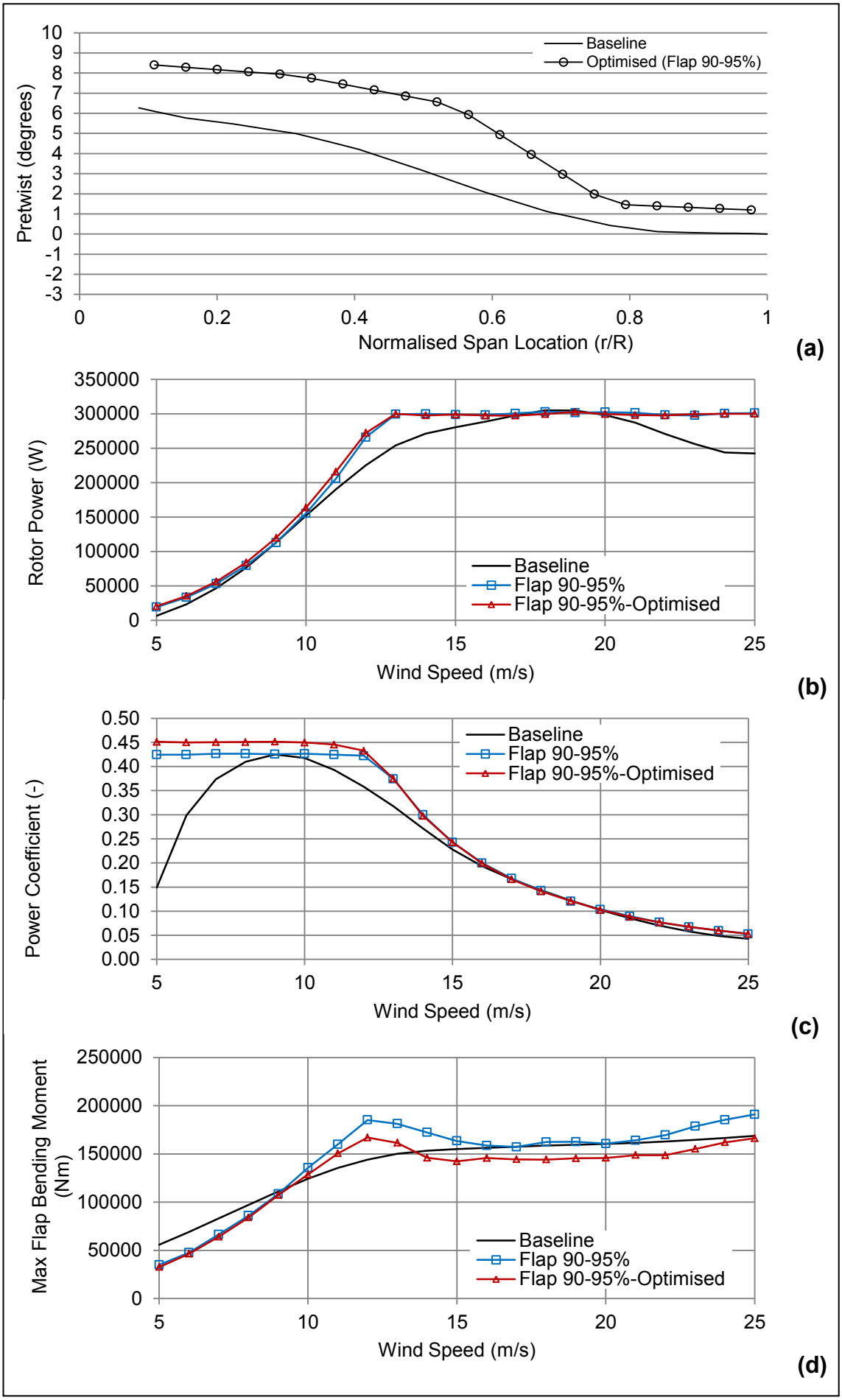

Figure C18-Flap 90-95%- variable speed

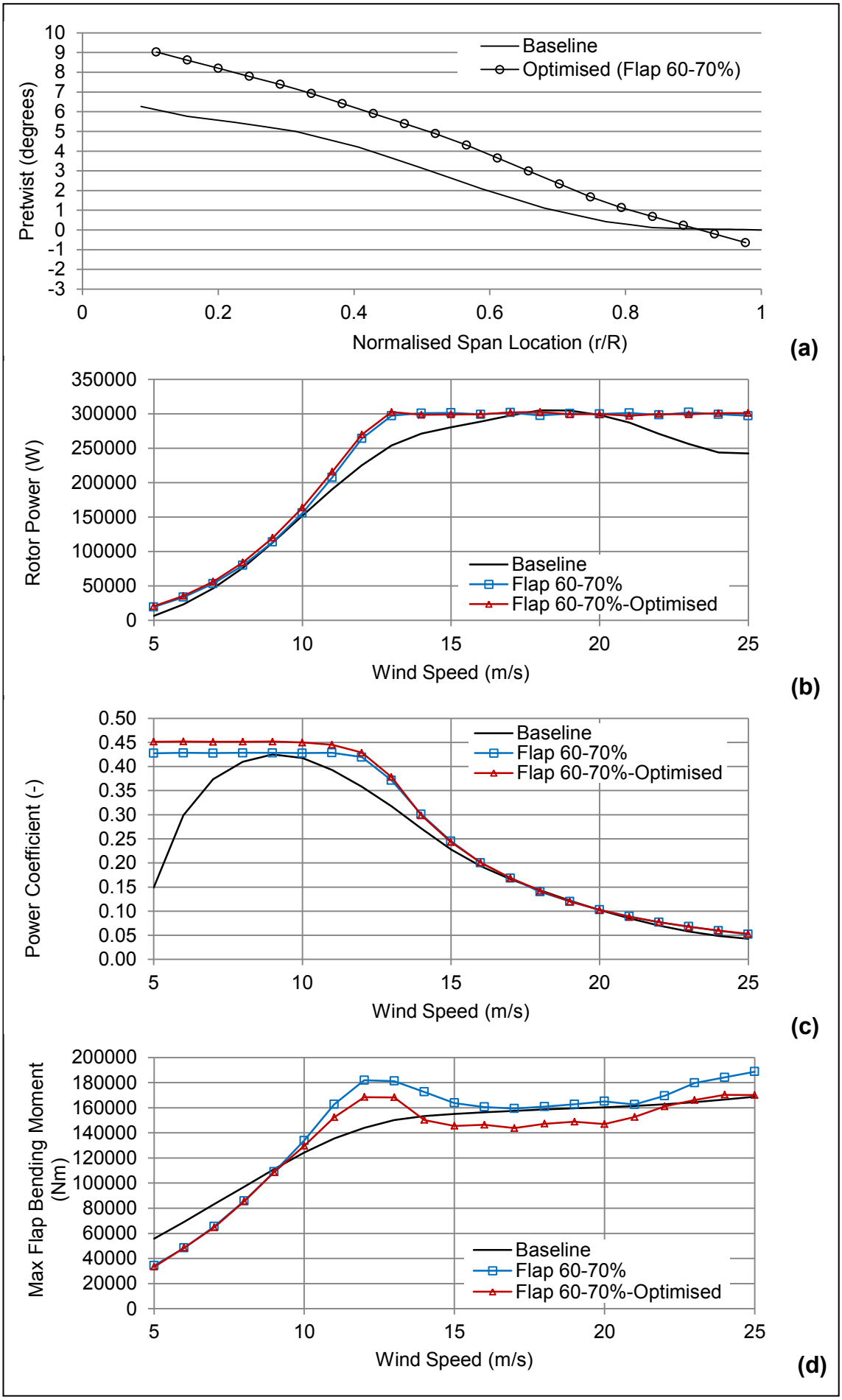

Figure C19-Flap 60-70%- variable speed

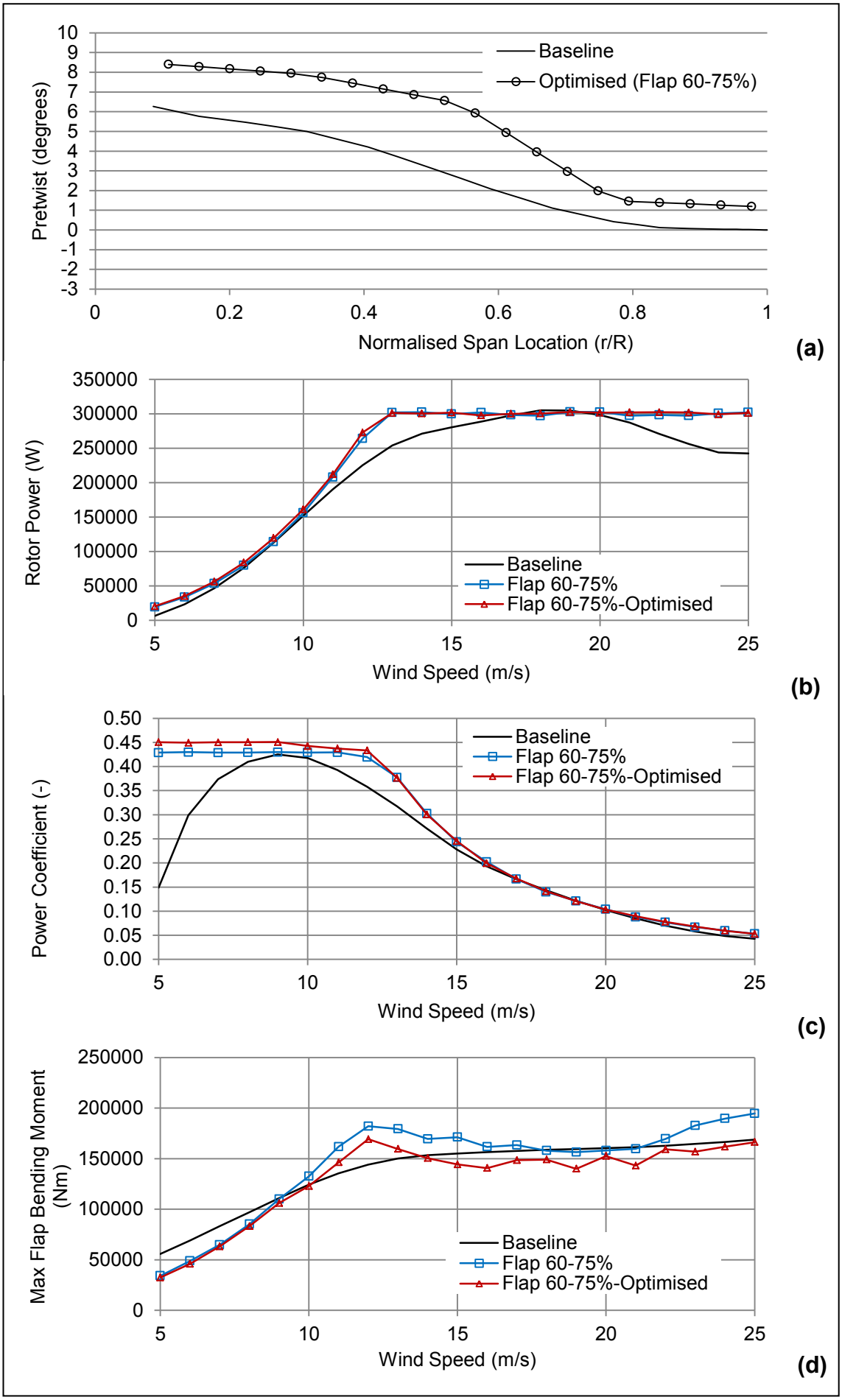

Figure C20-Flap 60-75%- variable speed

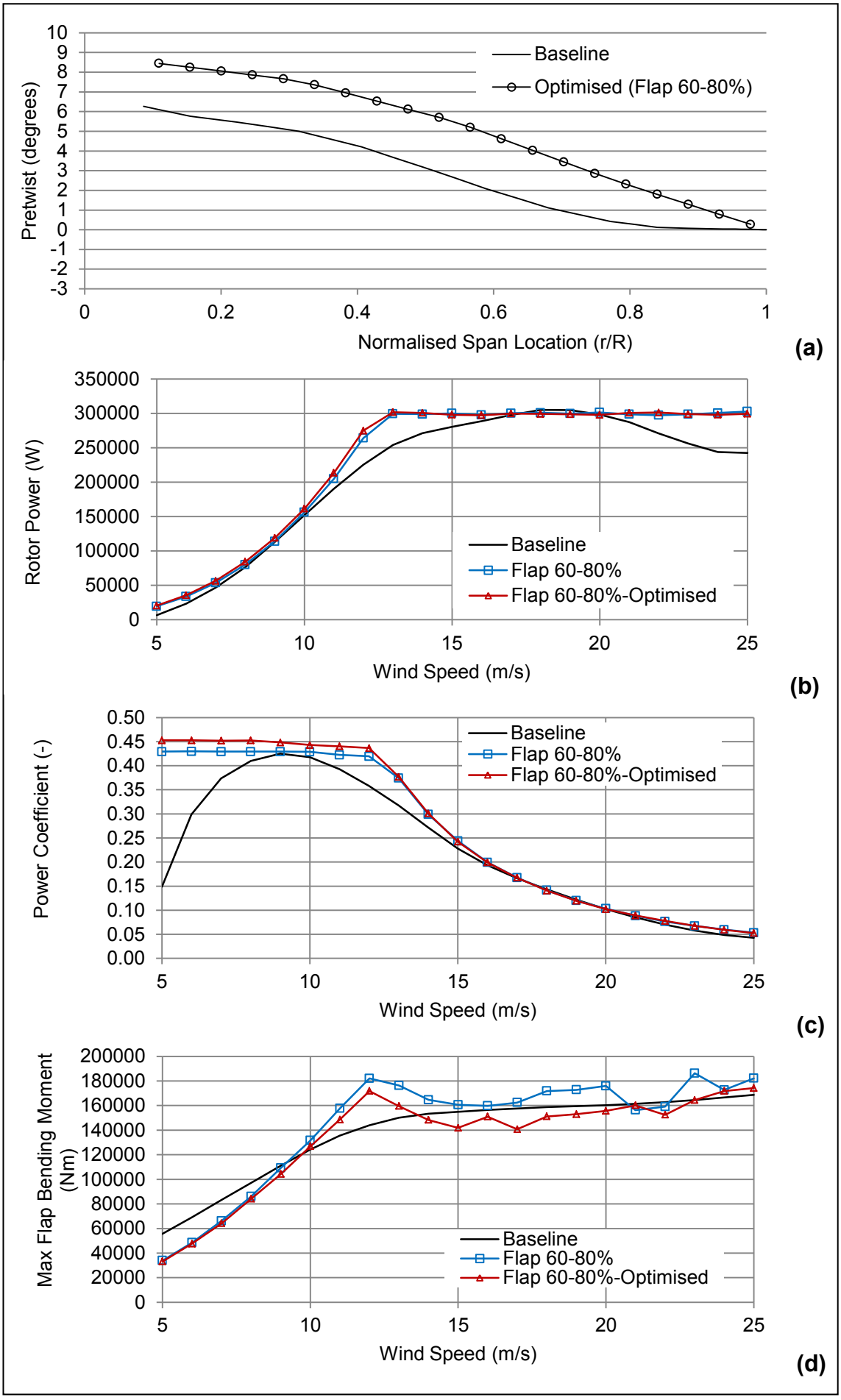

Figure C21-Flap 60-80%- variable speed

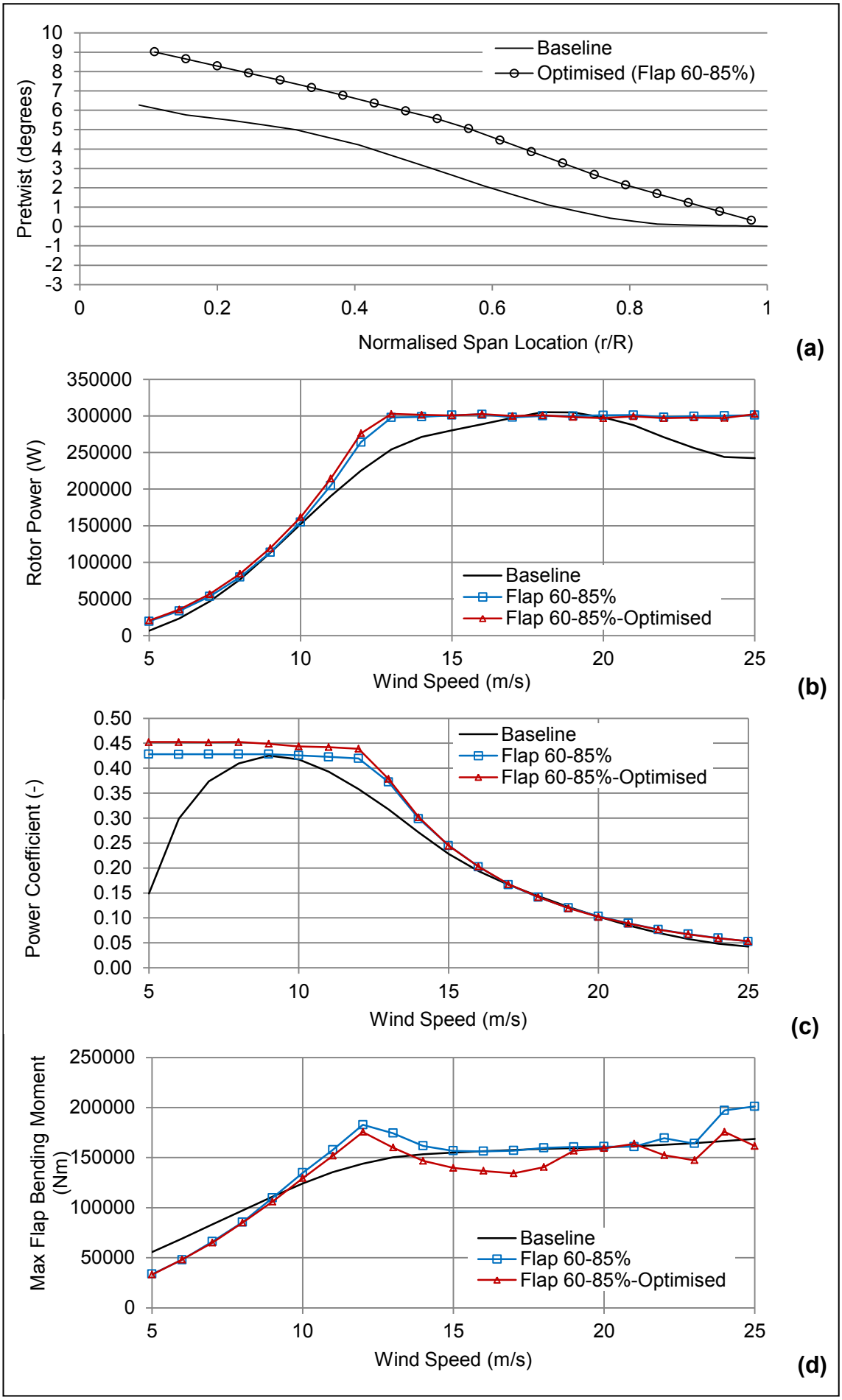

Figure C22-Flap 60-85%- variable speed